

Analysis of CERK1 ectodomain shedding and the role of XLG2 in *cerk1-4* cell death execution

Dissertation

zur Erlangung des mathematisch-naturwissenschaftlichen Doktorgrades

"Doctor rerum naturalium"

der Georg-August-Universität Göttingen

im Promotionsprogramm Biologie

der Georg-August University School of Science (GAUSS)

vorgelegt von

Christopher Meusel

aus Ankum

Göttingen, 2016

Betreuungsausschuss

Prof. Dr. Volker Lipka

Zellbiologie der Pflanze

Albrecht-von-Haller Institut für Pflanzenwissenschaften

PD. Dr. Thomas Teichmann

Zellbiologie der Pflanze

Albrecht-von-Haller Institut für Pflanzenwissenschaften

Dr. Elena K. Petutschnig

Zellbiologie der Pflanze

Albrecht-von-Haller Institut für Pflanzenwissenschaften

Mitglieder der Prüfungskommission

Referent: Prof. Dr. Volker Lipka

Zellbiologie der Pflanze

Albrecht-von-Haller Institut für Pflanzenwissenschaften

Korreferent: PD. Dr. Thomas Teichmann

Zellbiologie der Pflanze

Albrecht-von-Haller Institut für Pflanzenwissenschaften

Weitere Mitglieder der Prüfungskommission:

Prof. Dr. Ivo Feußner

Biochemie der Pflanze,

Albrecht-von-Haller Institut für Pflanzenwissenschaften

PD Dr. Martin Fulda

Biochemie der Pflanze,

Albrecht-von-Haller Institut für Pflanzenwissenschaften

Prof. Dr. Christiane Gatz

Molekularbiologie und Physiologie der Pflanze,

Albrecht-von-Haller Institut für Pflanzenwissenschaften

Prof. Dr. Andrea Polle

Forstbotanik und Baumphysiologie,

Fakultät für Forstwissenschaften und Waldökologie

Tag der mündlichen Prüfung: 18.04.2016

Promovierenden-Erklärung der Georg-August-Universität Göttingen

1. Die Gelegenheit zum vorliegenden Promotionsvorhaben ist mir nicht kommerziell vermittelt worden. Insbesondere habe ich keine Organisation eingeschaltet, die gegen Entgelt Betreuerinnen und Betreuer für die Anfertigung von Dissertationen sucht oder die mir obliegenden Pflichten hinsichtlich der Prüfungsleistungen für mich ganz oder teilweise erledigt.

2. Hilfe Dritter wurde bis jetzt und wird auch künftig nur in wissenschaftlich vertretbarem und prüfungsrechtlich zulässigem Ausmaß in Anspruch genommen. Insbesondere werden alle Teile der Dissertation selbst angefertigt; unzulässige fremde Hilfe habe ich dazu weder unentgeltlich noch entgeltlich entgegengenommen und werde dies auch zukünftig so halten.

3. Die Ordnung zur Sicherung der guten wissenschaftlichen Praxis an der Universität Göttingen wurde von mir beachtet.

4. Eine entsprechende Promotion wurde an keiner anderen Hochschule im In- oder Ausland beantragt; die eingereichte Dissertation oder Teile von ihr wurden nicht für ein anderes Promotionsvorhaben verwendet.

Mir ist bekannt, dass unrichtige Angaben die Zulassung zur Promotion ausschließen bzw. später zum Verfahrensabbruch oder zur Rücknahme des erlangten Grades führen.

Christopher Meusel

Göttingen, den 11.03.2016

Abstract

Conserved microbial signatures are perceived via plasma membrane localized pattern recognition receptors (PRRs). In *Arabidopsis*, perception of the fungal cell wall component chitin requires the LysM receptor-like kinase CERK1. CERK1 is post-translationally modified to release a soluble ectodomain derivative into the apoplast. The ectodomain fragment is likely to be generated by a proteolytic mechanism called ectodomain shedding. Ectodomain shedding is well documented in animals, where it fulfils diverse regulatory functions on a range of different proteins. In plants, ectodomain shedding has so far only been reported for CERK1 and the function of CERK1 ectodomain shedding is unknown. Some evidence for a role in cell death control comes from *cerk1-4*, a CERK1 mutant that lacks the soluble ectodomain fragment and is characterized by enhanced cell death upon pathogen attack and in senescence.

The first part of the present study focused on the analysis of CERK1 ectodomain shedding and its function in the development of the *cerk1-4* phenotype. *Arabidopsis* accessions were found to vary regarding the abundance of the shed CERK1 ectodomain. The presence of prolines within the extracellular stalk of CERK1 positively correlated with ectodomain abundance. CERK1 variants lacking specific proline residues showed reduced ectodomain abundance, but did not suppress the development of the *cerk1-4* phenotype. Point mutations targeting possible protease recognition motifs or variations in extracellular stalk length did not abolish CERK1 ectodomain shedding. Similarly, replacement of the CERK1 transmembrane domain and extracellular stalk with corresponding regions from the flagellin receptor FLS2 had little impact on ectodomain shedding. In mass spectrometry analyses of cell culture supernatants and apoplastic wash fluids, peptides corresponding to extracellular domains of numerous RLKs were identified. The peptides probably derived from ectodomain which were proteolytically released into the apoplast. These results indicate that ectodomain shedding might be a common post-translational modification in plants.

The second part of this study focused on the identification of signal transduction components which are essential for development of the *cerk1-4* phenotype. A novel mutant fully suppressing the *cerk1-4* phenotype was isolated from a genetic screen. The underlying mutation was mapped to the extra-large G-protein 2 (XLG2), which has recently been proposed to act as a G-protein α -subunit. In the suppressor mutant, a highly conserved glutamic acid was substituted by lysine in the N-terminal part of XLG2. Complementation studies showed that XLG2 fusions with an N-terminal fluorescence protein tag are functional,

while C-terminal fusions are not. Confocal microscopy of stably transformed *Arabidopsis* plants expressing Venus-XLG2 revealed localization to the cell periphery. A subpopulation of Venus-XLG2 accumulates in the nucleus upon diverse stimuli such as water and PAMP infiltration, wounding or pathogen attack. XLG2 has recently been shown to physically interact with canonical heterotrimeric G-protein $\beta\gamma$ -dimers. Also, G-protein β - and γ -subunits were shown to be required for full development of the *cerk1-4* phenotype. Interestingly, in the G-protein β -subunit mutant *agb1*, a subpopulation of Venus-XLG2 was localized to the nucleus already in untreated cells. These results suggest that XLG2 subcellular localization is modulated by interaction with G-protein $\beta\gamma$ -subunits, which in turn affects its action on downstream targets.

Zusammenfassung

Konservierte mikrobielle Strukturen werden von Plasmamembran lokalisierten Rezeptoren erkannt. In *Arabidopsis* erfordert die Wahrnehmung der Pilzzellwand-Komponente Chitin die LysM Rezeptor-ähnliche Kinase CERK1. CERK1 wird post-translational modifiziert was die Freisetzung seiner Ektodomäne in den Apoplasten zur Folge hat. Die Freisetzung der Ektodomäne erfolgt wahrscheinlich durch so genanntes Ektodomänen-Shedding. Ektodomänen-Shedding ist ein in Tieren gut dokumentierter Mechanismus, wo es diverse regulatorische Funktionen für eine Reihe von verschiedenen Proteinen erfüllt. In Pflanzen wurde Ektodomänen-Shedding bisher nur für CERK1 beschrieben, wobei die Funktion unbekannt ist. Anzeichen für eine Rolle der CERK1 Ektodomäne in Zelltodkontrolle kommen von *cerk1-4*, einer CERK1 Mutante der das lösliche Ektodomänen Fragment fehlt.

Der erste Teil der vorliegenden Arbeit konzentrierte sich auf die Analyse von CERK1 Ektodomänen-Shedding und dessen Funktion in der Entwicklung des *cerk1-4* Phänotyps. Die Abundanz der löslichen CERK1 Ektodomäne zwischen *Arabidopsis* Ökotypen variiert. Die Anwesenheit von Prolinen innerhalb des so genannten extrazellulären Stiels von CERK1 konnte positiv mit der Abundanz der Ektodomäne korreliert werden. CERK1 Varianten denen spezifische Proline fehlten zeigten reduzierte Ektodomänen Abundanz, konnten die Entwicklung des *cerk1-4* Phänotyps jedoch nicht unterdrücken. Punktmutationen möglicher Protease-Erkennungsmotive oder Längenvariationen des extrazellulären Stiels konnten das Ektodomänen-Shedding nicht supprimieren. In ähnlicher Weise hatten der Austausch der CERK1 Transmembran-Domäne und des extrazellulären Stiels mit korrespondierenden Regionen des Flagellin-Rezeptors FLS2 nur geringe Auswirkungen auf das Ektodomänen-Shedding von CERK1. Bei der massenspektrometrischen Analyse von Zellkulturen und apoplastischen Waschflüssigkeiten konnten Peptide identifiziert werden, die mit der extrazellulären Domäne zahlreicher Rezeptor-ähnlicher Kinasen korrespondierten. Die Peptide stammen wahrscheinlich von Ektodänen, die proteolytisch in den Apoplasten entlassen wurden. Diese Ergebnisse deuten an, dass Ektodomänen-Shedding eine verbreitete post-translational Modifikation in Pflanzen sein könnte.

Der zweite Teil der Arbeit konzentrierte sich auf die Identifizierung von Signalübertragungskomponenten, die für die Entwicklung des *cerk1-4* Phänotyps erforderlich sind. Eine neue Mutante, die den *cerk1-4* Phänotypen vollständig unterdrückt wurde aus einem genetischen Screen isoliert. Die zugrunde liegende Mutation wurde in dem extra großen G-Protein 2 (XLG2) lokalisiert, das vor kurzem als G-Protein α -Untereinheit vorgeschlagen wurde. In der Suppressor-Mutante wurde eine hoch konservierte Glutaminsäure durch Lysin in dem N-terminalen Teil von XLG2 ersetzt.

Komplementationsstudien zeigten, dass XLG2 Fusionen mit einem N-terminalen Fluoreszenz Protein-Tag funktionell sind, wohingegen C-terminale Fusionen es nicht sind. Konfokale Mikroskopie von stabil mit Venus-XLG2 transformierten *Arabidopsis* Pflanzen zeigten Lokalisierung an der Zellperipherie. Eine Subpopulation von Venus-XLG2 akkumuliert im Zellkern auf diverse Reize wie Wasser und PAMP Infiltration, Verletzung oder Pathogenbefall. Für XLG2 wurde vor kurzem die physische Interaktion mit kanonischen heterotrimeren G-Protein- $\beta\gamma$ Dimeren nachgewiesen. Auch β und γ G-Proteinuntereinheiten wurden als erforderlich für die vollständige Entwicklung des *cerk1-4* Phänotyps gezeigt. Interessanterweise war in der G-Protein β Mutante *agb1* eine Subpopulation von Venus-XLG2 bereits in unbehandelten Zellen im Zellkern lokalisiert. Diese Ergebnisse legen nahe, dass die subzelluläre Lokalisierung von XLG2 durch Wechselwirkung mit G-Protein $\beta\gamma$ -Untereinheiten moduliert wird, was wiederum seine Wirkung auf nachgeschaltete Ziele betrifft.

ABSTRACT	I
ZUSAMMENFASSUNG	III
TABLE OF ABBREVIATIONS	XI
1. INTRODUCTION	1
1.1 The plant innate immune system	1
1.1.1 Pattern recognition receptors perceive conserved microbial structures	3
1.1.1.1 Peptide ligands are perceived by LRR-proteins	4
1.1.1.2 LysM-proteins mediate perception of GlcNAc-containing oligosaccharides	5
1.1.1.2.1 Chitin perception	5
1.1.1.2.2 Peptidoglycan perception	8
1.1.2 Heterotrimeric G-proteins act as molecular switches	9
1.1.2.1 The role of heterotrimeric G-proteins in plant immunity and cell death	11
1.1.2.2 <i>Arabidopsis</i> Extra-large G-Proteins (XLGs) are alternative G α subunits	12
1.2 Ectodomain shedding and related proteolytic processes in metazoans	16
1.2.1 Well studied examples of ectodomain shedding in metazoans	17
1.2.2 Ectodomain shedding of metazoan receptor kinases and their ligands	20
1.2.3 Ectodomain shedding of plant receptor-like kinases	22
2. MATERIALS AND METHODS	26
2.1 Materials	26
2.1.1 Plant materials	26
2.1.1.1 <i>Arabidopsis thaliana</i>	26
2.1.1.1 <i>Nicotiana benthamiana</i>	29
2.1.2 Pathogens	29
2.1.2.1 Fungal pathogens	29
2.1.2.1.1 Powdery mildews	29
2.1.3 Bacterial strains used for cloning and transformation	29
2.1.3.1 <i>Escherichia coli</i>	29
2.1.3.2 <i>Agrobacterium tumefaciens</i>	29
2.1.4 Yeast strains used for cloning and transformation	29
2.1.5 Vectors used in this study	30

2.1.6	Oligonucleotides	32
2.1.7	Enzymes	36
2.1.7.1	Restriction endonucleases	36
2.1.7.2	Nucleic acid modifying enzymes	36
2.1.8	Chemicals	36
2.1.8.1	Antibiotics.....	36
2.1.8.2	Media	37
2.1.8.3	Buffers and solutions.....	38
2.1.8.4	Antibodies	41
2.2	Methods	42
2.2.1	Plant methods	42
2.2.1.1	Plant cultivation	42
2.2.1.2	Crossing of <i>Arabidopsis thaliana</i> plants.....	43
2.2.1.3	Stable transformation of <i>Arabidopsis thaliana</i> (floral dip).....	43
2.2.1.4	Transient transformation of <i>Nicotiana benthamiana</i>	43
2.2.1.5	Selection of transgenic <i>Arabidopsis</i> plants on soil.....	44
2.2.1.6	In-vitro selection of transgenic <i>Arabidopsis</i> plants.....	44
2.2.1.7	Chitin treatment of <i>Arabidopsis</i> plants	44
2.2.1.8	Cultivation and inoculation of <i>Blumeria graminis</i> f.sp. <i>hordei</i>	44
2.2.2	Biochemical methods	45
2.2.2.1	Protein extraction	45
2.2.2.1.1	Standard preparation of total protein extracts.....	45
2.2.2.1.2	Preparation of total protein extracts with SDS	45
2.2.2.2	Chitin pull-down.....	46
2.2.2.3	Microsomal preparation.....	46
2.2.2.4	Determination of protein concentration by the Bradford method	47
2.2.2.5	SDS-polyacrylamide gel electrophoresis (SDS-PAGE).....	47
2.2.2.6	Immunoblotting.....	47
2.2.2.7	Coomassie staining of PVDF membranes.....	48
2.2.2.8	Mass spectrometry analysis	49
2.2.3	Molecular biology methods.....	50
2.2.3.1	Preparation of genomic DNA from <i>Arabidopsis</i> leaves	50
2.2.3.2	Preparation of total RNA from <i>Arabidopsis</i> leaves.....	51
2.2.3.3	Plasmid preparation from <i>E.coli</i>	51
2.2.3.4	Plasmid preparation from <i>S. cerevisiae</i>	51
2.2.3.5	Synthesis of cDNA	52
2.2.3.6	Polymerase chain reaction (PCR)	52
2.2.3.7	Semi-quantitative reverse transcription-polymerase chain reaction (RT-PCR).....	53
2.2.3.8	Agarose gel electrophoresis.....	53
2.2.3.9	DNA purification from agarose gels	53
2.2.3.10	Measurement of DNA and RNA concentration	53
2.2.3.11	Restriction endonuclease digestion of DNA.....	54
2.2.3.12	Ligation of DNA fragments	54
2.2.3.13	Cloning by homologous recombination in <i>S. cerevisiae</i>	54
2.2.3.14	DNA sequencing and analysis.....	55

2.2.3.15	Preparation of chemically competent <i>E.coli</i> cells	55
2.2.3.16	Transformation of chemically competent <i>E.coli</i> cells	55
2.2.3.17	Preparation of electro-competent <i>A. tumefaciens</i> cells	56
2.2.3.18	Transformation of electro-competent <i>A. tumefaciens</i> cells	56
2.2.3.19	Preparation of chemically competent <i>S. cerevisiae</i> cells	56
2.2.3.20	Transformation of chemically competent <i>S. cerevisiae</i> cells	57
2.2.4	Confocal laser scanning microscopy (CLSM)	57
3.	RESULTS	58
3.1	Analysis of CERK1 ectodomain shedding.....	59
3.1.1	Investigation of CERK1 ectodomain shedding in <i>Arabidopsis thaliana</i> accessions	59
3.1.2	Mutational analysis of potential CERK1 protease cleavage motifs	62
3.1.3	The <i>cvg1</i> mutation does not suppress the <i>cerk1-4</i> phenotype.....	66
3.1.4	Variation of the CERK1 extracellular stalk length	71
3.1.5	CERK1-FLS2 domain swap experiments	73
3.1.6	CERK1 and FLS2 extracellular stalk harbor a KS motif	76
3.1.7	The extracellular domains of many receptor-like kinases can be found in supernatants of cell cultures.....	78
3.1.8	CERK1 ectodomain shedding is not altered in sphingolipid mutants	84
3.2	Extra-Large G-protein 2 (XLG2) plays a key role in <i>cerk1-4</i> cell death execution	85
3.2.2	Characterization of <i>cerk1-4</i> suppressor mutants	86
3.2.3	A single amino acid exchange in XLG2 (E293K) suppresses the <i>cerk1-4</i> phenotype	89
3.2.4	Localization studies with XLG2-GFP fusion protein	93
3.2.4.1	XLG2-GFP and <i>xlg2</i> -E293K-GFP are located to the nucleus and cell periphery in <i>N. benthamiana</i>	93
3.2.4.2	XLG2-GFP localizes to the cell periphery in unchallenged <i>Arabidopsis</i> plants and accumulates in the nucleus upon stress ...	94
3.2.4.3	C-terminal XLG2-GFP fusions are not functional.....	96
3.2.5	Localization studies with Venus-XLG2	97
3.2.5.1	Venus-XLG2 localizes to the nucleus, cytoplasm and plasma membrane in <i>Nicotiana benthamiana</i>	97
3.2.5.2	N-terminal XLG2 fusions are functional and restore the <i>cerk1-4</i> phenotype in <i>nole1-1</i> plants	99
3.2.5.3	Venus-XLG2 localises to the cell periphery in unchallenged <i>Arabidopsis</i> plants and accumulates in the nucleus upon stress	100
3.2.5.4	XLG2 is localized to the nucleus in <i>Bgh</i> attacked and surrounding cells	108

4. DISCUSSION	110
4.1 Analysis of CERK1 ectodomain shedding.....	110
4.1.1 Prolines within the extracellular stalk of CERK1 modulate the abundance of the CERK1 ectodomain fragment.....	110
4.1.2 Reduced abundance of the CERK1 ectodomain cannot suppress the <i>cerk1-4</i> phenotype	112
4.1.3 CERK1 ectodomain shedding cannot be suppressed by mutating potential protease cleavage motifs	113
4.1.4 Reduction of extracellular stalk length cannot suppress CERK1 ectodomain shedding.....	115
4.1.5 The CERK1 extracellular stalk and transmembrane domain are not critical for ectodomain shedding.....	115
4.1.6 The extracellular domain of many RLKs is proteolytically processed.....	117
4.1.7 Possible function of CERK1 ectodomain shedding.....	119
4.1.8 Conclusion	120
4.1.9 Outlook	120
4.2 Analysis of <i>nole1-2</i> and XLG2 subcellular localization	121
4.2.1 XLG2 is a key regulator of <i>cerk1-4</i> cell death execution.....	121
4.2.2 XLG2 localization is stimulus dependent.....	122
4.2.3 XLG2 localization in <i>Bgh</i> -infected <i>cerk1-4</i> plants does not differ from wild type plants	125
4.2.4 Conclusion	125
4.2.5 Outlook	126
5. REFERENCES	128
6. SUPPLEMENTAL MATERIAL.....	149
LIST OF TABLES.....	157
LIST OF FIGURES	158
LIST OF SUPPLEMENTAL TABLES	161
LIST OF SUPPLEMENTAL FIGURES	162
DANKSAGUNG.....	163
CURRICULUM VITAE.....	165

Table of abbreviations

::	fused to (gene fusions)	Eph	erythropoietin-producing
7TM	seven transmembrane		hepatoma
ADAM	A DESINTEGRIN AND METALLOPROTEINASE	ES	extracellular stalk
AGB1	<i>ARABIDOPSIS</i> G-PROTEIN BETA-SUBUNIT 1	et al.	Et alii; and others
AGG	<i>ARABIDOPSIS</i> G-PROTEIN GAMMA-SUBUNIT	ETI	effector triggered immunity
AP	Alkaline phosphatase	EtOH	ethanol
APP	AMYLOID PRECURSOR PROTEIN	ETS	effector triggered susceptibility
<i>A. thaliana</i>	<i>Arabidopsis thaliana</i>	FLS2	FLAGELLIN SENSING 2
<i>A. tumefaciens</i>	<i>Agrobacterium tumefaciens</i>	g	gram
APS	ammoniumpersulfat	xg	times gravity
AWF	apoplastic wash fluid	GAP	GTPase activating protein
BAK1	BRASSINOSTEROID INSENSITIVE1-ASSOCIATED RECEPTOR KINASE1	gDNA	genomic DNA
<i>Bgh</i>	<i>Blumeria graminis</i> forma specialis <i>hordei</i>	GDP	<i>guanosine</i> diphosphate
BIK1	BOTRYTIS-INDUCED KINASE1	GEF	guanine nucleotide exchange factor
BKK1	BAK1-LIKE 1	GTP	<i>guanosine</i> triphosphate
BRI1	BRASSINOSTEROID INSENSITIVE1	GFP	green fluorescent protein
bp	base pair(s)	GPA1	<i>ARABIDOPSIS</i> G-PROTEIN ALPHA SUBUNIT 1
°C	degree Celsius	GPI	glycosylphosphatidylinositol
C	carboxy terminal	GPCR	G-PROTEIN COUPLED RECEPTOR
cDNA	complementary DNA	h	hour(s)
CEBiP	CHITIN ELICITOR-BINDING PROTEIN	HB-EGF	heparin-binding EGF-like growth factor
CERK1	CHITIN ELICITOR RECEPTOR KINASE1	iCLIP	intramembrane-cleaving protease
CLSM	confocal laser scanning microscopy	ICD	Intracellular domain
CPD	chitin pull-down	kb	kilobase(s)
d	days	kDa	kiloDalton(s)
dCAPS	derived cleaved amplified polymorphic sequence	l	litre
ddH2O	double deionised water	LD	long-day
DAMP	damage-associated molecular pattern	LRR	leucine-rich repeats
DMSO	dimethylsulfoxide	LysM	lysine motif
DNA	deoxyribonucleic acid	M	molar (mol/L)
dNTP	deoxynucleosidetriphosphate	MAMP	microbe-associated molecular pattern
DSL	Delta/Serrate/LAG-2	MLD	malectin-like domain
DTT	dithiothreitol	MMP	MATRIX
<i>E. coli</i>	<i>Escherichia coli</i>	μ	micro
EDTA	ethylenediaminetetraacetic acid	min	minute(s)
EFR	EF-TU RECEPTOR	mM	millimolar
EF-Tu	ELONGATION FACTOR THERMO UNSTABLE	N	amino-terminal
EGF	EPIDERMAL GROWTH FACTOR	NADPH	nicotinamide adenine dinucleotide phosphate
EGFR	EPIDERMAL GROWTH FACTOR RECEPTOR	<i>N. benthamiana</i>	<i>Nicotiana benthamiana</i>
		NES	nuclear export signal
		NLS	nuclear localization signal
		PAMP	pathogen-associated molecular pattern
		PCR	polymerase chain reaction
		PAGE	polyacrylamide gel- electrophoresis
		PDF1.2	PLANT DEFENSIN 1.2

PDGF	platelet-derived growth factor	XLG	EXTRA-LARGE
PGN	peptidoglycan		G-PROTEIN
pH	negative decimal logarithm of the H ⁺ concentration		
PM	plasma membrane		
PR1	PATHOGENESIS RELATED 1		
PRR	pattern recognition receptor		
PTI	PAMP-triggered immunity		
PVDF	polyvinylidene fluoride		
R	resistance		
RGS	REGULATOR OF G-PROTEIN SIGNALING		
RHOBD	RESPIRATORY BURST OXIDASE-D		
RIP	regulated intramembrane proteolysis		
RLCK	receptor-like cytoplasmic kinase		
RLK	receptor-like kinase		
RLP	receptor-like protein		
RNA	ribonucleic acid		
ROS	reactive oxygen species		
rpm	rounds per minute		
RSK	receptor serine kinase		
RT	room temperature		
RTK	receptor tyrosine kinase		
RT-PCR	reverse transcription-polymerase chain reaction		
s	second (s)		
SA	salicylic acid		
<i>S. cerevisiae</i>	<i>Saccharomyces cerevisiae</i>		
SD	short-day		
SDS	sodium dodecyl sulphate		
sec	second(s)		
SNP	single nucleotide polymorphism		
SOBIR	SUPPRESSOR OF BIR1-1		
SP	signal peptide		
SYMRK	SYMBIOSIS RECEPTOR-LIKE KINASE		
TBS	Tris buffered saline		
TβRI	transforming growth factor beta receptor type I		
T-DNA	transfer DNA		
TEMED	N,N,N',N'-tetramethylethane-1,2-diamine		
TE	total extract		
TGF	transforming growth factor		
TM	transmembrane domain		
TMK	TRANSMEMBRANE KINASE		
Tris	Tris-(hydroxymethyl)-aminomethane		
TTSS	type III secretion system		
U	unit		
v/v	volume per volume		
WT	wild type		
w/v	weight per volume		
XA21	XANTHOMONAS RESISTANCE 21		

1. Introduction

Plants are in a constant battle against a variety of abiotic and biotic stresses. As sessile organisms, they cannot simply evade unfavorable conditions, but have to respond to the continuously changing environmental cues they are confronted with. In contrast to animals, plants do not possess mobile immune cells which are activated upon pathogen attack. Instead, they have developed a multi-layered innate immune system. Every plant cell is equipped with a set of receptor and defense proteins to detect pathogens and initiate defense responses (Dodds & Rathjen, 2010). This system is highly effective with disease being the exception and not the rule (Jones & Dangl, 2006).

The first layer of defense responses is initiated upon perception of conserved pathogen-associated molecular patterns (PAMPs) by pattern recognition receptors (PRRs) on the cell surface (Zipfel, 2014). PAMPs are molecules that are conserved among a whole class of pathogens and often derived from structural or motility components, like the cell wall or flagella (Newman *et al.*, 2013). The activation of PRRs leads to the induction of a wide range of signaling and defense responses which result in PAMP-triggered immunity (PTI). These defense responses together with preformed barriers are sufficient to stop the progression of a broad spectrum of non-adapted pathogens. This process is also known as non-host resistance (Nürnbergger & Lipka, 2005). Adapted pathogens developed specialized effector proteins which are able to suppress PTI leading to effector triggered susceptibility (ETS) (Jones & Dangl, 2006). Plants in turn developed mechanisms to recognize these effectors, thereby mounting a second layer of defense, which is called effector triggered immunity (ETI) (Jones & Dangl, 2006).

1.1 The plant innate immune system

Once a pathogen arrives on the plant surface, it is confronted with a variety of preformed obstacles, like the cell wall, anti-microbial substances and a waxy cuticle (Nürnbergger & Lipka, 2005). Pathogens which are able to overcome these barriers are then challenged by an efficient two-layered immune system (Dodds & Rathjen, 2010). Perception of microbial signatures on the cell surface by pattern recognition receptors (PRRs) activates the first layer called PAMP-triggered immunity (PTI, Figure 1, step 1). Microbial signatures, also referred to as pathogen associated molecular pattern (PAMPs) are molecules which are highly conserved among a class of pathogens and are absent from the host. To date, many PAMPs

of different classes of pathogens and their cognate receptors have been identified. Well studied examples in *Arabidopsis thaliana* include the perception of the bacterial PAMPs flagellin and elongation factor thermo unstable (EF-Tu) by the PRRs FLAGELLIN SENSING 2 (FLS2) and EF-Tu receptor (EFR), respectively (Gómez-Gómez & Boller, 2000; Zipfel *et al.*, 2006). The perception of chitin derived from fungal cell walls by the CHITIN ELICITOR RECEPTOR KINASE 1 (CERK1) is another well established example of PAMP perception (Miya *et al.*, 2007). Plants also possess PRRs to perceive self-molecules, which are released from damaged plant structures (Boller & Felix, 2009). These molecules are referred to as

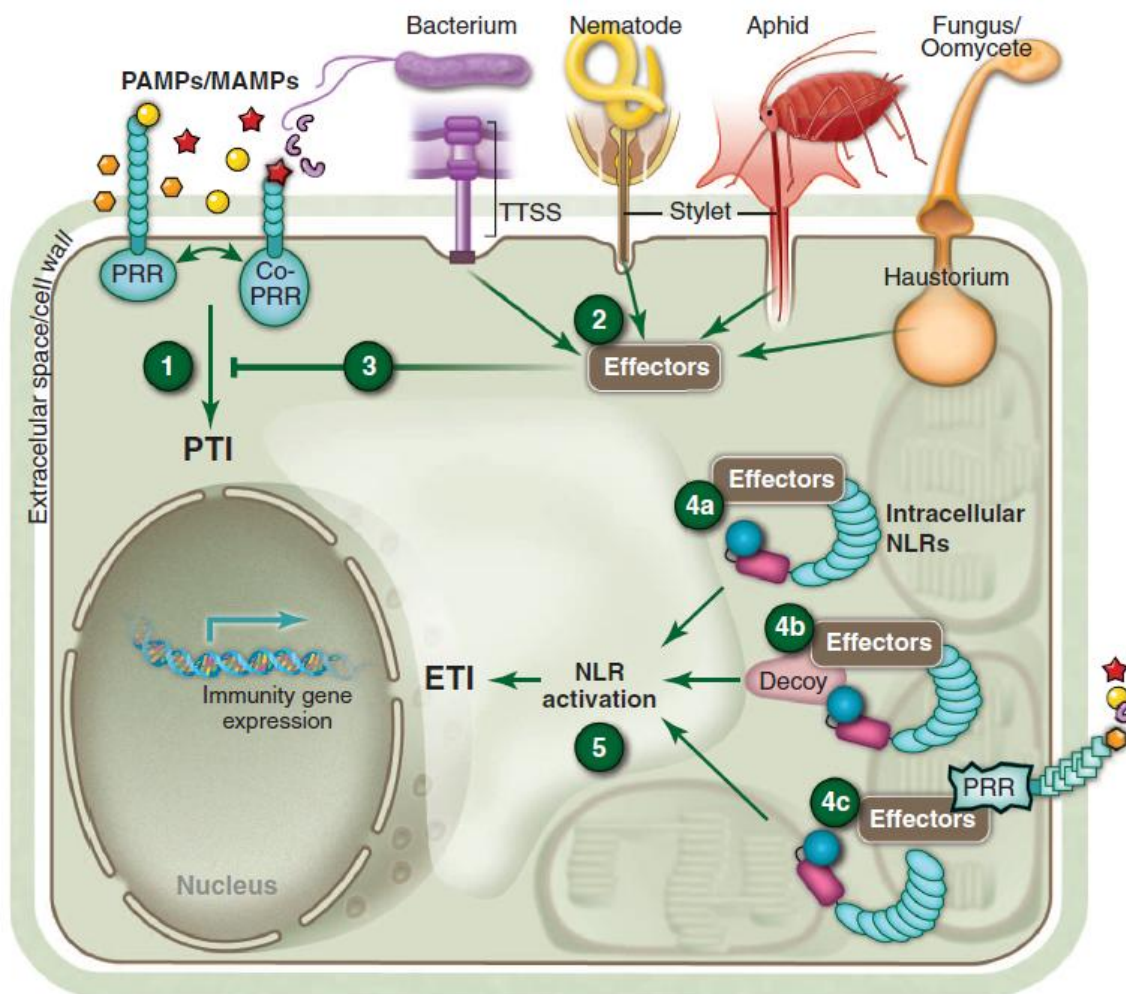


Figure 1. The plant immune system. Pathogen associated molecular patterns (PAMPs) are perceived by pattern recognition receptors at the cell surface. Signaling initiated by pattern recognition receptors leads to the onset of PAMP-triggered immunity (PTI) (1). Pathogens developed effector molecules (2) of which some are delivered into the cell to block PTI responses (3), leading to effector triggered susceptibility (ETS). Plants developed Resistance proteins (R-proteins) to cope with pathogen effector molecules. R-proteins either detect effectors by direct interaction with the effector molecules (4a) or sense the activity of effectors on other host proteins. This can be achieved by monitoring the integrity of a decoy protein, which resembles an effector target (4b) or by guarding the integrity of an effector target protein (4c). Perception of effector activity by an R-protein leads to the induction of effector triggered immunity (ETI) (5). Image from Dangl *et al.* (2013).

damage-associated molecular patterns (DAMPs). Characteristic PAMP (and DAMP) responses involve generation of reactive oxygen species (ROS), activation of mitogen activated protein (MAP) kinase cascades and induction of defense related genes (Dodds & Rathjen, 2010). The mechanisms of PTI are sufficient to establish resistance against most pathogens and, together with pre-formed physical barriers and toxins, are the basis of non-host resistance (Nürnberg & Lipka, 2005).

In order to establish a compatible interaction with the host plant, adapted pathogens developed effector molecules to prevent or inhibit PTI initiation (Jones & Dangl, 2006). Fungal pathogens and oomycetes secrete effector proteins into the apoplast (not shown) or deliver them into the host cell by a not yet identified mechanism (Lo Presti *et al.*, 2015), while bacterial pathogens use a type III secretion system (TTSS) to transport effector proteins into the host cell (Figure 1, step 2) (Hueck, 1998; Lo Presti *et al.*, 2015). Effector proteins can suppress PTI responses or prevent recognition of the pathogen by the host, resulting in effector-triggered susceptibility (ETS) (Figure 1, step 3). To detect effector protein activity and halt further pathogen ingress, plants have developed intracellular Resistance (R) proteins. Most R-proteins are NB-LRR proteins and contain a nucleotide-binding site (NB) and a leucine-rich repeat (LRR) domain. They may recognize the activity of intracellular effectors either directly or indirectly (Figure 1, step 4) (Spoel & Dong, 2012). Direct recognition occurs via binding of an effector to an R-protein, but is a rather uncommon mechanism. Indirect recognition is explained by the guard model, where R-proteins monitor the integrity of effector target proteins (van der Hoorn & Kamoun, 2008). Detection of target protein modifications, like phosphorylation or degradation, leads to the activation of the R-protein, resulting in effector triggered immunity (ETI) within the host plant (Axtell & Staskawicz, 2003; Liu *et al.*, 2011) (Figure 1, step 5). ETI is a strong defense response which typically results in a hypersensitive response leading to cell death of the infected tissue (Spoel & Dong, 2012).

1.1.1 Pattern recognition receptors perceive conserved microbial structures

Recognition of conserved microbial structures (PAMPs) is mediated by PRRs and takes place at the cell surface. PRRs are membrane localized proteins and contain extracellular ligand-binding domains. There are two kinds of PRRs: Receptor-like kinases (RLKs) contain a transmembrane domain and an intracellular kinase domain (Trdá *et al.*, 2015). Receptor-like proteins (RLPs) lack an intracellular kinase domain and are often linked to the extracellular leaflet of the plasma membrane via glycosylphosphatidylinositol (GPI) anchors (Zipfel, 2014).

Perception of peptide-based PAMPs like bacterial flagellin or EF-Tu is mediated by PRRs containing leucine-rich repeats (LRRs) within their extracellular domain (Chinchilla *et al.*, 2006; Zipfel *et al.*, 2006). Carbohydrate PAMPs that contain N-acetylglucosamine moieties, such as fungal chitin or bacterial peptidoglycan, are perceived by lysin motif (LysM) containing receptors (Kaku *et al.*, 2006; Kaku & Shibuya, 2011; Miya *et al.*, 2007; Willmann *et al.*, 2011).

Plant PRRs are often organized in multiprotein complexes, which contain components in addition to the PRR, such as co-receptors and receptor-like cytoplasmic kinases (RLCKs) to ensure proper and specific signaling (Macho & Zipfel, 2014).

1.1.1.1 Peptide ligands are perceived by LRR-proteins

LRR receptor-like kinases (LRR-RLKs) are the largest group of RLKs in *Arabidopsis* (Shiu & Bleecker, 2001). Several of them have been identified as receptors of peptide ligands involved in growth, development or defence. One of the most prominent members of this group is FLAGELLIN-SENSITIVE 2 (FLS2) which was the first PRR identified in *Arabidopsis* (Chinchilla *et al.*, 2006; Gómez-Gómez & Boller, 2000; Zipfel *et al.*, 2004). FLS2 harbors 28 extracellular leucine-rich repeats (LRRs) which can bind a conserved 22 amino-acid epitope (flg22) of flagellin, the building block of bacterial flagella (Chinchilla *et al.*, 2006). Flagellin perception by FLS2 is an essential part of defense against bacterial pathogens, as *fls2* mutants are severely impaired in resistance against avirulent and virulent *Pseudomonas syringae* pv. *tomato* strains (Zipfel *et al.*, 2004). Orthologs of *AtFLS2* can be found in genomes of many higher plants, such as tomato (Robatzek *et al.*, 2007), *Nicotiana benthamiana* (Hann & Rathjen, 2007) and rice (Takai *et al.*, 2008).

Another well studied member of the group of LRR-RLKs is the *Arabidopsis* ELONGATION FACTOR-TU RECEPTOR (EFR). The extracellular domain of EFR containing 21 LRR motifs binds an 18 amino acid N-terminal peptide (elf18) of the bacterial elongation factor Tu (EF-Tu) (Kunze *et al.*, 2004; Zipfel *et al.*, 2006). Similar to FLS2, EFR is a crucial part of the defense system against bacterial pathogens, as *efr* plants are more susceptible to *Agrobacterium* transformation (Zipfel *et al.*, 2006). Upon ligand binding, both FLS2 and EFR1 form a complex with the BRI1-ASSOCIATED RECEPTOR KINASE 1 (BAK1) which was shown to act as a co-receptor for a variety of LRR-RLKs and LRR-RLPs (Chinchilla *et al.*, 2007; Heese *et al.*, 2007; Liebrand *et al.*, 2014; Roux *et al.*, 2011; Schulze *et al.*, 2010). BAK1, also known as SOMATIC EMBRYOGENIC RECEPTOR KINASE 3 (SERK3), is a LRR-RLK and was discovered as a positive regulator of Brassinosteroid signaling (Li *et al.*, 2002). Heterodimerization of FLS2 or EFR with BAK1 followed by transphosphorylation

events is a prerequisite for proper defense signaling and *bak1* mutant plants exhibit severely reduced defense responses to flg22 and elf18 treatment (Chinchilla *et al.*, 2007; Roux *et al.*, 2011; Schwessinger *et al.*, 2011). FLS2 and EFR do not only associate with BAK1, but also with receptor-like cytoplasmic kinases (RLCKs). RLCKs possess kinase domains similar to RLKs, but lack extracellular and transmembrane domains (Shiu & Bleecker, 2001). Upon flg22 or elf18 perception, the RLCK BOTRYTIS-INDUCED KINASE1 (BIK1) is phosphorylated by BAK1 and subsequently phosphorylates BAK1 and FLS2 (Lu *et al.*, 2010). BIK1 also mediates flg22- and elf18- triggered ROS production by phosphorylating the NADPH oxidase RHOBD (Kadota *et al.*, 2014; Lu *et al.*, 2010; Zhang *et al.*, 2010). Apart from PAMP perception and signaling, BAK1 and the closely related RLK BKK1 were also shown to be negative regulators of cell death. Upon inoculation with different pathogens, *bak1* plants exhibit enhanced cell death (Kemmerling *et al.*, 2007). Double mutant *bak1 bkk1* plants show an even more severe phenotype and do not survive seedling stage (He *et al.*, 2007).

1.1.1.2 LysM-proteins mediate perception of GlcNAc-containing oligosaccharides

Lysin motif (LysM) containing proteins can be found in almost all living organisms (Buist *et al.*, 2008). The lysin motif was discovered in bacteriophage lysozymes that degrade bacterial cell walls during the lytic cycle (Garvey *et al.*, 1986). In plants, LysM domain containing receptor-like kinases (LysM-RLKs) and receptor-like proteins (LysM-RLPs) mediate the perception of N-acetyl-D-glucosamine (GlcNAc) containing carbohydrate molecules such as chitin and peptidoglycan, as well as Nod- and Myc-factors. They play important roles in establishment of symbiosis and defense (Antolín-Llovera *et al.*, 2012). The following part will focus on the roles of LysM-proteins in defense responses.

1.1.1.2.1 Chitin perception

Chitin is one of the main constituents of the fungal cell wall and the second most abundant naturally occurring biopolymer after cellulose. It is a polymer consisting of β -1-4 linked monomers of N-Acetyl-D-glucosamine (GlcNAc) (Muzzarelli, 1977). Plant-derived chitinases are able to degrade the fungal cell wall, thereby releasing chitin fragments (chito-oligosaccharides) which can serve as a PAMP and be perceived by plants (Eckardt, 2008). Chitin perception and signaling has been the subject of extensive research in rice and *Arabidopsis* (Gust *et al.*, 2012). In rice, two LysM motif containing proteins have been found

to be indispensable for chitin signaling (Kaku *et al.*, 2006; Shimizu *et al.*, 2010). The LysM-RLP CHITIN ELICITOR-BINDING PROTEIN (OsCEBiP) consists of three extracellular LysM domains, a transmembrane domain and was the first identified PRR to have chitin binding ability (Hayafune *et al.*, 2014; Kaku *et al.*, 2006). As OsCEBiP lacks an intracellular domain, it requires interaction with additional proteins for proper signal transduction. The LysM-RLK CHITIN ELICITATOR RECEPTOR-LIKE KINASE (OsCERK1) was found to form a heteromeric complex with OsCEBiP upon chitin perception (Shimizu *et al.*, 2010). As OsCERK1 has no chitin binding ability, it seems to be functionally important for signal transduction via its intracellular kinase domain (Shinya *et al.*, 2012). Knockout analyses confirmed that both, OsCEBiP and OsCERK1 are essential factors of rice chitin signaling and pathogen resistance. Chitin-induced generation of reactive oxygen species and transcriptional reprogramming are markedly impaired in *oscebip* and completely abolished in *oscerk1* mutants. Furthermore, both mutants showed reduced resistance against the rice blast fungus *Magnaporthe oryzae* (Kouzai *et al.*, 2014b; Kouzai *et al.*, 2014a).

The ectodomains of OsCEBiP and OsCERK1 are believed to form a sandwich-like tetrameric receptor complex for chitin perception and signaling (Hayafune *et al.*, 2014; Shimizu *et al.*, 2010). In this model, two OsCEBiP proteins bind opposing N-acetyl moieties of a chitin oligosaccharide, forming a homodimer, thereby inducing the dimerization of closely associated OsCERK1 (Figure 2a) (Hayafune *et al.*, 2014).

In addition to OsCEBiP, the two LysM-RLPs LYP4 and LYP6 were found to contribute to chitin perception in rice (Liu *et al.*, 2012a). They were reported to heterodimerize with OsCERK1 upon chitin binding and induce defense responses (Ao *et al.*, 2014). In agreement with that, knock-down of either LYP4 or LYP6 resulted in impaired chitin-induced defense gene expression and ROS production and enhanced susceptibility against bacterial and fungal pathogens (Liu *et al.*, 2012a). Interestingly, LYM2, the *Arabidopsis* homolog of OsCEBiP, has also chitin binding ability, but is not involved in canonical chitin signaling (Shinya *et al.*, 2012; Wan *et al.*, 2012). However, it was shown to regulate changes in plasmodesmata flux upon chitin treatment (Faulkner *et al.*, 2013; Shinya *et al.*, 2012; Wan *et al.*, 2012).

In *Arabidopsis*, CHITIN ELICITOR RECEPTOR-LIKE KINASE (AtCERK1/AtLysM-RLK1/AtLYK1), an ortholog of OsCERK1, was identified as an essential component of chitin signaling (Kaku *et al.*, 2006; Miya *et al.*, 2007). CERK1 T-DNA knockout mutants such as *cerk1-2*, are completely insensitive to chitin (Miya *et al.*, 2007; Wan *et al.*, 2008). Upon chitin treatment, *cerk1-2* plants do not generate reactive oxygen species, activate MAP kinase cascades or show induction of chitin responsive genes. In contrast to OsCERK1, direct chitin binding activity was shown for CERK1, pointing to possible differences between the chitin

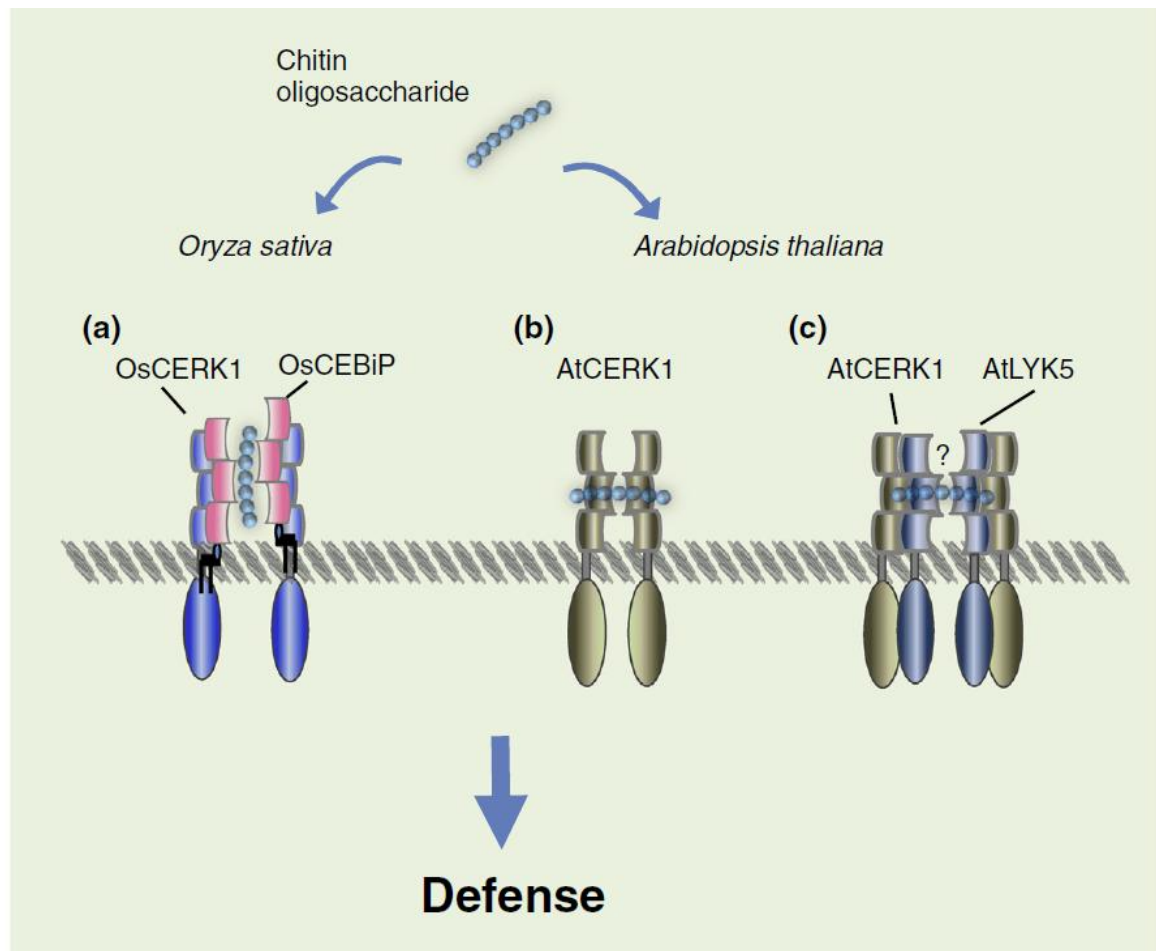


Figure 2. Chitin perception in plants. a) Chitin perception in rice. Homodimers of OsCEBiP bind chitin and recruit OsCERK1 to form a heteromeric complex. b) Model of chitin perception in *Arabidopsis* through AtCERK1 only. Upon chitin binding, AtCERK1 homodimerizes and is thereby activated. c) Model of chitin perception through a receptor complex. Chitin binding of AtLYK5 homodimers recruits AtCERK1 to form an active receptor complex. Image from Shinya *et al.* (2015).

perception systems of *Arabidopsis* and rice (Iizasa *et al.*, 2010; Liu *et al.*, 2012b; Petutschnig *et al.*, 2010). Chitin binding of CERK1 is mediated via its extracellular domain and transmitted into the cell via its intracellular kinase domain. Similar to rice OsCEBiP (Hayafune *et al.*, 2014), CERK1 forms homodimers through binding of chitooligosaccharides (Figure 2b) (Hayafune *et al.*, 2014; Liu *et al.*, 2012b). Homodimerization is a crucial step in receptor activation and leads to phosphorylation events at the intracellular juxtamembrane and kinase domains (Liu *et al.*, 2012b; Petutschnig *et al.*, 2010). Chitin-induced CERK1 phosphorylation is required for downstream signaling and results in an electrophoretic mobility shift of CERK1, which can be detected in immunoblot experiments (Petutschnig *et al.*, 2010). CERK1 kinase activity is crucial for both receptor phosphorylation and defense processes, as kinase dead (*cerk1-LOF*) variants of CERK1 are unable to complement *cerk1-2* knockout mutants (Petutschnig *et al.*, 2010).

Arabidopsis contains four more LysM-RLKs in addition to CERK1. Of these, the LysM-RLK LYK4 was shown to play a minor role in chitin perception, as *lyk4* mutant plants show reduced expression of chitin responsive genes and a moderately reduced calcium influx after chitin treatment (Wan *et al.*, 2012). As LYK4 appears to be an inactive kinase, it might act as a co-receptor and depend on CERK1 for signal transduction. The LysM-RLK LYK5 was also shown to be involved in chitin signaling, as chitin treatment leads to CERK1 dependent LYK5 endocytosis and phosphorylation (Erwig *et al.*, unpublished). Furthermore, LYK5 was shown to be phosphorylated by CERK1 *in vivo* and *in vitro*. The current model for chitin perception in *Arabidopsis* considers CERK1 as an ‘all-in-one’ receptor, which is the main protein responsible for direct chitin binding, signal transduction and activation of downstream signaling responses (Iizasa *et al.*, 2010; Liu *et al.*, 2012b; Miya *et al.*, 2007; Petutschnig *et al.*, 2010; Wan *et al.*, 2012). Recent results however, call this model into question and propose the LysM-RLK LYK5 to be the main chitin receptor in *Arabidopsis* forming a complex with CERK1 (Figure 2c) (Cao *et al.*, 2014). This new model is based on results revealing a higher chitin binding affinity for LYK5 than CERK1 and complete chitin insensitivity for *lyk5-2* mutants. These results however, are contradictory to previous results, assigning a higher chitin binding affinity to CERK1 and wild type-like chitin signaling for *lyk5-1* mutants (Cao *et al.*, 2014; Liu *et al.*, 2012b; Wan *et al.*, 2012). Due to these contradicting results the contribution of different LysM-RLKs to chitin perception and signaling is not yet clear and it is still a matter of debate whether there is a “main” chitin receptor in *Arabidopsis*.

Similar to FLS2 and EFR, the receptor-like cytoplasmic kinase BIK1 was also shown to interact with CERK1 and to be involved in ROS generation after chitin treatment (Zhang *et al.*, 2010). The related RLCK PBL27 mediates downstream responses like MAP kinase activation and induction of defense related genes. The importance of PBL27 for pathogen resistance is further corroborated by enhanced susceptibility of *pbl27* mutant plants to bacterial and fungal pathogens (Shinya *et al.*, 2014). Furthermore, the RLCK CLR1 was shown to be phosphorylated by CERK1 *in vivo* and *in vitro* and to be involved in chitin induced ROS production, MAPK activation and induction of defense genes (Ziegler, 2015).

1.1.1.2.2 Peptidoglycan perception

The cell wall of gram-negative and gram-positive bacteria contains peptidoglycan (PGN), a polymer of N-acetyl-D-glucosamine (GlcNAc) and N-acetylmuramic acid (MurNAc) that is crosslinked with peptide chains (Lovering *et al.*, 2012). PGN represents a classical PAMP and PRRs involved in PGN perception have been described in plants (Gust, 2015). The LysM-RLPs OsLYP4 and OsLYP6, homologs of OsCEBIP, were shown to be critical

components for PGN perception in rice (Liu *et al.*, 2012a). Similar to the rice chitin receptor OsCEBIP, OsLYP4 and OsLYP6 lack an intracellular kinase domain and depend on OsCERK1 for signal transduction (Ao *et al.*, 2014). The importance of OsLYP4 and OsLYP6 in PGN signaling is supported by knockdown and overexpression analyses. Knockdown of OsLYP4 and OsLYP6 led to enhanced susceptibility to bacterial pathogens, while the overexpression of both proteins resulted in enhanced resistance (Liu *et al.*, 2012a).

The *Arabidopsis thaliana* genome harbors three LysM-RLPs (LYM1-3). While LYM2 binds chitin (Petutschnig *et al.*, 2010; Shinya *et al.*, 2012), LYM1 and LYM3 were shown to physically bind to PGN (Willmann *et al.*, 2011). *lym1* and *lym3* mutants showed enhanced susceptibility to bacterial pathogens and altered defense gene expression upon PGN treatment (Willmann *et al.*, 2011). Interestingly, *cerk1* mutant plants were similarly altered in PGN perception. As LYM1 and LYM3 lack an intracellular kinase domain, complex formation of LYM1, LYM3 and CERK1 for proper PGN signaling was proposed (Willmann *et al.*, 2011). CERK1 is a target of the bacterial effector AvrPtoB, which mediates its degradation (Gimenez-Ibanez *et al.*, 2009). This provides further evidence for a role of CERK1 in perception of PGN and possibly other bacterial PAMPs.

1.1.2 Heterotrimeric G-proteins act as molecular switches

In order to adapt to constantly changing environmental conditions, eukaryotic cells need to transduce extracellular stimuli into intracellular signals through receptor proteins. In animals, G-protein coupled receptors (GPCRs) are an important class of receptors. These seven-transmembrane (7TM) containing proteins harbor an extracellular ligand binding site and are in complex with heterotrimeric G-proteins at the intracellular site of the plasma membrane (Urano & Jones, 2014). Heterotrimeric G-proteins consist of a G α -subunit, which can bind and hydrolyze GTP, as well as a G β - and G γ - subunit which form an obligate dimer. In animals, GPCRs act as guanine nucleotide exchange factors (GEFs) after ligand binding and promote GDP dissociation and GTP binding on G α (Figure 3a). The activated G α -subunit dissociates from the G $\beta\gamma$ -dimer. G α -subunit and G $\beta\gamma$ -dimer can now act as independent signaling units and regulate the activity of downstream targets (Urano *et al.*, 2013). The GTPase activity of G α terminates signaling by hydrolyzing GTP to GDP. This leads to the re-association of G α with the G $\beta\gamma$ -dimer, thereby returning the complex to its assembled and inactive state (Ross & Wilkie, 2000). GTP hydrolysis can be promoted by a group of GTPase activating proteins (GAPs) termed regulators of G-protein signaling (RGSs). Animals possess large numbers of GPCRs. The human genome, for example, encodes for over 800 GPCRs (Jones & Assmann, 2004). In plants however, the

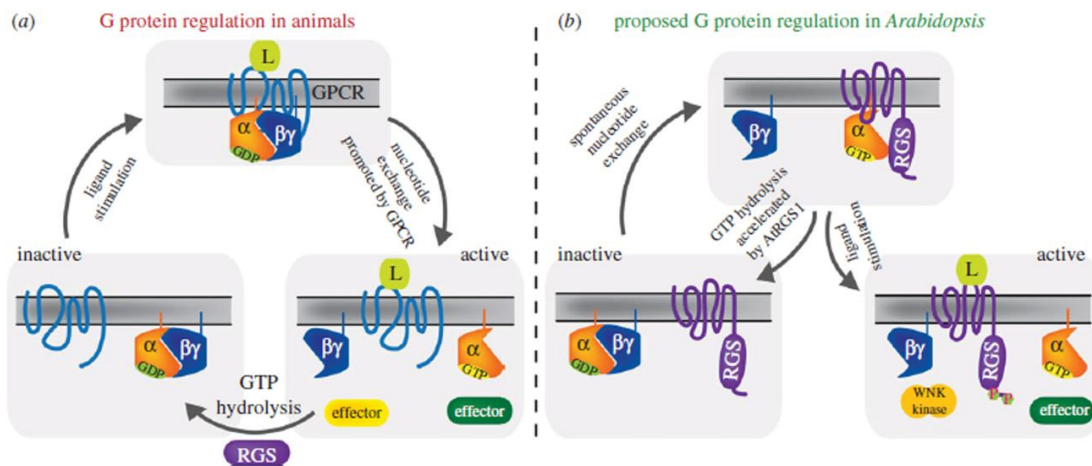


Figure 3. Cycle of heterotrimeric G-protein activation in animals and in *Arabidopsis*. a) G-protein activation in animals. Ligand binding leads to G-protein coupled receptor (GPCR) activation and nucleotide exchange at the α -subunit. The GTP-bound α -subunit dissociates from the $\beta\gamma$ -dimer, which can now independently interact with downstream targets (effectors). GTP hydrolysis at the α -subunit is promoted by regulators of G-protein signaling (RGS) leading to inactivation and reformation of the heterotrimeric complex. b) G-protein activation in *Arabidopsis*. Spontaneous release of GDP and binding of GTP leads to activation of the α -subunit. The low intrinsic GTPase activity of the α -subunit is enhanced by RGS, resulting in an inactive and assembled heterotrimeric complex. Ligand binding of RGS leads to its endocytosis, thereby preventing α inactivation. α and $\beta\gamma$ can now interact with downstream targets. Image from Urano *et al.* (2013).

situation is different. A number of proteins have been proposed as GPCRs, but whether GPCRs really exist in plants is still under debate (Urano *et al.*, 2013). *In vitro* analyses and structural studies suggest that the *Arabidopsis* α -subunit AtGPA1 does not need a GPCR for activation. It spontaneously releases GDP and binds GTP *in vitro* (Johnston *et al.*, 2007; Urano *et al.*, 2012a). The rate of GTP hydrolysis in AtGPA1 is slower than the rate of nucleotide exchange, resulting in a permanently GTP-bound state. This has led to a model of G-protein signaling in plants, where the G-proteins are active by default and regulated by deactivation through GAPs that enhance the intrinsic GTPase activity of α -subunits (Figure 3b). To date, only one GAP targeting AtGPA1 has been identified. AtRGS1 is a membrane localized protein with a 7TM and an RGS domain (Chen *et al.*, 2003) and has therefore been proposed to act as a hybrid G-protein coupled receptor GAP. AtRGS1 acts in sugar sensing and based on genetic evidence, glucose has been put forward as its ligand. AtRGS1-mediated GTP hydrolysis leads to the formation of the inactive $\alpha\beta\gamma$ heterotrimer (Figure 3b). Ligand binding of AtRGS1 triggers its phosphorylation and subsequent endocytosis, physically decoupling it from AtGPA1 (Urano *et al.*, 2012b). AtGPA1 and the $\beta\gamma$ -dimer are now able to relay signals to downstream targets (Figure 3b) (Urano *et al.*, 2013). The *Arabidopsis* genome encodes one α -subunit (GPA1), one β -subunit (AGB1) and three γ -subunits (AGG1-3) (Jones & Assmann, 2004; Thung *et al.*, 2012). AGG1 and AGG2 are

highly similar, while AGG3 is a much larger protein and shares little sequence homology with the other two G γ -subunits (Chakravorty *et al.*, 2011).

Knockout mutants of *Arabidopsis thaliana* heterotrimeric G-proteins have been subject of intensive research and have revealed many processes in which G-proteins play important roles including defense against fungal and bacterial pathogens, cell death, hormone signaling, oxidative stress, as well as seedling and root development (Chen *et al.*, 2006; Joo *et al.*, 2005; Liu *et al.*, 2013a; Nitta *et al.*, 2015; Trusov *et al.*, 2006).

Since *Arabidopsis* contains only one AtRGS1-like protein, it is not clear how heterotrimeric G-proteins are regulated in these pathways and how specificity is achieved. AtRGS1 might associate with RLKs, since AtRGS1 interacts with some RLKs in yeast (Klopffleisch *et al.*, 2011). RLK mediated phosphorylation of AtRGS1 might trigger endocytosis, thereby activating G-protein signaling (Urano *et al.*, 2013). However, cereals lack RGS1-like proteins, so alternative mechanisms for regulation of heterotrimeric G-proteins must be present in at least some plants (Urano *et al.*, 2012a).

1.1.2.1 The role of heterotrimeric G-proteins in plant immunity and cell death

Heterotrimeric G-proteins are involved in nearly all aspects of life. Research on plant G-proteins however, has mainly focused on their roles in immunity and functions for most G-proteins herein have been described (Liu *et al.*, 2013a; Llorente *et al.*, 2005; Trusov *et al.*, 2006; Trusov *et al.*, 2007). Furthermore, G-proteins have been found to be important regulators of cell death signaling in plants (Liu *et al.*, 2013a). The following section will focus on the roles that G-proteins play in these two pathways.

GPA1 and AGB1 were shown to be regulators of resistance against fungal pathogens. *gpa1* mutant plants exhibited enhanced resistance, while *agb1* plants were more susceptible to the necrotrophic fungal pathogens *Plectosphaerella cucumerina* (Llorente *et al.*, 2005), *Fusarium oxysporum* (Trusov *et al.*, 2006) and *Alternaria brassicola* (Trusov *et al.*, 2006). Studies about the role of GPA1 and AGB1 in resistance against bacterial pathogens are contradictory. Trusov and colleagues (2006) reported that resistance against *Pseudomonas syringae* pv. *tomato* DC3000 is independent of heterotrimeric G-proteins. Torres *et al.* (2013) however, found *agb1* mutant plants to be more susceptible to *Pseudomonas syringae* pv. *tomato* DC3000, while resistance against this pathogen is unaffected in *gpa1* plants. The situation is further complicated by reports that *gpa1* and *agb1* as well as *gpa1 agb1* double mutants showed similarly impaired resistance against virulent and avirulent *Pseudomonas syringae* pv. *maculicola* and pv. *tabaci* strains (Lee *et al.*, 2013a).

Several studies have reported partly redundant functions of the G γ -subunits AGG1 and

AGG2 in disease resistance (Lee *et al.*, 2013a; Liu *et al.*, 2013a). *Arabidopsis* plants lacking either AGG1 or AGG2 showed wild type-like resistance when inoculated with virulent or avirulent *Pseudomonas syringae* strains, while double knockout *agg1 agg2* plants were more susceptible (Lee *et al.*, 2013a). But not all defense responses are redundantly mediated by AGG1 and AGG2. Resistance against the necrotrophic fungal pathogen *Fusarium oxysporum* was impaired in *agg1* single and *agg1 agg2* double mutants, while *agg2* plants exhibited wild type-like resistance (Trusov *et al.*, 2007). To date, no defense related role has been postulated for AGG3.

AGB1, AGG1 and AGG2 have been found to be involved in PAMP triggered defense responses, while GPA1 seems not to play a role in these pathways (Liu *et al.*, 2013a). ROS production was reduced in *agb1* single and *agg1 agg2* double mutants upon flg22, elf18 and chitin treatment. Interestingly, ROS production in *agg1* plants was only reduced after elf18 treatment and wild type-like for flg22, elf18 and chitin treatment in *agg2* plants, pointing to partly redundant functions of AGG1 and AGG2 in PAMP responses. Furthermore, AGB1, AGG1 and AGG2 were required for activation of the MAPK4, but dispensable for MAPK3 and 6 activation (Liu *et al.*, 2013a).

Heterotrimeric G-proteins were also reported to play a role in cell death regulation (Liu *et al.*, 2013a). Knockout mutants of the BAK1 interacting kinase BIR1 (*bir1-1*) are characterized by constitutive activation of defense responses which result in cell death and stunted growth (Gao *et al.*, 2009). This phenotype could be suppressed by *agb1* single and *agg1 agg2* double knockout mutants, but not by *gpa1*, *agg1* or *agg2* single mutants (Liu *et al.*, 2013a). A mutant of the LRR-RLK SUPPRESSOR OF BIR1-1 (SOBIR1) was found to suppress the cell death phenotype of *bir1-1* and act as a positive regulator of cell death (Gao *et al.*, 2009). Overexpression of SOBIR1 resulted in a cell death phenotype similar to *bir1-1* (Gao *et al.*, 2009), which could be suppressed by *agb1* knockout, indicating that they act in the same pathway (Liu *et al.*, 2013a).

Given the fact that heterotrimeric G-proteins are involved in PAMP-triggered responses and cell death suggest that RLKs like FLS2, EFR, CERK1 and SOBIR1 might act upstream of G-proteins. Heterotrimeric G-proteins might act as converging point for these RLKs activating a common signaling pathway leading to the induction of PTI or cell death.

1.1.2.2 *Arabidopsis* Extra-large G-Proteins (XLGs) are alternative G α subunits

In addition to the canonical G α -subunit GPA1, the *Arabidopsis* genome encodes for so called extra-large G-proteins (XLGs), which are nearly twice the size of conventional G α -subunits

(Ding *et al.*, 2008; Lee & Assmann, 1999). The first extra-large G-protein was identified in 1999 and was named XLG1 (Lee & Assmann, 1999). Further research led to the discovery of two additional *Arabidopsis* XLGs (XLG2 and 3) (Ding *et al.*, 2008).

Extra large G-proteins contain a C-terminal domain which is homologous to GPA1 and mammalian Gas as well as an N-terminal domain of unknown function (Ding *et al.*, 2008; Lee & Assmann, 1999). In comparison to GPA1, the G α domains of XLGs lack several conserved amino acids which are involved in GTP binding and hydrolysis (Temple & Jones, 2007). Nevertheless, GTPase activity was confirmed for all *Arabidopsis* extra-large G-proteins *in vitro* (Heo *et al.*, 2012). In contrast to AtGPA1 and other canonical Gas which need Mg²⁺ as a cofactor, GTPase activity of XLG proteins depends on the presence of Ca²⁺ (Heo *et al.*, 2012). The N-terminal part of XLGs harbours a cysteine-rich region with four perfect CxxC motifs which is followed by a region that is highly conserved among all extra large G-proteins (Ding *et al.*, 2008; Lee & Assmann, 1999). The regularly spaced cysteines have been speculated to form a DNA binding domain, since they resemble elements found in DNA binding zinc finger domains (Ding *et al.*, 2008). Overall, the region containing the CxxC motifs does not match any known zinc-finger-like patterns and their function remains unknown.

Localization studies concerning extra-large G-proteins are contradictory. Ding *et al.* (2008) reported localization of GFP-XLG1/2/3 fusion proteins in nuclei when heterologously expressed in *Vicia faba* leaves. Due to the predicted nuclear localization signals in each of the XLG proteins, this was not unexpected. However, Maruta *et al.* (2015) reported GFP-XLG1 to be localized at the plasma membrane, and GFP-XLG2 and GFP-XLG3 to be localized to both, the plasma membrane and the nucleus when stably overexpressed in *Arabidopsis* or transiently in *N. benthamiana*. As the XLG-GFP fusion constructs in both these studies were overexpressed under control of the strong 35S promoter, Chakravorty *et al.* (2015) sought to investigate XLG localization using the weaker UBIQUITIN10 promoter for 'enhanced temporal resolution'. These localization studies were performed via transient expression in *N. benthamiana* and essentially confirmed the results of Maruta *et al.* (2015). Nevertheless, the reported XLG localization patterns might be the result of mild to strong overexpression and/or transient heterologous expression and may therefore not necessarily display the localization of the endogenous XLG proteins. A nuclear localization signal (NLS) was predicted in the N-terminal part of all three XLGs. Their functionality was confirmed by fusion of the N-terminal part of each XLG to GFP and heterologous expression in *Vicia faba* (Ding *et al.*, 2008). However, re-evaluation of nuclear localization signals of XLGs confirmed a classical NLS only for XLG3, while XLG2 harbors a non-canonical NLS. The functionality of the XLG2 NLS was confirmed by fusion to XLG1, which changed its localization pattern from

primarily extra-nuclear to mainly nuclear (Chakravorty *et al.*, 2015). No NLS could be identified for XLG1 in this study, which is expected according to localization studies. XLG3 contains an additional, non-canonical NES, whose functionality was confirmed by mutational analysis (Chakravorty *et al.*, 2015).

XLG knockout mutant analyses revealed functions of XLG proteins in root development, hormone signaling, pathogen resistance and cell death (Ding *et al.*, 2008; Maruta *et al.*, 2015; Pandey *et al.*, 2008; Zhu *et al.*, 2009) of which the latter two will be the focus of the following part. All three XLGs act as negative regulators of root growth, as indicated by *xlg* triple mutant seedlings grown in darkness. XLG3 has additional functions in the regulation of root-waving and root-skewing (Pandey *et al.*, 2008). *xlg* triple mutants were further found to be hypersensitive to osmotic stress and abscisic acid (Ding *et al.*, 2008).

XLG2 was found to be involved in resistance against bacterial pathogens (Maruta *et al.*, 2015; Zhu *et al.*, 2009). Inoculation of *xlg2* plants with virulent and avirulent *Pseudomonas syringae* pv. *tomato* strains led to enhanced bacterial growth in comparison to Col-0 wild type plants (Zhu *et al.*, 2009). The analysis of double (*xlg2 xlg3*) and triple (*xlg1 xlg2 xlg3*) mutants revealed no additive effect in susceptibility, indicating that XLG1 and XLG3 do not participate in resistance against *Pseudomonas syringae* (Maruta *et al.*, 2015). Transcription of XLG2 and XLG3 is induced upon *Pseudomonas* infection, even though only XLG2 contributes to resistance (Zhu *et al.*, 2009). XLG2 and XLG3 were shown to exhibit functions in resistance against fungal pathogens. Inoculation of *xlg2* mutants with the incompatible biotrophic pathogen *Erysiphe pisi* led to enhanced cell penetration in comparison to wild type plants (Humphry *et al.*, 2010). Resistance against the hemibiotrophic fungal pathogen *Fusarium oxysporum* is impaired in *xlg2* and *xlg3* single and even more impaired in *xlg2 xlg3* double mutants, indicating that XLG2 and XLG3 have redundant functions in resistance against this pathogen (Maruta *et al.*, 2015). Similar to experiments with *Pseudomonas*, *xlg2* mutants showed enhanced susceptibility to the necrotrophic pathogen *Alternaria brassicola* but there was no additive effect regarding *Alternaria* susceptibility in *xlg2 xlg3* double or *xlg* triple mutants (Maruta *et al.*, 2015). Interestingly, *agb1* mutants were similarly impaired in resistance against *P. syringae*, *F. oxysporum* and *A. brassicola* as *xlg2* single and/or *xlg2 xlg3* double mutants, indicating that they are involved in the same defense signalling pathway. Another hint for XLG2 and AGB1 acting in the same signalling pathways came from experiments showing that the *bir1-1* cell death phenotype not only depends on AGB1, but also on XLG2 (Liu *et al.*, 2013a; Maruta *et al.*, 2015).

For a long time it was thought that there are only 3 possible heterotrimeric complexes in *Arabidopsis* consisting of GPA1/AGB1 and one of the three Gy-subunits AGG1-3. Interaction of XLGs with AGB1/AGG was deemed unlikely because of considerable sequence

divergence between extra-large G-proteins and conventional G α -subunits, particularly in regions thought to mediate GPA1-AGB1 interaction (Temple & Jones, 2007). This view was supported by the fact that in contrast to GPA1 (Klopfleisch *et al.*, 2011), XLG2 did not interact with AGB1 in yeast (Zhu *et al.*, 2009).

The situation changed recently, when XLGs were reported to bind G $\beta\gamma$ -dimers in yeast and upon transient transformation of *Arabidopsis* protoplasts or *Nicotiana benthamiana* leaves (Chakravorty *et al.*, 2015; Maruta *et al.*, 2015). XLG proteins were shown to interact with AGB1 in yeast, when one of the AGG proteins was also expressed. Interaction in plants occurs at the plasma membrane and also depends on the presence of at least one of the G γ -subunits (Chakravorty *et al.*, 2015; Maruta *et al.*, 2015). One possible explanation is that the G γ -subunits are required for stabilization of AGB1. This is consistent with recent results showing that AGB1 abundance is decreased in *agg1 agg2* double mutants and barely detectable in *agg1 agg2 agg3* triple mutants (Wolfenstetter *et al.*, 2015). Alternatively, XLG proteins could directly bind the G γ -subunits. However, contradicting results were reported about the direct interaction of XLGs with the G γ -subunits in absence of AGB1. Maruta *et al.* (2015) could detect XLG2 interaction with each G γ -subunit in *agb1* protoplasts in bimolecular fluorescence experiments. These results could not be confirmed by Chakravorty *et al.* (2015), who could detect XLG – AGG1/2/3 interaction only in the presence of AGB1. It therefore remains unclear, if direct interaction between XLGs and G γ -subunits alone is possible. Also, the interaction specificity between the three XLG proteins and the three possible G $\beta\gamma$ -dimers is not yet entirely clear. While Maruta *et al.* (2015) reported that XLG2 equally interacted with all G $\beta\gamma$ -dimers, Chakravorty *et al.* (2015) found that XLG1 and XLG2 preferentially interact with G $\beta\gamma$ -dimers containing either AGG1 or AGG2, whereas XLG3 bound strongly to all three possible G $\beta\gamma$ -dimers (AGB1 + AGG1/2/3). In this study, GPA1 interacted preferentially with G $\beta\gamma$ -dimers containing AGG3.

Taken together, these recent findings (Chakravorty *et al.*, 2015; Maruta *et al.*, 2015) confirmed XLG proteins as components of heterotrimeric G-protein complexes, expanding the G α family in *Arabidopsis* from one to four members: GPA1, XLG1, XLG2 and XLG3. This increases the number of potential heterotrimeric G-protein complexes from three to twelve. The involvement of extra-large G-proteins and their possible direct interaction with G γ -subunits is an uncommon theme in G-protein signaling and clearly distinguishes plant heterotrimeric G-protein signalling from its animal counterpart.

1.2 Ectodomain shedding and related proteolytic processes in metazoans

The proteolytic cleavage of transmembrane proteins to release the extracellular domain is referred to as ectodomain shedding (Figure 4) (Arribas & Borroto, 2002). In animals, it acts as a regulatory mechanism in a wide range of proteins, such as growth factors, cytokines, cell adhesion molecules and receptors (Hayashida *et al.*, 2010). Ectodomain shedding leads to the release of a soluble ectodomain into the extracellular space which may then act as a signaling module in paracrine signaling (Blobel, 2005). Cells can also use ectodomain shedding as a regulatory mechanism to control the abundance or function of proteins on the cellular surface and it may also be a prerequisite for further proteolytic processing steps. Basal ectodomain shedding takes place in unstimulated cells, but it can also be induced by different stimuli such as protein kinase C activating chemicals or ligand binding (Hayashida *et al.*, 2010).

For most vertebrate proteins, proteolytic processing of the extracellular domain depends on the catalytic activity of metalloproteases belonging either to the A Disintegrin and Metalloproteinase (ADAM) or Matrix Metalloproteinases (MMPs) family (Hayashida *et al.*, 2010). In addition to the catalytic metalloprotease domain, MMPs and ADAMs share an N-terminal pro-domain, which is cleaved off to activate the protein. ADAMs contain additional disintegrin and EGF-like domains (Khokha *et al.*, 2013). Members of the ADAM and MMP family are either soluble or membrane bound by transmembrane domains (MMPs + ADAMs) or GPI anchors (MMPs). Despite their involvement in distinct cellular processes, many different proteins may be cleaved by the same sheddase and many sheddases may be involved in the cleavage of one substrate (Hayashida *et al.*, 2010). The activity of a sheddase on a certain substrate is thought to also depend on spatio-temporal expression of protease and substrate and on the presence of activators (Chow & Fernandez-Patron, 2007).

Proteolytic cleavage of the extracellular domain is often followed by cleavage within the transmembrane domain (Figure 4). This mechanism is referred to as regulated intramembrane proteolysis (RIP) and is a common mechanism to release the intracellular domain, which can serve as signaling molecule or is subject to degradation (Lichtenthaler *et al.*, 2011). Intramembrane proteolysis is carried out by intramembrane-cleaving proteases (iCLIPs), which are either aspartyl proteases (presenilin, signal peptide peptidase and related proteases), metallo proteases (Membrane-bound transcription factor site-2 protease) or serine proteases (Rhomboids) (Kopan & Ilagan, 2004; Lal & Caplan, 2011). The protease type most frequently reported to perform RIP after ectodomain shedding is presenilin, which interacts with additional proteins to form the γ -secretase complex. Ectodomain shedding is a

prerequisite for intramembrane cleavage by most iCLIPs. Rhomboid proteases are an exception to this rule, since they are able to cleave substrates containing long ectodomains (Freeman, 2009).

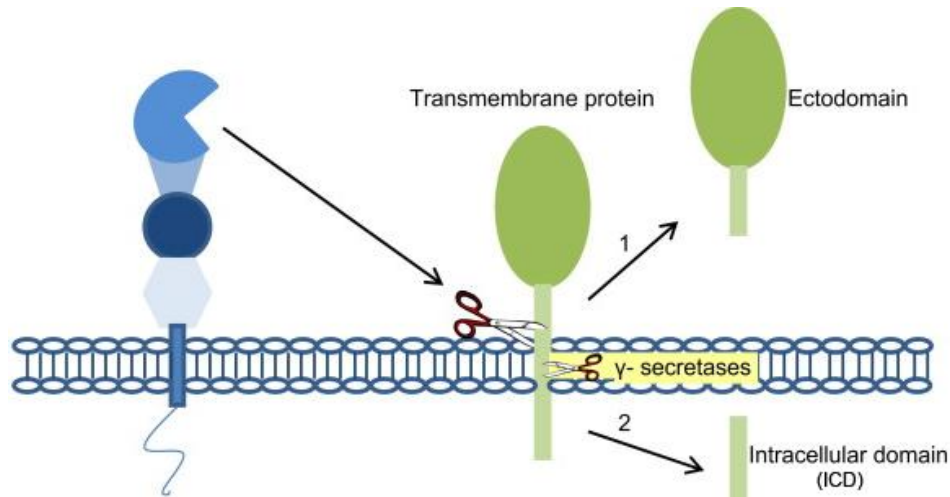


Figure 4. Ectodomain shedding and RIP of integral membrane proteins. An integral transmembrane protein is cleaved in close vicinity to the plasma membrane. The cleaved ectodomain is released into the extracellular space and can act as signaling module. The remaining membrane bound fragment is then subject to iCLIP mediated cleavage (for example by γ -secretase). This leads to release of the intracellular domain (ICD) which can now function as a cytosolic or nuclear effector. Image from herrlichlab.org (modified).

1.2.1 Well studied examples of ectodomain shedding in metazoans

Many different signaling pathways in animals are regulated via proteolytic processing of extracellular domains. Tight regulation of this process is of great importance and dysregulation often results in disease (Saftig & Reiss, 2011). The Notch signaling pathway is a well-documented pathway which is regulated by ectodomain shedding. Notch receptors are a family of transmembrane proteins and are important regulators of cell to cell communication (Kopan & Ilagan, 2009). Notch is conserved in metazoans with homologs in *Drosophila*, *Caenorhabditis* and mammals (Chillakuri *et al.*, 2012; Kopan & Ilagan, 2009). Notch receptors are constitutively cleaved in the *trans*-Golgi resulting in an N-terminal ligand binding part and a C-terminal transmembrane domain containing part (Guruharsha *et al.*, 2012). Noncovalent heterodimerization of both parts constitutes the mature receptor. Notch receptors are activated upon binding of DSL (Delta/Serrate/LAG-2) ligands on opposing cell surfaces (Chillakuri *et al.*, 2012). Ligand binding leads to structural changes, rendering the Notch ectodomain accessible for proteolytic cleavage by either ADAM10 or ADAM17/TACE (Bozkulak & Weinmaster, 2009). Subsequent to ectodomain shedding, the transmembrane domain of Notch is cleaved by the γ -secretase complex to release the intracellular domain,

which translocates into the nucleus, where it can interact with transcription factors (Guruharsha *et al.*, 2012). Amino acid substitutions and insertions resulting in reduced heterodimer stability or ligand-independent ectodomain shedding lead to inappropriate activation of the Notch receptor and are frequently associated with leukemia (Aster *et al.*, 2008).

The amyloid precursor protein (APP) is a type I transmembrane protein which has drawn much attention because of its involvement in the development and progression of Alzheimer's disease and can be found in mammalian and non-mammalian cells (Dawkins & Small, 2014). Intriguingly, the molecular function of APP is still elusive, but it has been proposed as a regulator of growth and maturation of many cells in the nervous system (Dawkins & Small, 2014). The amyloid plaques associated with Alzheimer's disease are caused by production and accumulation of a proteolytic cleavage product of APP (Murphy & LeVine, 2010). Post-translational processing of APP can occur in two different ways (Haass *et al.*, 2012). The enzymes involved in the so-called anti-amyloidogenic pathway are similar to those of Notch ectodomain shedding. APP is first cleaved by ADAM10, which leads to the release of the extracellular APP_{sα} fragment (Figure 5A) (Postina *et al.*, 2004). The remaining membrane bound part of APP is then cleaved by the γ -secretase complex, leading to generation of the p3 peptide.

The second possible processing mechanism is the amyloidogenic pathway, which involves proteolytic cleavage of APP near the transmembrane domain by the aspartic protease beta-secretase 1 (BACE1). This leads to the release of a large part of the APP ectodomain (APP_{sβ}, Figure 5B) (Seubert *et al.*, 1993). A second cleavage of the remaining membrane-bound fragment of APP mediated by the γ -secretase complex results in generation of A β (Haass *et al.*, 1993). The A β peptide accumulates and aggregates in the brain, forming senile plaques, which is characteristic for Alzheimer's disease (Selkoe, 2001).

The anti-amyloidogenic and the amyloidogenic pathways are in competition with each other. Postina *et al.* (2004) showed that overexpression of ADAM10 leads to enhanced generation of the APP_{sα} fragment and reduced the formation of A β . A C-terminal intracellular fragment (ICD) is released in both pathways, which is believed to engage in nuclear signaling thereby inducing its own expression to restore full length APP (Rotz *et al.*, 2004). L-selectin is a cell-adhesion molecule that is expressed on most leukocytes. It consists of a large extracellular domain and a small cytoplasmic tail (Smalley & Ley, 2005). L-selectin is involved in adhesion of leukocytes to the endothelium, the initial step of leukocyte recruitment to sites of

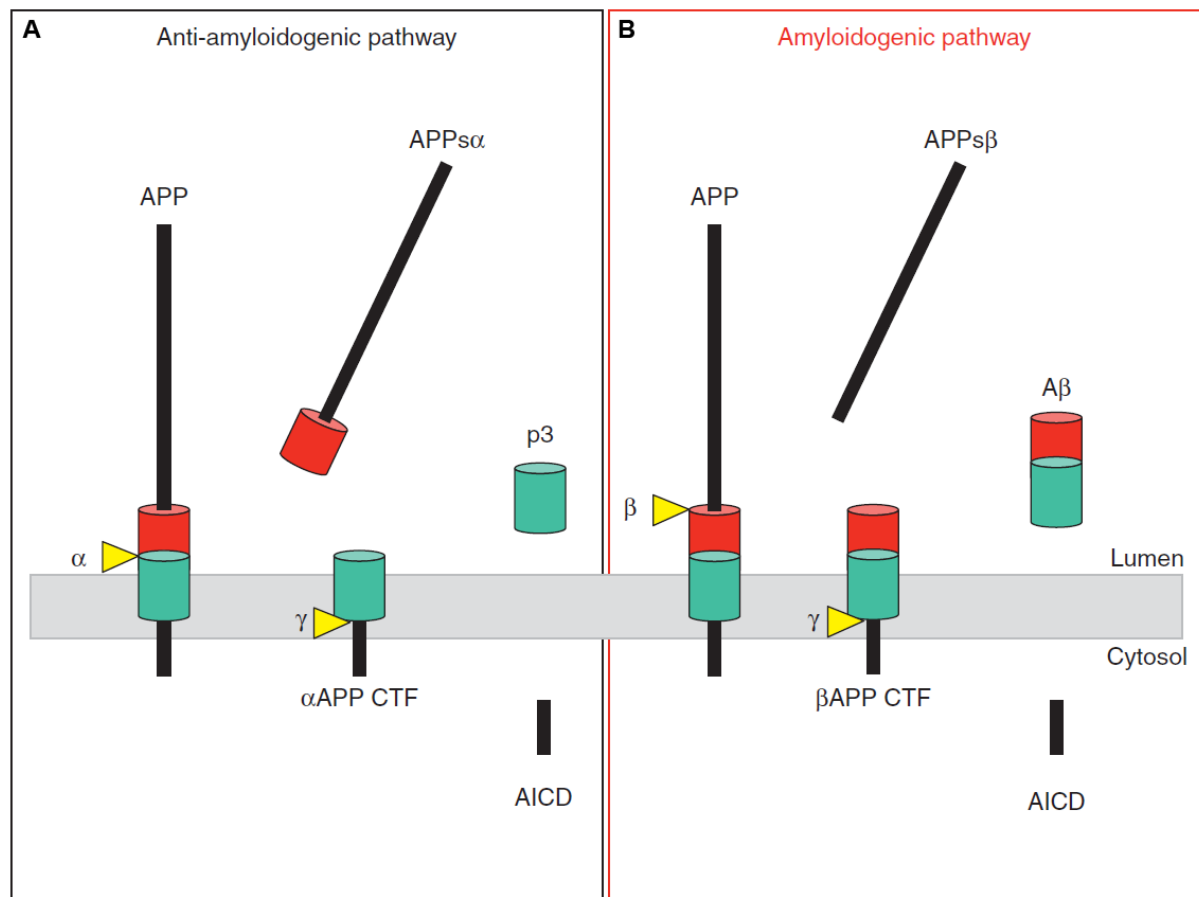


Figure 5. Proteolytic processing of amyloid precursor protein. A) In the anti-amyloidogenic pathway, APP is cleaved by ADAM10 (α -secretase) close to the transmembrane domain to release the extracellular APPs α fragment. Subsequent cleavage of the remaining truncated C-terminal fragment (α APP CTF) by a γ -secretase releases an extracellular peptide (p3) and the intracellular domain (AICD). B) In the amyloidogenic pathway, cleavage by BACE (β -secretase) releases the extracellular fragment APPs β . BACE cleavage occurs closer to the N-terminus in comparison to ADAM10 cleavage. The remaining C-terminal fragment (β APP CTF) is subsequently cleaved to release the neurotoxic A β peptide and the intracellular domain (AICD). Image from Haass *et al.* (2012).

inflammation (Raffler *et al.*, 2005). The ectodomain of L-selectin is cleaved by ADAM17/TACE and other sheddases (Walcheck *et al.*, 2003), which is important for directional migration of monocytes to sites of inflammation (Rzeniewicz *et al.*, 2015).

An example for ectodomain shedding by MMPs is E-cadherin, a transmembrane glycoprotein that mediates cell to cell adhesion in a calcium dependent manner (van Roy & Berx, 2008). The ectodomain of E-cadherin consists of 5 cadherin domain repeats which mediate interactions between cadherin molecules on adjacent cells (David & Rajasekaran, 2012). Cleavage of the extracellular part of E-cadherin by a number of different metalloproteinases releases the soluble ectodomain (sE-cad) into the extracellular space. One function of sE-cad is the disruption of cell-to-cell contacts, probably by interacting with unshed E-cadherin molecules (Noe *et al.*, 2001). sE-cad further acts as a paracrine/autocrine signaling molecule and was shown to activate receptor-like tyrosine kinases (David & Rajasekaran, 2012).

1.2.2 Ectodomain shedding of metazoan receptor kinases and their ligands

Receptor kinases are single-span transmembrane proteins with an extracellular ligand binding domain, and an intracellular kinase domain (Ganten *et al.*, 2006). They share a common mechanism of activation, which involves ligand binding, receptor oligomerization and subsequent transphosphorylation events at the intracellular kinase domains (Ganten *et al.*, 2006; Schlessinger, 2000). Based on the amino acids they phosphorylate, receptor kinases can be grouped into receptor serine/threonine kinases (RSKs) and receptor tyrosine kinases (RTKs). The human genome encodes 12 RSKs which serve as receptors for members of the transforming growth factor beta (TGF- β) superfamily of secreted peptides and are involved in many processes of metazoan life such as embryogenesis, tissue fibrosis and cancer (Ganten *et al.*, 2006; Josso & Di Clemente, 1997). RTKs are a large gene family in humans with 58 members that fall into 20 families. Most of the ligands, which are perceived by RTKs are polypeptides including insulin, epidermal growth factor (EGF) and platelet-derived growth factor (PDGF) (Schlessinger, 2000). RTKs play key roles in metabolism, growth, differentiation and motility (Hubbard & Miller, 2007; Schlessinger, 2000). An important regulatory step of receptor kinase mediated signaling is the availability of the ligand to the receptor. Ligands of RSKs are secreted, while many ligands of RTKs are synthesized as transmembrane ligand precursors (Singh & Harris, 2005; Weiss & Attisano, 2013). Ectodomain shedding of the precursor protein leads to release of the active ligand which can then participate in juxtacrine/paracrine signaling and activate RTKs. A particularly well-substantiated example is heparin-binding EGF-like growth factor (HB-EGF) which plays a role in cell proliferation and migration (Faull *et al.*, 2001; Piepkorn *et al.*, 1998). HB-EGF can be cleaved by members of the ADAMs family of proteases to release its N-terminal domain which can then bind to epidermal growth factor receptors (EGFRs) (Singh *et al.*, 2004). Both, mice expressing an uncleavable or a soluble form of HB-EGF suffered from heart problems indicating that regulated shedding is essential for normal development and health (Yamazaki *et al.*, 2003).

The release of the extracellular domain of the EGF-like growth factor spitz in *Drosophila* is an example for rhomboid-mediated ectodomain shedding. Spitz is synthesized as an inactive transmembrane bound precursor (Rutledge *et al.*, 1992). Proteolytic cleavage within the transmembrane domain by Rhomboid-1 releases the extracellular domain of spitz (Urban *et al.*, 2001) which is then suggested to engage in paracrine signaling to activate EGFR signaling.

Not only ligands, but also receptor kinases themselves are subject to proteolytic cleavage of their extracellular domain. The transforming growth factor beta receptor type I (T β RI) is a

RSK and part of the receptor complex that perceives transforming growth factor beta (TGF- β) ligands (Feng & Derynck, 2005). T β RI is subject to ADAM17/TACE-mediated proteolytic cleavage of its ectodomain, which is thought to downregulate its presence on the cellular surface (Liu *et al.*, 2009). Downstream responses mediated by T β RI include growth inhibition (Siegel & Massagué, 2003). Enhanced ectodomain shedding of T β RI might therefore be a strategy of cancer cells to inhibit tumor suppression (Liu *et al.*, 2009; Siegel & Massagué, 2003).

Ectodomain shedding is a fairly common process in RTKs. Out of the 20 RTK-subfamilies, 10 contain members for which ectodomain shedding has been reported. In the majority of these cases, ectodomain shedding is mediated by ADAM17/TACE or ADAM10 and often followed by intramembrane cleavage by γ -secretase (Chen & Hung, 2015). The released intracellular domains are usually short lived (Carpenter & Liao, 2009), but can be stabilized by post-translational modifications or interaction with other proteins such as chaperones. This way they may be transported into various intracellular compartments. Most commonly translocation occurs into the nucleus, where RTK intracellular domains may interact with transcriptional regulators (Chen & Hung, 2015).

Ectodomain shedding has been characterized well in the epidermal growth factor receptor (EGFR) sub-family of RTKs. In humans, the EGFR group consists of four members (erbB1-erbB4). Ligand binding induces homo- or heterodimerization of erbBs, which are then able to activate signaling cascades within the cell, leading to cell proliferation, differentiation and migration (Higashiyama *et al.*, 2011).

The erbB4 receptor occurs in two isoforms which are generated by alternative splicing and differ in their juxtamembrane amino acid composition (Elenius *et al.*, 1997). Only the Jm-a isoform harbors the ADAM17/TACE cleavage site (Cheng *et al.*, 2003) and is therefore subject to ectodomain shedding. erbB4 ectodomain shedding is constitutive, but can also be induced by ligand binding (Rio, 2000; Zhou & Carpenter, 2000). After ectodomain shedding, γ -secretase cleavage releases the erbB4 intracellular domain (ICD), which then translocates to the nucleus (Ni *et al.*, 2001). High levels of erbB4 ectodomain can be found in breast cancer cells (Hollmén *et al.*, 2009). Tumor growth can be stopped by inhibition of erbB4 ectodomain shedding underlining the importance of a tight regulation of this process (Hollmén *et al.*, 2012).

erbB2 (Her2/neu2) is the only EGFR family receptor for which no direct ligand has been described so far. The erbB2 ectodomain was shown to be shed into the extracellular space by ADAM10 (Liu *et al.*, 2006). Overexpression of erbB2 in breast cancer cells leads to frequent cleavage of the extracellular domain. This also generates a C-terminal fragment with constitutive, ligand-independent kinase activity (Gajria & Chandarlapaty, 2011). This

constitutive activation of growth factor signaling pathways by erbB2 serves as an oncogenic driver in breast cancer.

Investigations of the erbB2 cleavage site led to the discovery of a signature motif within the extracellular juxtamembrane domain (Yuan *et al.*, 2003). A five to seven amino acid stretch flanked by either a proline or a glycine (P/G-X₅₋₇-P/G) was found to be conserved from human to chicken EGFRs and was therefore proposed as a common cleavage motif for the EGFR family.

There are also examples of RTK ectodomain shedding by MMPs. EphB2 belongs to the RTK subfamily of erythropoietin-producing hepatoma (Eph) receptors. Ephs are activated by binding membrane bound ligands (ephrins) on adjacent cells. Thereby, they regulate adhesion between neuronal cells which is critical for the development of the nervous system (Kullander & Klein, 2002). EphB2 was reported to undergo ectodomain shedding driven by MMP-2 and MMP-9 upon ligand binding, which triggers repulsion between neurons (Lin *et al.*, 2008). Similar to ectodomain shedding by ADAMs, proteolytic cleavage of the EphB extracellular domain by MMPs is a prerequisite for intramembrane cleavage by the γ -secretase complex to release the intracellular domain (ICD) (Litterst *et al.*, 2007).

1.2.3 Ectodomain shedding of plant receptor-like kinases

Plant receptor-like kinases (RLKs) are transmembrane proteins composed of an extracellular domain and an intracellular kinase domain and thus have a domain organization similar to animal RSKs and RTKs (Shiu & Bleecker, 2001). They are involved in a plethora of developmental and stress responses including hormone signaling, defense and symbiosis (Tax & Kemmerling, 2012). Despite the importance of ectodomain shedding for regulation of many animal RTKs, there are hardly any studies on this topic concerning plant RLKs. In recent years however, reports emerged indicating that ectodomain shedding or related processes might also be important regulatory mechanisms of receptor kinases in the plant kingdom.

A process that is similar to, but distinct from ectodomain shedding regulates the function of *Lotus japonicus* SYMBIOSIS RECEPTOR-LIKE KINASE (SYMRK). SYMRK is involved in the early stages of symbiosis establishment between plants and rhizobia or mycorrhizal fungi (Stracke *et al.*, 2002). The ectodomain of SYMRK contains three LRRs and an N-terminal malectin-like domain (MLD). Recently, it was shown that the MLD of SYMRK is proteolitically released in absence of symbiotic stimulation (Antolín-Llovera *et al.*, 2014). Cleavage occurred at a GDPC motif that connects the MLD domain with the LRR domain (Antolín-Llovera *et al.*, 2014) and can be found in many MLD-LRR-RLKs (Hok *et al.*, 2011). Mutation of this motif

abolished the release of the MLD domain (Antolín-Llovera *et al.*, 2014). The release of the MLD domain is of striking physiological importance, as plants expressing SYMRK constructs unable to release MLD were severely impaired in the establishment of symbiotic interactions. Conversely, deletion of the entire SYMRK extracellular domain led to a massive induction of infection threads which points to important regulatory functions of the SYMRK ectodomain (Antolín-Llovera *et al.*, 2014). This was confirmed by the finding that proteolytic cleavage of the SYMRK extracellular domain seemed to be a prerequisite for complex formation of SYMRK with Nod factor receptor 5 (NFR5) (Antolín-Llovera *et al.*, 2014).

Evidence for proteolytic processing of plant RLKs also came from *Xanthomonas* resistance 21 (XA21), a rice LRR-RLK mediating resistance to the Gram-negative bacterium *Xanthomonas oryzae* pv. *oryzae* (Xoo) (Song *et al.*, 1995). A sulfated, 17-amino acid peptide (AxY^S22) derived from the Ax21 protein of *Xanthomonas* was initially reported to induce XA21 mediated defense responses (Lee *et al.*, 2009). These studies however were later retracted and a new ligand candidate was presented (Lee *et al.*, 2013b; Pruitt *et al.*, 2015). The newly proposed ligand, RaxX, is a *Xanthomonas* protein of unknown function. A 21-amino acid tyrosine-sulfated peptide derived from RaxX (RaxX21-sY) is sufficient to trigger Xa21-mediated defence responses in rice (Pruitt *et al.*, 2015). Immunoblot analyses of transgenic rice plants expressing a labeled version of XA21 with a myc-tag inserted into the extracellular domain, revealed the presence of an XA21 N-terminal cleavage product. This cleavage product was found in microsomal protein fractions and accumulated together with full length XA21 protein after infection with the Xoo strain PXO99Az (Park *et al.*, 2010; Xu *et al.*, 2006) or treatment with the now controversial ligand AxY^S22 (Lee *et al.*, 2009). Interestingly, the intracellular juxtamembrane domain of XA21 harbors a P/G-X₅₋₇-P/G motif similar to extracellular juxtamembrane domain of EGFRs. This signature was proposed as a cleavage site in XA21 and auto-phosphorylation of residues within this motif was positively correlated with protein stability and resistance (Xu *et al.*, 2006). Park & Ronald (2012) showed that XA21 accumulation upon Xoo or AxY^S22 treatment is also associated with the release of a C-terminal fragment. The authors demonstrated the presence of XA21-GFP at the plasma membrane and in the endoplasmic reticulum in unstimulated protoplasts. Upon AxY^S22 treatment, the C-terminal XA21-GFP fragment translocated to the nucleus. The nuclear translocation of the XA21-GFP C-terminus was shown to be critical for XA21-mediated immunity. However, since the role of AxY^S22 as a XA21 ligand is questionable, the significance of this report (Park & Ronald, 2012) is not clear.

Another hint for the existence of ectodomain shedding in plants comes from BRI1. BRI1 is an LRR-receptor-like kinase and the *Arabidopsis* brassinosteroid receptor (Wang *et al.*, 2001). Immunoblots on plant extracts using an N-terminal BRI1 antibody revealed the presence of

an N-terminal fragment in addition to the full-length receptor (Wang et al., 2001). Since the BRI1 gene consists of only one exon, this fragment is likely generated by proteolytic cleavage. The presence of a soluble, N-terminal BRI1 fragment was confirmed in our laboratory (Elena Petutschnig, unpublished data).

Ectodomain shedding similar to animal receptor kinases was reported for CERK1 (Petutschnig *et al.*, 2014). In addition to full-length CERK1, an N-terminal fragment can be detected in immunoblots using an N-terminal CERK1 antibody. This fragment lacks the CERK1 transmembrane domain, as it can be found in soluble fractions of microsomal preparations and in apoplastic wash fluids. Therefore, it represents the free CERK1 ectodomain. The abundance of the CERK1 ectodomain fragment increases in older plants and after inoculation with the non-adapted pathogen *Blumeria graminis* f. sp. *hordei* (*Bgh*) (Petutschnig *et al.*, 2014).

A CERK1 mutant (*cerk1-4*) lacking the N-terminal cleavage product was identified (Petutschnig *et al.*, 2014). *cerk1-4* plants harbor a leucine to phenylalanine (L->F) exchange within the second LysM domain of CERK1. These plants exhibit normal chitin signaling but are characterized by an enhanced salicylic acid-dependent cell death phenotype upon inoculation with *Bgh*. This phenotype is independent of CERK1 kinase activity and does not require the intracellular domain of CERK1. CERK1-GFP and *cerk1-4*-GFP fusion proteins revealed the presence of a C-terminal fragment in both cases. This suggests that the ectodomain fragment is missing in *cerk1-4* plants because of the instability of the released *cerk1-4* ectodomain, rather than shedding deficiency of the full length *cerk1-4* protein. However, the mechanism of CERK1 ectodomain shedding and its role in cell death regulation remain unclear (Petutschnig *et al.*, 2014).

The proteases acting on plant RLKs are currently not known. While ADAMs, one of the main actors in ectodomain shedding in vertebrates, do not exist in the plant kingdom (Seals & Courtneidge, 2003) there are five homologs of the vertebrate family of MMPs in *Arabidopsis thaliana* (At1-MMP – At5-MMP) (Maidment *et al.*, 1999; Seals & Courtneidge, 2003). All five At-MMPs were shown to have protease activity *in vitro* and (with the exception of At5-MMP) showed similar cleavage site specificity to human MMPs (Marino *et al.*, 2014).

Of these five MMPs, only At2-MMP was functionally characterized in plants. At2-MMP knockout mutants showed early senescence, smaller growth and early flowering (Golldack *et al.*, 2002). A tomato MMP was recently reported to mediate resistance against fungal as well as bacterial pathogens (Li *et al.*, 2015).

Rhomboids are another family of proteases which are engaged in animal ectodomain shedding and can be found in plants. 13 rhomboid homologs can be found in *Arabidopsis* (Koonin *et al.*, 2003), but studies on plant rhomboids are scarce. Rhomboid activity and

specificity were demonstrated *in vitro* for heterologously expressed AtRBL2 (Kanaoka *et al.*, 2005). Also, the subcellular localization has been investigated for several *Arabidopsis* RBLs and ranges from golgi apparatus to chloroplasts and mitochondria (Kmiec-Wisniewska *et al.*, 2008). However, the information on the function of RBLs in *Arabidopsis* is very limited. Mutants of AtRBL8 were reported to show defects in floral development, but no substrates were identified (Adam, 2013; Thompson *et al.*, 2012). The examples about proteolytic processing and ectodomain shedding of plant RLKs presented in this section might just be the beginning of many more studies to come. Results from this study (compare section 3.1.7) suggest that ectodomain shedding may be a common process in plant RLKs. Future work may elucidate the function of RLK ectodomain shedding and the proteases involved in it.

2. Materials and Methods

2.1 Materials

2.1.1 Plant materials

2.1.1.1 *Arabidopsis thaliana*

Arabidopsis accessions, mutant and transgenic lines used in this work are listed in Table 1, Table 2 and Table 3.

Table 1. *Arabidopsis* accessions used in this study.

Accession	Abbr.	Source / NASC Stock number
Columbia-0	Col-0	J. Dangl, University of North Carolina, USA.
Columbia-3	Col-3	N908
Argentat	Ag-0	N901
Barcelona-Tibidabo	Bar-1	N77689
Bensheim	Be-0	N964
Landsberg erecta	Ler-0	N77020
Lipowiec	Lip-0	N1336
Mühlen	Mh-1	N1368
Moscow	Ms-0	N905
N	N14	N22492
N	N6	N22484
N	N7	N22485
Nossen	No-0	N77128
Oberursel	Ob-0	N1418
Pitztal	Pi-0	N1454
Poppelsdorf	Po-0	N1470
Richmond	Ri-0	N1492
Rschew	Rsch-4	N1494
Slavice	Sav-0	N1514
Shakdara	Shakdara	N929
Sorbo	Sorbo	N931
Spandau	Sp-0	N1530

Table 1 (continued).

San Feliu	Sf-0	N1510
Stobowal	Stw-0	N1538
Wilna	Wil-2	N1596
Wietze	Wt-5	N1612

Table 2. Mutant *Arabidopsis* lines used in this study.

Genotype / Name	AGI locus identifier	Accession	T-DNA / mutagen	Reference / source
Col-3 <i>gl1</i>	AT3G27920	Col-3	EMS	Volker Lipka
<i>cerk1-2</i>	AT3G21630	Col-0	T-DNA insertion	Miya <i>et al.</i> (2007)
<i>cerk1-4</i>	AT3G21630	Col-3 <i>gl1</i>	EMS	Petutschnig <i>et al.</i> (2014)
<i>fah1 fah2</i>	AT2G34770 AT4G20870	Col-0	T-DNA	König <i>et al.</i> (2012)
<i>fah1 fah2 loh1</i>	AT2G34770 AT4G20870 AT3G25540	Col-0	T-DNA	Prof. Dr. Ivo Feussner
<i>fah1 fah2 loh2</i>	AT2G34770 AT4G20870 AT3G19260	Col-0	T-DNA	Prof. Dr. Ivo Feussner
<i>fah1 fah2 loh3</i>	AT2G34770 AT4G20870 AT1G13580	Col-0	T-DNA	Prof. Dr. Ivo Feussner
<i>pad4-1</i>	AT3G52430	Col-0	EMS	Glazebrook <i>et al.</i> (1996)
<i>sid2-2</i>	AT1G74710	Col-0	EMS	Dewdney <i>et al.</i> (2000)
<i>agb1-2</i>	AT4G34460	Col-0	T-DNA insertion	Ullah <i>et al.</i> (2003)
<i>nole1-1</i>	AT3G21630 AT4G34390	Col-3 <i>gl1</i>	EMS	Marnie Stolze
<i>nole1-2</i>	AT3G21630 AT4G34390	Col-3 <i>gl1</i>	EMS	This work
<i>nole2/7</i>	unknown	Col-3 <i>gl1</i>	EMS	This work
<i>nole3/4</i>	unknown	Col-3 <i>gl1</i>	EMS	This work
<i>nole3/8</i>	unknown	Col-3 <i>gl1</i>	EMS	This work

Table 3. Transgenic *Arabidopsis* lines used in this study.

Background	Construct	Resistance	Reference
<i>cerk1-2</i>	pGreenII0229-PREP- pCERK1:: <i>CERK1</i>	Basta	This work
<i>cerk1-2</i>	pGreenII0229-PREP- pCERK1:: <i>cerk1 cvg1</i>	Basta	This work
<i>cerk1-2</i>	pGreenII0229-PREP- pCERK1:: <i>cerk1-4 cvg1</i>	Basta	This work
<i>cerk1-2</i>	pGreenII0229-PREP- pCERK1:: <i>cerk1 cvg2</i>	Basta	This work
<i>cerk1-2</i>	pGreenII0229-PREP- pCERK1:: <i>cerk1 cvg3</i>	Basta	This work
<i>cerk1-2</i>	pGreenII0229-PREP- pCERK1:: <i>cerk1 clx</i>	Basta	This work
<i>cerk1-2</i>	pGreenII0229-PREP- pCERK1:: <i>cerk1 Del1</i>	Basta	This work
<i>cerk1-2</i>	pGreenII0229-PREP- pCERK1:: <i>cerk1 Del2</i>	Basta	This work
<i>cerk1-2</i>	pGreenII0229-PREP- pCERK1:: <i>cerk1 cerk1 fls2tm</i>	Basta	This work
<i>cerk1-2</i>	pGreenII0229-PREP- pCERK1:: <i>cerk1 fls2tmex1</i>	Basta	This work
<i>cerk1-2</i>	pGreenII0229-PREP- pCERK1:: <i>cerk1 fls2tmex2</i>	Basta	This work
<i>cerk1-2</i>	pGreenII0229-PREP- pCERK1:: <i>cerk1 fls2tmex3</i>	Basta	This work
<i>cerk1-2</i>	pGreenII0229-PREP- pCERK1:: <i>cerk1 -ks</i>	Basta	This work
<i>cerk1-2</i>	pGreenII0229-PREP- pCERK1:: <i>cerk1 ks->aa</i>	Basta	This work
<i>cerk1-2</i>	pGreenII0229-PREP- pCERK1:: <i>cerk1 -ks</i>	Basta	This work
<i>nole1-2 cerk1-4</i>	pGreenII0229-PREP- pXLG2:: <i>XLG2</i>	Basta	This work
Col-3 <i>gl1</i> , <i>nole1-2</i> <i>cerk1-4</i>	pGWB604-pXLG2:: <i>XLG2-GFP</i>	Basta	This work
Col-3 <i>gl1</i>	pGWB604-pXLG2:: <i>xlg2</i> <i>E293K-GFP</i>	Basta	This work
Col-0, <i>cerk1-2</i> , Col-3 <i>gl1</i> , <i>cerk1-4</i>	pGreenII0229-PREP - pXLG2:: <i>Venus-XLG2</i>	Basta	This work

2.1.1.1 *Nicotiana benthamiana*

N. benthamiana seeds were originally provided by T. Romeis (Biochemistry of Plants, Institute of Biology, Freie Universität Berlin). *N. benthamiana* plants were used for transient expression mediated by *Agrobacterium tumefaciens*.

2.1.2 Pathogens

2.1.2.1 Fungal pathogens

2.1.2.1.1 Powdery mildews

The non-adapted filamentous powdery mildew *Blumeria graminis* f.sp. *hordei* (Lipka *et al.*, 2005) was used for inoculation experiments of *Arabidopsis* plants.

2.1.3 Bacterial strains used for cloning and transformation

2.1.3.1 *Escherichia coli*

Chemically competent *E. coli* TOP10 (F- mcrA Δ (mrr-hsdRMS-mcrBC) Φ 80lacZ Δ M15 Δ lacX74 deoR recA1 araD139 Δ (ara-leu)7697 galU galK rpsL (StrR) endA1 nupG) cells (Thermo Scientific™, Waltham, USA) were used for cloning and transformation.

2.1.3.2 *Agrobacterium tumefaciens*

Electro-competent *Agrobacterium tumefaciens* GV3101 were used in this study containing resistance against rifampicin and gentamycin (Koncz & Schell, 1986). Agrobacteria contained the additional helper plasmid pSoup conferring tetracycline resistance (Hellens *et al.*, 2000).

2.1.4 Yeast strains used for cloning and transformation

For transformation and cloning by drag and drop the *Saccharomyces cerevisiae* strain S288c BY4741 (*MATa*, *his3 Δ 1*, *leu2 Δ 0*, *met15 Δ 0*, *ura3 Δ 0*) (Brachmann *et al.*, 1998) was used.

2.1.5 Vectors used in this study

Table 4 lists the vectors used or generated in this study.

Table 4. Vectors used in this study.

Name	Description	Resistance	Reference
pGreenII0229PREP- pCERK1:: <i>CERK1</i>		Bacterial resistance: Kan Plant resistance: Basta	This work
pGreenII0229PREP- pCERK1:: <i>cerk1 cvg1</i>	Synthesized by GeneWiz (South Plainfield) and subcloned into pGreenII0229PREP	Bacterial resistance: Kan Plant resistance: Basta	This work
pGreenII0229PREP- pCERK1:: <i>cerk1-4 cvg1</i>	Synthesized by GeneWiz (South Plainfield) and subcloned into pGreenII0229PREP	Bacterial resistance: Kan Plant resistance: Basta	This work
pGreenII0229PREP- pCERK1:: <i>cerk1 cvg2</i>	Synthesized by GeneWiz (South Plainfield) and subcloned into pGreenII0229PREP	Bacterial resistance: Kan Plant resistance: Basta	This work
pGreenII0229PREP- pCERK1:: <i>cerk1 cvg3</i>	Synthesized by GeneWiz (South Plainfield) and subcloned into pGreenII0229PREP	Bacterial resistance: Kan Plant resistance: Basta	This work
pGreenII0229PREP- pCERK1:: <i>cerk1 clx</i>	Synthesized by GeneWiz (South Plainfield) and subcloned into pGreenII0229PREP	Bacterial resistance: Kan Plant resistance: Basta	This work
pGreenII0229PREP- pCERK1:: <i>cerk1 Del1</i>		Bacterial resistance: Kan Plant resistance: Basta	This work
pGreenII0229PREP- pCERK1:: <i>cerk1 Del2</i>		Bacterial resistance: Kan Plant resistance: Basta	This work
pGreenII0229PREP- pCERK1:: <i>cerk1 cerk1 fls2tm</i>		Bacterial resistance: Kan Plant resistance: Basta	This work

Table 4 (continued).

pGreenII0229PREP- pCERK1:: <i>cerk1</i> <i>fls2tmex1</i>	Bacterial resistance: Kan Plant resistance: Basta	This work
pGreenII0229PREP- pCERK1:: <i>cerk1</i> <i>fls2tmex2</i>	Bacterial resistance: Kan Plant resistance: Basta	This work
pGreenII0229PREP- pCERK1:: <i>cerk1</i> <i>fls2tmex3</i>	Bacterial resistance: Kan Plant resistance: Basta	This work
pGreenII0229PREP- pCERK1:: <i>cerk1 -ks</i>	Bacterial resistance: Kan Plant resistance: Basta	This work
pGreenII0229PREP- pCERK1:: <i>cerk1 ks-</i> <i>>aa</i>	Bacterial resistance: Kan Plant resistance: Basta	This work
pGreenII0229PREP- pCERK1:: <i>cerk1 -ks</i>	Bacterial resistance: Kan Plant resistance: Basta	This work
pGreenII0229PREP- pXLG2:: <i>XLG2</i>	Bacterial resistance: Kan Plant resistance: Basta	Elena Petutschnig (unpublished)
pENTR TM /D-TOPO®	Kan	Inivitrogen TM
pGWB604; no promoter, C-sGFP	Bacterial resistance: Spc Plant resistance: Basta	Nakamura <i>et al.</i> (2010)
pGWB604+ pXLG2:: <i>XLG2-GFP</i>	Bacterial resistance: Spc Plant resistance: Basta	This work
pGWB604- pXLG2:: <i>xlg2 E293K-</i> <i>GFP</i>	Bacterial resistance: Spc Plant resistance: Basta	This work
pGreenII0229PREP - pXLG2:: <i>Venus-</i> <i>XLG2</i>	Bacterial resistance: Kan Plant resistance: Basta	This work
pGreenII0229-JE - pLYK5:: <i>LYK5-mKate</i>	Bacterial resistance: Kan Plant resistance: Basta	Jan Erwig
pHG34 + p35S- <i>mCherry</i>	Bacterial resistance: Amp Plant resistance: Basta	Hassan Ghareeb
pHG77p-H2B- TagRFP-T-TQ2- LTI6b	Bacterial resistance: Kan Plant resistance: Hyg	Hassan Ghareeb
pGreenII-0229	Bacterial resistance: Kan Plant resistance: Basta	Hellens <i>et al.</i> (2000)
pRS426	Bacterial resistance: Amp Yeast marker: Uracil	Christianson <i>et al.</i> (1992)

2.1.6 Oligonucleotides

Oligonucleotides used in this study are given in Table 5.

Table 5. Primer used in this study.

Name	Sequence 5' -> 3'	Description
Primer used for cloning		
CM1	GTAACGCCAGGGTTTTCCAGTCACGACAA GCTTCAAAATGAAGCTAAAGATTTCTCTAATC	Forward primer for amplification of CERK1 with additional HindIII restriction site and pRS426 overhang
CM2	ACCAACACCATCTTGTTTACTTG	Reverse primer for amplifying CERK1 without transmembrane domain
CM3	TTCAAATCAAGTAAACAAGATGGTGTGGTG TCATCCTGATTATTCTTGATCAGCCGC	Forward primer for amplification of FLS2 transmembrane domain with overhang homologues to CERK1
CM4	CTTCGACTTATTCTTCCGGTAAGCATAATATA GAATCAGAACAAGAAGCAGGACAAGAAG	Reverse primer for amplification of FLS2 transmembrane domain with overhang homologues to CERK1
CM5	TATTATGCTTACCGGAAGAATAAGTCG	Forward primer for amplifying CERK1 without transmembrane domain
CM7	CTATACCAGCAATAACTCCAGCACCAACACC TCCAGGCACATAAACGATTCCATTCCCGG	Reverse primer for amplification of CERK1 for deletion of 16 amino acids
CM8	GGTGTGGTGCTGGAGTTATTGCTGGTATAG	Forward primer for amplification of CERK1 for deletion of 16 amino acids
CM9	GCGGATAACAATTTACACAGGAAACAGCTG GATCCCCCGGGCTGCAGGAATTCTAC	Reverse primer for amplification of CERK1 with additional SmaI restriction site and pRS426 overhang
CM12	AACTCCAGCACCAACTGATTTGAATGGTGGA AATGCACC	Reverse primer for deletion of 5 amino acids within the CERK1 extracellular stalk
CM13	CCACCATTCAAATCAGTTGGTGCTGGAGTTA TTGCTGGT	Forward primer for deletion of 5 amino acids within the CERK1 extracellular stalk

Table 5 (continued).

CM33	GATCCAAATGGTGCATTTCCACCATTCAAAA TCAACGCCTCTGATCTAATGGGAAAC	Forward primer for amplification of FLS2 extracellular stalk with overhang homologues to CERK1
CM34	TTTGAATGGTGGAAATGCACC	Reverse Primer for amplification of CERK1 ectodomain for FLS2 fusion
CM35	GATCCAAATGGTGCATTTCCACCATTCAAAA GCCACTTCTCGAAGAGAACCAGAGTC	Forward primer for amplification of FLS2 extracellular stalk and transmembrane domain with overhang homologues to CERK1
CM36	AGGCACATAAACGATTCCATTCCCGG	Reverse Primer for amplification of CERK1 ectodomain for FLS2 fusion
CM37	AACTCCGGGAATGGAATCGTTTATGTGCCTA TCAACGCCTCTGATCTAATGGGAAAC	Forward primer for amplification of FLS2 extracellular stalk and transmembrane domain with overhang homologues to CERK1
CM55	TGGTGCATTTCCACCATTCCGAGCAAGTAAA CAAGATGGTGTG	Forward primer for replacement of CERK1 KS with AA
CM56	CAACACCATCTTGTTTACTTGCTGCGAATGG TGGAATGCACCA	Reverse primer for replacement of CERK1 KS with AA
CM57	GAATGGTGGAAATGCACCATTTGG	Reverse primer for CERK1 KS deletion
CM58	AGAGATCCAAATGGTGCATTTCCACCATTCA GTAAACAAGATGGTGTGGTGCTGGAGTTAT TG	Forward primer for CERK1 KS deletion
CM82	GTAACGCCAGGGTTTTCCAGTCACGACGG GCGCGCCCTGGAGGAGCATAGTGTGATTA TTTACGAGAGTG	Forward primer for amplification of the XLG2 promoter with additional pRS426 homology and Ascl site
CM83	GCGGATAACAATTTACACAGGAAACAGCG GATCCTCAAGAGGACGAGCTGGCCTCTATG CTAGTAG	Reverse primer for amplification of XLG2 with additional pRS426 homology and BamHI site

Table 5 (continued).

CM92	GGTGAACAGCTCCTCGCCCTTGCTCACCAT CTTCTTACCCAATCAAGCACACATACAAACC C	Reverse primer for amplification of <i>XLG2</i> promoter with overhang homologues to Venus
CM93	AGGTAATAACTTTCTTATAACTGCAGCCATC GCTCCAGCGCCCTTGACAGCTCGTCCATG CCGAGAGTGATCCC	Reverse primer for amplification of Venus with homology to <i>XLG2</i> with additional YAGA linker
CM94	ATGGCTGCAGTTATAAGAAAGTTATTACCTTT C	Forward primer for <i>XLG2</i> amplification
JE23	ATGGTGAGCAAGGGCGAGGAGC	Forward primer for Venus amplification
EP209	ACTGCAGGCGCGCCTGGAGGAGCATAGTGT GATTATTTAC	Forward primer for generation of genomic <i>XLG2</i> construct for complementation containing Ascl site
EP210	TGAGCTGGATCCTCAAGAGGACGAGCTGGC CTCTATG	Reverse primer for generation of genomic <i>XLG2</i> construct for complementation containing BamHI site
EP314	cacc TGGAGGAGCATAGTGTGATTATTTAC	Forward primer for generation of <i>XLG2</i> -GFP and <i>XLG2</i> E293K-GFP with cacc gateway site
EP315	AGAGGACGAGCTGGCCTCTATGC	Reverse primer for generation of <i>XLG2</i> -GFP and <i>xlg2</i> E293K-GFP without <i>XLG2</i> stop codon
Primer used for sequencing		
35S GC359	CTATAAGAACCCTAATTCCCTTATCTG	35S terminator reverse
CM73	GATTCTGAACTTCGACAAGTCATGAATCTC	Forward dCAPS primer introducing containing a partly XhoI restriction site for genotyping <i>xlg2</i> E293K
CM75	GTAGTTAAAAATCCTTCAAATTC	<i>AGB1</i> sequencing
CM76	CAATAAGACCAAACCTATATGTTG	<i>AGB1</i> sequencing
CM77	GTTTCAGGTGATCAAACCTTGATCTTATGGG	<i>AGB1</i> sequencing
CM78	CTTGCTCGGATTTGAAAACCACTACC	<i>AGB1</i> sequencing
CM74	CCAATAGTGTCCGGGTTTTAGCTTCTTGG	Reverse dCPAPs primer for genotyping <i>xlg2</i> E293K

Table 5 (continued).

EP164	GACTGGTGATTTTTGCGGACTC	35S terminator reverse
CM81	CATGAATGTATCTTCACACTAC	<i>XLG2</i> sequencing
EP219	CCTAACCCGCGTTGACGGCAAG	<i>XLG2</i> sequencing
EP221	CCGGGAAATAACCAAGCCAGAG	<i>XLG2</i> sequencing
EP233	AACTGGCAGAGAGAACACAGC	<i>XLG2</i> sequencing
MS226	GGCGCTTGAGCATTCTTGAACAC	<i>XLG2</i> sequencing
JH15	CCGGTAAGCATAATATACGATA	<i>CERK1</i> sequencing
MS122	TCGAAACAGTTCTTGGCGGAAC	<i>CERK1</i> sequencing
MS148	TGGACCTACCTTTCACAGCATTTC	<i>PAD4</i> sequencing
MS149	ACGGACGTGATGGCATACAAAC	<i>PAD4</i> sequencing
MS150	CCACCATTTGGAATATGTCATTG	<i>PAD4</i> sequencing
MS151	ACGCCACTTGTGTCATCGTTAGAG	<i>PAD4</i> sequencing
MS152	CACCGAGGAACATCAGAGGTACG	<i>PAD4</i> sequencing
MS153	ACATGAGAACTCTTTGCACATTG	<i>PAD4</i> sequencing
MS154	GCTACATCAGTCCCCTATTTATATC	<i>SID2</i> sequencing
MS155	CCTTGCCTTTACAACAAATTGG	<i>SID2</i> sequencing
MS156	TAGTGTGGCCATGCTAAG	<i>SID2</i> sequencing
MS157	AAGACCTACCGTGTTTCC	<i>SID2</i> sequencing
MS158	TGGCTAGCACAGTTACAG	<i>SID2</i> sequencing
MS159	AGGTCCCGCATAACCTCCTATC	<i>SID2</i> sequencing
MS160	ATTGGCTGCTCTGCATCCAAC	<i>SID2</i> sequencing
MS161	AAAGGCCCAAGCATTCTACGG	<i>SID2</i> sequencing
MS164	GTCTCCAATAGCCAAAGAGTC	<i>EDS1</i> sequencing
MS165	GCAAGAACATGAGGCAAAG	<i>EDS1</i> sequencing
MS166	AATGGAGCCGGTTCTTTGTG	<i>EDS1</i> sequencing
MS167	GCTCAACTAATCTGCGGTATCG	<i>EDS1</i> sequencing
MS168	CGAGGTGCTTGGTTTAATG	<i>EDS1</i> sequencing
MS169	TAGTGCTCCGTTTGGTTAG	<i>EDS1</i> sequencing
UL154	TCTTCTTCCCCACAGAGCAACGACG	<i>CERK1</i> sequencing
UL166	TTCCAGGCACATAAACGATTCC	<i>CERK1</i> sequencing
UL167	TTACGTATCCGTTTCGTCTGAAG	<i>CERK1</i> sequencing
Primer used for semi-quantitative RT-PCR		
EP13	AGACTCATACACTCTGGTGGGCCTT	<i>PR1</i> fw
EP14	CGTCCTTTATGTACGTGTGTATGCA	<i>PR1</i> rev
EP15	TAATCATCATGGCTAAGTTTGCTTC	<i>PDF1.2</i> fw
EP16	GCATGTCATAAAGTTACTCATAGAGTG	<i>PDF1.2</i> rev
Act fw	TGCGACAATGGAAGTGAATG	<i>Actin</i> fw
Act rev	GGATAGCATGTGGAAGTGCATAC	<i>Actin</i> rev

2.1.7 Enzymes

2.1.7.1 Restriction endonucleases

Restriction endonucleases were obtained from New England BioLabs (Frankfurt/Main, Germany) or Thermo Scientific™ (Life Technologies GmbH, Darmstadt, Germany) and were used according to the manufacturer's manual.

2.1.7.2 Nucleic acid modifying enzymes

Homemade Taq polymerase was used for colony and genotyping PCRs. For cloning, iProof High-Fidelity DNA Polymerase (BioRad, München, Germany) was used.

2.1.8 Chemicals

Chemicals were obtained from Bio-Rad (Munich, Germany), Difco (Heidelberg, Germany), Duchefa (Haarlem, Netherlands), Thermo Scientific™ (Waltham, USA), GE Healthcare (Munich, Germany), Macherey Nagel (Düren, Germany), Merck (Darmstadt, Germany), New England BioLabs (NEB) (Frankfurt/Main, Germany), Roche (Mannheim, Germany), Roth (Karlsruhe, Germany), Serva (Heidelberg, Germany), Sigma-Aldrich (Deisenhofen, Germany) or VWR™ (Darmstadt, Germany).

2.1.8.1 Antibiotics

The following antibiotic stock solutions were used. Stock solutions were filter sterilized and stored at -20 °C. For the final working concentration, stocks were used at a dilution of 1:1000.

Ampicillin	100 mg/ml in ddH ₂ O
Gentamycin	15 mg/ml in ddH ₂ O
Phosphinothricin	25 mg/ml in ddH ₂ O
Rifampicin	20 mg/ml in methanol
Spectinomycin	100 mg/ml in ddH ₂ O
Tetracyclin	5 mg/ml in ethanol

2.1.8.2 Media

Media were sterilized by autoclaving at 121 °C for 20 minutes. Antibiotics were added after media were cooled down. The following media were used in this work:

½ Murashige and Skoog (MS) medium

MS powder: 2.2 g/l

Sucrose: 0.5 %

The pH was adjusted to pH 5.7 with KOH. For ½ MS plates, 4.5 g/l plant agar were added. Phosphinothricin (25 µg/µl) was added for selection of transgenic plants expressing phosphinothricin acetyltransferase (PAT) conferring BASTA resistance.

Lysogeny broth (LB) medium:

Peptone: 10 g/l

Yeast extract: 5 g/l

NaCl: 10 g/l

For LB agar plates, 1.5 % (w/v) bacterial grade agar was added before autoclaving.

Yeast extract-peptone dextrose (YPD) medium:

Yeast extract: 10 g/l

Peptone: 20 g/l

Glucose 20 g/l

For YPD agar plates, 1.5 % (w/v) bacterial grad agar was added before autoclaving.

Synthetic complete (SC) medium (-Uracil, +Glucose):

Yeast nitrogen base (YNB)

w/o amino acids: 13.4 g/l (2x)

Amino acid drop-out mix (-Ura): 4.0 g/l (2x)

Adjust to ph 5.6 with NaOH

Agar: 40.0 g/l (2x)

Glucose: 40.0 g/l (2x)

Glucose was prepared and autoclaved separately from the remaining components. After autoclaving, the glucose solution and the medium prepared with the other components were mixed in a 1:1 ratio before pouring plates.

2.1.8.3 Buffers and solutions

Buffers and solutions used in this work are listed in Table 6. Ultra-pure water was used for the preparation of all buffers and solutions. Sterilization was either carried out by autoclaving at 121 °C for 20 minutes or by filter-sterilization.

Table 6. Buffers used in this study.

Buffer for bacterial infiltration		
Agrobacterium	MgCl ₂	10 mM
Infiltration medium	Acetosyringone	150 µM
PCR and gel electrophoresis		
TAE (50x)	Tris base	242 g/l
	Glacial acetic acid	51.1 ml/l
	EDTA (0.5 M; pH 8.0)	100 ml/l
Homemade <i>Taq</i> buffer (10x)	Tris	100 mM
	KCl	500 mM
	MgCl ₂	15 mM
	Triton X-100	1 %
	Adjust to pH 9.0	
TE buffer	Tris-HCl, pH 8.0	2 M
	EDTA	1 mM
DNA loading dye (6x)	Sucrose	4 g
	EDTA (0.5M)	2 ml
	Bromophenol blue	25 mg
	Add ddH ₂ O to 10 mL	
Extraction of genomic DNA		
Extraction buffer	Tris-HCl, pH 7.5	0.2 M
	NaCl	1.25 M
	EDTA	25 mM
	SDS	0.5 %
Plasmid preparation (alkaline lysis)		
P1 buffer	Tris-HCl, pH 8.0	50 mM
	EDTA, pH 8.0	10 mM
	RNase A (DNase free)	100 µg/µl
	Storage at 4 % after RNase A addition	
P2 buffer	NaOH	200 mM
	SDS	1 %
P3 buffer	KOAc	3 M
	Acetic acid	2 M

Table 6 (continued).

Buffers for preparation of chemically competent <i>E.coli</i> cells		
CCMB80 buffer	KOAc pH 7.0	10 mM
	CaCl ₂	80 mM
	MnCl ₂	20 mM
	MgCl ₂	10 mM
	Glycerol	10% (v/v)
	Adjust to pH 6.4	
	Filter sterilize before use	
Buffers for cloning by homologous recombination in yeast		
Li-PEG buffer	Lithium acetate	100 mM
	Tris-HCl, pH 8.0	10 mM
	EDTA, pH 8.0	1 mM
	PEG 4000	50 % (w/v)
	Autoclave before use	
SORB buffer	Lithium acetate	100 mM
	Tris-HCl, pH 8.0	10 mM
	EDTA, pH 8.0	1 mM
	Sorbitol	1 M
	Autoclave before use	
Solutions for mass spectrometry analysis		
	Ammonium bicarbonate (ABC)	100 mM
	Iodoacetamide (IAA)	500 mM
	D-1,4-dithiothreitol	100 mM
ABC/DTT solution	mix 1 vol DTT with 4 vol of ABC	
	NaCl	625 mM
	Tris-HCl pH 8.0	100 mM
	Ammonium formate (AF) pH 10	20 mM
Trypsin stock solution	Trypsin	100 ng/μl
	HCl (MS grade, Promega, Madison, USA)	10 mM
Protein extraction, SDS PAGE and Immunoblotting		
CERK1 extraction buffer	Sucrose	250 mM
	HEPES-KOH, pH 7.5	100 mM
	Glycerol	5 % (v/v)
	Na ₄ P ₂ O ₇	50 mM
	Na ₂ MoO ₄	1 mM
	NaF	25 mM
	EDTA	10 mM
	DTT	1 mM
	Triton X-100	0.5 % (v/v)
	Add PIC (1:100) prior to use	

Table 6 (continued).

Protease inhibitor cocktail (PIC, 100x)	4-(2-aminoethyl)benzenesulfonyl fluoride hydrochloride (AEBSF)	1 g
	Bestatin hydrochloride	5 mg
	Pepstatin A	10 mg
	Leupeptin hemisulfate	100 mg
	E-64 (trans-epoxysuccinyl-L-leucylamido-(4-guanidino)butane)	10 mg
	Phenanthroline (1, 10-phenanthroline monohydrate)	10 g
	DMSO	Ad 2 ml
SDS sample Buffer (4x)	Tris-HCl, pH 6.8	200 mM
	DTT	400 mM
	SDS	8 %
	Glycerol	40 %
	Bromophenol blue	0.1 %
Stacking gel	Tris-HCl, pH 6.8	125 mM
	SDS	0.1 %
	acrylamide/bis-acrylamide, 37.5:1	5 %
Resolving gel (8 %)	Tris-HCl, pH 8.8	375 mM
	SDS	0.1 %
	acrylamide/bis-acrylamide, 37.5:1	8 %
Resolving gel (10 %)	Tris-HCl, pH 8.8	375 mM
	SDS	0.1 %
	acrylamide/bis-acrylamide, 37.5:1	10 %
Stacking gel buffer	Tris-HCl, pH 6.8	150 mM
	SDS	0.12 %
Resolving gel buffer (8 %)	Tris-HCl, pH 8.8	525 mM
	SDS	0.14 %
Resolving gel buffer (10 %)	Tris-HCl, pH 8.8	575 mM
	SDS	0.15 %
Mixtures for frequent use in SDS-PAGE and Immunoblotting		
Stacking gel buffer	Tris-HCl, pH 6.8	125 mM
	10 % SDS	3.06 ml
	H ₂ O	208.36 ml
Resolving gel buffer (8 %)	1 M Tris, pH 8.8	130.9 ml
	10 % SDS	3.46 ml
	H ₂ O	115.64 ml
Resolving gel buffer (10 %)	1 M Tris, pH 8.8	143.6 ml
	10 % SDS	3.79 ml
	H ₂ O	102.53 ml

Table 6 (continued).

Stacking gel (per gel)	Stacking gel buffer	4.08 ml
	30% acrylamide/bis-acrylamide, 37.5:1	0.83 ml
	TEMED	0.025 ml
	10% APS	0.0025 ml
Resolving gel (8 %) (per gel)	Resolving gel buffer (8 %)	7.2 ml
	30% acrylamide/bis-acrylamide, 37.5:1	2.7 ml
	TEMED	0.1 ml
	10% APS	0.006 ml
Resolving gel 10 % (per gel)	Resolving gel buffer (10 %)	6.6 ml
	30 % acrylamide/bis-acrylamide, 37.5:1	3.3 ml
	TEMED	0.1 ml
	10 % APS	0.004 ml
SDS running Buffer (10x)	Tris	30.28 g/l
	Glycine	144.13 g/l
	SDS	10 g/l
Transfer buffer (20x)	Tris	1 M
	Boric acid	1 M
	Adjust pH to 8.3	
TBS-T (20x)	NaCl	3 M
	Tris-HCl, pH 8.0	200 mM
	Tween-20	1 %
Alkaline phosphatase (AP) buffer	Tris, pH 9.5	100 mM
	NaCl	100 mM
	MgCl ₂	50 mM
Staining solution for PVDF membranes	Methanol	45 % (v/v)
	Acetic acid	10 % (v/v)
	Coomassie R250	0.05 % (w/v)
Destaining solution for PVDF membranes	Methanol	45 % (v/v)
	Acetic acid	10 % (v/v)
	Add H ₂ O	
Buffer stocks were diluted to 1x with ddH ₂ O before use		

2.1.8.4 Antibodies

The following table lists the antibodies used in this work. Antibodies were aliquoted and stored at -80 °C. Aliquots in use were stored at 4 °C. Secondary antibodies are conjugated to alkaline phosphatase (AP).

Table 7. Antibodies used in this study.

Antibody	Source	Dilution	Reference
α -CERK1	Rabbit, polyclonal	1:3000	Eurogentec Deutschland GmbH, Köln, Germany
α -GFP	Rat, monoclonal	1:3000	Chromotek GmbH, Planegg-Martensried, Germany
α -FLS2	Rabbit, polyclonal	1:10000	Agrisera, Vännäs, Sweden
α -BRI1	Rabbit, polyclonal	1:5000	Agrisera, Vännäs, Sweden
α -Rabbit (AP conjugated)	Goat, polyclonal	1:5000	Sigma-Aldrich Chemie GmbH, Taufkirchen, Germany
α -Rat (AP conjugated)	Rabbit, polyclonal	1:5000	Sigma-Aldrich Chemie GmbH, Taufkirchen, Germany

2.2 Methods

2.2.1 Plant methods

2.2.1.1 Plant cultivation

Seeds were frozen (-20 °C, 2-3 days) to eliminate potential pest contaminations before they were sown. The seeds were placed directly on damp soil (Frühstorfer Erde, Type T25, Str1, Archut) which was steam-sterilized before it was filled into plant pots. To promote germination, the pots were covered with a transparent lid and transferred to growth chambers (Johnson Controls, Milwaukee, WI, USA) with short day (SD) conditions (8 h light, 22 °C, 140 mol m⁻² sec⁻¹, 65 % rel. humidity). After germination, lids were removed. To induce flowering, plants were transferred to long day (LD) conditions (16 h light, 22 °C, 140-160 μ mol m⁻² sec⁻¹, 65 % rel. humidity).

Nicotiana benthamiana seeds were treated as described for *Arabidopsis*. However, *Nicotiana* seeds were immediately placed under LD conditions (16 h light, 26 °C, 200 μ mol m⁻² sec⁻¹, 65 % rel. humidity) to ensure rapid growth.

For in-vitro cultivation of plants, *Arabidopsis* seeds were placed in reaction tubes and washed with 70 % ethanol three times in a sterile hood. During these washing steps, reaction tubes were inverted several times to ensure proper washing of the seeds. Ethanol was removed between each washing step. After that, a final washing step with 96 % ethanol was performed. Tubes were put on a tube rack to allow sinking of the seeds. Ethanol was

removed and seeds were put on a Whatman® paper placed in a petri dish to allow evaporation of the ethanol.

2.2.1.2 Crossing of *Arabidopsis thaliana* plants

For crossing of *Arabidopsis* plants, carpels of closed buds were uncovered by removing all other parts of the flowers using magnifying glasses and fine tweezers. Stamina of the donor line (male parent) were collected and used to pollinate the stigmas of the receptor line (female parent). Crossings were performed both ways, with each of the parental lines being acceptor and donor to exclude effects of the respective parental genotypes.

2.2.1.3 Stable transformation of *Arabidopsis thaliana* (floral dip)

The generation of stably transformed *Arabidopsis* plants was performed by the 'floral dip' method (Clough & Bent, 1998). To induce flowering, *Arabidopsis* plants were transferred from SD to LD conditions. To induce the growth of additional shoots, the first developed apical meristem was removed. Transformed *Agrobacterium tumefaciens* strains were grown (28 °C) in 5 ml LB containing the appropriate antibiotics overnight. This culture was used to inoculate 300 ml LB containing appropriate antibiotics which were incubated at 28 °C with shaking for 1-2 days until the culture reached an $OD_{600} > 1.6$. *Agrobacterium* cells were pelleted (4000 xg, 20 min, RT) and resuspended in 300 ml 5 % glucose containing 0.05 % Silwet-77. Plants were then dipped into the *Agrobacterium* solution until the inflorescence was completely submerged. This was repeated 2 - 3 times. Plants were then transferred to a plastic bag to ensure high humidity and were kept in the laboratory over night. The next day, the plastic bag was removed and plants were transferred back to the growth chamber (LD conditions).

2.2.1.4 Transient transformation of *Nicotiana benthamiana*

Transformed *Agrobacterium tumefaciens* strains were used to inoculate 5 ml LB containing the appropriate antibiotics and were grown at 28 °C overnight. Cells were pelleted (4000 xg, 20 min, RT) and resuspended in 1 ml infiltration buffer. OD_{600} was measured and cultures were diluted to an OD_{600} of 0.4. Cultures were left on the bench for several hours before use. 4 week old *Nicotiana benthamiana* plants were watered several hours before use and placed on the bench covered by a lid to increase humidity. A 1 ml needle-less syringe was used to infiltrate whole leaves and infiltrated areas were marked. Plants were transferred back to the

growth chamber (LD conditions). After 2 – 3 days, samples for protein extraction were taken or leaves were analyzed by confocal laser scanning microscopy.

2.2.1.5 Selection of transgenic *Arabidopsis* plants on soil

Surface-sterilized T1 seeds were sown densely on damp soil and covered with a plastic lid. After germination, seedlings were sprayed with a 1:1000 diluted herbicide BASTA® (200 g/l glufosinate [phosphinothricin ammonium] solution, Bayer CropScience AG, Monheim, Germany) every two days for a total of three times. The surviving and therefore transformed plants were transferred into single pots.

2.2.1.6 In-vitro selection of transgenic *Arabidopsis* plants

To select or analyse the segregation pattern of transgenic *Arabidopsis* plants, ethanol sterilized seeds were spread sparsely on ½ MS plates containing 25 µg/ml phosphinothricin. Plants were grown under SD conditions until a clear difference between resistant and non-resistant plants became visible. Resistant plants were transferred onto soil for further propagation.

2.2.1.7 Chitin treatment of *Arabidopsis* plants

For investigation of the chitin-induced band-shift of CERK1, 2-6 *Arabidopsis* leaves were collected and divided into two 15 ml falcons, one half for mock treatment and the other half for chitin treatment. The leaves were fully covered with water. 10 mg Polymeric chitin (shrimp shell chitin) were transferred to a 1 ml reaction tube. 100 µl H₂O were added and the mixture was ground until no chitin chunks were visible anymore. 900 µl H₂O were added to reach a final stock concentration of 10 mg/ml. Chitin was then added to one half of the samples to a final concentration of 100 µg/ml. The falcons were then placed in a desiccator and a vacuum was applied for 5 minutes. Vacuum was released leading to leaf infiltration. Leaves were incubated for 12 minutes and then blotted on paper tissue for drying. The leaves were transferred to 1.5 ml reaction tubes, frozen in liquid nitrogen and stored at -80 °C.

2.2.1.8 Cultivation and inoculation of *Blumeria graminis* f.sp. *hordei*

Cultivation of the obligate biotrophic ascomycete *Blumeria graminis* f.sp. *hordei* (Bgh) was performed on barley plants (*Hordeum vulgare* cv. Golden Promise) under short day

conditions (16 h light, 22 °C, 140-160 $\mu\text{mol m}^{-2} \text{sec}^{-1}$, 65 % rel. humidity) in a growth cabinet (CLF Plant Climatics, Wertingen, Germany). 6 day old barley plants were inoculated with *Bgh* spores formed on older infected barley plants. After one week, they were ready to be used for inoculation of *Arabidopsis* plants. For phenotype investigation of *cerk1-4* and *cerk1-4* suppressor lines, 5 – 6 week old plants were placed in an inoculation tower and were inoculated evenly by shaking the infected barley plants over the tower. For macroscopical analysis, plants were photographed 7 days after infection.

2.2.2 Biochemical methods

2.2.2.1 Protein extraction

2.2.2.1.1 Standard preparation of total protein extracts

50 – 100 mg plant material were harvested in a 1.5 ml reaction tube and frozen in liquid nitrogen. A spatula of quartz sand and 300 μl CERK1 extraction buffer were added. A drill equipped with a glass pestel (IKA-Werke GmbH & Co. KG, Staufen, Germany) fitting 1.5 ml tubes was used to grind the plant material thoroughly. Afterwards, additional 700 μl of CERK1 extraction buffer were added and samples were centrifuged to sediment cell debris (15 min, 17000 xg, 4 °C). The supernatants were transferred to new reaction tubes and kept on ice. Protein concentrations were measured by the Bradford method (2.2.2.4) and were adjusted to the concentration of the lowest sample using CERK1 extraction buffer. For immunoblotting, equalized samples were mixed with 4x SDS loading dye and stored at -20°C until use.

2.2.2.1.2 Preparation of total protein extracts with SDS

To extract proteins that are not sufficiently soluble in CERK1 extraction buffer and/or prevent any degradation processes during extraction, proteins were extracted with 2x SDS loading dye. This method excludes determination of protein concentrations. Therefore, a defined amount of thoroughly ground plant material was transferred to a reaction tube. 200 μl 2x SDS buffer were added per 100 mg plant material. A spatula of quartz sand was added and samples were ground with a glass pestil. Samples were centrifuged (10 min, 17000 xg, RT) and supernatants were transferred to new reaction tubes and stored at -20 °C until use in immunoblots.

2.2.2.2 Chitin pull-down

Chitin pull-downs were performed to enrich chitin-binding proteins from protein extracts. Therefore, chitin magnetic beads (NEB, Frankfurt/Main, Germany) were washed three times and finally resuspended in ultra-pure H₂O. 20 µl chitin beads were added to protein extracts containing 1 – 1.5 mg total protein. Samples were then incubated on a wheel for 45 minutes at 4 °C. Reaction tubes were then transferred to a magnet rack to pellet chitin magnetic beads. The supernatants were discarded and the beads were washed with 1 ml ice-cold TBS-T. This step was repeated twice. A last washing step was performed using ice-cold ultra-pure water. Samples were centrifuged (1 min, 10000 xg, 4 °C) to collect residual water at the bottom of the reaction tubes. The reaction tubes were transferred to a magnet rack and water was removed using a pipette. 20 µl 1.5x SDS sample buffer were added and samples were centrifuged to mix beads with SDS buffer. Samples were then stored at -20 °C.

2.2.2.3 Microsomal preparation

As a first step, a protein extract was prepared with CERK1 extraction buffer without Triton X-100. For small scale preparations, the extraction was performed with a glass pestil as described in Chapter 2.2.2.1.1. For larger scale microsomal preparations, the plant material was ground to a fine powder with mortar, pestle and quartz sand under liquid nitrogen. Then the CERK1 extraction buffer lacking Triton X-100 was added at 2-3 ml per g plant material. Sedimentation of cell debris was performed at 2000g at 4 °C for 5 minutes. 60 µl of supernatant were taken as total protein extract and mixed with 4x SDS buffer. The remaining supernatant was transferred to ultracentrifugation tubes (Eppendorf, Hamburg, Germany) and centrifuged at 100000 xg in a Sorvall ultracentrifuge (Thermo Scientific™, Waltham, USA) for 1 hour at 4 °C. The supernatant was collected. Soluble proteins can be found in this fraction. The remaining pellet was washed with CERK1 extraction buffer without Triton-X 100 and was centrifuged again (1 h, 100000 xg, 4 °C). The final pellet was resuspended with CERK1 extraction buffer containing Triton-X 100 to dissolve membrane bound proteins (microsomal fraction). The microsomal fraction was transferred to new 1.5 ml reaction tubes. The protein concentration of microsomal and soluble fractions was determined by the Bradford method. The fractions were then either used for chitin pull downs or mixed with 4x SDS loading dye and stored at -20 °C until further use.

2.2.2.4 Determination of protein concentration by the Bradford method

In order to determine the protein concentration of extracts, a method based on (Bradford, 1976) was used. A calibration curve using determined concentrations of bovine serum albumin (BSA) was generated. For this, 0 μ l, 3 μ l, 7 μ l, 10 μ l and 15 μ l of a 1 mg/ml BSA solution was pipetted into cuvettes. 1 ml Bradford solution (Roti®-Quant, Roth, Karlsruhe, Germany) (diluted 1:5 with H₂O) was added and incubated for 5 minutes at room temperature. Absorbance at 595 nm was measured using a WPA Biowave II photometer (Biochrom, Berlin, Germany). The absorption was plotted against the protein concentration to generate the calibration curve. Samples (typically 3 μ l) were pipetted in duplicate into cuvettes, 1 ml Bradford solution was added and after 5 min of incubation, absorption was measured at 595 nm. The calibration curve was used to calculate the protein concentrations of each sample.

2.2.2.5 SDS-polyacrylamide gel electrophoresis (SDS-PAGE)

Proteins were separated according to their molecular mass by SDS-PAGE. The Mini-PROTEAN 3 system (BioRad, Munich, Germany) was used for casting of discontinuous gels. The system was assembled according to manufacturer's instructions. Resolving gels containing 8 % or 10 % acryl amide were poured between two glass plates spaced 1.5 mm apart and overlaid with isopropanol to remove air bubbles. After polymerization, isopropanol was removed and the stacking gel was poured on top of the resolving gel and a comb for formation of samples pockets was inserted. After the gels were completely polymerized, they were either used directly or wrapped in damp paper tissue and stored in plastic bags at 4 °C. Gels were placed in a PROTEAN 3 vertical gel chamber which was filled with 1x SDS running buffer. The comb was removed and gel pockets were rinsed with running buffer. Samples were mixed with SDS sample buffer and boiled at 95 °C for 3 minutes. Samples were then loaded in the sample pockets. PageRuler™ Prestained Protein Ladder Plus (Thermo Scientific™, Waltham, USA) was used as size standard. SDS PAGE was then performed at 30 mA until the desired separation was achieved. Gels were then used for immunoblot analysis (2.2.2.6).

2.2.2.6 Immunoblotting

For the transfer of proteins from a SDS-polyacrylamide gel to a PVDF membrane, the Mini Trans-Blot® system (BioRad, Munich, Germany) or Trans-Blot® system (BioRad, Munich,

Germany) was used, depending on the number of gels to be blotted. The glass plates containing the SDS-gel were disassembled and the stacking gel was removed. Next, sponges and Whatman paper were thoroughly soaked in blotting buffer and a “sandwich” was assembled on the the cathode side of the blotting cassette. First, a sponge was placed on the cassette, followed by layers of Whatman® paper. The resolving gel was then placed on the Whatman® paper and a methanol-activated PVDF membrane was arranged on top of the gel. After adding another Whatman® paper and sponge, air bubbles were removed by rolling with a 50 ml tube. Then the blotting cassette was closed and placed into the blotting tank (BioRad, Munich, Germany) which was then filled to the top with 1x blotting buffer. Blotting was carried out at 75 V for 2 hours. The blotting cassettes were disassembled and PVDF membranes were incubated in 1x TBS-T containing 3 % milk powder for 1 hour to block unspecific binding sites. After blocking, membranes were incubated with primary antibody solution (primary antibody diluted in 1x TBS-T containing 3 % milk powder) and were incubated over night at 4 °C with shaking. The next day, membranes were washed 5 times for at least 10 minutes with 1x TBS-T containing 3 % milk powder. Membranes were then incubated with secondary antibody (secondary antibody diluted in 1x TBS-T containing 3 % milk powder) solution for 2 hours at room temperature. Membranes were washed 5 times for at least 10 minutes with 1x TBS-T. Afterwards, membranes were incubated for 10 minutes in AP buffer. Membranes were then incubated with Immun-Star™ AP substrate (BioRad, Munich, Germany) for 5 minutes and then placed in a plastic bag, which was subsequently transferred to an exposure cassette. The membranes were then exposed to an X-ray Screen Film Blue Sensitive (CEA, Hamburg, Germany) to detected chemiluminescence.

To enhance signal intensity and reduce background signals of GFP-immunoblots, the SuperSignal™ Western Blot Enhancer (Thermo Scientific™, Westham, USA) was used according to manufacturer’s instructions.

2.2.2.7 Coomassie staining of PVDF membranes

For visualization of total protein content, PVDF membranes were stained with Coomassie Brilliant Blue. Membranes were placed in a plastic box and incubated with staining solution until they were fully stained. Staining solution was decanted and membranes were rinsed with water. To remove background staining membranes were incubated with destaining solution until only stained protein bands remained. The staining solution was removed, membranes were rinsed with water and placed on a paper tissue under a fume hood to dry.

2.2.2.8 Mass spectrometry analysis

Mass spectrometry analysis (Sample preparation and LC-ESI-MS analysis) were performed by Dr. Andrzej Majcherczyk (Georg-August University of Göttingen) according to the following protocol (provided by Dr. Andrzej Majcherczyk). Data analysis was performed by Christopher Meusel.

Sample preparation

Samples from *Arabidopsis* cell culture supernatants and *Arabidopsis* apoplastic wash fluids in 15 ml Falcon-tubes were frozen at -80 °C and freeze-dried for about 5 days at -30 °C. Dry samples were re-dissolved in 80 µl ABC/DTT, centrifuged at 2000 rpm for 3 minutes and 75 µl liquid was transferred to a new 1.5 ml reaction tube. 75 µl of TFE were added to extract proteins and precipitate polysaccharides. Samples were shaken for 15 minutes, sonicated for 5 minutes, shaken for 15 minutes again and incubated for 30 minutes at 60 °C. After centrifugation for 10 minutes (16000 xg), 100 µl supernatant were carefully collected into a new 1.5 ml LoBind tube (Eppendorf, Hamburg, Germany) Proteins were alkylated with IAA (5 µl IAA stock solution) in dark for 30 minutes and thereafter diluted with 50 µl water.

Protein purification was performed by chloroform/methanol precipitation according to Wessel and Fluegge (1984). Protein precipitates were suspended in 50 µl Tris-HCl pH 8.0 by careful sonication for about 3 minutes and 5 µl trypsin stock solution were added to each sample (protein to trypsin ratio was about 1:100). Protein digestion was performed overnight at 37 °C in a water bath.

Thereafter, the digestion was stopped by addition of 20 µl of 20 mM AF (pH 10) and samples were vortexed and centrifuged for 20 minutes at 16000 xg. 60 µl of peptide solutions were immediately purified by StageTips (Rappsilber et al., 2007) prepared from 3 layers of 3M-C18 filter (3M, Minnesota, USA). Purification was performed with 20 mM AF pH 10 and peptides eluted with 60 % acetonitrile (Ultima LC-MS grade, Fisher Scientific, Schwerte, Germany) in 20 mM AF buffer. After drying for 10 minutes in vacuum, concentrated peptides were stored at -20 °C or immediately dissolved in 2 % acetonitrile in water with 0.1 % formic acid (all solvents were Ultima LC-MS quality) and analyzed by LC-ESI-MS. Peptide concentration was measured by Micro-BCA (Thermo Scientific™, Waltham, USA) method using BSA-digest as calibration standard.

LC-ESI-MS analysis

Peptides were analyzed by trap & elute mode (Eksigent 420, Sciex, Framingham, USA) using 2.5 cm (Ø 100 µm) pre-column packed with 5 µm Reprosil-Pur C18-AQ (Dr. Maisch GmbH, Ammerbuch, Germany) and 30 cm (Ø 50 µm) analytical column packed with 3 µm

Reprosil-Gold C18. Peptide samples (5µl corresponding to 0.1 - 0.2 µg) were separated in a gradient mode at 260 nl/minute solvent flow. Solvent A consisted of 100% water with 0.1% formic acid and solvent B of 100% acetonitrile with 0.1% formic acid. Peptide elution from the analytical column was performed in a gradient of solvent B: initially 5%, 100 minutes to 35 %, 20 minutes to 50 % and 2 minutes to 95 %.

Mass spectrometry system consisted of Hybrid Quadrupole-TOF LC/MS/MS Mass Spectrometer TripleTOF 5600+ (Sciex, Framingham, USA), nano-spray source Nanospray III (Sciex, Framingham, USA) and Analyst 1.7 software (Sciex, Framingham, USA). MS spectra in a positive mode were detected in a range of 300 to 2000 Da and 30 most intensive ions with charge 2+ to 5+ were fragmented in a MS/MS mode. Analysis of MS spectra and protein identification was performed by ProteinPilot 5.0 (Sciex, Framingham, USA), and database consisted of *Arabidopsis* TAIR10 (<https://phytozome.jgi.doe.gov>) protein sequences combined with a common contaminants dataset (Sciex, Framingham, USA). Carbamidomethylation of cysteine and trypsin cleavage were set as fixed modifications and searches were performed in FDR mode with thorough settings including biological modifications and amino acid substitutions.

Data analysis

Data obtained by mass spectrometry was analyzed using ProteinPilot 5.0 (Sciex, Framingham, USA) and Microsoft Excel 2007 (Microsoft, Redmond, USA). Only proteins were considered of which at least 2 peptides were found and which had an unused score of at least 2.

2.2.3 Molecular biology methods

2.2.3.1 Preparation of genomic DNA from *Arabidopsis* leaves

One small *Arabidopsis* leaf was harvested and transferred to a 1.5 ml reaction tube. 300 µl warm extraction buffer were added and a plastic pestle driven by an IKA drill (IKA-Werke GmbH & Co. KG, Staufen, Germany) was used to disrupt the plant tissue. The sample was centrifuged (5 min, 17000 xg, RT) and the resulting supernatant was transferred to a new reaction tube which was filled with 300 µl isopropanol. After mixing by pipetting up and down the sample was incubated for 5 minutes at room temperature. After an additional centrifugation step (5 min, 17000 xg, RT) the supernatant was carefully and completely

removed and the pellet was air-dried. The pellet was resuspended in 50 μ l H₂O and stored at -20 °C.

2.2.3.2 Preparation of total RNA from *Arabidopsis* leaves

Arabidopsis leaf material was harvested and ground to a fine powder a TissueLyser LT (Qiagen, Hilden, Germany). 70 – 100 mg powder were transferred to a reaction tube. For extraction of total RNA, the innuPREP Plant RNA kit (Analytik Jena, Jena, Germany) was used according to the manufacturer's instructions. RNA extraction in the present study was performed using the lysis buffer RL. RNA quality was checked on a 1 % agarose gel. Therefore, 3 μ l total RNA were mixed with 7 μ l H₂O and 2 μ l 6x loading dye. RNA concentration was then measured using the TECAN Infinite® 200 PRO NanoQuant plate reader (2.2.3.10) and samples were then adjusted to the lowest RNA concentration using RNase free H₂O.

2.2.3.3 Plasmid preparation from *E.coli*

Plasmid preparation was performed according to the protocol of alkaline lysis (Birnboim & Doly, 1979). Single *E.coli* colonies were inoculated in 3 ml LB containing the appropriate antibiotics and grown overnight at 37 °C. Cells were pelleted by centrifugation (1 min, 17000 xg, RT). The supernatant was discarded and the pellet was resuspended in 200 μ l P1 buffer. 200 μ l P2 buffer were added and mixed by inverting the tube. The preparation was incubated for 3 minutes. 200 μ l P3 buffer were added and the reaction was inverted several times until a white precipitate formed. After centrifugation (10 min, 17000 xg, RT), the supernatant was transferred to a new reaction tube and mixed with 1 ml 96 % Ethanol. The mixture was centrifuged (10 min, 17000 xg, RT) and the supernatant was discarded using a pipette. The remaining pellet was washed with 70 % ethanol and a last centrifugation step was performed (5 min, 17000 xg, RT). Residual ethanol was removed and the pellet was air dried. Subsequently, the pellet was resuspended in 30 – 50 μ l ddH₂O and stored at -20 °C.

2.2.3.4 Plasmid preparation from *S. cerevisiae*

S.cerevisiae colonies were washed from plates using 1 ml H₂O and a pipette tip and were transferred to a reaction tube. Cells were pelleted by centrifugation (5 min, 4000 xg, RT) and resuspended in 200 μ l P1 buffer from the QIAGEN® Plasmid Midi Kit (art.nr. 12145). 0.3 g glass beads (425 - 600 micron) were added and the mixture was shaken on a Vibrax VXR

basic (1500 rpm, 15 min) (IKA-Werke GmbH & Co. KG, Staufen, Germany). Subsequently, glass beads were pelleted by centrifugation (5 min, 4000 xg, RT). The next steps were performed according to the manufacturers' manual of the QIAGEN® Plasmid Midi Kit.

2.2.3.5 Synthesis of cDNA

For expression analysis, cDNA was synthesized from RNA samples using the RevertAid™ H Minus First Strand cDNA Synthesis kit (Thermo Scientific™, Westham, USA) according to manufacturer's instructions. 1 - 4 µg total RNA were used and cDNA synthesis was performed at 42 °C for 60 minutes. The synthesis reaction was terminated by incubation at 70°C for 10 minutes. The generated cDNA was diluted (1:5) with water and directly used for RT-PCR (2.2.3.7) or stored at -20 °C.

2.2.3.6 Polymerase chain reaction (PCR)

To amplify DNA fragments, polymerase chain reaction (PCR) was performed (Mullis *et al.*, 1986). PCR for cloning was carried out using iProof™ High-Fidelity DNAPolymerase (BioRad, Munich, Germany) according to manufacturer's instructions. Genotyping, colony PCR and RT-PCR were carried out using homemade Taq polymerase. Standard reactions using homemade Taq polymerase (20 µl) were prepared as followed:

10x Taq buffer:	2.0	µl
10 mM dNTPs:	0.5	µl
10 mM Primer 1:	1.0	µl
10 mM Primer 2:	1.0	µl
Taq DNA polymerase:	0.5	µl
H ₂ O:	15.0	µl
Template: 1 µl DNA or bacterial colony		

The following PCR program was used for homemade Taq polymerase:

1.	95 °C	5 min	(initial denaturation)
2.	95 °C	30 s	(denaturation)
3.	50-60 °C	30 s	(annealing)
4.	72 °C	1 min/kb	(extension)
5.	72 °C	5 -10 min	(final extension)
6.	4 °C	10 min	(cooling)

Steps 2 – 4 were repeated 29 – 35x

The annealing temperature was adjusted to the primers used and the extension time to the length of the fragment to be amplified.

2.2.3.7 Semi-quantitative reverse transcription-polymerase chain reaction (RT-PCR)

Semi-quantitative RT-PCR was performed according to the standard PCR method (2.2.3.6). The number of amplification cycles was adjusted to the gene of interest and the cDNA used.

2.2.3.8 Agarose gel electrophoresis

DNA fragments were separated according to their length on 1 – 3 % agarose gels using horizontal Sub-Cell GT electrophoresis apparatuses (BioRad, Munich, Germany). The appropriate amount of agarose was mixed with 1x TAE buffer and boiled in a microwave until the agarose was dissolved. Subsequently, the mixture was cooled down to about 60 °C and ethidium bromide to a final concentration of 1 - 5 µg/ml was added. The solution was poured into a casting chamber. After the gel solidified it was placed in the Sub-Cell GT tank filled with 1x TAE buffer. Samples were mixed with 6x DNA loading dye and loaded into the prepared pockets. Generuler™ ladders (Thermo Scientific™) were used as size standards. The DNA fragments were then separated by applying a voltage from 90 – 120 V for 20 – 60 minutes depending on the gel percentage and fragment size. The gel was exposed to UV light (312 nm) to visualize the DNA fragments. Pictures were taken using a gel documentation and analysis system (VWR, Lutterworth, UK).

2.2.3.9 DNA purification from agarose gels

Agarose gel electrophoresis was performed to separate DNA fragments (2.2.3.8). The fragments of interest were excised from the gel under UV-light (365 nm) and purified using the NucleoSpin® Gel and PCR Clean-up kit (Macherey-Nagel, Düren, Germany) according to the manufacturer's instructions.

2.2.3.10 Measurement of DNA and RNA concentration

Measurement of DNA and RNA concentration was performed using the TECAN Infinite® 200 PRO NanoQuant plate reader (Tecan Group Ltd, Männedorf, Switzerland). 1 µl of sample

was pipetted onto the NanoQuant Plate™. Absorbance was measured at 260 nm and 280 nm. The ratio of absorbance at 260 nm and 280 nm indicates the purity of the sample. For DNA samples, the optimal ratio is about 1.8. For RNA samples the optimal ratio is about 2.0.

2.2.3.11 Restriction endonuclease digestion of DNA

Digestion of DNA was performed using restriction endonucleases from Thermo Scientific™ or New England Biolabs and the corresponding buffer systems. Buffer and enzyme concentration as well as incubation temperature were chosen according to manufacturer's instructions.

2.2.3.12 Ligation of DNA fragments

Covalent linkage of DNA fragments was performed using T4-DNA Ligase (Thermo Scientific™, Waltham, USA) For cloning an insert into a linearized plasmid, the following reaction mixture was used:

Linearized plasmid DNA:	50 ng
Insert:	150 - 500 ng
T4-DNA Ligase:	0.5 U
T4-DNA Ligase Buffer:	2 µl
H ₂ O fill up to	20 µl

The sample was incubated for 4 hours at room temperature or at 16 °C overnight and subsequently transformed into chemo-competent *E.coli* (2.2.3.16).

2.2.3.13 Cloning by homologous recombination in *S. cerevisiae*

Constructs were cloned by homologous recombination using a modified version of the 'drag and drop' method (Colot *et al.*, 2006). In this method the yeast is used to recombine DNA-fragments with short regions of homology (about 29 base pairs) with high efficiency. This method is exemplified by the generation of *cerk1 fls2tm*, a construct where the CERK1 transmembrane domain was replaced by the FLS2 transmembrane domain. The N-terminal part of CERK1 up to the transmembrane domain was amplified by PCR. The forward primer was designed to harbor a 29 bp homology region to the shuttle vector pRS426 at the 5' end (Fragment 1) followed by a HindIII restriction site. The C-terminal part of CERK1 beginning

right after the transmembrane domain was also amplified. The reverse primer was designed to harbor a 29 bp homology region to pRS426 at the 3' end (Fragment 2). The FLS2 transmembrane domain was amplified adding 30bp homology to fragment 1 at the 5' end and 30 bp homology to fragment 2 at the 3' end. The vector pRS426 was linearized by digestion with BamHI and KpnI. For transformation of *S. cerevisiae* see 2.2.3.20. 500 ng of each fragment and 200 ng of the linearized vector were used. Recombined plasmids were purified (see 2.2.3.4) and transformed into *E.coli* (see 2.2.3.16) for further analysis.

2.2.3.14 DNA sequencing and analysis

DNA sequencing was performed by Seqlab (Göttingen, Germany). Samples were premixed with suitable primers according to Seqlab's sequencing instructions. Sequencing data was analyzed using the bioinformatics software Geneious 7.1.5 (Kearse *et al.*, 2012).

2.2.3.15 Preparation of chemically competent *E.coli* cells

25 ml LB containing the appropriate antibiotics were inoculated with a single colony from a fresh *E.coli* TOP10 plate and grown overnight at 37 °C. The next day, the overnight culture was used to inoculate a main culture of 300 ml LB to an OD₆₀₀ of 0.2. The main culture was grown at 37 °C until it reached an OD₆₀₀ of 0.6. The cells were chilled on ice for 15 minutes and then centrifuged (2500 xg, 10 min, 4 °C). The resulting cell pellet was then resuspended in 80 ml ice-cold CCMB80 buffer and incubated on ice for 15 minutes. After an additional centrifugation step (2500 xg, 10 min, 4 °C), the cells were resuspended in 10 ml ice-cold CCMB80 buffer and aliquots of 50 µl were prepared. Aliquots were frozen in liquid nitrogen and stored at -80 °C.

2.2.3.16 Transformation of chemically competent *E.coli* cells

For transformation of chemo-competent *E.coli*, up to 10 µl of ligations or 200 – 700 ng plasmid DNA were mixed with 50 µl of competent cells and incubated on ice for 10 minutes. Subsequently, cells were heat shocked at 42 °C for 1 minute and incubated on ice again for 2 minutes. 1 ml LB was added and cells were regenerated at 37 °C and 180 rpm for 1 hour. Next, the cells were centrifuged (1 min, 17000 xg, RT), most of the supernatant was discarded and the pellet was resuspended in residual LB. The resuspended cells were then plated on LB-agar plates containing the appropriate antibiotics and incubated at 37 °C overnight.

2.2.3.17 Preparation of electro-competent *A. tumefaciens* cells

2 ml LB containing the appropriate antibiotics was inoculated with a single colony of *A. tumefaciens* GV3101 pSoup and grown overnight at 28 °C. This culture was used to inoculate 50 ml LB containing the appropriate antibiotics, which was again grown over night at 28 °C. This culture was then used to inoculate the main culture of 300 ml LB without antibiotics to and OD of 0.3. The main culture was incubated at 28 °C until the OD₆₀₀ reached 0.6 and was chilled on ice for 15 – 30 minutes. The culture was then centrifuged (15 min, 6000 xg, 4 °C). The supernatant was discarded and the cells were resuspended in ice-cold 1mM HEPES, pH 7.0 and centrifuged again (15 min, 6000 xg, 4 °C). This step was repeated twice. Pellets were then resuspended in 30 ml ice-cold 10 % glycerol and centrifuged (15 min, 6000 xg, 4 °C). The supernatant was discarded and pellets were resuspended in 2 ml ice-cold 10 % glycerol. 50 µl aliquots were frozen in liquid nitrogen and stores at -80 °C until further use.

2.2.3.18 Transformation of electro-competent *A. tumefaciens* cells

Transformation of electro-competent *A. tumefaciens* GV3101 pSoup cells was performed by electroporation (Koncz & Schell, 1986). An aliquot of competent cells was thawed on ice and gently mixed with 100 ng plasmid DNA. The bacterial suspension was then transferred to a pre-chilled electroporation cuvette (0.1 electrode distance). For electroporation, the MicroPulser™ (Bio-Rad, Munich, Germany) was used (25 µF, 2.5 kV and 400 Ω). 1 ml LB was then added and the bacteria were transferred to a reaction tube. Cells were then incubated at 28 °C for 2 hours for regeneration. Cells were then centrifuged (1 min, 17000 xg, RT) and most of the supernatant was discarded. The pellet was then resuspended in residual LB, plated on LB agar containing the appropriate antibiotics and incubated at 28 °C for 2 - 3 days.

2.2.3.19 Preparation of chemically competent *S. cerevisiae* cells

For the preparation of chemically competent cells, 3 ml YPD were inoculated with *S. cerevisiae* and grown overnight at 30 °C. This overnight culture was used to inoculate 20 ml YPD to an OD₆₀₀ of 0.1, which was then grown at 30 °C for 6 hours. Cells were pelleted by centrifugation (3 min, 3000 xg, RT) and washed once with 10 ml sterile H₂O and once with 2 ml volumes SORB-buffer. Subsequently, the cells were resuspended in 180 µl SORB-buffer

and mixed with 20 μ l ss-DNA (2 mg/ml). Aliquots of 50 μ l were generated and directly used or stored at -80 °C. It is important not to freeze the cells in liquid nitrogen.

2.2.3.20 Transformation of chemically competent *S. cerevisiae* cells

Chemically competent *S. cerevisiae* cells were mixed with linearized pRS426 vector and each of the fragments to be recombined. 300 μ l Li-PEG were added and samples were incubated for 30 minutes on a wheel at room temperature. Subsequently, cells were heat-shocked at 42 °C for 15 minutes and then centrifuged (2 min, 3000 xg, RT). Most of the supernatant was discarded and the cells were resuspended in residual liquid. The cell suspension was then plated on SC plates (-Ura +Gluc) and incubated at 28 °C for 2 – 3 days.

2.2.4 Confocal laser scanning microscopy (CLSM)

Confocal laser scanning microscopy was performed using a TCS SP5 DM6000 CS confocal laser scanning microscope (Leica, Wetzlar, Germany) equipped with an argon laser and HyD hybrid detectors as well as the appropriate software (LAS AF Leica Application Suite, Version 2.7.2). For microscopy, small leaf pieces cut and placed onto an object slide. A drop of water was placed in the middle and silicone to the corners of a cover glass. The cover glass was then placed onto the object slide with the water drop covering the leaf piece. For visualization of fungal structures in tissues, Fluorescent Brightener 28 (FB28, 10 μ g/ml solution) (Sigma-Aldrich Deisenhofen, Germany) was used instead of water. Table 8 provides an overview of excitation and emission spectra for the fluorophores used in this study. Chloroplast autofluorescence was detected at 700 – 750 nm. For co-localization studies sequential scanning was used.

Table 8. Settings for fluorophore detection

Fluorophore	Excitation	Emission
Fluorescent Brightener 28 (FB28)	405 nm	420 – 460 nm
GFP	488 nm	500 – 540 nm
Venus	514 nm	525 – 560 nm
TagRFP-T	514 nm	560 – 600 nm
RFP	561 nm	580 – 620 nm
mCherry	561 nm	590 – 630 nm
mKate2	561 nm	590 – 640 nm

3. Results

This work analyzed proteolytic processing of the LysM-RLK CERK1 as well as its role in cell death regulation. In immunoblot experiments, a specific CERK1 antibody that recognizes an epitope near the N-terminus of CERK1 detects the full length CERK1 receptor protein and an additional band of lower molecular weight. Previous research showed that this smaller band corresponds to the soluble extracellular domain of CERK1, also called the CERK1 ectodomain (Petutschnig *et al.*, 2014). A CERK1 mutant was identified that shows no ectodomain signals in immunoblots, likely due to reduced stability of the ectodomain fragment. This mutant, *cerk1-4*, exhibits an enhanced cell death phenotype upon inoculation with powdery mildews and during senescence (Petutschnig *et al.*, 2014).

The results of this thesis are divided into two parts. The aim of the first part was to analyze CERK1 ectodomain shedding. In particular, possible functions of ectodomain shedding in the wild type CERK1 protein and its role in formation of the *cerk1-4* phenotype should be investigated. To do so, CERK1 mutants should be generated that are defective in ectodomain shedding. Therefore, a CERK1 antibody is used, which detects an epitope within the ectodomain of CERK1. Bands detected in immunoblots are therefore either full length protein or N-terminal fragments. The non-shedding CERK1 variants should be analyzed with regard to their chitin signaling capacity, such as chitin binding and chitin-induced receptor phosphorylation. The mutant plants should then be used to analyze if CERK1 ectodomain shedding is a prerequisite for development of the *cerk1-4* phenotype.

The second part of this thesis aimed at identification of signal transduction components required for cell death formation in *cerk1-4*. For this purpose, a *cerk1-4* suppressor screen with an EMS mutagenized population was previously established. In this work, a novel mutant fully suppressing the *cerk1-4* phenotype was identified and the underlying mutation was mapped to the extra-large G-protein 2 (XLG2). The analysis of this mutant and the investigation of the subcellular localization of XLG2 was the focus of the second part of this work.

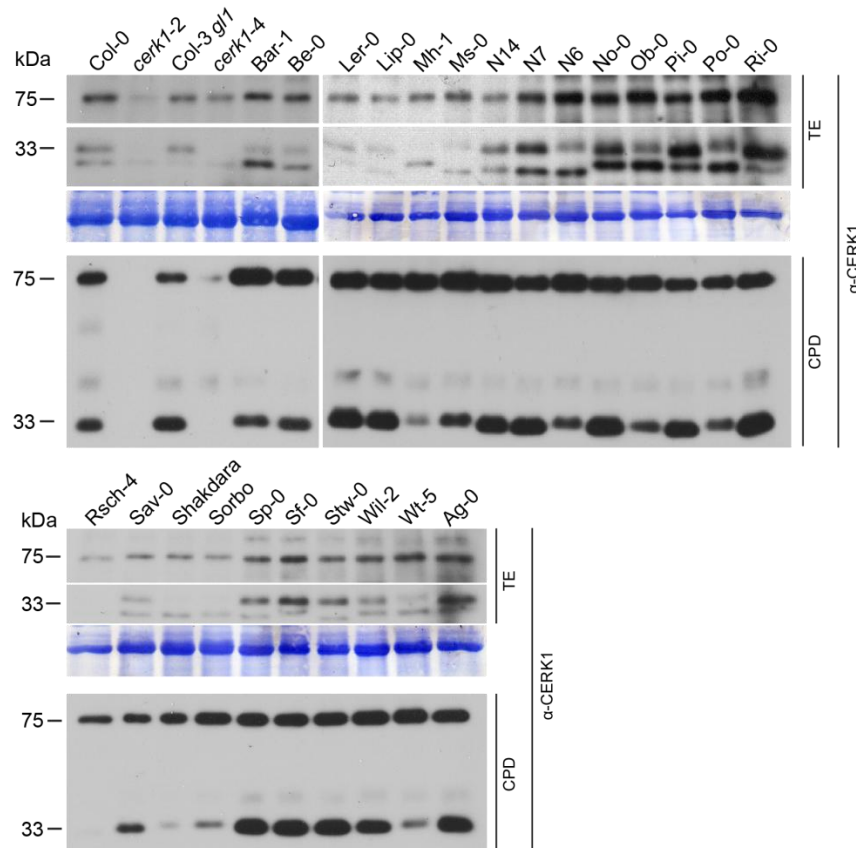
3.1 Analysis of CERK1 ectodomain shedding

3.1.1 Investigation of CERK1 ectodomain shedding in *Arabidopsis thaliana* accessions

Arabidopsis thaliana can be naturally found in different habitats throughout the northern hemisphere (Weigel & Mott, 2009). Plants from different locations exhibit genetic and morphological variety in order to adapt to their environments. *Arabidopsis* accessions also vary with regard to their PRR- and NB-LRR-type immune receptors (Gomez-Gomez *et al.*, 1999; Noel *et al.*, 1999; Rose *et al.*, 2004; Stahl *et al.*, 1999). To investigate this, different *Arabidopsis thaliana* accessions were analyzed for CERK1 ectodomain shedding and variations in the CERK1 amino acid sequence. Immunoblot analysis of 24 *Arabidopsis* accessions using the specific N-terminal CERK1 antibody was carried out. The immunoblots were performed with total protein extracts as well as pull-downs with chitin magnetic beads that are enriched for chitin binding proteins such as CERK1 (Petutschnig *et al.*, 2010). As expected, wild type Col-0 and Col-3 *gl1* controls showed a signal at 75 kDa corresponding to full length CERK1 receptor protein, as well as a signal at 33 kDa representing the soluble ectodomain (Figure 6A). As described previously (Petutschnig *et al.*, 2014), the *cerk1-4* mutant showed the 75 kDa full length signal, but lacked the 33 kDa band corresponding to the soluble ectodomain. After chitin pull-down, additional faint bands around 40 kDa became apparent in Col-0, Col-3 *gl1* and *cerk1-4*, which can be typically observed for CERK1 (Petutschnig, unpublished data). Occasionally, low levels of 33 kDa and 40 kDa fragment can be detected in the CERK1 knockout mutant *cerk1-2*. This is due to the localization of the T-DNA near the 3' end of the CERK1 gene which results in residual upstream transcript (Miya *et al.*, 2007). However, no signal for any of these bands could be detected in the CERK1 knockout mutant *cerk1-2*, indicating that all described signals are CERK1-specific. In all tested *Arabidopsis* ecotypes, the 75 kDa full length CERK1 signal could be observed at similar abundance levels. Also, most accessions showed the faint 40 kDa band. The 33 kDa CERK1 ectodomain shedding product was also visible in all tested lines, however its abundance appeared to be clearly reduced in Mh-1, Rsch-4, Shakhara, Sorbo and Wt-5 (Figure 6A). Furthermore, the soluble ectodomain of Rsch-4 had a lower molecular size in comparison to Col-0. This was expected as one N-glycosylation site in Rsch-4 is mutated (not shown). The CERK1 ectodomain fragment is soluble and thus does not contain a functional transmembrane domain (TM). The size of the fragment as well as proteomic analyses narrow the possible CERK1 cleavage site down to a region comprising 20 amino acids N-terminal of the TM and the TM itself (Petutschnig *et al.*, 2014) (Figure 8A). This

sequence overlaps with the extracellular stalk, which is defined as the region between transmembrane domain and third LysM domain. Interestingly, all accessions found to exhibit reduced CERK1 ectodomain shedding harbor amino acid substitutions within the extracellular stalk in comparison to Col-0 (Figure 6B).

A



B

		extracellular stalk										transmembrane domain																																									
Col-0	207	I	V	Y	V	P	G	R	D	P	N	G	A	F	P	P	F	K	S	S	K	D	G	V	G	A	G	V	I	A	G	I	V	I	G	V	I	V	A	L	L	L	I	L	F	I	V	Y	Y	A	Y	257	
Sorbo	207	I	V	Y	V	P	G	R	D	P	S	G	A	F	P	A	F	K	A	S	K	Q	G	G	I	G	A	V	V	I	A	G	I	V	V	G	V	I	V	A	L	L	L	I	L	F	I	I	Y	Y	A	Y	257
Shakdara	207	I	V	Y	V	P	G	R	D	P	S	G	A	F	P	A	F	K	A	S	K	Q	G	G	I	G	A	V	V	I	A	G	I	V	V	G	V	I	V	A	L	L	L	I	L	F	I	I	Y	Y	A	Y	257
Wt-5	207	I	V	Y	V	P	G	R	D	P	S	G	A	F	P	A	F	K	A	S	K	Q	G	G	I	G	A	V	V	I	A	G	I	V	V	G	V	I	V	A	L	L	L	I	L	F	I	I	Y	Y	A	Y	257
Mh-1	207	I	V	Y	V	P	G	R	D	P	S	G	A	F	P	A	F	K	A	S	K	Q	G	G	I	G	A	V	V	I	A	G	I	V	V	G	V	I	V	A	L	L	L	I	L	F	I	I	Y	Y	A	Y	257
Rsch-4	207	I	V	Y	V	P	G	R	D	P	S	G	A	F	P	A	F	K	A	S	K	Q	G	G	I	G	A	V	V	I	A	G	I	V	V	G	V	I	V	A	L	L	L	I	L	F	I	I	Y	Y	A	Y	257

Figure 6. CERK1 ectodomain shedding is reduced in some *Arabidopsis* accessions. A) Anti-CERK1 immunoblot of different *Arabidopsis* accessions. Col-0, *cerk1-2*, Col-3 *gl1* and *cerk1-4* were used as controls. Upper panel, total extracts (TE). Lower panel, chitin pull-downs (CPD) prepared from total extracts shown in the upper panel. Full length CERK1 can be detected at 75 kDa and CERK1 ectodomain at 33 kDa. CBB, Coomassie Brilliant Blue membrane (loading control). For Mh-1, Rsch-4, Sha Sorbo and Wt-5, reduced CERK1 ectodomain signal was observed in 3 independent experiments. B) Alignment of the extracellular stalk and transmembrane region of CERK1 from different *Arabidopsis* accessions with reduced CERK1 ectodomain shedding in comparison to Col-0.

It has to be noted that Sorbo, Shakdara, Wt-5, Mh-1 and Rsch-4 repeatedly showed decreased signals for the 33 kDa CERK1 ectodomain fragment in several independent experiments, but in some blots they exhibited ectodomain shedding similar to Col-0. The abundance of the soluble ectodomain fragment increases with plant age and positively correlates with salicylic acid levels (Petutschnig *et al.*, 2014). This raised the question whether the reduced abundance of the soluble ectodomain in Sorbo, Shakdara, Wt-5, Mh-1 and Rsch-4 is caused by differences in the developmental status of these lines, which in turn might be influenced by slightly variable growth conditions between experiments. To test if the reduction of CERK1 ectodomain shedding in these accessions is indeed caused by changes in the CERK1 amino acid sequence a construct containing the Wt-5 CERK1 coding sequence was generated and transformed into the CERK1 knockout *cerk1-2*, which is in the Col-0 background. Three independent transgenic *cerk1-2* lines expressing Wt-5 CERK1 were tested in immunoblot analyses for CERK1 ectodomain shedding (Figure 7). A signal at 75 kDa could be detected for all plants, except *cerk1-2* and an ectodomain signal (33 kDa) could be observed for all plants except *cerk1-2* and *cerk1-4*. Abundance of the ectodomain fragment in transgenic *cerk1-2* plants expressing Wt-5 CERK1 was slightly reduced in comparison to Col-0, indicating that the amino acid sequence of CERK1 might play a role in ectodomain shedding. However, Wt-5 control plants exhibited CERK1 ectodomain shedding comparable to wild type in this experiment and the transgenic lines had lower overall abundance of the CERK1 protein compared to the controls, making interpretation of the data difficult.

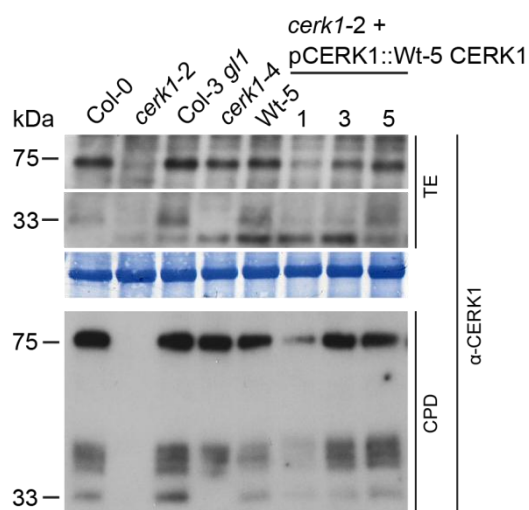


Figure 7. Wt-5 ectodomain shedding is also reduced in *cerk1-2*. Immunoblot of three independent transgenic lines expressing *Wt-5 CERK1* using a specific CERK1 antibody. Col-0, *cerk1-2*, Col-3 *gl1*, *cerk1-4* and *Wt-5* were used as controls. Upper panel, total extracts (TE). Lower panel, chitin pull-down (CPD) using total extracts of the upper panel. CBB, Coomassie Brilliant Blue stained protein served as loading control.

3.1.2 Mutational analysis of potential CERK1 protease cleavage motifs

Arabidopsis accessions with amino acid exchanges in the extracellular stalk region and TM show reduced abundance of the CERK1 ectodomain fragment in comparison to Col-0. The substitution from proline to alanine in position 221 is of special interest, as prolines are secondary structure disrupters (Vanhoof *et al.*, 1995) which might be of importance for proper cleavage. Also, proline-containing motifs have been shown to be sites of ectodomain shedding in metazoan receptor kinases (Thorp *et al.*, 2011; Yuan *et al.*, 2003), which are structurally and functionally related to plant receptor-like kinases. In animals, ectodomain shedding of receptor kinases is performed by proteases belonging to two related families, A Disintegrin And Metalloproteinases (ADAMs) and matrix metalloproteases (MMPs) (Hayashida *et al.*, 2010). ADAM and MMP cleavage motifs are not clearly defined but cleavage sites of some receptor kinases are known. Yuan *et al.* (2003) analyzed ectodomain shedding of the human receptor tyrosine kinase Her2/neu/erbB2, a member of the epidermal growth factor receptor (EGFR) family and identified a short peptide signature within the extracellular stalk that is required for cleavage. This motif consists of two prolines or glycines flanking any five to seven amino acids (P/G-X₅₋₇-P/G). Another member of the EGFR family, erbB4/Her4 is also subject to ectodomain shedding by ADAMs. Its cleavage site contains a P-X₇-P motif and a splice form that lacks this signature is not cleavable (Cheng *et al.*, 2003). Proline-containing cleavage motifs have also been reported in RTKs outside the EGFR family. For example, ADAM-mediated ectodomain shedding of Mer tyrosine kinase (MerTK) is dependent on a P-X₅-P motif (Thorp *et al.*, 2011). Moreover, many mammalian MMP cleavage motifs contain the P/G-X₅₋₇-P/G signature (Turk *et al.*, 2001).

Interestingly, the proline in position 221, which was found to be replaced by alanine in diverse accessions with reduced CERK1 ectodomain shedding (Figure 6B), is part of several potential EGFR cleavage motifs (Figure 8A), suggesting that this type of motif may also play a role in ectodomain shedding of CERK1. The neighboring amino acid in position 220 is also a proline, which is still present in the *Arabidopsis* accessions with reduced CERK1 ectodomain abundance. It may provide an alternative cleavage site and might explain why CERK1 ectodomain shedding is not completely abolished in these ecotypes. Thus, a construct was generated, where also the neighboring proline at position 220 was mutated to alanine. The mutation was denoted *cerk1* cleavage1 (cvg1) (Figure 8B).

In addition to ADAMs and MMPs, Rhomboid proteases can mediate ectodomain shedding. They are intramembrane proteases which cleave their substrate within the transmembrane domain (Urban *et al.*, 2001). Studies from *Drosophila melanogaster* revealed that Rhomboid-1 specifically recognizes a short amino acid sequence (ASIASGA) within the N-

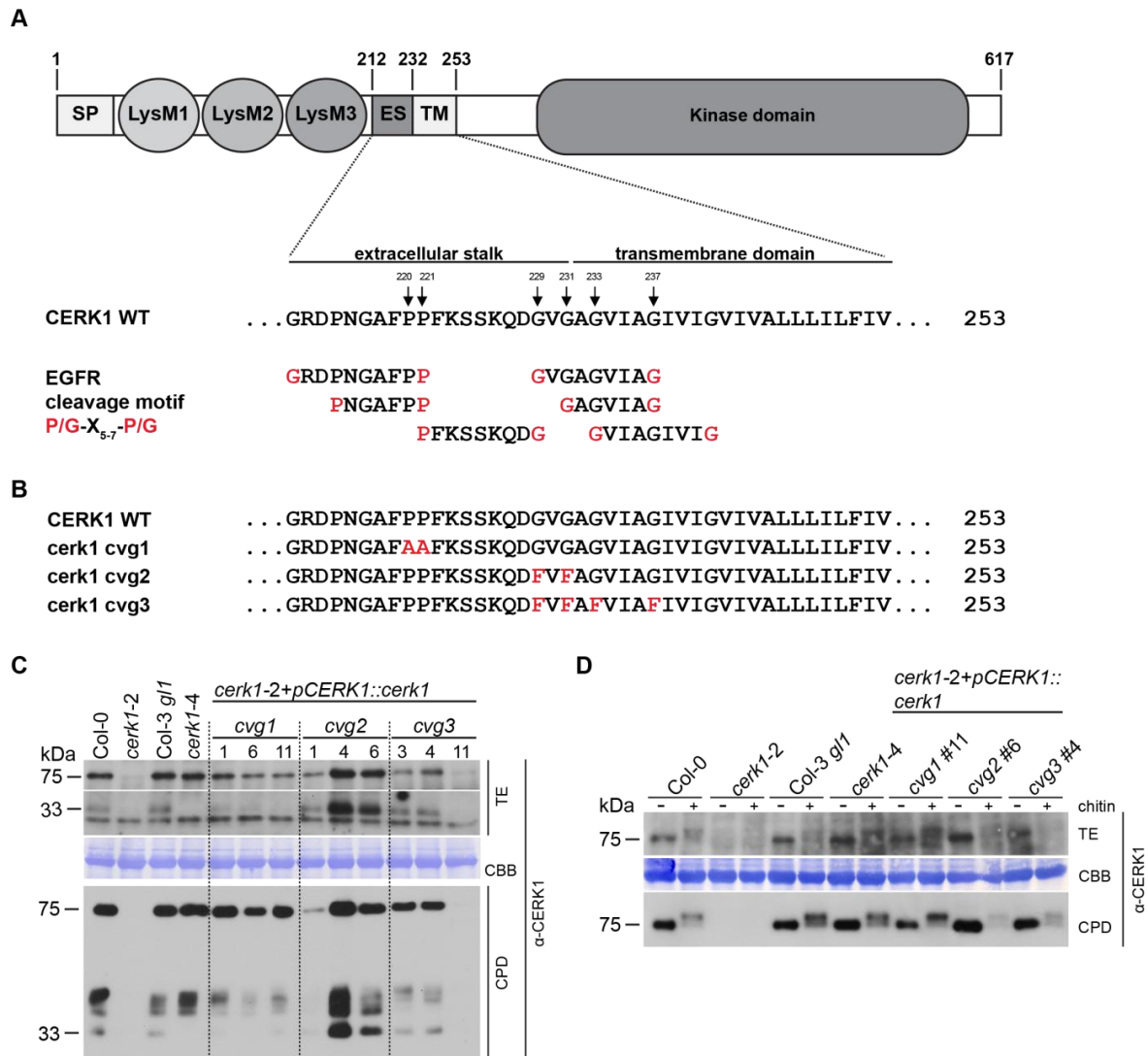


Figure 8. CERK1 cleavage motif mutants could not fully suppress CERK1 ectodomain shedding. A) Domain organization of CERK1 showing signal peptide (SP), lysin motifs (LysMs), extracellular stalk (ES), transmembrane domain (TM) and kinase domain. Positions of introduced mutations are indicated by arrows and numbers above arrows indicate amino acid positions. Potential EGFR-type cleavage motifs are aligned to the CERK1 extracellular stalk and transmembrane sequence and amino acids matching motifs are highlighted in red (CERK1 domain structure adapted from (Petutschnig *et al.*, 2014)). B) Alignment of CERK1 wild type sequence to protease cleavage mutants. Mutated amino acids are highlighted in red. C) Anti-CERK1 immunoblot of three independent *cerk1-2* transgenic lines per cleavage construct expressed in *cerk1-2*. T2 transformants were selected for Basta® resistance and three whole rosettes per line were pooled and used for protein extraction. Samples from Col-0, *cerk1-2*, Col-3 *gl1* and *cerk1-4* were pooled the same way and served as controls. The upper panel shows total extracts (TE). To visualize both, the 75 kDa full length fragment and the 33 kDa ectodomain fragment optimally, different exposure times are shown. Lower panel, chitin pull-downs (CPD) prepared using total extracts shown in the upper panel. CBB, Coomassie Brilliant Blue stained membrane (loading control). D) Band shift assay of CERK1 cleavage mutants. Plant leaves were vacuum-infiltrated with 100 µg ml⁻¹ shrimp shell chitin and were then incubated for 12 minutes. An anti-CERK1 immunoblot of one chitin-treated transgenic line per CERK1 cleavage mutant is shown. Upper panel, total extracts of either mock-infiltrated (-) or chitin-infiltrated (+) leaves. Lower panel, chitin pull-downs prepared from the total extracts shown in the upper panel. This experiment was repeated four times with similar results.

terminal part of the transmembrane domain of its substrate, the TGF α homologue spitz (Urban & Freeman, 2003). Detailed mutational analysis showed that the presence of the glycine residue in this motif is essential for cleavage and the adjacent alanine has an enhancing effect. Introduction of the GA motif turned synthetic transmembrane proteins into substrates for a number of different eukaryotic and prokaryotic rhomboid proteases. The small amino acids glycine and alanine were proposed to break the alpha helix and thereby increase the accessibility of the peptide backbone for rhomboid proteases (Urban & Freeman, 2003). As rhomboid proteases are present in *Arabidopsis* (Koonin *et al.*, 2003), it is possible that CERK1 might be a substrate of an *Arabidopsis* rhomboid protease.

The CERK1 transmembrane domain as well as the CERK1 extracellular stalk harbor several glycines, which might be part of potential Rhomboid cleavage motifs. Therefore, CERK1 mutants were generated where these glycines were mutated to the large hydrophobic amino acid phenylalanine. The mutants were designed in such a way, that also P/G-X₅₋₇-P/G motifs overlapping with the transmembrane domain were mutated. In one mutant CERK1 variant, glycines at position 229 and 231 within the extracellular stalk were mutated (*cerk1 cvg2*, Figure 8B). In a second variant, additionally glycines in the transmembrane domain (position 233 and 237) were mutated to phenylalanine (*cerk1 cvg3*, Figure 8B) resulting in four glycine to phenylalanine substitutions. The *cerk1 cvg1*, *cvg2* and *cvg3* mutant variants were generated in the pGreenII-0229 vector containing the endogenous CERK1 promoter. The resulting constructs were transformed into the CERK1 knockout mutant *cerk1-2* and transgenic plants were analyzed by immunoblotting using the specific CERK1 antibody. As expected, wild type Col-0, Col-3 *gl1* and *cerk1-4* controls showed a full length protein signal (75 kDa), whereas only Col-0 and Col-3 *gl1* controls showed an ectodomain signal (33 kDa) (Figure 8C). Additional bands at 40 kDa appeared in Col-0, Col-3 *gl1* and *cerk1-4* after chitin pull-down (Figure 8C). No CERK1 specific signal was detected in *cerk1-2*. Transgenic plants expressing the *cvg1*, *cvg2* or *cvg3* constructs showed both the full length CERK1 signal at 75 kDa, as well as the 33 kDa ectodomain band. The expression levels differed between individual lines, which would be expected for transgenic plants. Chitin binding ability was maintained in all tested CERK1 variants, as all of them could be pulled down by chitin magnetic beads at similar levels to the wild type controls (Figure 8C). Comparison of signals intensities of the 75 kDa and 33 kDa bands in both total extracts and chitin pull-downs, suggested that ectodomain shedding was reduced in *cerk1 cvg1* lines compared to Col-0 or Col-3 *gl1*. In contrast, ectodomain shedding in *cerk1 cvg2* and *cerk1 cvg3* seemed to be enhanced. CERK1 was reported to be phosphorylated after chitin treatment. This results in an electrophoretic mobility shift of phosphorylated CERK1 and can be detected in immunoblot experiments (Petutschnig *et al.*, 2010). Each of the CERK1 variants showed the

chitin-induced band shift in immunoblots, which was comparable to Col-0, Col-3 *gl1* and *cerk1-4*, indicating functionality of the generated CERK1 variants (Figure 8D).

Several potential EGFR cleavage motifs can be found within an eleven amino acid stretch in the intracellular juxtamembrane domain of CERK1 (Figure 9A). Interestingly, this motif can also be found in the intracellular juxtamembrane domain of several rice RLKs (Ding *et al.*, 2009) and autophosphorylation within this cleavage motif was suggested to prevent cleavage of the rice RLK XA21 (Xu *et al.*, 2006). CERK1 cleavage within or near this motif would result in a fragment with a molecular weight of about 40 kDa. As already shown, fragments of this size can be detected in CERK1 immunoblots after chitin pull-down (see Figure 8C) and might represent precursors, which are subsequently cleaved to produce the soluble CERK1 ectodomain fragment. Therefore, a CERK1 variant was generated, where this amino acid stretch was deleted (*cerk1 clx*, Figure 9A). This construct was expressed in the CERK1 knockout mutant *cerk1-2* under control of the endogenous CERK1 promoter. Immunoblot analysis of three independent transgenic *cerk1 clx* expressing lines was performed using the specific CERK1 antibody (Figure 9B). Full length CERK1 protein at 75 kDa and CERK1 ectodomain at 33 kDa could be detected for Col-3 *gl1* and Col-0. As expected, only full length protein and no ectodomain could be detected for *cerk1-4*. Full length protein and ectodomain were missing in *cerk1-2*, confirming the specificity of the described bands. *cerk1 clx* full length protein and ectodomain could be detected for all tested transgenic lines, albeit at lower molecular weights as their wild type counterparts. Lower molecular weight was expected and is caused by deletion of eleven amino acids. *cerk1 clx* maintained the ability to bind chitin, as for all tested transgenic lines full length protein and ectodomain could be pulled down with chitin magnetic beads. The abundance of full length CERK1, but not the ectodomain shedding product, is lower in *cerk1 clx* expressing lines than in the wild type controls, which can be observed in total extracts as well as chitin pull-downs. This led to the conclusion that ectodomain shedding in *cerk1 clx* is actually enhanced in comparison to wild type. Multiple bands around 40 kDa were detected in chitin pull-downs of Col-0, Col-3 *gl1* and *cerk1-4*, but not in *cerk1-2*. This is frequently observed, but the exact identity of these CERK1 signals is not known. The approximately 40 kDa signals also occurred in the *cerk1 clx* expressing plants, indicating that the deleted amino acid stretch in the intracellular juxtamembrane domain is not critical for their generation. Thus CERK1 is probably not cleaved within the deleted sequence. The apparent molecular weight of the 40 kDa bands was altered in the *cerk1 clx* expressing plants, which suggests that the cleavage site(s) might be shifted C-terminally of the *clx* deletion (Figure 9B). *cerk1 clx* is still able to autophosphorylate, as indicated by an electrophoretic mobility shift after chitin treatment, suggesting functionality of the construct (Figure 9C).

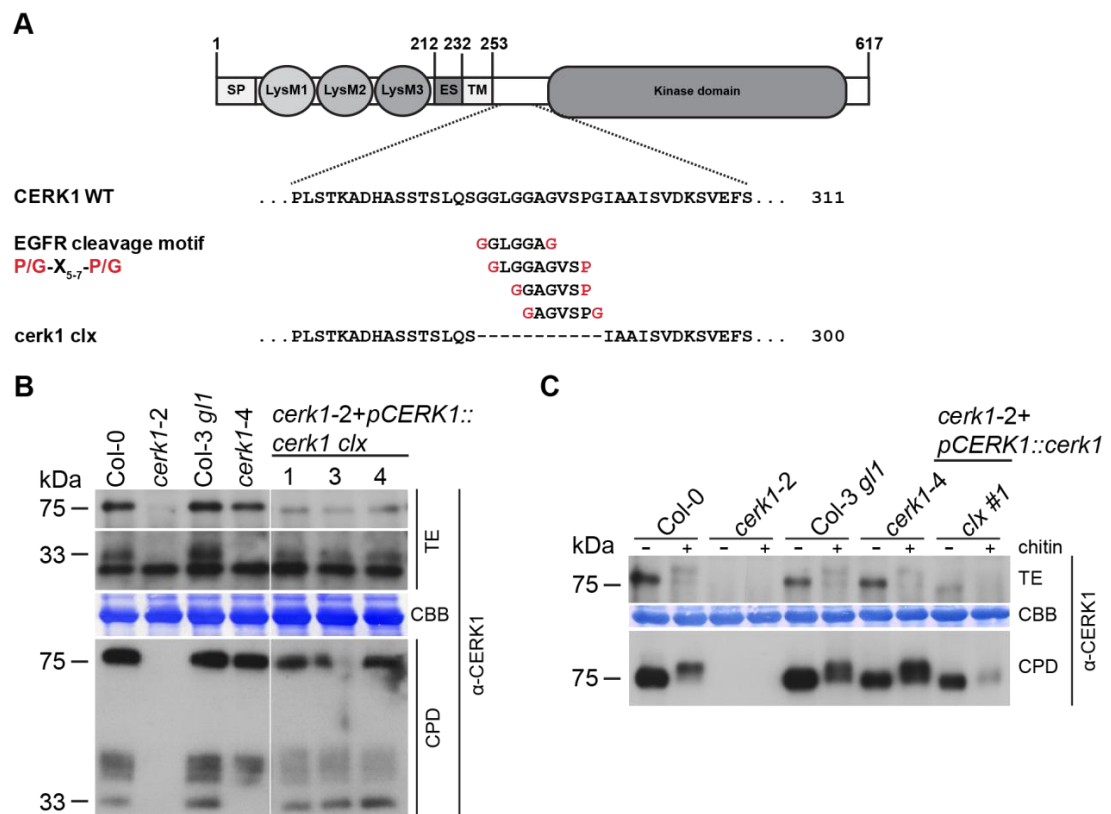


Figure 9. Deletion of potential intracellular cleavage motifs could not suppress CERK1 ectodomain shedding. Domain organization of CERK1 illustrating signal peptide (SP), lysin motifs (LysMs), extracellular stalk (ES), transmembrane domain (TM) and kinase domain. Deleted amino acids in *cerk1 clx* are indicated by dashes. EGFR-type cleavage motifs are aligned to the CERK1 intracellular juxtamembrane domain. Amino acids of EGFR-type cleavage motifs matching the CERK1 sequence are highlighted in red (CERK1 domain structure adapted from (Petutschnig *et al.*, 2014)). B) Immunoblot of three individual transgenic *cerk1-2* lines expressing *cerk1 clx* using the specific CERK1 antibody is shown. T2 transformants were selected for Basta® resistance and three whole rosettes per line were pooled and used for protein extraction. Col-0, *cerk1-2*, Col-3 *gl1* and *cerk1-4* plants were harvested the same way and served as controls. Upper panel shows total extracts (TE). To visualize both, the 75 kDa full length fragment and the 33 kDa ectodomain fragment optimally, different exposure times are shown. Lower panel shows chitin pull-downs (CPD) using total extracts shown in the upper panel. C) Band shift assay of *cerk1 clx*. Leaves were vacuum-infiltrated with 100 $\mu\text{g ml}^{-1}$ shrimp shell chitin and incubated for 12 minutes. Immunoblot of one transgenic *cerk1-2* line expressing *cerk1 clx* using the specific CERK1 antibody is shown. Upper panel, total extracts of either mock-infiltrated (-) or chitin-infiltrated (+) leaves. Lower panel, chitin pull-down prepared of total extracts shown in upper panel. CBB, Coomassie Brilliant Blue stained membrane (loading control). This experiment was repeated three times with similar results

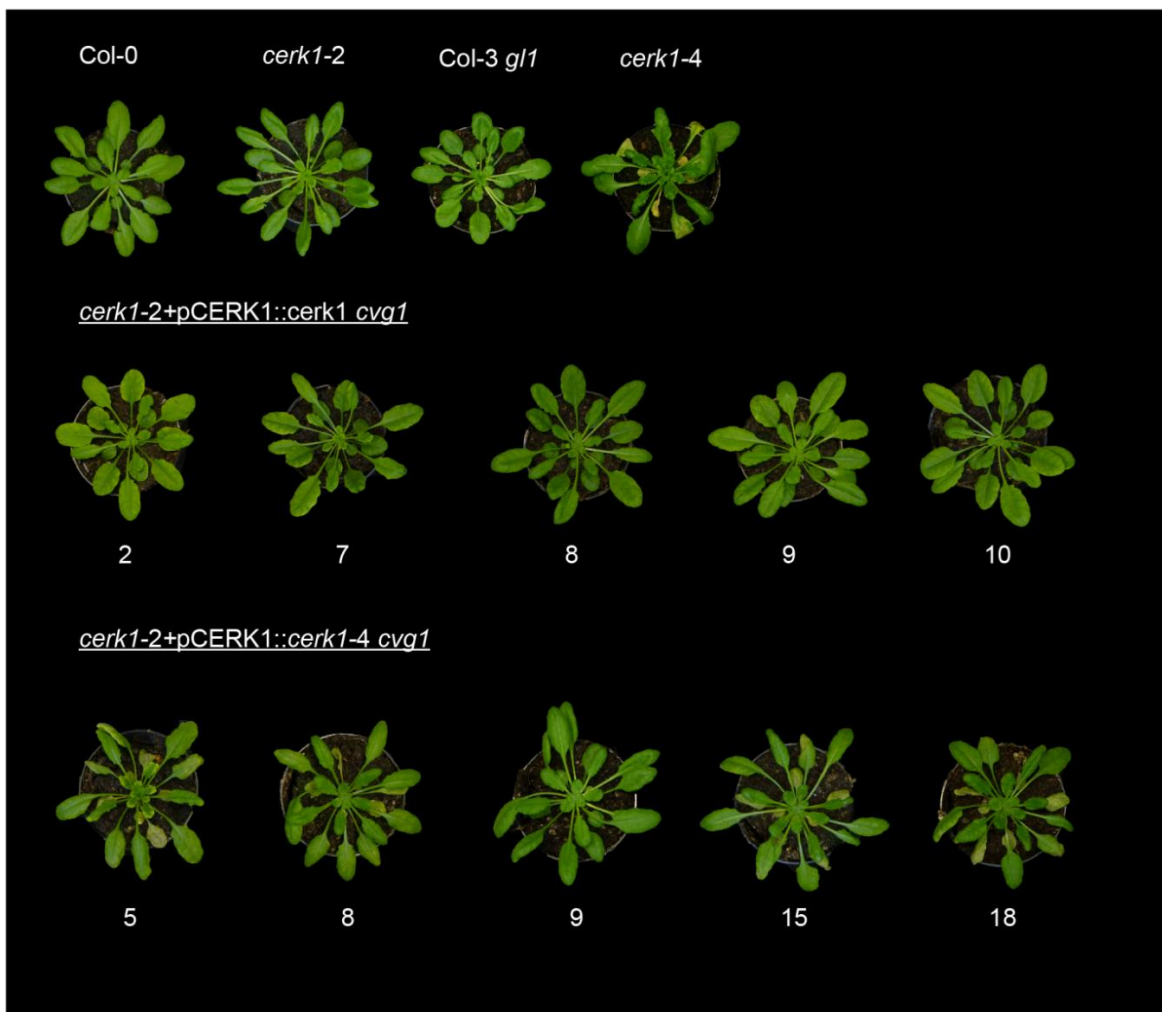
3.1.3 The *cvg1* mutation does not suppress the *cerk1-4* phenotype

Mutational analysis of CERK1 potential proteolytic cleavage sites led to the identification of a CERK1 mutant (*cerk1 cvg1*) with reduced ectodomain shedding. This mutant was used to investigate if reduced ectodomain shedding can suppress the development of the *cerk1-4* phenotype. Therefore, the *cerk1-4* mutation was introduced into the vector pGreenII-0229PREP harbouring *cerk1 cvg1*. The resulting construct (*cerk1-4 cvg1*) was transformed

into the CERK1 knockout mutant *cerk1-2* and expressed under the control of the endogenous promoter. The resulting transgenic lines were assessed for *cerk1-4* phenotype development after pathogen inoculation (Figure 10) and of senescent plants (Figure 11). Five independent transgenic lines either expressing *cerk1-4 cvg1* or *cerk1 cvg1* were inoculated with *Blumeria graminis* f.sp *hordei* (Figure 10A). The controls Col-0, *cerk1-2* and Col-3 *gl1* did not show any macroscopically visible phenotype. As expected, *cerk1-4* plants exhibited cell death and chlorosis, particularly on lower leaves. A similar phenotype was shown by four out of five transgenic plant lines expressing *cerk1-4 cvg1*, indicating that reduced ectodomain shedding cannot suppress the *cerk1-4* phenotype. *cerk1 cvg1* expressing plants looked like wild type, confirming that the cell death phenotype of *cerk1-4 cvg1* plants is caused by the *cerk1-4* and not by the *cvg1* mutation.

Immunoblot analysis of *Bgh* inoculated plants was performed to check for CERK1 protein levels and CERK1 band pattern in the transgenic plant lines (Figure 10B). Full length protein (75 kDa) could be observed for Col-0, Col-3 *gl1* and *cerk1-4* and an ectodomain fragment (33 kDa) for Col-0 and Col-3 *gl1*. No CERK1-specific bands were detected for *cerk1-2*. As expected, ectodomain abundance in *cerk1 cvg1* expressing plants was reduced compared to wild type. However, it has to be noted that none of the *cerk1 cvg1* lines tested in this experiment reached the overall CERK1 protein levels of the controls. Surprisingly, in plants expressing the double mutant *cerk1-4 cvg1* version, only very low levels of full length *cerk1* protein could be detected compared to wild type. In spite of the low abundance of *cerk1-4 cvg1*, the protein amount was apparently still sufficient to trigger the *cerk1-4* phenotype. Also, the *cerk1-4 cvg1* protein maintained the ability to bind chitin, as indicated by pulldown experiments with chitin magnetic beads (Figure 10B). Interestingly, an ectodomain fragment could be detected in chitin pull-downs after long exposure for *cerk1-4 cvg1* expressing plants, which is not present in *cerk1-4* plants.

A



B

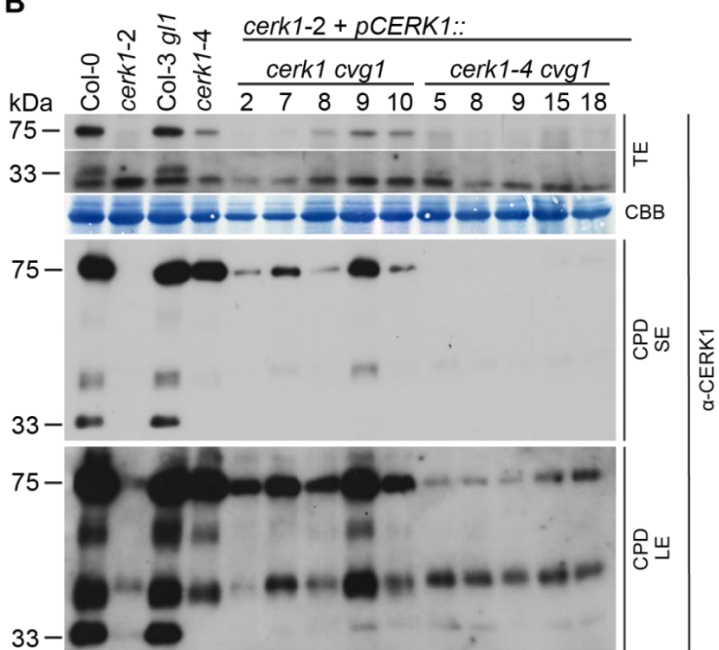


Figure 10 on page 68. The *cvg1* mutation cannot suppress the *Bgh*-induced *cerk1-4* phenotype. Five independent transgenic lines either expressing *cerk1 cvg1* or *cerk1-4 cvg1* under control of the CERK1 promoter as well as control plants were inoculated with *Blumeria graminis* f.sp. *hordei* (*Bgh*). T1 plants were selected for Basta® resistance and Col-0, *cerk1-2*, Col-3 *gl1* and *cerk1-4* served as controls. A) The macroscopical phenotype was assessed seven days after inoculation and pictures were taken. This experiment was repeated twice with similar results. B) Anti-CERK1 immunoblot using protein samples prepared from plants shown in A). 2-3 leaves were harvested from each plant. Col-0, *cerk1-2*, Col-3 *gl1* and *cerk1-4* plants were harvested the same way. The upper panel shows total protein extracts (TE). To visualize both, the 75 kDa full length fragment and the 33 kDa ectodomain fragment optimally, different exposure times are shown. Lower panel shows chitin pull-downs (CPD) using total extracts shown in the upper panel. Two exposure times are shown to optimally visualize the ectodomain of *cerk1-4 cvg1* expressing plants. CBB, Coomassie Brilliant blue staining (loading control); SE, short exposure; LE, long exposure. This experiment was repeated twice with similar results.

In addition to the exaggerated cell death phenotype upon inoculation with *Bgh*, *cerk1-4* plants also exhibit a typical phenotype during senescence, which is characterised by a reduced rosette size and enhanced cell death on older leaves (Petutschnig *et al.*, 2014). To test if the *cvg1* mutation could suppress the *cerk1-4* senescence phenotype, five independent transgenic plants expressing *cerk1-4 cvg1* or *cerk1 cvg1* were assessed after five and ten weeks of growth, respectively (Figure 11A). At the age of five weeks, all plants, including the *cerk1-4* control, looked like wild type with no macroscopically visible cell death. At ten weeks, *cerk1-4* and all tested *cerk1-4 cvg1* expressing plants showed the characteristic *cerk1-4* senescence phenotype (Figure 11A). *cerk1 cvg1* expressing plants looked like wild type plants, confirming that the senescence phenotype is caused by *cerk1-4* and not the *cvg1* mutation. Immunoblot analysis was performed to assess CERK1 expression and band pattern (Figure 11B). The control plants Col-0, *cerk1-2*, Col-3 *gl1* and *cerk1-4* showed the expected band pattern. The transgenic lines expressing *cerk1 cvg1* showed CERK1 full length signals (75 kDa) that were comparable to wild type or weaker. In agreement with earlier results, the soluble ectodomain fragment was hardly visible in these lines. For *cerk1-4 cvg1* expressing plants, only a weak 75 kDa signal corresponding to full length protein could be detected, which is very similar to the results obtained with *Bgh* infected *cerk1-4 cvg1* expressing plants. Taken together, the immunoblot data suggest that the *cvg1* mutation has a destabilizing effect on CERK1 which predominantly affects the soluble CERK1 ectodomain fragment as a single mutation. In combination with the *cerk1-4* mutation, the effect seems to become more severe and to also destabilize the full length CERK1 protein. The results of the phenotypic analyses suggest that the *cvg1* mutation could neither suppress the enhanced cell death phenotype after pathogen challenge nor the characteristic *cerk1-4* senescence phenotype.

Figure 11 on page 70. The *cvg1* mutation cannot suppress the *cerk1-4* senescence phenotype. Five independent transgenic lines expressing either *cerk1 cvg1* or *cerk1-4 cvg1* in the *cerk1-2* background under control of the endogenous CERK1 promoter were grown under short day conditions. T1 plants were selected for Basta® resistance and Col-0, *cerk1-2*, Col-3 *gl1* and *cerk1-4* served as controls. A) Phenotype was macroscopically assessed after 5 and 10 weeks of growth and pictures were taken. B) Immunoblot analysis using the specific CERK1 antibody. Total extracts (TE) were prepared plants shown in A). 2 – 3 leaves were harvested from each plant including controls. The upper panel shows total protein extracts (TE). To visualize both, the 75 kDa full length fragment and the 33 kDa ectodomain fragment optimally, different exposure times are shown. Lower panel shows chitin pull-down which was performed using the total extracts shown in the upper panel. CBB, Coomassie Brilliant blue. This experiment was repeated twice with similar results.

3.1.4 Variation of the CERK1 extracellular stalk length

Point mutations targeting potential cleavage motifs in the extracellular juxtamembrane domain (extracellular stalk) of CERK1 did not fully suppress its ectodomain shedding. Furthermore, deletion of a potential cleavage motif within the intracellular juxtamembrane domain had no effect on the CERK1 band pattern. Therefore, other factors than the amino acid sequence might be of importance for proteolytic processing of the extracellular domain. Migaki *et al.* (1995) showed that cleavage of the leukocyte adhesion molecule L-selectin could be inhibited by reduction of the extracellular stalk length. Deletion of five amino acids within the extracellular stalk could suppress cleavage of the L-selectin extracellular domain completely, even if the native cleavage site of L-selectin was maintained. Similar effects were reported for other transmembrane proteins that undergo ectodomain shedding such as the interleukin 6-receptor (Baran *et al.*, 2013) or the p75 neurotrophin receptor (Weskamp *et al.*, 2004). This raised the idea that proteolytic cleavage of the CERK1 ectodomain might also depend on the length of the extracellular stalk. Therefore, CERK1 mutants were generated, where amino acids of the extracellular stalk were deleted (Figure 12A). In one mutant construct, five amino acids close to the transmembrane domain were deleted (*cerk1 del1*). In a second construct a deletion of 11 amino acids within the extracellular stalk was generated (*cerk1 del2*). In this construct, only a short amino acid stretch of the extracellular stalk was left as a linker between the third LysM domain and the transmembrane domain. Both mutant *cerk1* variants were cloned into the pGreenII-0229PREP vector containing the native CERK1 promoter and expressed in the CERK1 knockout mutant background *cerk1-2*. Three independent transgenic plants expressing *cerk1 del1* were analyzed in immunoblot experiments together with control lines (Figure 12B).

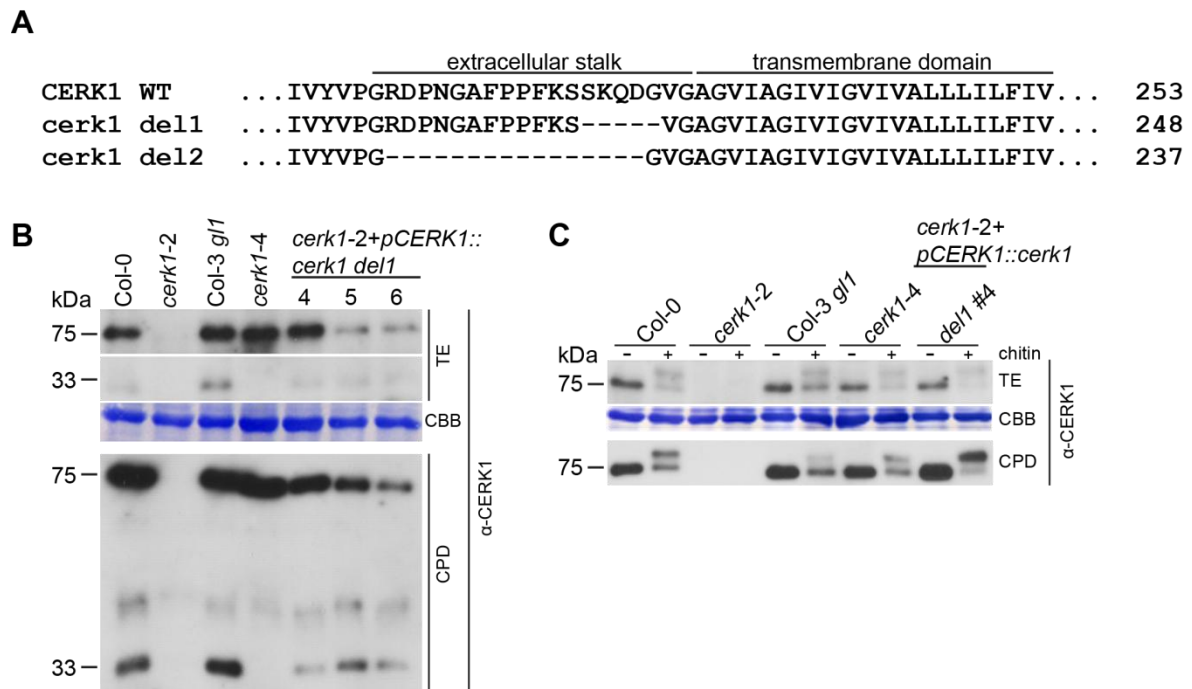


Figure 12. Deletion within the extracellular stalk did not suppress CERK1 ectodomain shedding. A) Alignment of generated CERK1 deletion mutants to wild type CERK1. Deleted amino acids are indicated by dashes. B) Anti-CERK1 immunoblot of three transgenic lines expressing *cerk1 del1* in the CERK1 knockout background *cerk1-2* under control of the native CERK1 promoter. Col-0, *cerk1-2*, Col-3 *gl1* and *cerk1-4* were used as controls. Upper panel, total extracts (TE). Lower panel, chitin pull-down (CPD) using total extracts shown in the upper panel. CBB, Coomassie Brilliant Blue stained membrane (loading control). C) Band shift assay. Leaves of one transgenic line expressing *cerk1 del1* and control plants were vacuum infiltrated with 100 $\mu\text{g ml}^{-1}$ shrimp shell chitin and were then incubated for 12 minutes. An immunoblot using the specific CERK1 antibody is shown. Upper panel, total extract of either mock-infiltrated (-) or chitin-infiltrated (+) plants. Lower panel, chitin pull-down performed with total extracts shown in upper panel. Immunoblot analysis was repeated 3 times, band shift assay was repeated 2 times.

The expected band pattern could be detected for the control plants. For all three plants lines expressing *cerk1 del1*, a 75 kDa signal corresponding to the full length protein and a 33 kDa ectodomain fragment could be detected (Figure 12B) even though the overall CERK1 abundance between the transgenic lines was variable. Full length protein and ectodomain fragment of *cerk1 del1* could be pulled down using magnetic chitin beads demonstrating chitin binding capacity (Figure 12B). In addition to chitin binding, functionality of *cerk1 del1* is further indicated by chitin-induced receptor phosphorylation, which appears as a characteristic band shift in immunoblot experiments (Figure 12C).

In transgenic plants expressing *cerk1 del2* neither full length protein nor ectodomain fragment could be detected (not shown), even though 17 independent transformants were analyzed. Deletion of 16 amino acids within the CERK1 extracellular stalk did probably cause structural instability of the protein.

3.1.5 CERK1-FLS2 domain swap experiments

CERK1 cleavage motif and short deletion mutants were not successful to suppress CERK1 ectodomain shedding. Longer deletions affected the stability of the CERK1 protein and thus the position of CERK1 proteolytic cleavage remains unknown. To generate shedding deficient CERK1 variants and/or to narrow down the area where CERK1 ectodomain shedding occurs, domain swap constructs with FLS2 were generated. FLS2 is the *Arabidopsis* flagellin receptor (Chinchilla *et al.*, 2006) and one of the best characterized plant RLKs. To date there are no reports of any proteolytic modification of FLS2, suggesting that FLS2 may not be subject to ectodomain shedding. By replacing the CERK1 transmembrane domain and parts of the CERK1 extracellular stalk with the respective parts of FLS2, chimeric CERK1 FLS2 mutants were generated (Figure 13A). CERK1 FLS2 chimeras lacking the CERK1 sequences critical for ectodomain shedding should not generate any soluble ectodomain fragments and possibly extend our knowledge about the CERK1 cleavage site. A series of chimeric CERK1-FLS2 constructs were generated. In *cerk1 fls2tm*, the CERK1 transmembrane domain was replaced by the FLS2 transmembrane domain (*cerk1 fls2tm*). In a second variant, the amino acid sequence of the CERK1 extracellular stalk beginning with serine at position 224 was replaced by the entire extracellular stalk of FLS2 including the FLS2 transmembrane domain (*cerk1 fls2tmex1*). In *cerk1 fls2tmex2*, the CERK1 transmembrane domain and eight amino acids N-terminal of the transmembrane domain were replaced with the respective sequences of FLS2. A fourth domain swap construct was generated where the entire extracellular stalk and the transmembrane domain of CERK1 were replaced by the entire extracellular stalk and transmembrane domain of FLS2 (*cerk1 fls2tmex3*). The chimeric CERK1-FLS2 constructs were cloned into the vector pGreenII-0229PREP and heterologously expressed in *Nicotiana benthamiana* under control of the endogenous CERK1 promoter. A CERK1 wild type construct was transformed as control. To confirm specificity of the observed bands, a sample of a non-transformed *N. benthamiana* leaf was included. Immunoblot analysis using the specific CERK1 antibody revealed expression of all constructs in *N. benthamiana* (Figure 13B). A signal at 75 kDa corresponding to the full length CERK1 protein and a 33 kDa fragment corresponding to the soluble ectodomain could be detected for wild type CERK1. Full length protein at 75 kDa and an ectodomain fragment at 33 kDa could also be observed for *cerk1 fls2tm* and *cerk1 fls2tmex2*. Leaves expressing *cerk1 fls2tmex1* and *cerk1 fls2tmex3* showed a full length signal with a higher molecular weight than wild type CERK1. This was expected due to the insertion of the FLS2 extracellular stalk, which is longer than the CERK1 extracellular stalk. Interestingly, even though *cerk1 fls2tmex3* full

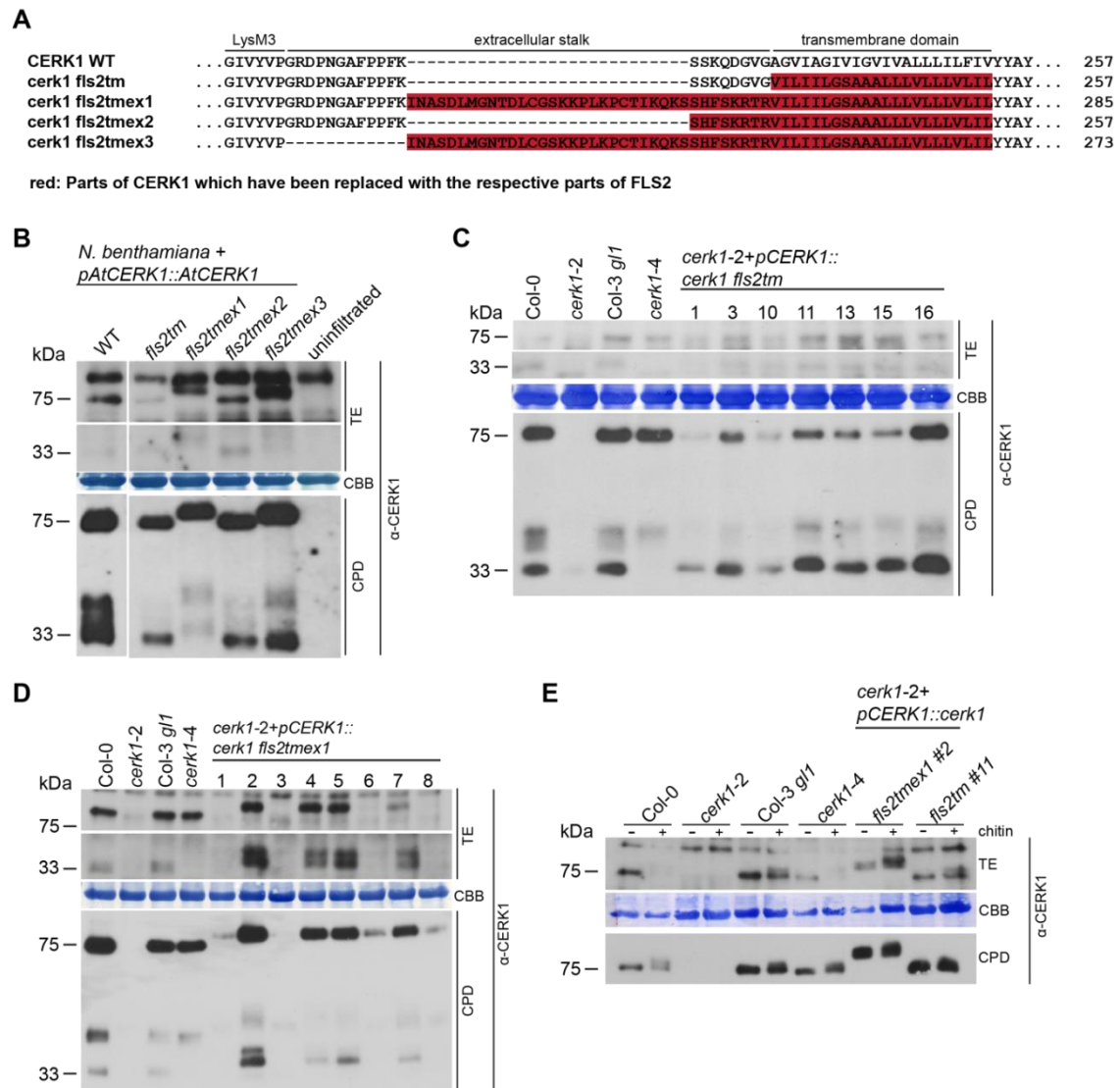


Figure 13. Replacement of the CERK1 extracellular stalk and transmembrane domain could not suppress CERK1 ectodomain shedding. A) Alignment of generated CERK1-FLS2 domain-swap mutants to the wild type CERK1 sequence. Sequences highlighted in red derive from FLS2 and have been used to replace the respective parts of CERK1. B) Anti-CERK1 immunoblot of CERK1-FLS2 domain swap proteins expressed transiently under control of the native CERK1 promoter in *Nicotiana benthamiana*. Wild type CERK1 was expressed as a control protein and uninfiltrated *Nicotiana benthamiana* leaves served as a negative control. Samples were harvested 3 days after infiltration. Upper panel, immunoblot with total protein extracts (TE). Lower panel, immunoblot with chitin pull-downs (CPD) of total extracts shown in upper panel. CBB, Coomassie Brilliant Blue stained membrane (loading control). C) Anti-CERK1 immunoblot of seven individual transgenic lines expressing *cerk1 fls2tm* under control of the native CERK1 promoter in the *cerk1-2* background. Col-0, *cerk1-2*, Col-3 *gl1* and *cerk1-4* were used as controls. Upper panel, total extracts. Lower panel, chitin pull-down of total extracts. D) Anti-CERK1 immunoblots of eight individual transgenic lines expressing *cerk1 fls2tmex1* under control of the native CERK1 promoter in *cerk1-2*. Col-0, *cerk1-2*, Col-3 *gl1* and *cerk1-4* were used as controls. Upper panel, total extracts showing two different exposure times to visualize both, the full length protein and the ectodomain. Lower panel, chitin pull-down of total extracts. E) Band shift assay. Leaves of transgenic lines expressing *cerk1 fls2tmex1* and *cerk1 fls2tm* as well as control plants were vacuum infiltrated with $100 \mu\text{g ml}^{-1}$ shrimp shell chitin and were then incubated for 12 minutes. Immunoblots using the specific CERK1 antibody is shown. Upper panel, total extracts of mock-infiltrated (-) or chitin-infiltrated (+) samples. Lower panel, chitin pull-downs of total extracts shown in upper panel. This experiment was repeated three times with similar results.

length protein had a higher apparent molecular weight than wild type CERK1, it showed an ectodomain fragment that was very similar in size to the wild type variant. In contrast, the N-terminal fragment of *cerk1 fls2tmex1* ectodomain had a higher apparent molecular weight and gave only a very weak signal. All CERK1-FLS2 domain swap constructs retained chitin binding ability, as full length protein and ectodomain could be detected for all domain swap constructs after chitin pulldown (Figure 13B).

cerk1 fls2tm and *cerk1 fls2tmex1* were also stably transformed into the CERK1 knockout mutant *cerk1-2*. Seven independent transgenic lines expressing *cerk1 fls2tm* were tested for ectodomain shedding in immunoblot experiments using the CERK1 specific antibody (Figure 13C). All controls (Col-0, Col-3 *gl1*, *cerk1-4* and *cerk1-2*) showed the expected CERK1 band pattern. Confirming the results obtained by transient expression in *N. benthamiana*, full length *cerk1 fls2tm* protein (75 kDa) and ectodomain (33 kDa) could be detected for all tested transgenic *cerk1 fls2tm* lines. These results indicate that CERK1 ectodomain shedding does not depend on the CERK1 transmembrane domain. Full length *cerk1 fls2tm* as well as *cerk1 fls2tm* ectodomain could be detected after pulldown with chitin magnetic beads indicating that chitin binding ability of this CERK1 variant is not disturbed in *Arabidopsis*.

Eight transgenic *cerk1 fls2tmex1* expressing lines were analyzed for CERK1 ectodomain shedding in immunoblot experiments (Figure 13D). As expected, full length CERK1 signal (75 kDa) could be detected for Col-0, Col-3 *gl1* and *cerk1-4*, while an ectodomain fragment (33 kDa) could only be detected in Col-0 and Col-3 *gl1* and was missing in *cerk1-4*. As already observed in heterologous expression experiments in *N. benthamiana*, full length *cerk1 fls2tmex1* had a bigger apparent molecular weight than its wild type CERK1 counterpart. While *cerk1 fls2tmex1* had shown a very weak N-terminal fragment signal in *N. benthamiana*, the signal was quite strong in several *cerk1 fls2tmex1* expressing *Arabidopsis* plants. The putative *fls2tmex1* ectodomain signal appeared as a double band at a size clearly larger than the wild type CERK1 soluble ectodomain (Figure 13D). *cerk1 fls2tmex1* maintained chitin binding ability, as for all tested transgenic lines full length protein and N-terminal fragments could be detected after pull-down with chitin magnetic beads. While the two putative ectodomain fragment bands were of similar intensity in blots performed with total extracts, the lower band was predominant after chitin pull-down. This suggests that the upper band might be cleaved *in vitro*.

One *cerk1 fls2tm* and one *cerk1 fls2tmex1* expressing line were chosen to be tested for receptor phosphorylation after chitin treatment (Figure 13E). Both tested lines showed an electrophoretic mobility shift, which was comparable to Col-0, Col-3 *gl1* and *cerk1-4*. This suggests that signaling initiated by ligand binding to the extracellular chitin binding domain

can still be transmitted into the cell via the FLS2 extracellular stalk and the FLS2 transmembrane domain.

3.1.6 CERK1 and FLS2 extracellular stalk harbor a KS motif

Based on the results of the cleavage motif, deletion and domain swap mutants, it remained unclear which amino acids or structural characteristics are critical for CERK1 ectodomain shedding. In particular, the N-terminal fragments of the *cerk1 fls2tmex1* and *cerk1 fls2tmex3* protein variants were puzzling. The putative ectodomain fragment of *fls2tmex1* appeared as a double band and the ectodomain fragment of *cerk1 fls2tmex3* was the same size as in wild type CERK1, although the full length protein was larger. A closer look at the amino acid sequences of the extracellular stalk of CERK1 and the generated domain swap constructs revealed the presence of a lysine followed by a serine (KS) within the extracellular stalk (Figure 14). This motif is also present in the tested protease cleavage motif and deletion mutants.

	LysM3	extracellular stalk			
CERK1 WT	...GIVYVPGRDPNGAFPPFK	-----SSKQDGVG...	231	→	33 kDa
<i>cerk1 fls2tm</i>	...GIVYVPGRDPNGAFPPFK	-----SSKQDGVG...	231	→	33 kDa
<i>cerk1 fls2tmex1</i>	...GIVYVPGRDPNGAFPPFK	INASDLMGNTDLCGSKKPLKPC TIKQKS SHFSKRTR...	259	→	37 kDa
<i>cerk1 fls2tmex2</i>	...GIVYVPGRDPNGAFPPFK	-----SHFSKRTR...	231	→	33 kDa
<i>cerk1 fls2tmex3</i>	...GIVYVP	-----INASDLMGNTDLCGSKKPLKPC TIKQKS SHFSKRTR...	247	→	36 kDa

Figure 14. CERK1 and FLS2 extracellular stalk share a lysine-serine (KS) motif. Alignment of CERK1 extracellular stalk amino acid sequence with the generated CERK1 FLS2 domain swap constructs. The shared lysine-serine (KS) motif is indicated in red letters. Molecular masses were calculated based on the N-terminal part of each CERK1 FLS2 domain swap construct up to the marked serine. 10 kDa were added for 5 glycosylation sites present in the CERK1 ectodomain.

Figure 14 shows the calculated masses of the ectodomain for CERK1 wild type and the CERK1 FLS2 domain swap constructs if cleavage of the CERK1 ectodomain would occur at or near the KS motif. This would explain the size differences of the ectodomains between *cerk1 fls2tmex1* and wild type CERK1 after transient expression in *Nicotiana benthamiana* (Figure 13B). The double band of *cerk1 fls2tmex1* ectodomain fragment and the wild type-like size of the *cerk1 fls2tmex3* ectodomain signal could then be explained by an additional genuine cleavage site within the FLS2 extracellular stalk.

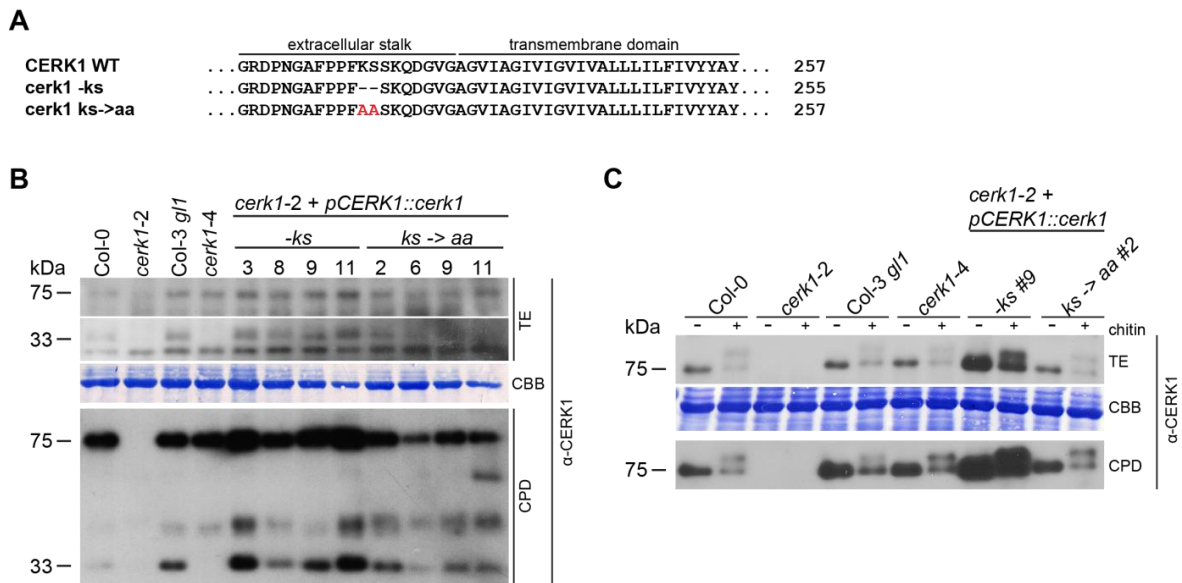


Figure 15. The KS motif within the FLS2 and CERK1 extracellular stalk is most likely not a cleavage motif.

A) Alignment of KS motif mutants to the wild type CERK1 sequence. Deleted amino acids are indicated with dashes, while replaced amino acids are shown in red letters. B) CERK1 immunoblots of three individual transgenic plants lines either expressing *cerk1*-ks or *cerk1* ks->aa under control of the native CERK1 promoter in *cerk1-2*. Col-0, *cerk1-2*, Col-3 *gl1* and *cerk1-4* were used as controls. Upper panel, total extracts (TE); lower panel, chitin pull-downs (CPD) prepared from the total extracts shown in upper panel. CBB, Coomassie Brilliant Blue stained membrane (loading control). C) Band shift assay using one transgenic line per KS motif mutant construct. Leaves were vacuum infiltrated with 100 $\mu\text{g ml}^{-1}$ shrimp shell chitin and incubated for 12 minutes. Immunoblot using the specific CERK1 antibody is shown. Upper panel, total extracts of mock-infiltrated (-) or chitin-infiltrated (+) samples. Lower panel, chitin pull-downs of total extracts shown in upper panel. Ectodomain shedding immunoblot was repeated 3 times with similar results and band shift assay was repeated twice with similar results.

To explore the hypothesis explained above, additional CERK1 variants were generated by either deleting the KS (*cerk1* -ks) motif or replacing it by two alanines (*cerk1* ks->aa) (Figure 15A). These variants were cloned into the vector pGreenII-0229PREP including the endogenous CERK1 promoter and the resulting constructs were used to generate transgenic lines in the CERK1 knockout mutant *cerk1-2*. Ectodomain shedding of four independent transgenic lines per construct was tested by immunoblotting with the specific CERK1 antibody (Figure 15B). Col-0, Col-3 *gl1* and *cerk1-4* showed a full length CERK1 signal (75 kDa). An ectodomain fragment could be detected for Col-0 and Col-3 *gl1*, but was missing in *cerk1-4* plants. No CERK1 signal was detected for *cerk1-2*. For each of the tested transgenic lines, a signal at 75 kDa corresponding to full length protein and a signal at 33 kDa corresponding to the soluble ectodomain could be observed (Figure 15B). The abundance of full length protein and ectodomain fragment seemed to be enhanced in plants expressing *cerk1* -ks. Full length protein as well as ectodomain fragments could be detected for all transgenic lines after chitin pull-down, indicating chitin binding ability of both, *cerk1* -ks and *cerk1* ks->aa.

One transgenic line per construct was tested for chitin induced autophosphorylation of CERK1 (Figure 15C). Both lines showed a characteristic band shift after chitin treatment comparable to Col-0 and Col-3 *gl1*, indicating functionality of both CERK1 variants.

3.1.7 The extracellular domains of many receptor-like kinases can be found in supernatants of cell cultures

The extensive mutational studies described above failed to generate a shedding deficient CERK1-variant and also could not pinpoint the CERK1 cleavage motif. This raised the idea that ectodomain shedding may not require any specific motifs and might be a common phenomenon in plant receptor-like kinases (RLKs). To investigate this theory, supernatants of *Arabidopsis* Col-0 cell cultures were collected and analyzed by mass spectrometry. These supernatants were expected to be enriched in apoplastic proteins and might contain shed extracellular domains of receptor-like kinases and possibly also receptor-like proteins. Thus, this approach could reveal additional RLKs which are subject to ectodomain shedding. The collected cell culture supernatant was filtered and concentrated by protein precipitation. Subsequent mass spectrometric analyses identified 588 proteins. The subcellular localization of these proteins was then predicted by SUBA3 (Tanz *et al.*, 2013) and results are summarized in Table 9. Proteins predicted to be localized to the extracellular space represented more than one third of all proteins found and half of all peptides in the sample and were thus the biggest fraction of all identified proteins. Cytosolic proteins accounted for 23.8 % of all proteins and 19.5 % of all peptides.

Table 9. Predicted localization of proteins from cell culture supernatants. SUBA3 localization prediction of proteins found in supernatants of *Arabidopsis* cell cultures.

Predicted localization	Proteins	%	Peptides	%
Extracellular	201	34.2	3678	50
Cytosol	140	23.8	1432	19.5
Plasma membrane	79	13.4	772	10.5
Plastid	60	10.2	497	6.8
Mitochondrion	42	7.1	334	4.5
Vacuole	29	4.9	472	6.4
Peroxisome	11	1.9	48	0.7
ER	10	1.8	64	0.9
Nucleus	16	2.7	58	0.7
Total	588	100	7355	100

The majority of detected cytosolic, plastid and mitochondrial proteins are highly abundant proteins involved in primary metabolism (Supplemental file 2) and are therefore likely contaminants. Furthermore, 13.4 % of all identified proteins (corresponding to 10.5% of all peptides) were predicted to be localized to the plasma membrane. Apoplastic and plasma membrane (PM)-localized proteins were probably underestimated in this study, because they are typically glycosylated and glycosylated peptides cannot be identified by the method used.

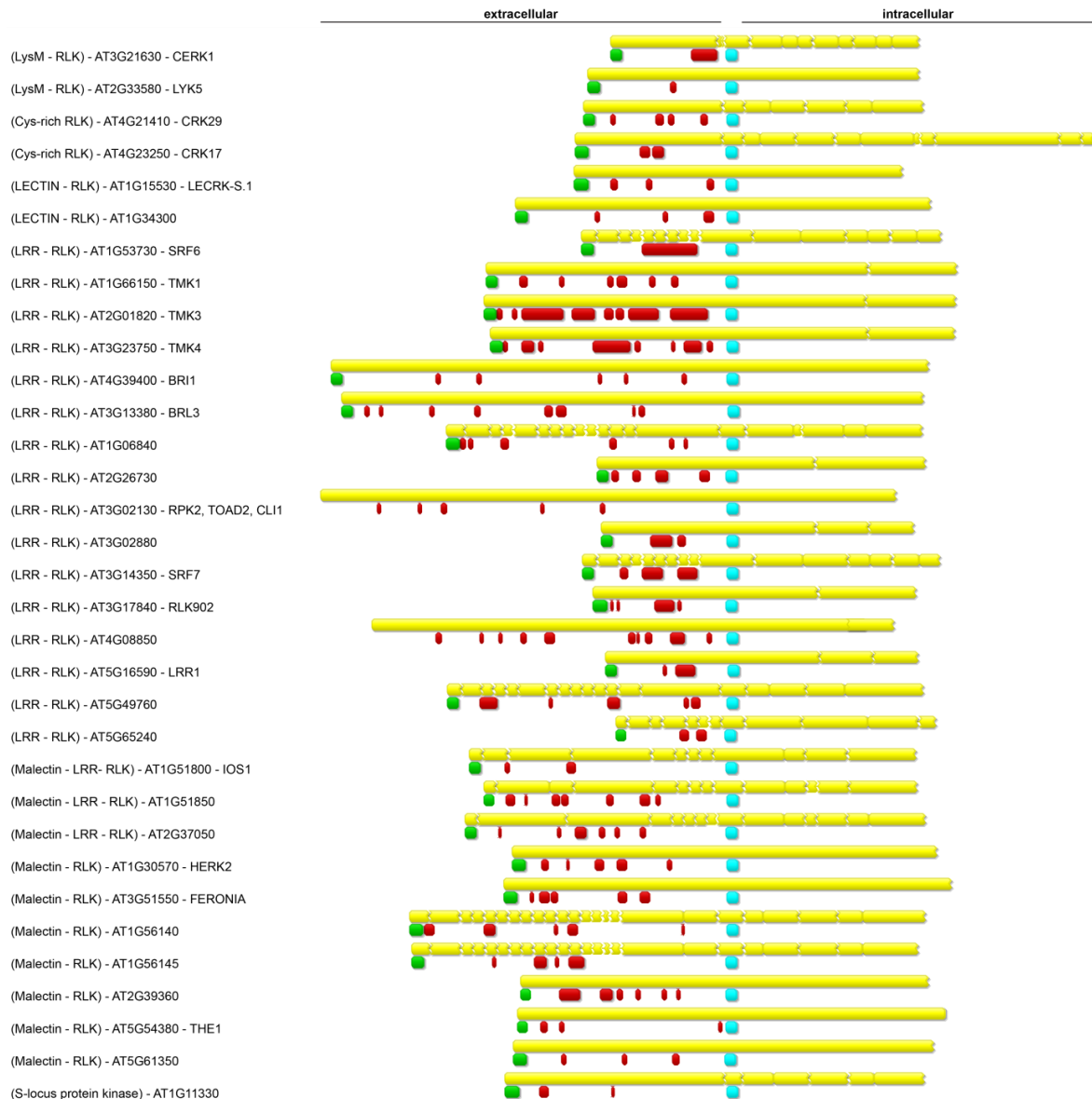


Figure 16. Receptor-like kinases found in Col-0 cell culture supernatants. The coding sequence of the proteins is shown as a yellow bar and breaks indicate the positions of introns. Identified peptides were mapped to the amino acid sequence of the respective RLK and peptide coverage is shown in red. The transmembrane domains are shown in light blue and predicted signal peptides are given in green. For easier comparison, the RLKs were aligned by their transmembrane domains.

Among the 588 identified proteins, 33 were found to be receptor-like kinases and 4 receptor-like proteins. Thus RLKs and RLPs account for 46.8 % of all identified PM proteins. Most of the identified receptor-like kinases were LRR-RLKs, but cysteine-rich RLKs, Lectin-RLKs, CrRLKs and the LysM-RLKs CERK1 and LYK5 were also found. Peptides corresponding to the identified receptor-like kinases were then aligned to their full length amino acid sequences (Figure 16). Interestingly, only peptides corresponding to extracellular parts of the receptor-like kinases could be found in supernatants of cell cultures. Despite the presence of cytosolic and plasma membrane localized proteins in the sample, peptides corresponding to intracellular parts of receptor-like kinases were not detected. Therefore, the peptides corresponding to extracellular domains of receptor-like kinases might derive from ectodomains released by shedding or a similar mechanism. Peptides corresponding to all 3 members of the TRANSMEMBRANE KINASE (TMK) group of LRR-RLKs (comprising a total of 4 members) which are expressed in leaves (Winter *et al.*, 2007) were found. The ectodomain of TMKs consists of LRR-motifs which are separated by a non-LRR domain (Liu *et al.*, 2013b). To test whether the non-LRR domain is the cleavage site for release of the N-terminal fragment, the mapping positions of peptides found in the supernatant of cell cultures were compared to the domain organization of the TMK proteins (Figure 17A). Peptides N- and C-terminal of the non-LRR domain could be found indicating that the non-LRR domain is not the site where the soluble extracellular derivative of the TMK proteins is generated. AT1G51800 (IOS1), AT1G51850 and AT2G37050 are Malectin-LRR-RLKs and resemble members of the symbiosis receptor-like kinase family (Hok *et al.*, 2011). They contain a malectin-like domain and short LRR motif stretches. The *L. japonicus* symbiosis receptor-like kinase

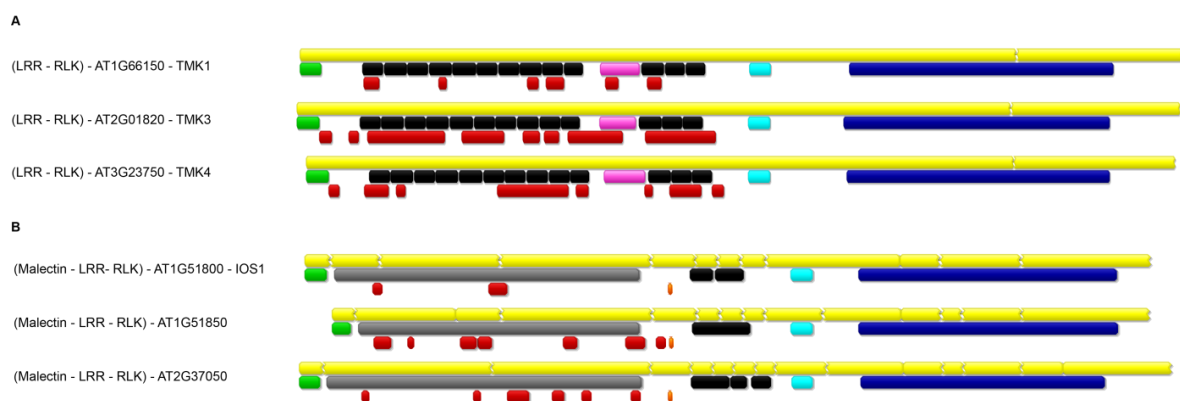


Figure 17. Detailed analysis of TMK1-3 and Malectin-LRR-RLKs. Domain organization of TMK1, TMK3 and TMK4. B) Domain organization of Malectin – LRR – RLKs. The coding sequence of the proteins is given as yellow bar with breaks indicating introns. As in Figure 16 peptides are aligned to the amino acid sequence and peptide coverage is shown in red. Green: Signal peptide; Black: LRR-repeats; Pink: non-LRR domain; light blue: transmembrane domain; blue: kinase domain; gray: malectin-like domain; orange: GDPC motif.

SYMRK was reported to be proteolytically processed to release its malectin-like domain (Antolín-Llovera *et al.*, 2014). A GDPC motif connecting the malectin-like domain and LRRs was found to be critical for this process. The three Malectin-LRR-RLKs found in this study also harbored a GDPC motif and only peptides N-terminal of this motif were found (Figure 17B). This points to a SYMRK-like release of the malectin-like domain in *Arabidopsis*. In addition to receptor-like kinases, peptides corresponding to four receptor-like proteins were found (Figure 18). These are either anchored to the outer leaflet of the plasma membrane via GPI anchor (LYM1-3) or via a transmembrane domain (RLP51). GPI anchors are known to be cleaved by lipases, such as phospholipase D (Paulick & Bertozzi, 2008), while the release of the RLP51 N-terminal domain probably occurs via ectodomain shedding or a related process. This experiment was performed with two different *Arabidopsis* cell culture lines (Ath-1, Ath-2) after one week or two weeks of subculturing (4 samples in total). The sample shown here (Sample02) yielded the highest number of RLKs and RLPs and the best peptide coverages, but overall the other three samples gave similar results (Table S1, Table S2, Table S3, Table S4, Table S5, Figure S1, Figure S2, Figure S3).

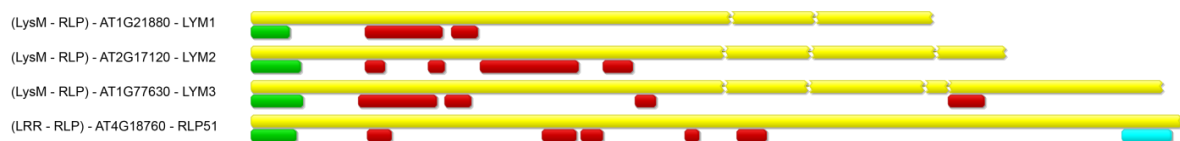


Figure 18. Receptor like proteins found in Col-0 cell culture supernatant. The exon structure of receptor-like proteins found in supernatants of Col-0 cell culture is shown in yellow. Identified peptides were aligned to the amino acid sequence and peptide coverage is shown in red. Predicted signal peptides are given in green and transmembrane domains are shown in light blue.

To validate the quality of the supernatant samples, total protein extracts from the cultured cells were prepared (Figure 19) and compared by immunoblotting to the supernatant samples analyzed by mass spectrometry. The proteomic analysis suggested ectodomain shedding of CERK1 and BRI1. For both receptor kinases, N-terminal antibodies are available that can detect ectodomain fragments. An immunoblot with a C-terminal antibody against FLS2 was included as a control. The full length receptor proteins could be detected for CERK1 (75 kDa), BRI1 (140 kDa) and FLS2 (175 kDa) in total extracts (lane A+B), but not in supernatants. Ectodomain fragments could be detected for CERK1 (33 kDa) and BRI1 (95 kDa) in total extracts and were enriched in most of the supernatants (lane C). As a C-terminal FLS2 antibody was used, no fragments corresponding to extracellular domains were detectable.

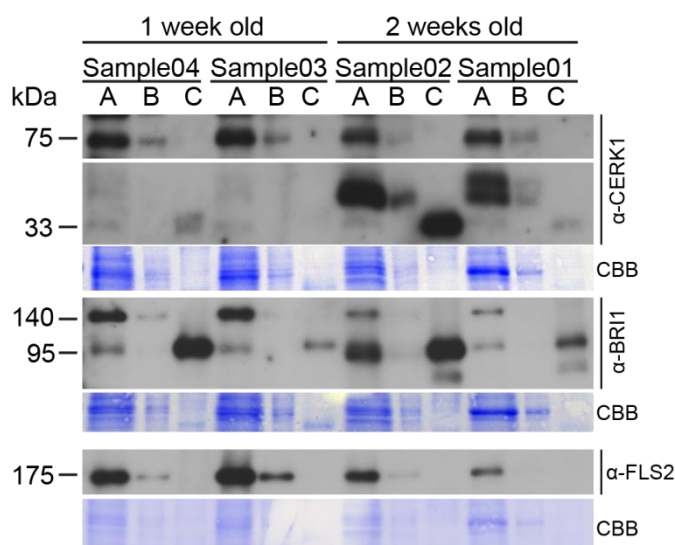


Figure 19. Only soluble ectodomain can be found in cell culture supernatants. Protein samples were prepared from one or two week old subcultured *Arabidopsis* cell culture lines. Total extracts of each cell culture sample were prepared and either 15 μ g (A) or 3 μ g (B) protein were loaded. Supernatants were collected and 3 μ g of precipitated proteins was used (C). Anti-CERK1, anti-BRI1 and anti-FLS2 immunoblots are shown. CBB, Coomassie Brilliant Blue membranes (loading control).

The absence of full length proteins from supernatants indicated good quality of the samples. To confirm the data of cell culture supernatants, apoplastic wash fluids (AWF) of *Arabidopsis thaliana* Col-3 *gl1* leaves were prepared. Col-3 *gl1* was chosen as a starting material to avoid contamination caused by broken trichomes. The AWF was subjected to analysis by mass spectrometry and 1005 proteins were identified (Table 10). AWFs are more difficult to harvest than cell culture supernatants. Even though great care was taken not to injure the leaves during the process, the quality of the AWF sample was lower than the cell culture supernatant preparation. In contrast to cell culture supernatants, the proportion of extracellular proteins was much lower. Only 15.9 % of the identified proteins (corresponding to 20.5 % of all peptides) were predicted to be localized to the apoplast (Table 10).

Table 10. Predicted localization of proteins from apoplastic wash fluids. SUBA3 localization prediction of proteins found in apoplastic wash fluids of *Arabidopsis thaliana* Col-0 leaves.

Predicted localization	Proteins	%	Peptides	%
Extracellular	160	15.9	2519	20.5
Cytosol	338	33.6	3200	26
Plasma membrane	51	5.1	442	3.6
Plastid	275	27.4	4085	33.1
Mitochondrion	76	7.6	946	7.7
Vacuole	23	2.3	384	3.1
Peroxisome	51	5.1	553	4.5
ER	13	1.3	112	0.9
Nucleus	18	1.7	72	0.6
Total	1005	100	12313	100

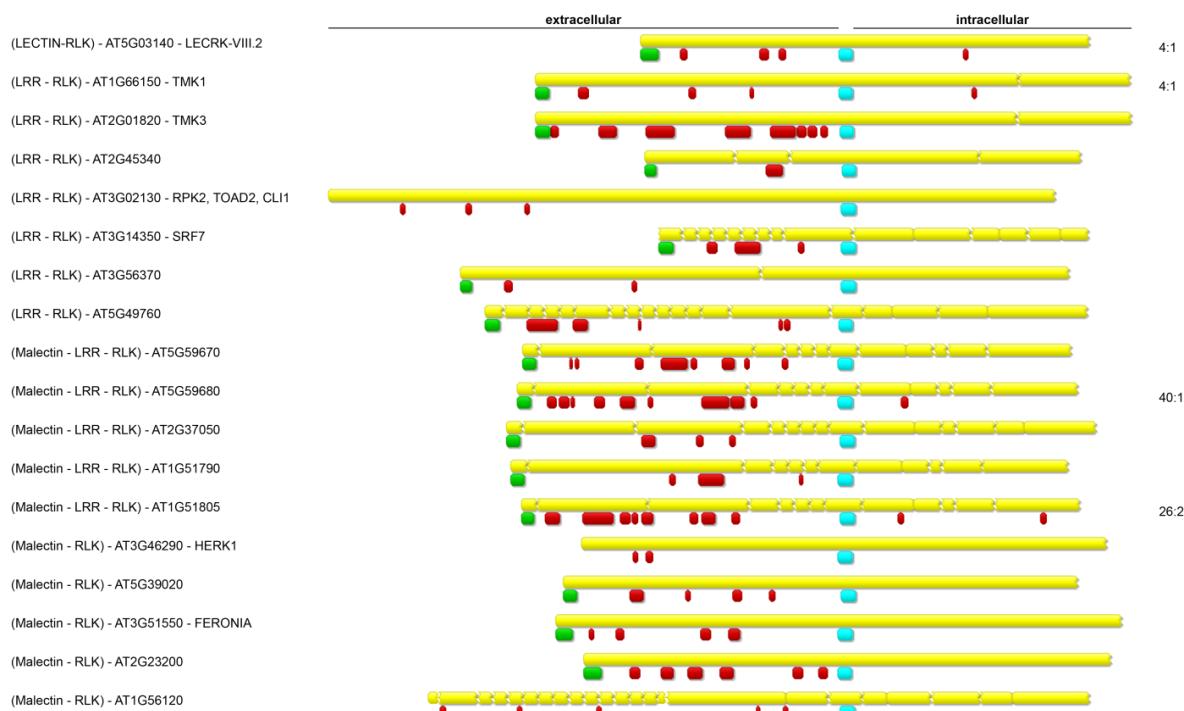


Figure 20. Receptor-like kinases found in apoplastic wash fluids of Col-3 *gl1* leaves. The exon structure of receptor-like kinases which were found in apoplastic wash fluids is shown in yellow. Peptides were aligned to amino acid sequence and peptide coverage is shown in red. Proteins were arranged by the transmembrane domain for easier comparison. Transmembrane domain is shown in light blue. Predicted signal peptides are given in green. Numbers indicate ratio of extracellular to intracellular peptides.

Cytosolic proteins and corresponding peptides accounted for over one third of the total proteins and over one fourth of the peptides found. Plasma membrane localized proteins accounted for 5.1 % of the identified proteins and 3.6 % of the identified peptides. In contrast to cell cultures, leaves are fully autotrophic which is in agreement with a higher number of plastid proteins (27.4 %) in the AWFs. Despite the higher number of proteins detected in *Arabidopsis* apoplastic wash fluids, in comparison to cell culture supernatant, fewer RLKs were identified. 18 RLKs were found that belonged to the classes of LRR-RLKs, Malectin-LRR-RLKs, Malectin-RLKs and LECTIN-RLKs. 9 out of these had also been detected in the cell culture supernatant. The matching peptides were aligned to the RLK amino acid sequences (Figure 20). Similar to cell culture supernatants, the vast majority of peptides mapped to the extracellular domains of the RLKs.

However, a few peptides aligned to intracellular kinase domains: 1 out of 4 peptides (25 %) for AT5G03140, 2 of 26 peptides of AT1G51805 (7.7 %), 1 out of 4 peptides for AT1G66150 (25 %) and 1 of 40 peptides of AT5G59680 (2.5 %). A higher number (5) of Malectin-LRR-RLKs were found in AWFs than in cell culture supernatant. Most of them also harbored a GPDC motif connecting the malectin with the LRR domain. Almost all peptides matching these Malectin-LRR-RLKs mapped to the area N-terminal to the GPDC motif. However, in

one case, one peptide each was found that mapped to an area C-terminal of the GIPC motif. Peptides corresponding to intracellular domains and LRR-domains in Malectin-LRR-RLKs are most likely an artefact caused by the high levels of intracellular contamination. However, additional experiments will be necessary to confirm this. In addition to RLKs, LYM2 (AT2G17120) was the only RLP which could be found in *Arabidopsis* apoplastic wash fluids (Figure 21).



Figure 21. Receptor-like proteins found in Col-3 *g/l1* apoplastic wash fluids. The exon structure of receptor-like proteins found in apoplastic wash fluids is shown in yellow. Peptides were aligned to the amino acid sequence and peptide coverage is shown in red. Predicted signal peptides are given in green.

3.1.8 CERK1 ectodomain shedding is not altered in sphingolipid mutants

Lipid rafts are microdomains within plasma membranes, where sterols and sphingolipids are enriched (Cacas *et al.*, 2012). Receptor-like kinases were reported to localise to these lipid rafts in *Medicago truncatula* (Lefebvre *et al.*, 2007) and *Nicotiana tabacum* (Morel *et al.*, 2006) and it seems conceivable that CERK1 may also localize to lipid rafts. Localization to lipid rafts can be critical for ectodomain shedding in animals (Wakatsuki *et al.*, 2004); (Zimina *et al.*, 2005). CERK1 ectodomain shedding might also occur in lipid rafts and changes of lipid raft composition might lead to alterations in CERK1 ectodomain shedding. Double mutants of sphingolipid fatty acid hydroxylases (*fah1 fah2*) and single mutants of three *Arabidopsis* ceramide synthases (*loh1*, *loh2*, *loh3*) show alterations in sphingolipid composition (König *et al.*, 2012; Ternes *et al.*, 2011).

Interestingly, later in development *fah1 fah2* and *loh1* mutants exhibit a growth phenotype which resembles *cerk1-4*. Therefore, double mutants defective in sphingolipid fatty acid hydroxylation (*fah1 fah2*) (König *et al.*, 2012) or triple mutants where *fah1 fah2* was combined with mutants of each of the *Arabidopsis* ceramide synthases (Ternes *et al.*, 2011) were tested for CERK1 ectodomain shedding. The respective mutant lines were provided by Prof. Ivo Feussner (Georg-August University of Göttingen). At ten weeks of age, double mutant plants (*fah1 fah2*) as well as each of the triple mutant plants (*fah1 fah2 loh1/2/3*) exhibited a growth phenotype characterized by smaller crinkly leaves and the development of cell death (Figure 22A). This phenotype looked similar, but not identical to *cerk1-4* plants of the same age.

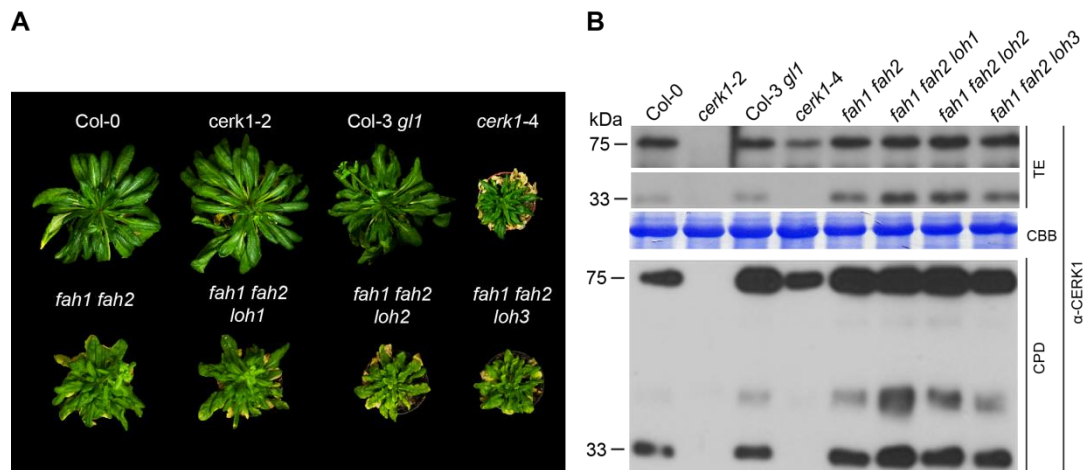


Figure 22. Spingolipid mutants show enhanced CERK1 ectodomain shedding. A) Plants of the indicated genotypes were grown under short day conditions and pictures were taken after 10 weeks of growth. B) CERK1 immunoblots of the plant lines shown in A). Leaves of three plants per genotype were pooled and to prepare total protein extracts (TE, upper panel). Total extracts were used to prepare chitin pull-downs (CPD, lower panel). CBB, Coomassie Brilliant Blue stained membranes (loading control).

Immunoblot analysis of ten-week-old plants was performed (Figure 22B). Full length CERK1 protein (75 kDa) could be detected in all tested lines, except *cerk1-2*. Furthermore, a CERK1 ectodomain fragment (33 kDa) was observed for all tested plant lines, except *cerk1-2* and *cerk1-4*. The abundance of ectodomain fragments seemed to be slightly enhanced in all of the tested sphingolipid mutant lines. CERK1 ectodomain shedding is enhanced by high levels of salicylic acid (Petutschnig *et al.*, 2014); unpublished data). Since *fah1 fah2* mutants contain higher levels of salicylic acid (König *et al.*, 2012), this could be the cause of the enhanced CERK1 ectodomain fragment abundance in these lines.

3.2 Extra-Large G-protein 2 (XLG2) plays a key role in *cerk1-4* cell death execution

To identify components which are involved in *cerk1-4* cell death execution, a forward genetic screen was initiated (Marnie Stolze, unpublished). *cerk1-4* seeds were mutagenized with EMS and screened in the F2 generation for plants that had lost the *cerk1-4* phenotype. The first *cerk1-4* suppressor mutant isolated from the screen was named *nole1-1* (*no lesions 1-1*). *nole1-1* suppressed *cerk1-4*-mediated cell death formation upon *Bgh* inoculation and during senescence. It also restored susceptibility to *Golovinomyces orontii* and reduced pathogen induced elevation of SA levels to wild type levels. The underlying mutation was mapped to the lower arm of chromosome 4 by a new next generation sequencing approach (Hartwig *et al.*, 2012). Analysis of single nucleotide polymorphisms (SNPs) in this region revealed the

introduction of a stop codon into the gene encoding Extra-Large G-protein 2 (XLG2, AT4G34390). Complementation analysis using the genomic sequence of XLG2 expressed under the native XLG2 promoter in *nole1-1* plants confirmed that suppression of the *cerk1-4* phenotype is caused by the premature stop codon within XLG2.

3.2.2 Characterization of *cerk1-4* suppressor mutants

In addition to *nole1-1*, the *cerk1-4* EMS mutagenesis screen yielded several other potential *cerk1-4* suppressing mutants (Marnie Stolze, not published), which were named *noce2/4* to *noce4/6* (no cerk1-4). The first digit of the mutant designation indicates the batch number and the second refers to the plant number. These suppressor mutant candidates were analyzed in more detail and re-evaluated for full suppression of the *cerk1-4* phenotype. For each of these mutant lines, M3 plants were inoculated with *Bgh* and their phenotype was assessed seven days after infection (Figure 23A).

All mutants except *noce2/7* suppressed macroscopically visible lesions after *Bgh* infection. The rosettes of *noce2/4* and *noce3/4* plants appeared smaller compared to wild type plants. Next, the *noce* mutants were analyzed on the molecular level. Since knock-out of CERK1 would suppress the *cerk1-4* phenotype, CERK1 immunoblots were performed.

The controls showed the expected CERK1 band patterns with full length CERK1 and ectodomain fragment in Col-0 and Col-3 *g1/1*, only full length protein in *cerk1-4* and no CERK1-specific signal (or just very weak 40 kDa and 33 kDa bands) in *cerk1-2* and in all tested mutant lines. All *noce* mutants showed a CERK1 band pattern that matched *cerk1-4* (Figure 23B). This was expected, since all mutants were derived from EMS-mutagenized *cerk1-4* seeds. In all *noce* mutants, the *cerk1-4* protein could be pulled down by chitin magnetic beads, which demonstrates normal chitin binding activity.

Since development of the *cerk1-4* phenotype is associated with elevated levels of SA levels upon *Bgh* inoculation (Petutschnig *et al.*, 2014), infected *noce* mutants were tested for expression of the SA-responsive gene PR1 in RT-PCR experiments (Figure 23C). PR1 is strongly induced after *Bgh* inoculation in wild type plants, but the induction is even stronger in *cerk1-4* (Petutschnig *et al.*, 2014). In mutants affected in SA synthesis or signalling, PR1 is not induced upon pathogen inoculation (Nawrath & Métraux, 1999; Zhou *et al.*, 1998). As expected, *cerk1-4* plants showed an exaggerated increase of PR1 expression after *Bgh* infection, while no clear induction was seen in *sid2* or *pad4* plants. The *noce2/7* and *noce3/4* mutations could not suppress the increased PR1 induction of

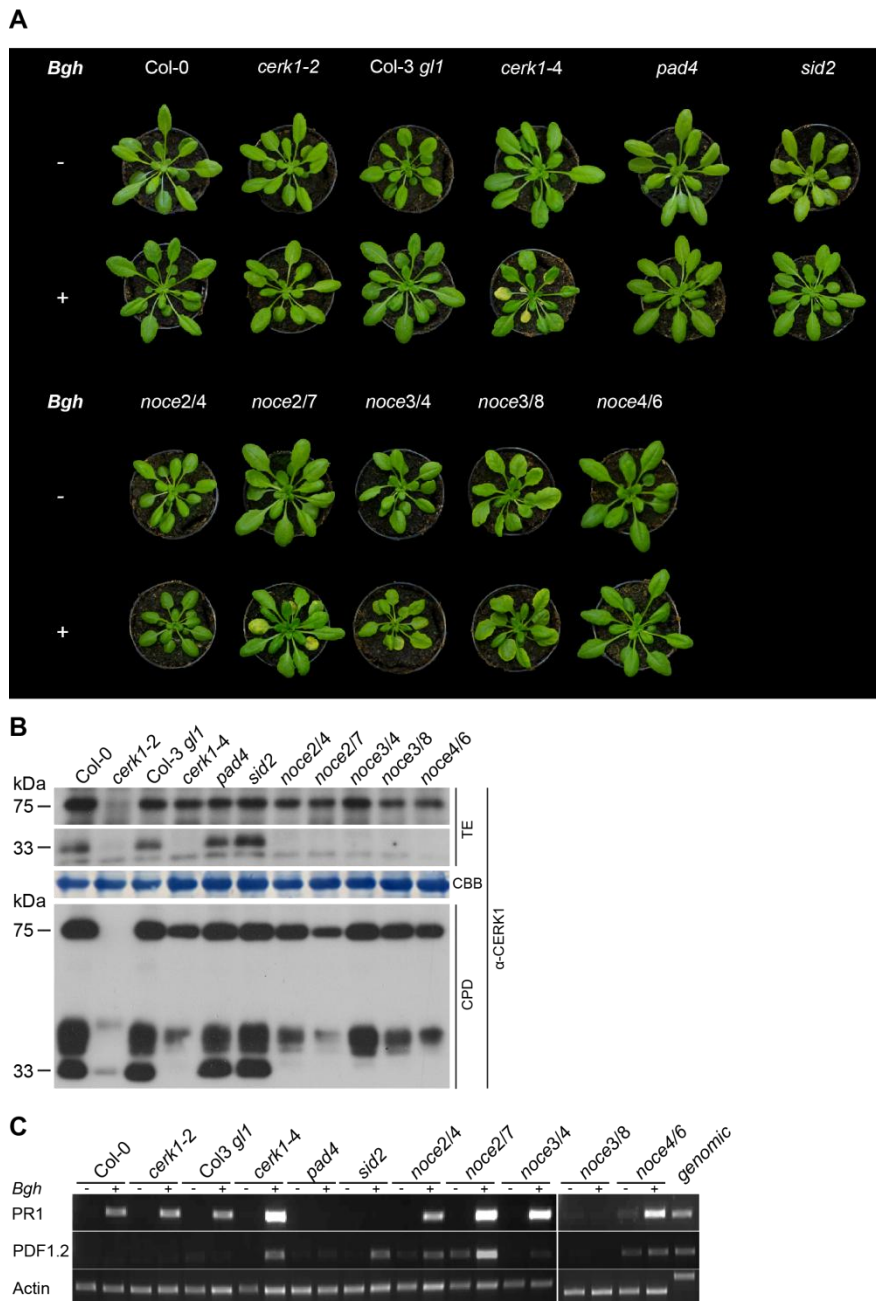


Figure 23. Different *noce* mutants fully suppress the *cerk1-4* phenotype. A) Re-mutagenized *cerk1-4* plants derived from an EMS based mutagenesis screen (Marnie Stolze, unpublished) were inoculated with *Bgh* and the phenotype was assessed seven days after infection. Col-0, *cerk1-2*, Col-3 *gl1*, *cerk1-4*, *pad4* and *sid2* were used as controls. B) Total protein extracts (TE) were prepared from 6-week-old plants and chitin pull-downs (CPD) were performed using these total extracts. Immunoblot analysis was performed using the specific CERK1 antibody. CBB, Coomassie Brilliant Blue stained membranes (protein loading control) C) PR1 and PDF1.2 expression was analyzed by semi-quantitative RT-PCR. Actin was used as control. Samples were prepared from three whole rosettes per genotype that were either either not inoculated (-) or inoculated with *Bgh* (+).

cerk1-4, whereas PR1 induction was wild type-like in *noce2/4* and *noce4/6*. PR1 expression in *noce3/8* was comparable to the SA signalling mutant *pad4* (Glazebrook *et al.*, 1996) and the salicylic acid synthesis mutant *sid2* (Wildermuth *et al.*, 2001), pointing to mutations within the SA synthesis or signalling pathways. Suppressor candidates were also assessed for

expression levels of the ethylene and JA responsive marker gene PDF1.2 (Figure 23C) (Manners *et al.*, 1998). Elevated levels of PDF1.2 expression could be observed for *cerk1-4*, *sid2*, *noce3/4* and *noce3/8*. For wild type plants, as well as *pad4*, *noce2/4* and *noce4/6* no induction of PDF1.2 expression was measurable.

Mutations in several genes are already known to suppress the *cerk1-4* phenotype (Petutschnig *et al.*, 2014). These are *SID2*, which encodes isochorismate synthase 1 (*ICS1*) (Wildermuth *et al.*, 2001) a key enzyme in SA biosynthesis, *PAD4* and *EDS1* two genes encoding lipase-like proteins (Falk *et al.*, 1999; Jirage *et al.*, 1999) involved in SA signaling and the Extra-Large G-Protein *XLG2*, previously identified in this screen. To investigate if the *noce* mutants had mutations in any of these proteins, the respective genes were sequenced (Table 11). *noce2/4* was wild type for all sequenced genes. As *noce2/7* did not suppress the *cerk1-4* cell death phenotype, no genes were sequenced. *noce4/6* turned out to harbor a mutation within *XLG2*, where a guanine was substituted by an adenine. This mutation causes a glutamic acid to lysine substitution at position 293 (E293K). As for all other *noce* mutants, *XLG2* turned out to be wild type, the following analyses were carried out with *noce4/6*.

Table 11. Summary of characteristics of *noce* mutants including results from sequencing of candidate suppressor genes. nd, not determined.

	<i>noce2/4</i>	<i>noce2/7</i>	<i>noce3/4</i>	<i>noce3/8</i>	<i>noce4/6</i>
Characteristics					
Suppression of <i>cerk1-4</i> cell death	yes	no	yes	yes	yes
CERK1 pattern like	<i>cerk1-4</i>	<i>cerk1-4</i>	<i>cerk1-4</i>	<i>cerk1-4</i>	<i>cerk1-4</i>
PR1 induction like	wild type	<i>cerk1-4</i>	<i>cerk1-4</i>	<i>sid2/pad4</i>	wild type
Sequence of candidate suppressor genes					
<i>CERK1</i>	<i>cerk1-4</i>	<i>cerk1-4</i>	<i>cerk1-4</i>	<i>cerk1-4</i>	<i>cerk1-4</i>
<i>SID2</i>	wt	nd	nd	nd	nd
<i>PAD4</i>	wt	nd	nd	nd	nd
<i>EDS1</i>	wt	nd	nd	nd	nd
<i>XLG2</i>	wt	nd	wt	wt	G->A, (E293K)

A derived cleaved amplified polymorphic sequence (dCAPS) marker was designed to detect the *noce4/6* mutation by PCR and subsequent restriction digestion. Primers were designed to introduce an *Xho*I cleavage site into PCR products derived from the wild type *XLG2* sequence (Figure 24A). After *Xho*I digestion of the PCR product, an uncleaved 169 bp product should be detected for the mutant (E293K) *XLG2* allele, while a cleaved 137 bp fragment should be observed with the wild type *XLG2* allele. From the backcrossed F2 population, 41 suppressor and 28 non-suppressor plants were thus analyzed to investigate the linkage between the suppressor phenotype and the *noce4/6* mutation. All non-suppressing plants were either heterozygous for the *xlg2* E293K mutation or homozygous for the *XLG2* wild type allele (Figure 24B).

Plants suppressing the *cerk1-4* phenotype were all homozygous for the *xlg2* E293K mutation, as only the non-cleaved 169bp fragment could be detected. This result indicates that the *xlg2* E293K mutation is highly linked with *cerk1-4* phenotype suppression, making it a very likely candidate for the causal suppressor mutation. Genotyping revealed that all *cerk1-4* suppressing plants derived from *noce4/6* backcrosses were homozygous for *xlg2* E293K. To confirm that *xlg2* E293K is indeed the causal mutation for suppression of the *cerk1-4* phenotype, *noce4/6* plants were transformed with a genomic fragment containing the wild type *XLG2* gene including the *XLG2* promoter. The resulting transformants were tested for restoration of the *cerk1-4* phenotype. Transformed plants were inoculated with *Bgh* and the phenotype was assessed seven days after infection.

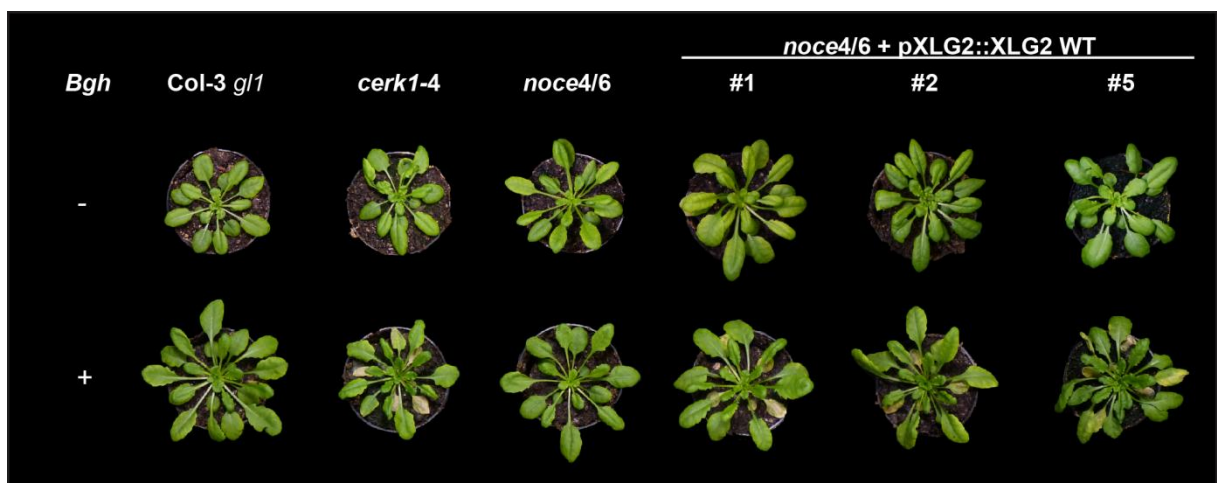


Figure 25. Expression of a genomic wild type *XLG2* fragment can restore the *cerk1-4* phenotype in *nole6-1* plants. *noce4/6* plants were transformed with a genomic fragment derived from wild type plants containing the *XLG2* gene including its promoter. Positive transformants, as well as *Col-3 gl1*, *cerk1-4* and *nole6-1* controls were inoculated with *Bgh*. Pictures of non-inoculated (-) and inoculated (+) plants were taken seven days after infection.

Expression of wild type XLG2 could restore the *cerk1-4* phenotype in all tested lines thereby delivering the last piece of evidence for *xlg2* E293K being the causal mutation of *noce4/6* (Figure 25). Since the *nole1-1* mutant also harbours a mutation within XLG2, *noce4/6* was renamed to *nole1-2 cerk1-4*.

E293 (which is mutated to K in *nole1-2* plants) is located to the N-terminal part of XLG2 in a highly conserved part C-terminal to the CxxC-motifs. Like the CxxC motifs, this glutamic acid is highly conserved in XLG proteins from mosses to flowering plants (Figure 26).

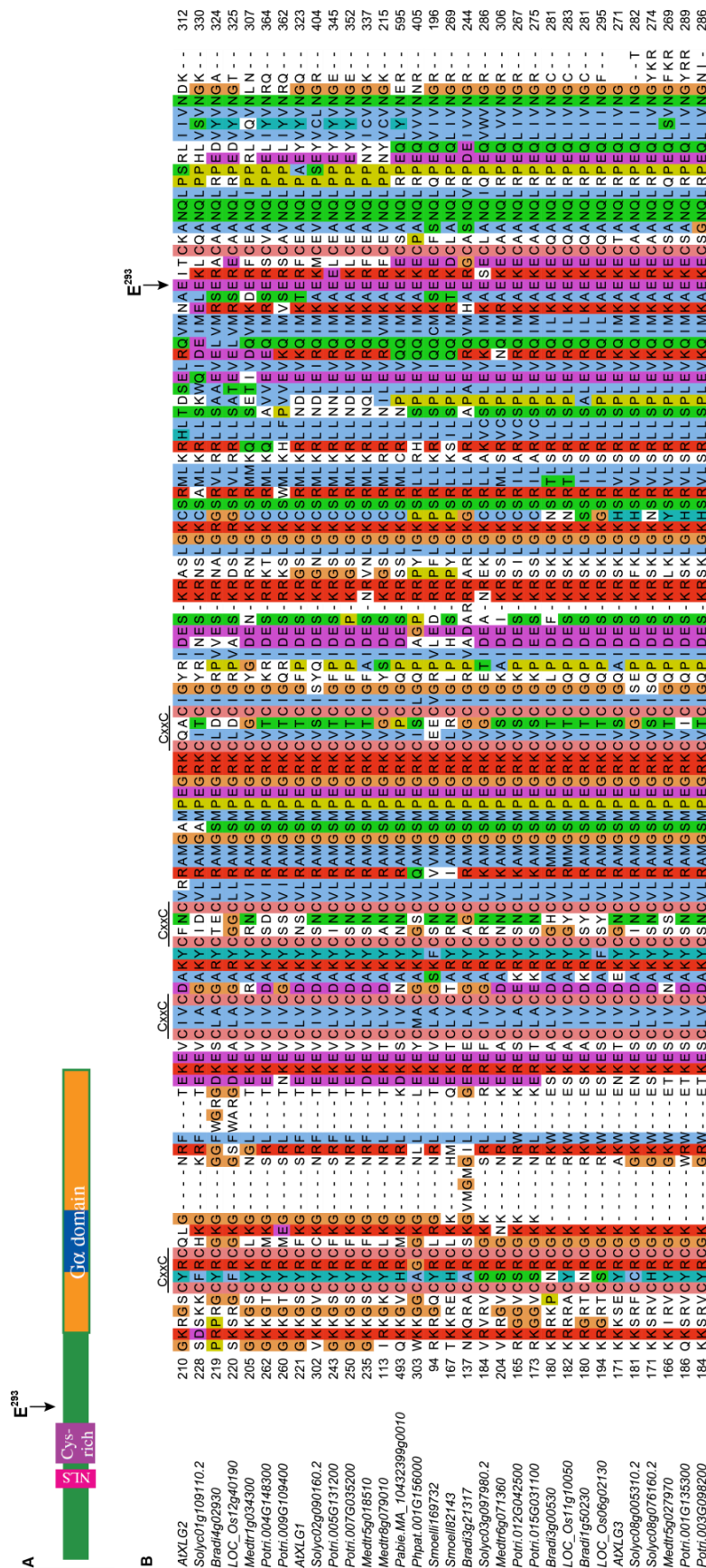


Figure 26. The glutamic acid mutated in *nole1-2*, E293, is located within a highly conserved region of the N-terminal part of XLG2. A) Domain organization of XLG2. Arrow indicates the amino acid which is mutated in *nole1-2* (E293) (adapted from Urano et al. (2013)). B) The alignment shows a highly conserved region within the N-terminal domain of XLG proteins from different plant species. The figure shows the cysteine rich region with four highly conserved and perfect CxxC motifs, and a highly conserved domain C-terminal of it. The glutamic acid which is mutated in *nole1-2* (E293) can be found in all aligned extra-large G-proteins. Plant species abbreviations: At, *Arabidopsis thaliana*; Solyc, *Solanum lycopersicum*; Bradi, *Brachypodium distachyon*; Os, *Oryza sativa*; Medtr, *Medicago truncatula*; Potri, *Populus trichocarpa*; Pabie, *Picea abies*; Ppbat, *Physcomitrella patens*; Smoelli, *Selaginella moellendorffii*

3.2.4 Localization studies with XLG2-GFP fusion protein

3.2.4.1 XLG2-GFP and *xlg2*-E293K-GFP are located to the nucleus and cell periphery in *N. benthamiana*

Previous studies reported localization of XLG2 to the nucleus, cytoplasm and plasma membrane when heterologously expressed in *Nicotiana benthamiana* (Chakravorty *et al.*, 2015; Maruta *et al.*, 2015) or to the nucleus and plasma membrane in stably transformed *Arabidopsis thaliana* plants (Chakravorty *et al.*, 2015; Maruta *et al.*, 2015). However, in these studies XLG2 expression was under control of the strong 35S or UBIQUITIN10 promoters and the reported localization patterns might be influenced by overexpression.

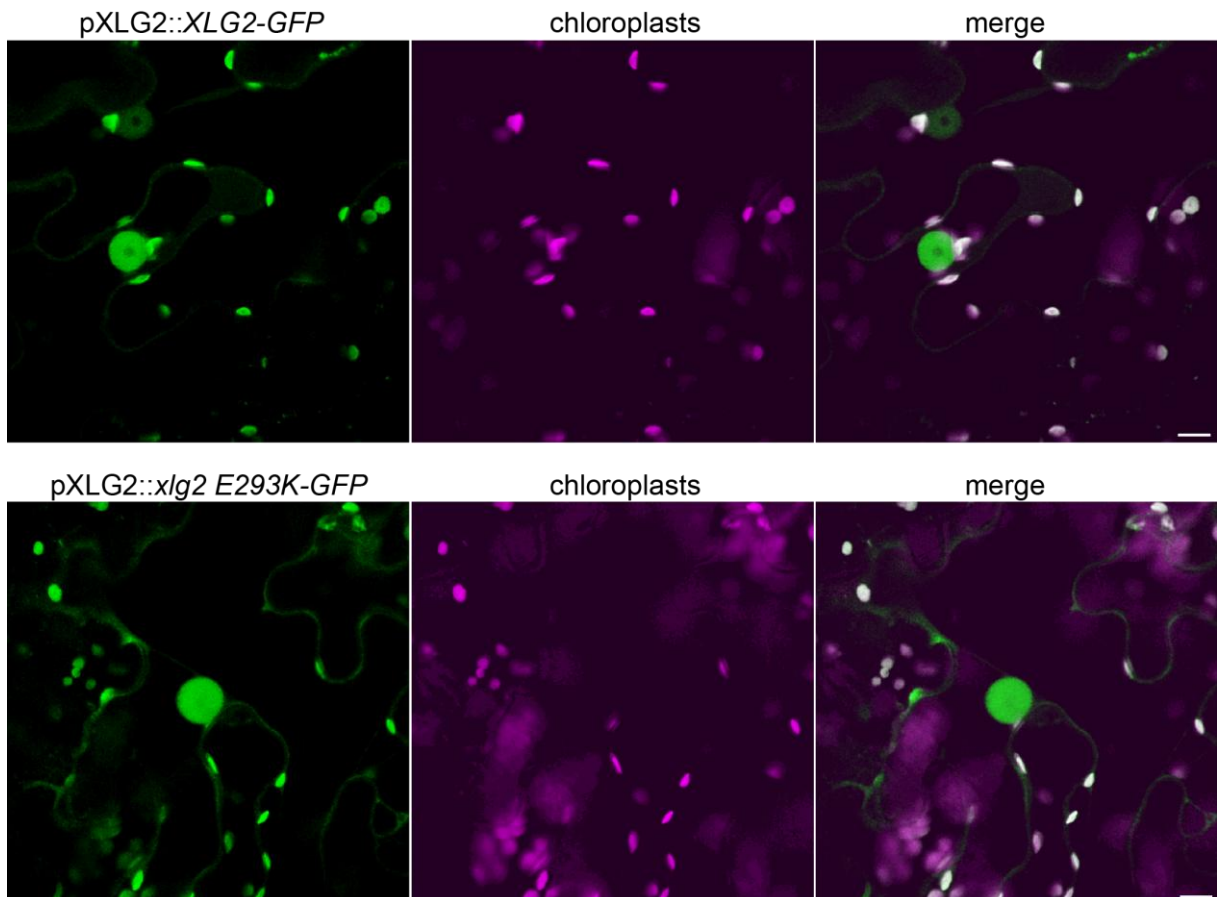


Figure 27. XLG2-GFP and *xlg2* E293K-GFP are located to the nucleus and the cell periphery in *N. benthamiana*. *Agrobacteria* either carrying a plasmid expressing XLG2-GFP or *xlg2* E293K-GFP under control of the native XLG2 promoter were infiltrated into *N. benthamiana*. Confocal laser scanning microscopy (CLSM) was carried out two days after infiltration. Size bar indicates 10 μ m.

To re-assess the subcellular localization of XLG2 and to investigate the localization of *xlg2* E293K, C-terminal GFP fusions under control of the endogenous XLG2 promoter were generated in the pGWB604 vector. Transient expression of XLG-GFP constructs in *Nicotiana benthamiana* confirmed localization of XLG2 to the nucleus but not the nucleolus. Also, weak localization of XLG-GFP to the cell periphery was seen (Figure 27). The same localization pattern was observed for *xlg2* E293K-GFP (Figure 27).

3.2.4.2 XLG2-GFP localizes to the cell periphery in unchallenged *Arabidopsis* plants and accumulates in the nucleus upon stress

The XLG2-GFP fusion construct was transformed into *Arabidopsis thaliana* plants. The resulting transformants were used to study the subcellular localization of XLG2 when stably expressed in *Arabidopsis*. Expression levels of XLG2-GFP in leaves of *Arabidopsis* Col-3 *gl1* plants were very low (Figure 28A, upper panel) and no signal could be detected for *xlg2* E293K-GFP expressing lines (data not shown). Nevertheless, a signal at the cell periphery was detectable for XLG2-GFP. Surprisingly, no signal in nuclei could be observed. Thus, the localization of XLG2-GFP upon PAMP treatment was investigated. Leaf discs were vacuum infiltrated with either chitin or H₂O as control, to test for any localization changes (Figure 28A, lower panels). Short incubation times did not cause any discernible alterations in XLG2-GFP localization (data not shown). An anti-GFP immunoblot revealed a signal at 130 kDa corresponding to full length fusion protein for *XLG2-GFP* and *xlg2* E293K-GFP expressing plants (Figure 28B). No difference between wild type XLG2-GFP and *xlg2* E293K-GFP concerning the band pattern was observable. However, after incubation for 16 hours in either H₂O or chitin, the overall signal for XLG2-GFP appeared to be increased and a clear GFP-signal in nuclei became visible. These results suggest that in unstimulated plants, XLG2 is localized only to the cell periphery, whereas upon exposure to stress, XLG2 also accumulates in the nucleus. The fact that water infiltration also caused this change in localization indicates that XLG2 responds either to mechanical stimuli or unspecifically to any stress.

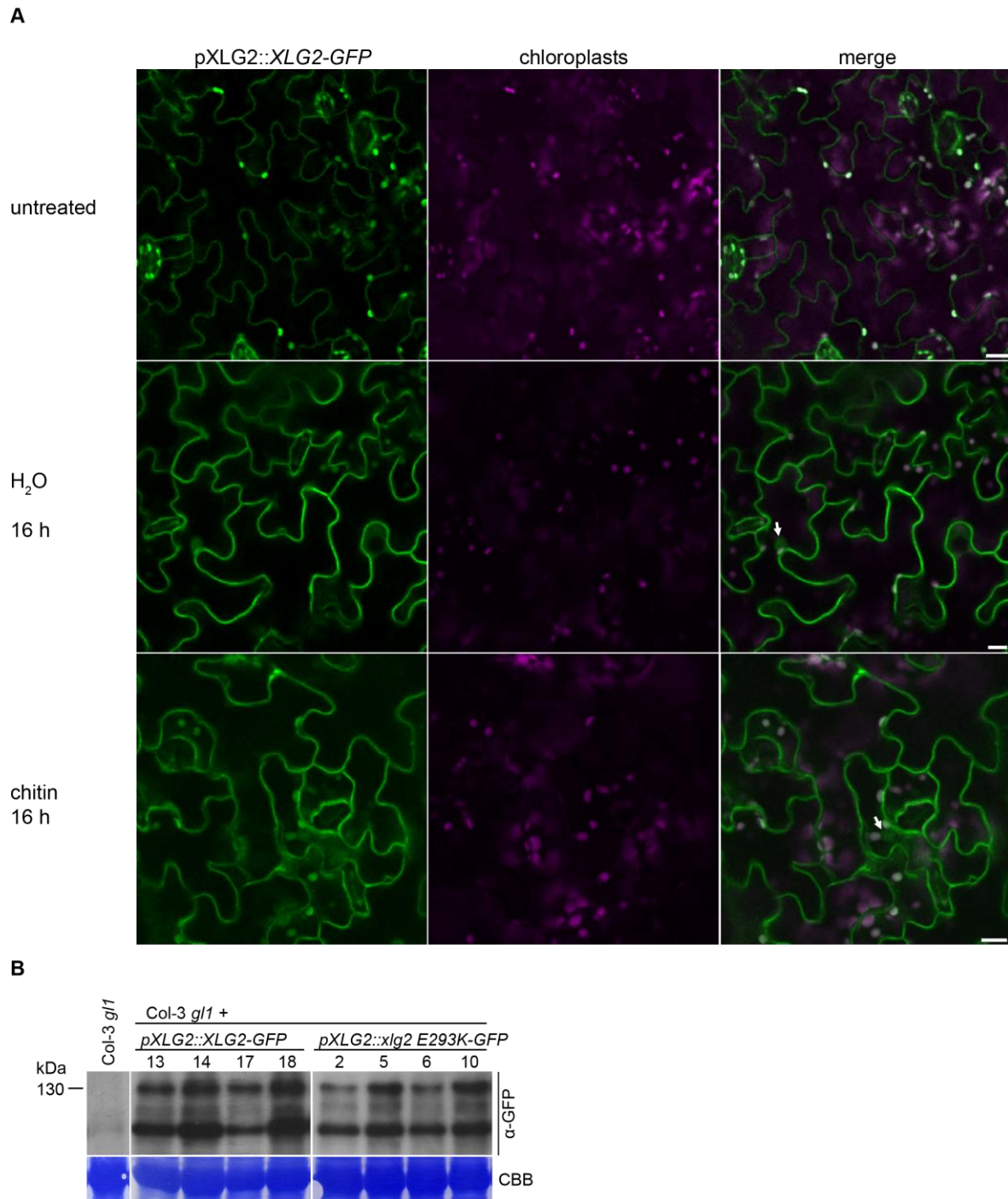


Figure 28. XLG2-GFP localization is stimulus dependent. A) Localization of XLG2 was investigated in leaf discs of Col-3 *gl1* plants stably expressing XLG2-GFP by confocal laser scanning microscopy. Leaf discs were either untreated or infiltrated with H₂O or 100 µg ml⁻¹ shrimp shell chitin and incubated for 16h. Pictures show maximum projections of 10 single focus plane images taken 1 µm apart. Size bar indicates 10 µm. B) Anti-GFP immunoblot of four individual transgenic T1 plants either expressing *XLG2-GFP* or *xlg2 E293K-GFP* under control of the endogenous XLG2 promoter. Total protein extracts were prepared from leaves. CBB, Coomassie Brilliant blue stained membrane.

3.2.4.3 C-terminal XLG2-GFP fusions are not functional

The *nole1-1 cerk1-4* and *nole1-2 cerk1-4* mutants offer the possibility to test XLG2 fusion constructs for functionality. These mutants harbor the *cerk1-4* mutation, but do not exhibit the characteristic *cerk1-4* phenotype, because they lack functional XLG2 (Chapter 3.2.3). Transformation with a functional XLG2 construct can restore the *cerk1-4* phenotype in *nole1-1 cerk1-4* (Elena Petutschnig, unpublished) and *nole1-2 cerk1-4* (Figure 25) upon *Bgh* infection. Therefore, functionality of XLG2-GFP was tested by expression in *nole1-1 cerk1-4* and subsequent *Bgh* infection (Figure 29). *nole1-1 cerk1-4* plants expressing XLG2-GFP developed lesions after *Bgh* infection, but to a much lesser extent than *cerk1-4* mutants and more resembled Col-3 *gl1* control plants (Figure 29A). This experiment was performed twice with similar results and eleven transgenic plants were tested in total. Immunoblot analysis using a GFP antibody revealed expression of full length XLG2-GFP (130 kDa) in all tested transgenic lines (Figure 29B). Additional signals below the full length signal could be detected for all tested lines and might represent degradation products. Since a specific XLG2 antibody is not available, it cannot be inferred from these blots whether the abundance of XLG2-GFP matches that of the endogenous XLG2 protein. Overall it can be concluded that XLG2-GFP is not functional, either because the tag inhibits XLG2 function, or because protein levels are insufficient. Based on the lack of functionality of XLG2-GFP, studies using this construct should be taken with caution since XLG2-GFP localization might not represent the localization of the endogenous XLG2 protein.

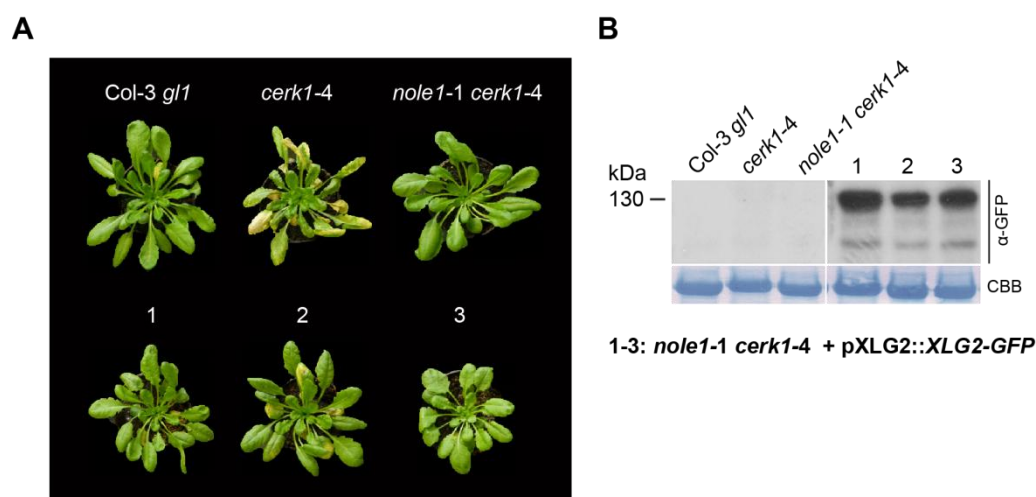


Figure 29. XLG2-GFP is not functional. A) *nole1-1 cerk1-4* plants were transformed with constructs containing XLG2-GFP under control of the native XLG2 promoter. Positive transformants were inoculated with *Bgh* and pictures were taken seven days after infection. Col-3 *gl1*, *cerk1-4* and *nole1-1 cerk1-4* were used as controls. B) Total protein extracts prepared from leaves of plants shown in A) were used for immunoblot analysis using a GFP antibody. CBB, Coomassie Brilliant Blue stained membrane (loading control).

For this reason, no further, more detailed localization studies were carried out with XLG2-GFP and related fusion proteins.

3.2.5 Localization studies with Venus-XLG2

3.2.5.1 Venus-XLG2 localizes to the nucleus, cytoplasm and plasma membrane in *Nicotiana benthamiana*

Since XLG2-GFP fusion constructs were shown not to be fully functional, N-terminal fusions of XLG2 with the fluorescence protein Venus (Venus-XLG2) were generated. This construct was used for further analysis of the subcellular localization of XLG2. To allow co-localization studies with marker proteins for different subcellular compartments, Venus-XLG2 was expressed transiently in *N. benthamiana*. These transient expression assays showed localization to the cell periphery, cytoplasm and the nucleus. This localization pattern resembled the localization pattern of C-terminal XLG2-GFP fusions, even though fluorescence intensity of the N-terminal Venus-XLG2 fusion appeared much stronger. Nuclear localization was confirmed by co-infiltration with a nuclear marker construct expressing TagRFP-T fused to Histone2B (Figure 30).

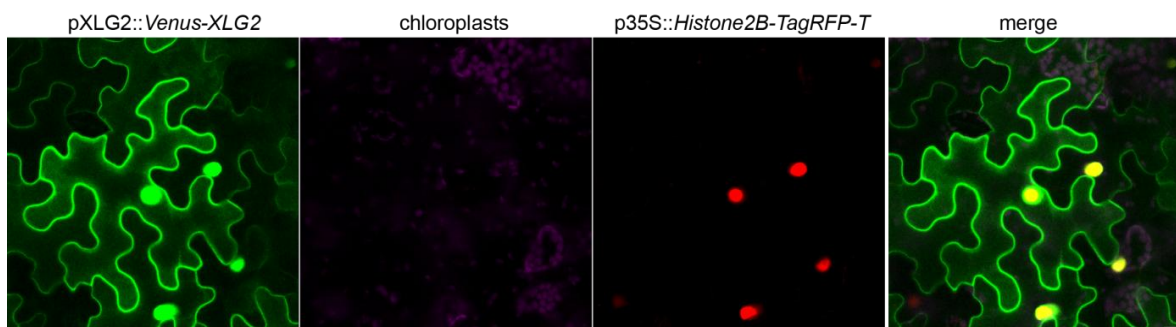


Figure 30. N-terminal XLG2 fusions are localized to the cell periphery and the nucleus. *Agrobacteria* carrying constructs for pXLG2::Venus-XLG2 and p35S::Histone2B tagged with TagRFP-T were co-infiltrated into *N. benthamiana* leaves. Confocal laser scanning microscopy (CLSM) was carried out two days after infiltration. Images represent a maximum projection of 10 single focal planes recorded 1 μ m apart. Size bar indicates 10 μ m.

To confirm localization to the plasma membrane, Venus-XLG2 was co-expressed in *Nicotiana benthamiana* leaves with the LysM-RLK LYK5 fused to the far red fluorescence protein mKate2 (LYK5-mKate2). LYK5 was shown to localise to the plasma membrane (Erwig *et al.*, unpublished) and was therefore considered a suitable plasma membrane marker. Venus-XLG2 co-localized with LYK5-mKate2 and both fusion proteins could be

found in Hechtian strands after plasmolysis, indicating plasma membrane localization (Figure 31).

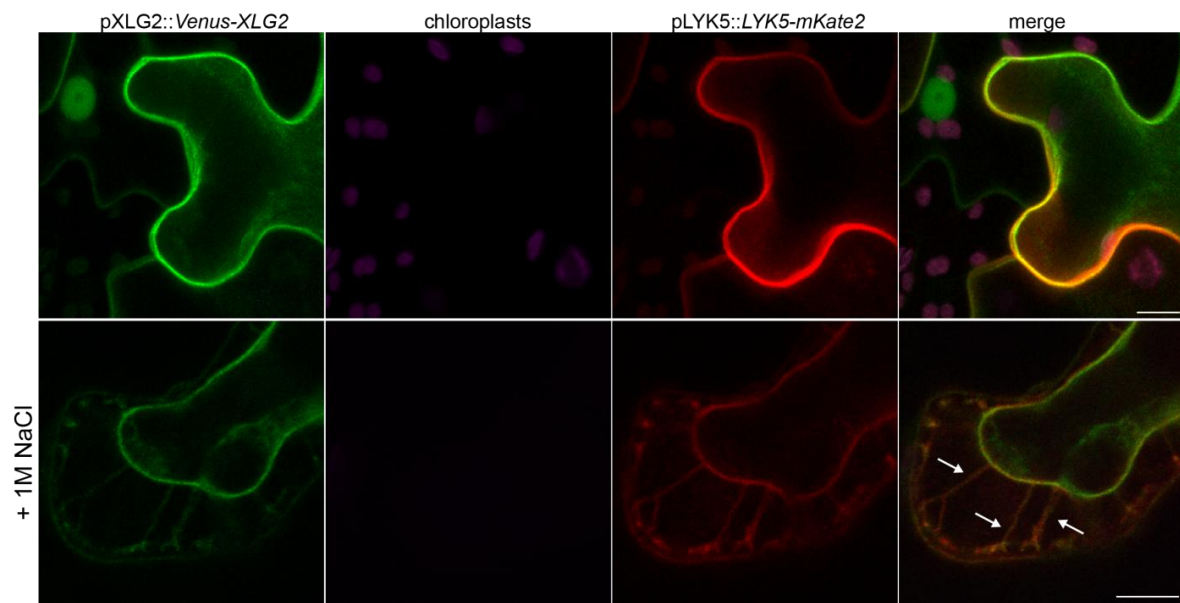


Figure 31. Venus-XLG2 co-localizes with LYK5-mKate at the plasma membrane. Venus-XLG2 and LYK5-mKate were co-expressed under control of their respective native promoters in *Nicotiana benthamiana*. Confocal laser scanning microscopy was performed 2 days after infiltration. Upper panel, Venus-XLG2 and LYK5-mKate2 co-localize at the plasma membrane; Lower panel, 1M NaCl was used to plasmolyse cells. White arrows indicate Hechtian strands. Size bar indicates 10 μm .

In order to confirm cytoplasmic localization, XLG2 was co-expressed with free mCherry under control of the 35S promoter (Figure 32). Venus-XLG2 showed a weak signal for a few cytoplasmic strands, whereas free mCherry strongly labelled cytoplasmic strands throughout the cell. This confirms that Venus-XLG2 is also present in the cytoplasm, but this appears to be only a minor pool compared to XLG2 in the nucleus or the PM.

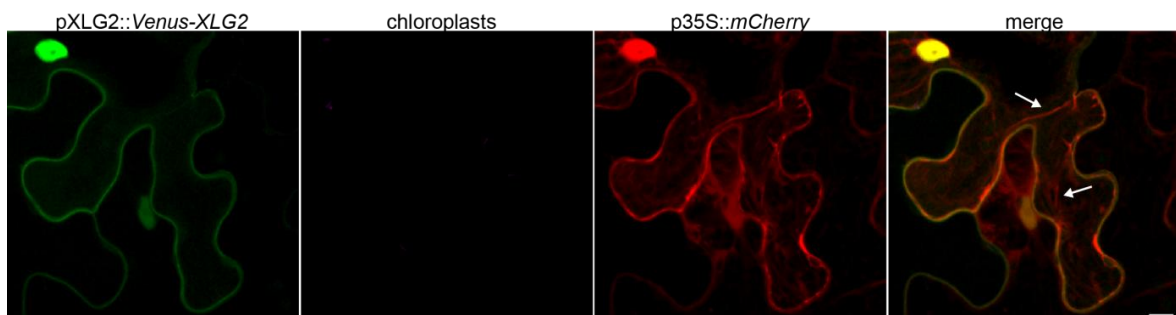


Figure 32. Venus-XLG2 is also found in cytoplasmic strands. Venus-XLG2 expressed under control of its native promoter and mCherry under control of the 35S promoter were co-expressed in *Nicotiana benthamiana* and confocal laser scanning microscopy was performed two days after infiltration. Arrows indicate cytoplasmic strands. Size bar indicates 10 μm .

3.2.5.2 N-terminal XLG2 fusions are functional and restore the *cerk1-4* phenotype in *nole1-1* plants

Prior to investigating subcellular localization of Venus-XLG2 in transgenic *Arabidopsis* plants, Venus-XLG2 was tested for functionality. Therefore, *nole1-1 cerk1-4* plants were transformed with the Venus-XLG2 construct under control of the native XLG2 promoter and transformants that gave a good signal in confocal microscopy were inoculated with *Bgh* (Figure 33A).

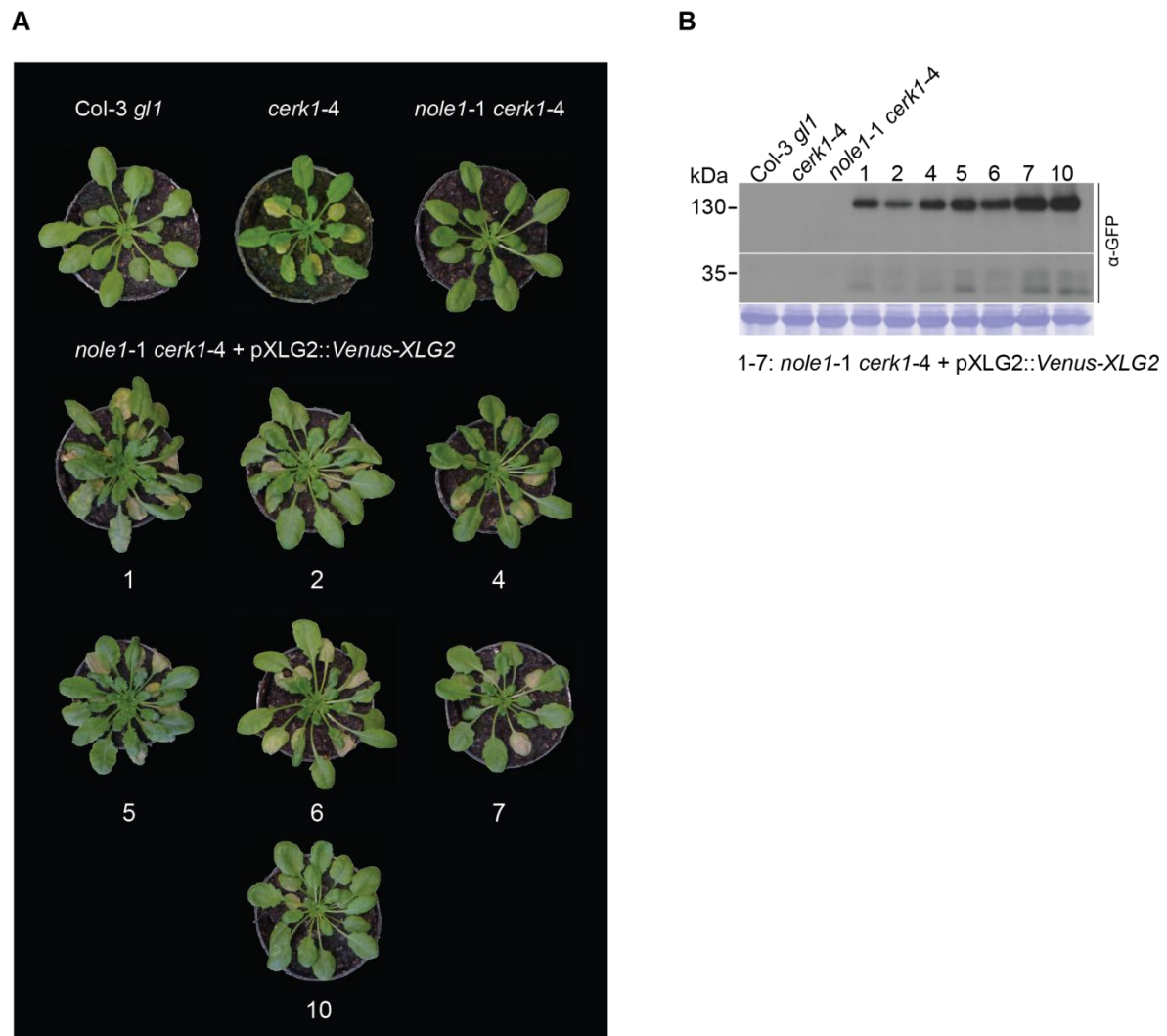


Figure 33. N-terminal XLG2 fusions are functional. A) *nole1-1 cerk1-4* plants were transformed with a construct containing Venus-XLG2 under control of the XLG2 promoter. Transformants were checked for fluorescence intensity by confocal laser scanning microscopy (not shown) and strong expressors were chosen for inoculation with *Bgh*. Col-3 *gl1*, *cerk1-4* and *nole1-1 cerk1-4* were used as controls. Pictures were taken seven days after *Bgh* infection. B) Total protein extracts prepared from leaves of *Bgh* infected plants shown in A) were used for immunoblot analysis with a GFP antibody. CBB, Coomassie Brilliant Blue stained membrane (loading control).

Transgenic plants developed macroscopically visible lesions comparable to *cerk1-4* plants seven days after infection. No lesions were visible in Col-3 *gl1* or *nole1-1* *cerk1-4* mutants. In immunoblot analysis with a GFP antibody, a 130 kDa band corresponding to Venus-XLG2 full length protein could be detected for all transgenic lines (Figure 33B). A weak signal of about 30 kDa was present in all transgenic lines, which might correspond to free Venus. Nevertheless, these results strongly indicate functionality of the N-terminal Venus-XLG2 fusion.

3.2.5.3 Venus-XLG2 localises to the cell periphery in unchallenged *Arabidopsis* plants and accumulates in the nucleus upon stress

XLG2 localization studies in *Nicotiana benthamiana* confirmed previous studies (Chakravorty *et al.*, 2015; Maruta *et al.*, 2015) which found XLG2 to be localized to the nucleus, cytoplasm and plasma membrane. In order to investigate the subcellular localization of XLG2 in *Arabidopsis thaliana*, pXLG2::Venus-XLG2 was transformed into Col-0, *agb1-2*, Col-3 *gl1* and *cerk1-4* plants. Confocal laser scanning microscopy revealed localization of XLG2 to the cell periphery in unchallenged Col-0 plants. These results confirm the localization studies conducted with C-terminal GFP fusions in this study and are in contrast to a recent study with stably transformed *Arabidopsis* plants overexpressing *GFP-XLG2* from the 35S promoter (Maruta *et al.*, 2015). To address the question if XLG2 localization might be stimulus dependent, leaves of Col-0 plants expressing *Venus-XLG2* were infiltrated with H₂O, chitin or flg22. Analysis by confocal laser scanning microscopy revealed that 3 hours after each of these treatments, the Venus-XLG2 fluorescence signal increased overall and a distinct signal within nuclei appeared. After one day of incubation, the Venus-XLG2 signal intensity was increased further, with pronounced labelling of nuclei. These data suggest that in the wild type background, infiltration stress causes Venus-XLG2 abundance to increase and triggers its accumulation in nuclei. No clear difference in the subcellular behaviour of Venus-XLG2 could be seen between water and PAMP treatment. To investigate if the accumulation of Venus-XLG2 in nuclei is specifically caused by infiltration, leaves of Col-0 plants expressing *Venus-XLG2* were analyzed after wounding. Leaf discs were cut out and analyzed either directly by confocal laser scanning microscopy or stored in water for 3 and 24 hours, respectively. Similar to infiltration of H₂O, chitin or flg22, a Venus-XLG2 signal in the nucleus appeared 3 hours after wounding and became more intense after 24 hours. Thus it seems likely that different types of abiotic and biotic stress can trigger nuclear accumulation of Venus-XLG2 (Figure 34, Figure 35, Figure 36, Figure 37)

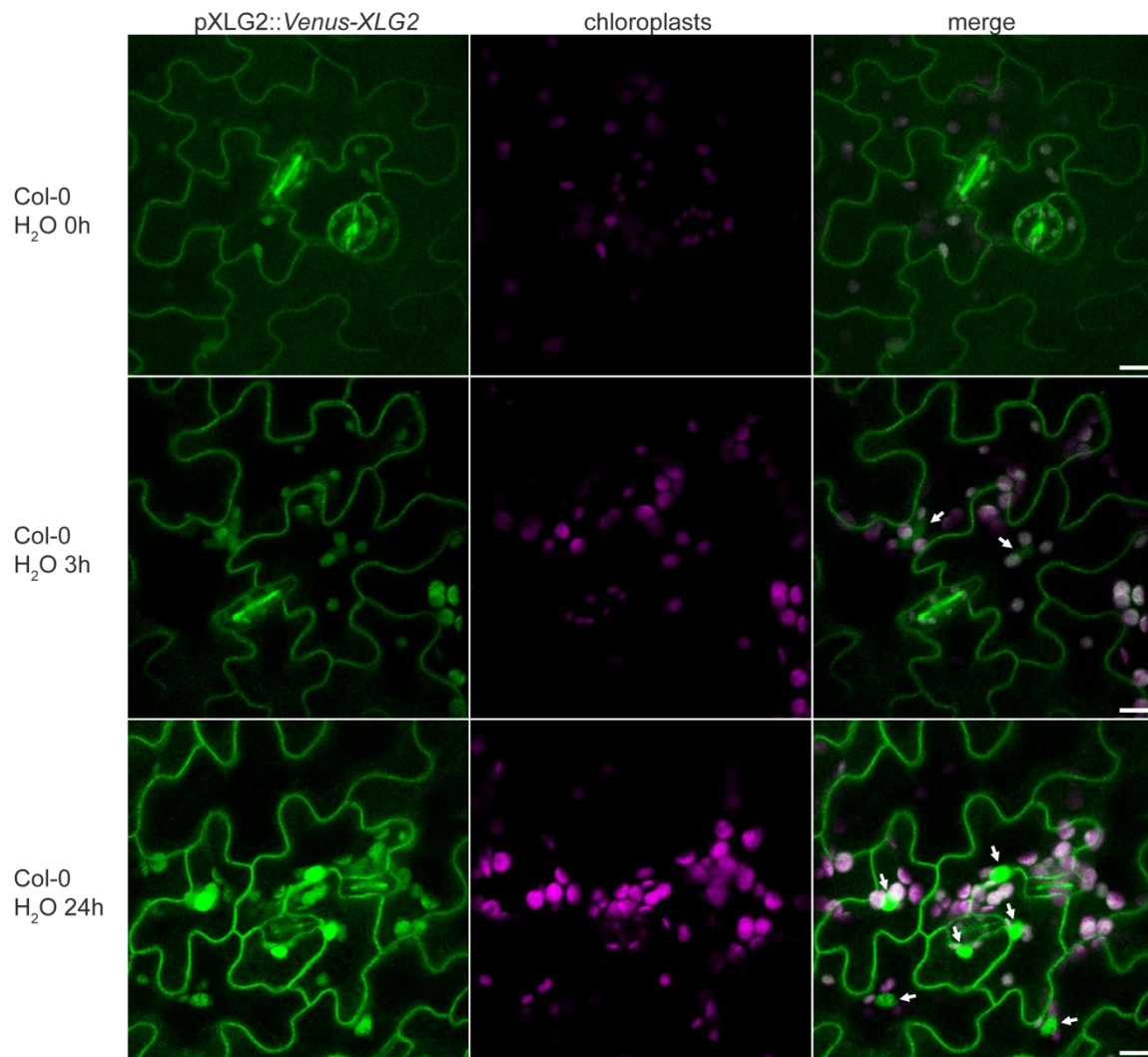


Figure 34. XLG2 is localized to the cell periphery in unchallenged plants and appears in nuclei after H₂O infiltration in Col-0 plants. Stably transformed Col-0 plants expressing Venus-XLG2 from the XLG2 promoter were analyzed by Confocal laser scanning microscopy. Leaf discs were cut out and vacuum-infiltrated with H₂O using a syringe. Leaf discs were either used for microscopy directly after infiltration or were incubated in H₂O for the indicated time points. Images represent maximum projections of 10 single focal plane images taken 1 μ m apart. White arrows denote nuclei. Size bar indicates 10 μ m.

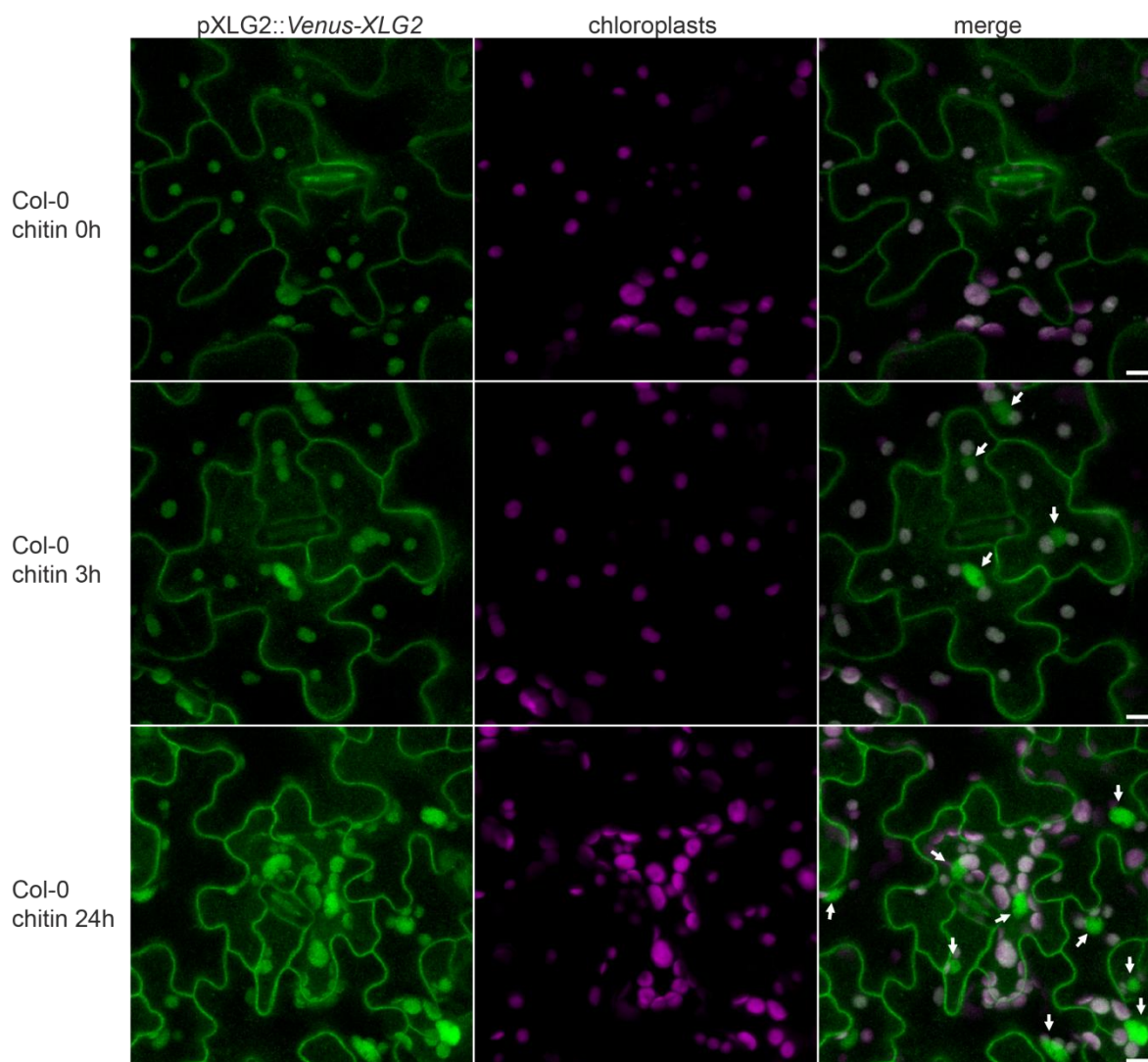


Figure 35. XLG2 is localized to the cell periphery in unchallenged plants and appears in nuclei after chitin infiltration in Col-0 plants. Stably transformed Col-0 plants expressing Venus-XLG2 from the XLG2 promoter were analyzed by Confocal laser scanning microscopy. Leaf discs were cut out and vacuum-infiltrated with 100 mg ml^{-1} chitin using a syringe. Leaf discs were either used for microscopy directly after infiltration or were incubated in 100 mg ml^{-1} chitin solution for the indicated time points. Images represent maximum projections of 10 single focal plane images taken $1 \mu\text{m}$ apart. White arrows denote nuclei. Size bar indicates $10 \mu\text{m}$.

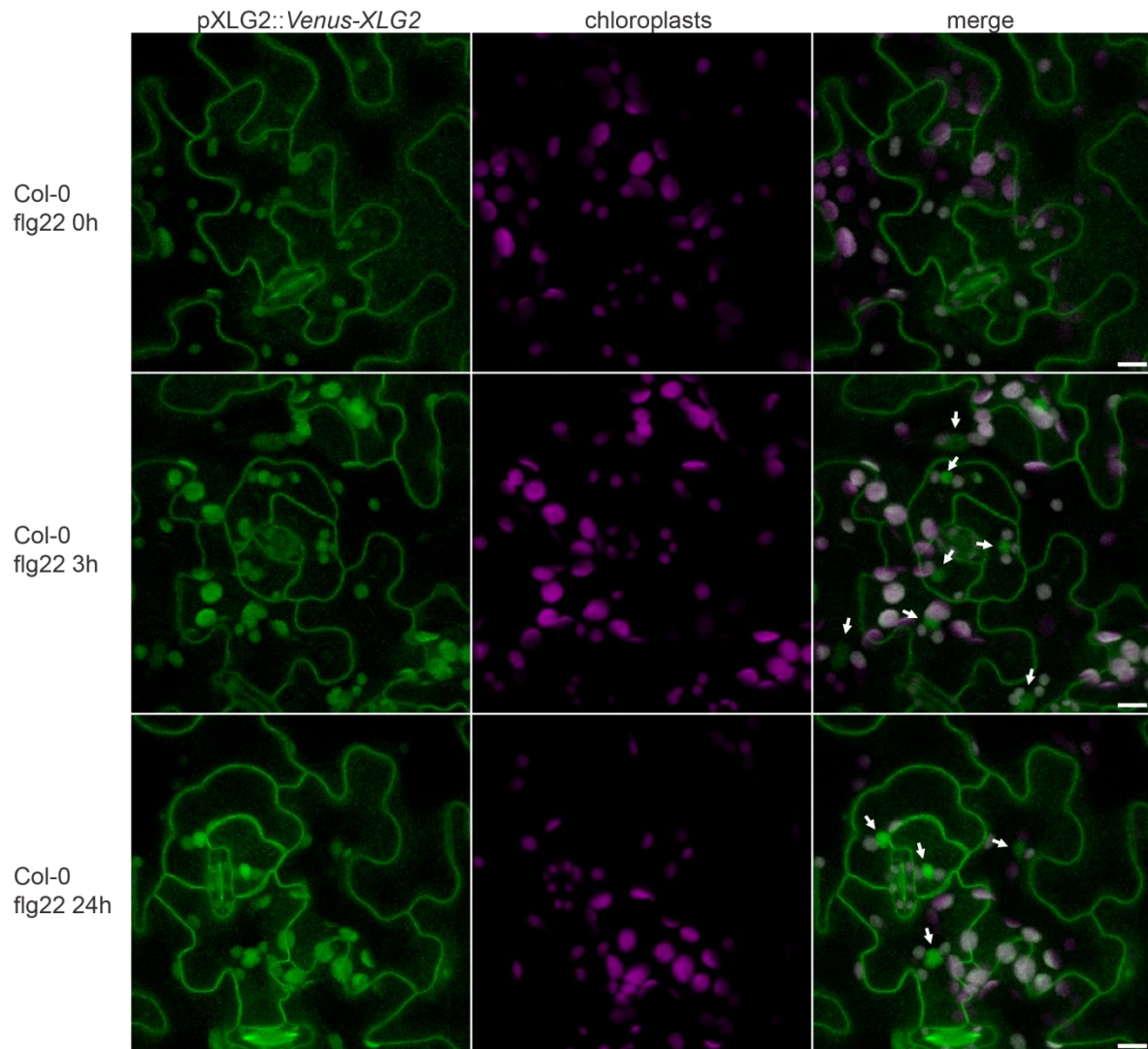


Figure 36. XLG2 is localized to the cell periphery in unchallenged plants and appears in nuclei after flg22 infiltration in Col-0 plants. Stably transformed Col-0 plants expressing Venus-XLG2 from the XLG2 promoter were analyzed by Confocal laser scanning microscopy. Leaf discs were cut out and vacuum-infiltrated with 100nm flg22 using a syringe. Leaf discs were either used for microscopy directly after infiltration or were incubated in 100nm flg22 solution for the indicated time points. Images represent maximum projections of 10 single focal plane images taken 1 μ m apart. White arrows denote nuclei. Size bar indicates 10 μ m.

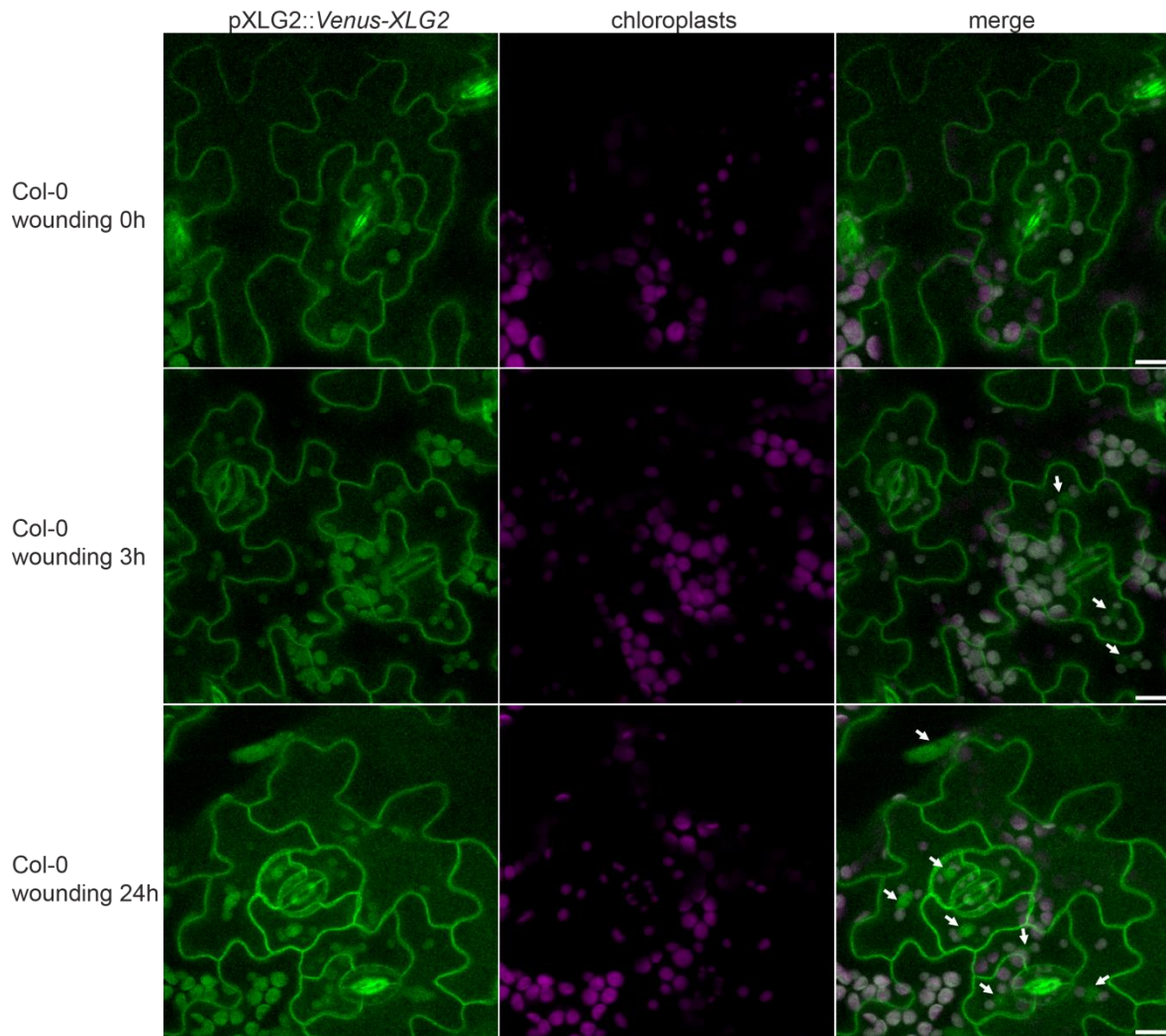


Figure 37. XLG2 is localized to the cell periphery in unchallenged plants and appears in nuclei after wounding in Col-0 plants. Stably transformed Col-0 plants expressing Venus-XLG2 from the XLG2 promoter were analyzed by Confocal laser scanning microscopy. Leaf discs were cut out and directly used for microscopy or were left in water for the indicated time points. Images represent maximum projections of 10 single focal plane images taken 1 μm apart. White arrows denote nuclei. Size bar indicates 10 μm .

Since XLG2 is required for the formation of the *cerk1-4* phenotype, the localization of Venus-XLG2 was also analyzed in the *cerk1-4* mutant and the corresponding wild type control, Col-3 *gl1*. The situation was the same as observed in Col-0. Venus-XLG2 localized to the cell periphery in unchallenged plants and showed an increase in overall signal intensity as well as accumulation in the nucleus upon water infiltration (Figure 38, Figure 39). Interestingly, when expressed in *agb1-2* plants, Venus-XLG2 was localized to the cell periphery as well as the nucleus even in unchallenged plants. Upon infiltration of water, the signal at the cell periphery did not increase much, but the signal intensity in nuclei became very strong after 3 and 24 hours (Figure 40). The localization of Venus-XLG2 appeared to be shifted towards the nucleus in *agb1-2* mutants.

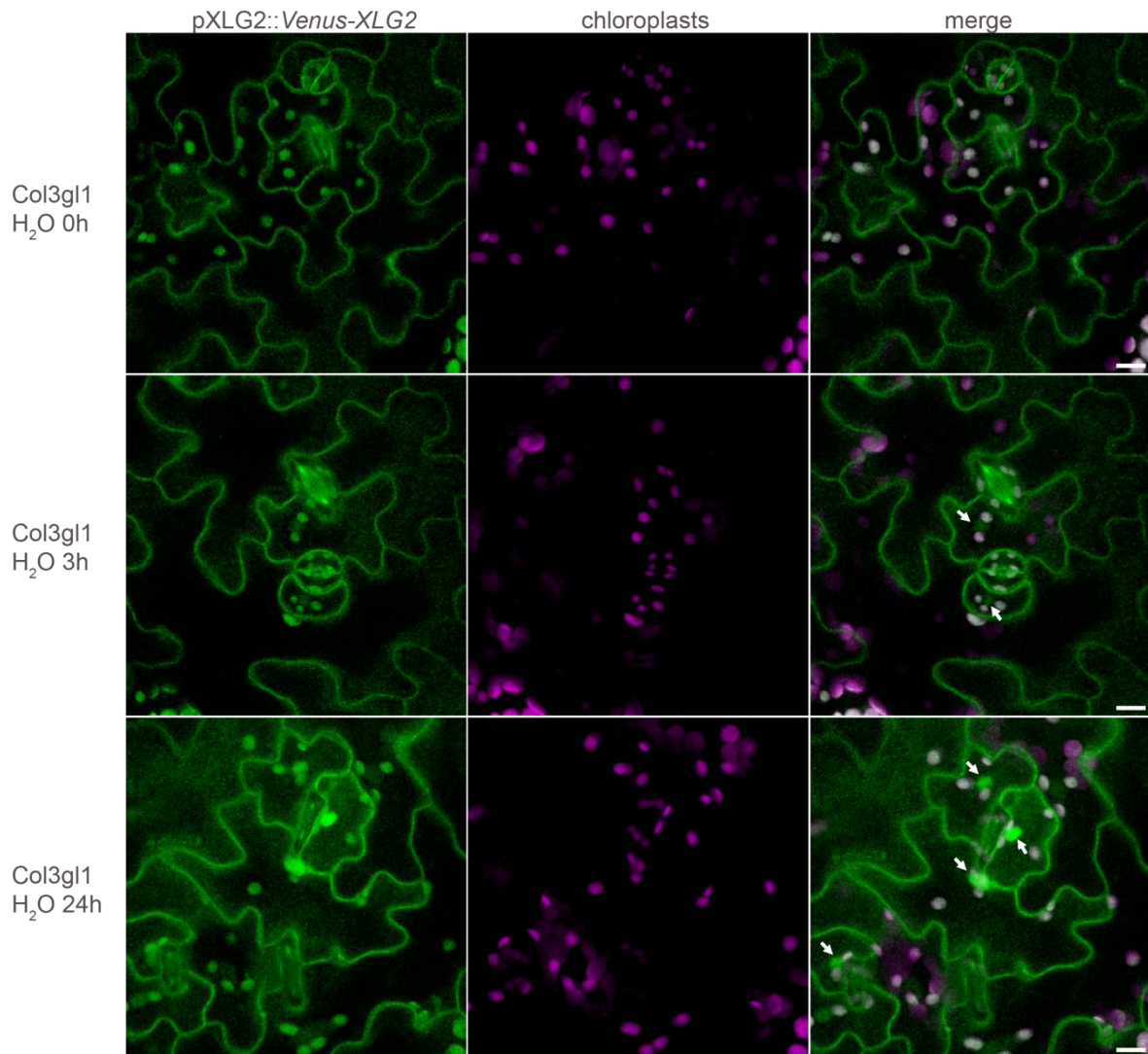


Figure 38. XLG2 is localized to the cell periphery in unchallenged plants and appears in nuclei after H₂O infiltration in Col-3 *g/1* plants. Stably transformed Col-3 *g/1* plants expressing Venus-XLG2 from the XLG2 promoter were analyzed by Confocal laser scanning microscopy. Leaf discs were cut out and vacuum-infiltrated with H₂O using a syringe. Leaf discs were either used for microscopy directly after infiltration or were incubated in H₂O for the indicated time points. Images represent maximum projections of 10 single focal plane images taken 1 μ m apart. White arrows denote nuclei. Size bar indicates 10 μ m.

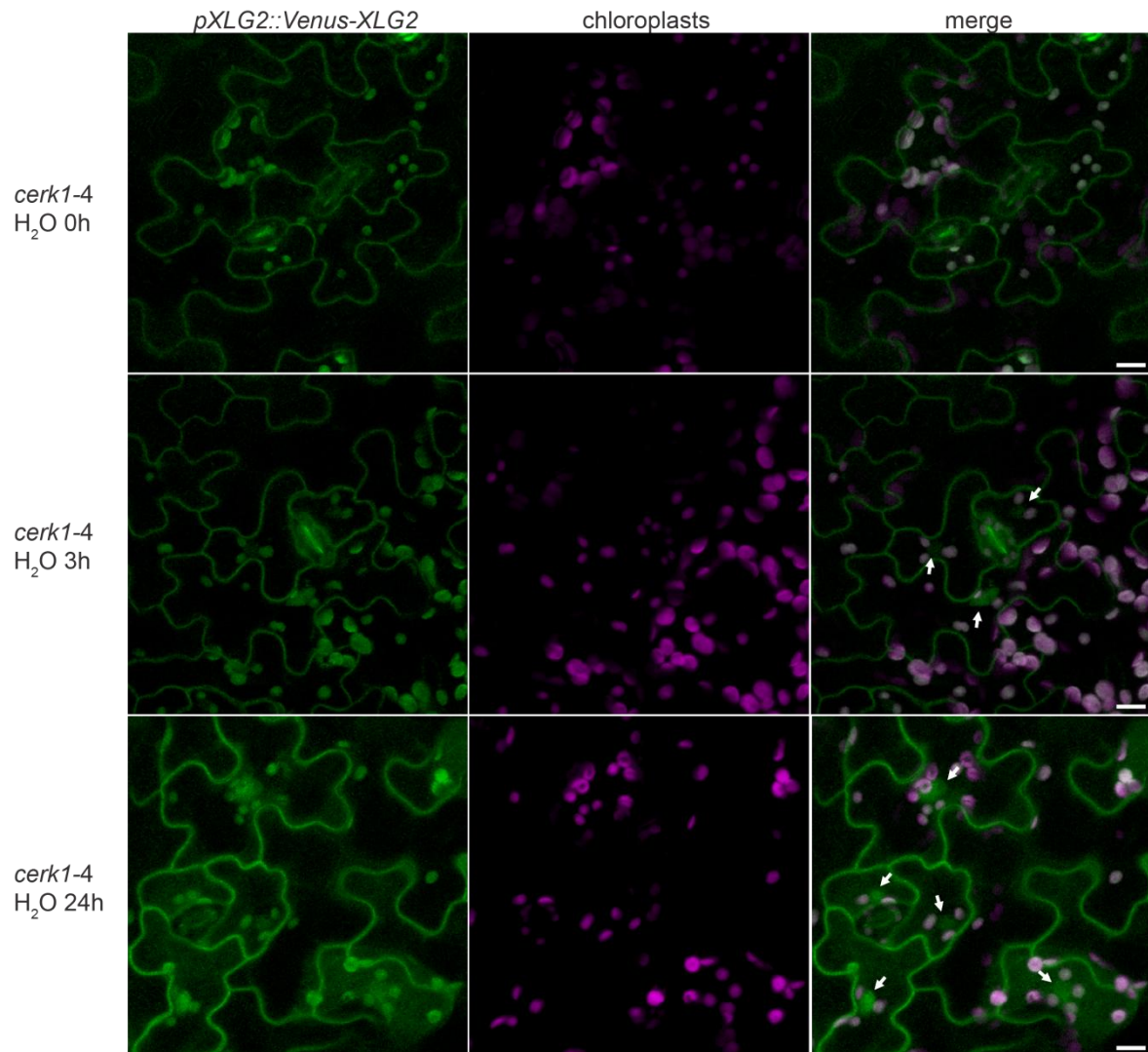


Figure 39. XLG2 is localized to the cell periphery in unchallenged plants and appears in nuclei after H₂O infiltration in *cerk1-4* plants. Stably transformed *cerk1-4* plants expressing Venus-XLG2 from the XLG2 promoter were analyzed by Confocal laser scanning microscopy. Leaf discs were cut out and vacuum-infiltrated with H₂O using a syringe. Leaf discs were either used for microscopy directly after infiltration or were incubated in H₂O for the indicated time points. Images represent maximum projections of 10 single focal plane images taken 1 μ m apart. White arrows denote nuclei. Size bar indicates 10 μ m.

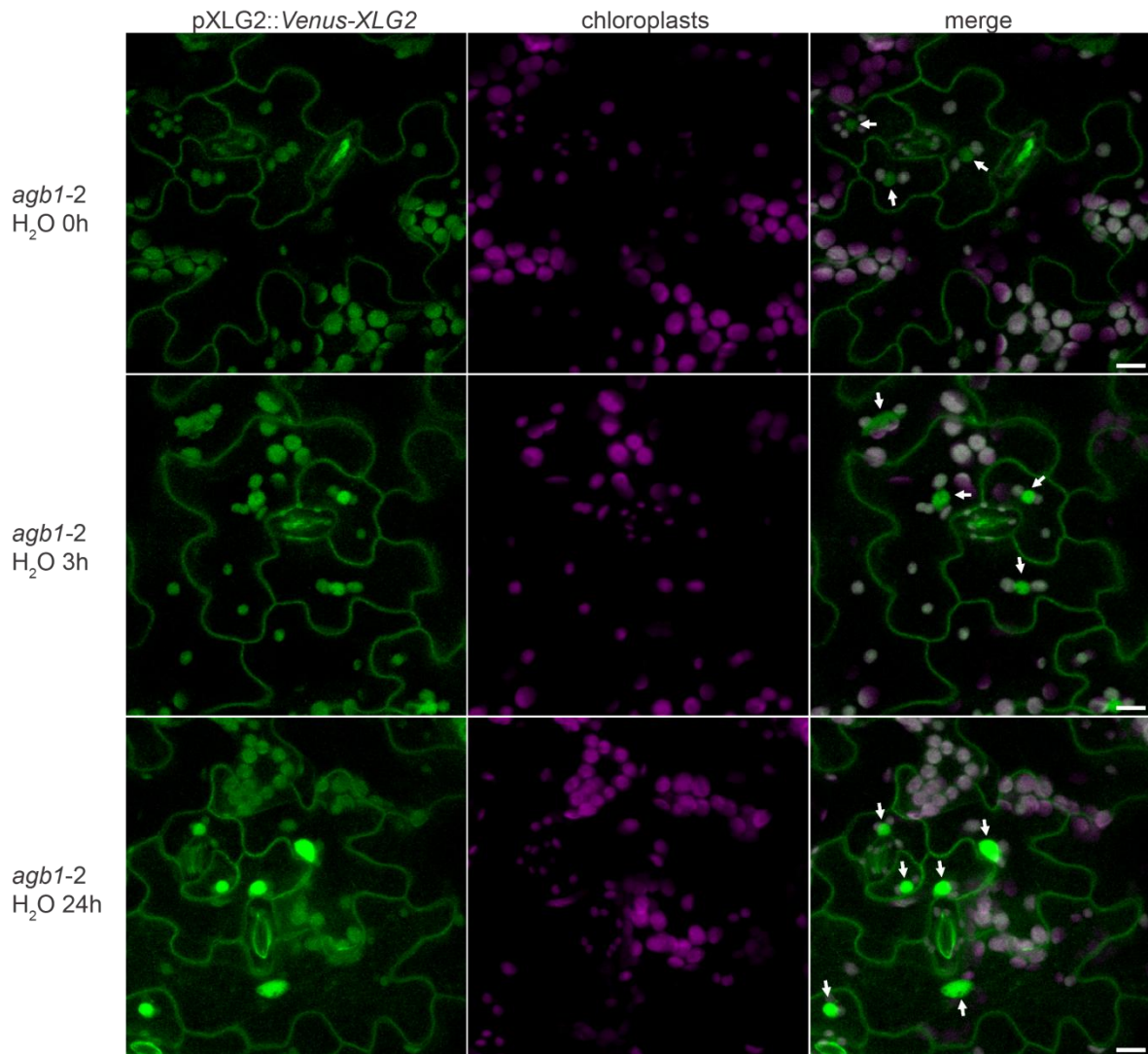


Figure 40. XLG2 is localized to the cell periphery and nucleus in unchallenged and challenged *agb1-2* plants. Stably transformed *agb1-2* plants expressing Venus-XLG2 from the XLG2 promoter were analyzed by Confocal laser scanning microscopy. Leaf discs were cut out and vacuum-infiltrated with H₂O using a syringe. Leaf discs were either used for microscopy directly after infiltration or were incubated in H₂O for the indicated time points. Images represent maximum projections of 10 single focal plane images taken 1 μ m apart. White arrows denote nuclei. Size bar indicates 10 μ m.

To complement confocal laser scanning microscopy analyses, membrane association of Venus-XLG2 was investigated by immunoblotting. To do so, microsomal fractions were prepared from untreated transgenic plants expressing Venus-XLG2 in the Col-0, *agb1-2*, Col-3 *gl1* or *cerk1-4* backgrounds. For all genotypes, immunoblot analysis using a GFP antibody revealed the presence of Venus-XLG2 in total extracts and in soluble fractions, but not in microsomal fractions for all genotypes (Figure 41). Since microscopy indicated a plasma membrane localization of Venus-XLG2, the membrane association of Venus-XLG2 might be disrupted by the extraction process. A CERK1 immunoblot was performed using the same samples to validate the identity of the prepared fractions. Full length CERK1 (75 kDa) is

membrane bound and can only be found in total extracts and microsomal fractions, whereas the CERK1 ectodomain (33 kDa) can be found in total extracts and soluble fractions (Figure 41) (Petutschnig *et al.*, 2014).

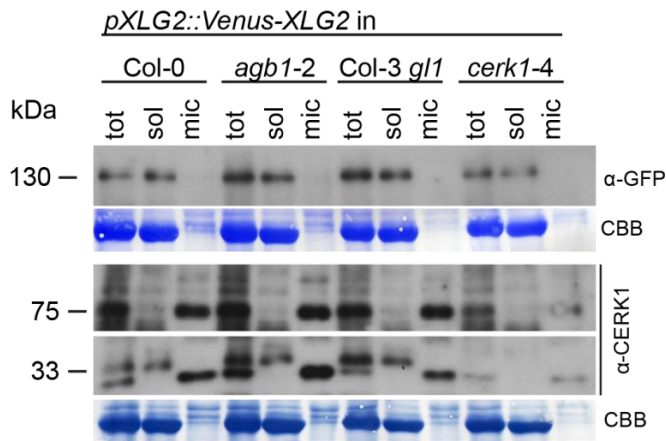


Figure 41. Venus-XLG2 can be found in soluble protein fractions, but not in microsomes. Microsomes were prepared from leaves of transgenic plants expressing Venus-XLG2. Samples were analyzed in immunoblot using a GFP antibody to detect Venus-XLG2 and with a specific CERK1 antibody, to validate microsomal and soluble fractions. Samples which have been used for GFP and CERK1 immunoblot are identical. CBB, Coomassie Brilliant Blue (loading control). Tot, total extracts; sol, soluble; mic, microsomal fraction.

3.2.5.4 XLG2 is localized to the nucleus in *Bgh* attacked and surrounding cells

The extra-large G-protein XLG2 appears to be a key regulator in cell death execution and is essential for development of the characteristic *cerk1-4* phenotype upon *Bgh* treatment (Marnie Stolze, unpublished, and this study). It was therefore of great interest to study XLG2 localization in *Bgh* infected plants. Especially localization of XLG2 in *Bgh* infected *cerk1-4* plants might help deciphering cellular changes that lead to development of the *cerk1-4* phenotype.

Transgenic plants expressing *pXLG2::Venus-XLG2* were inoculated with *Bgh* and analysis by confocal laser scanning microscopy was performed two days after infection (Figure 42). By staining fungal structures with FB28, penetrated cells could easily be detected. Penetrated cells were characterized by an accumulation of Venus-XLG2 fluorescence signal around the penetration site. XLG2 clearly accumulated in the nucleus of cells under *Bgh* attack. Interestingly, also cells surrounding the penetration site which are not under attack, show localization of XLG2 to the nucleus. This could be observed for Col-0, *agb1-2*, Col-3 *gl1* and *cerk1-4* plants. This supports the notion that XLG2 accumulates in nuclei after stress. However, no differences between wild type lines and *cerk1-4* could be observed.

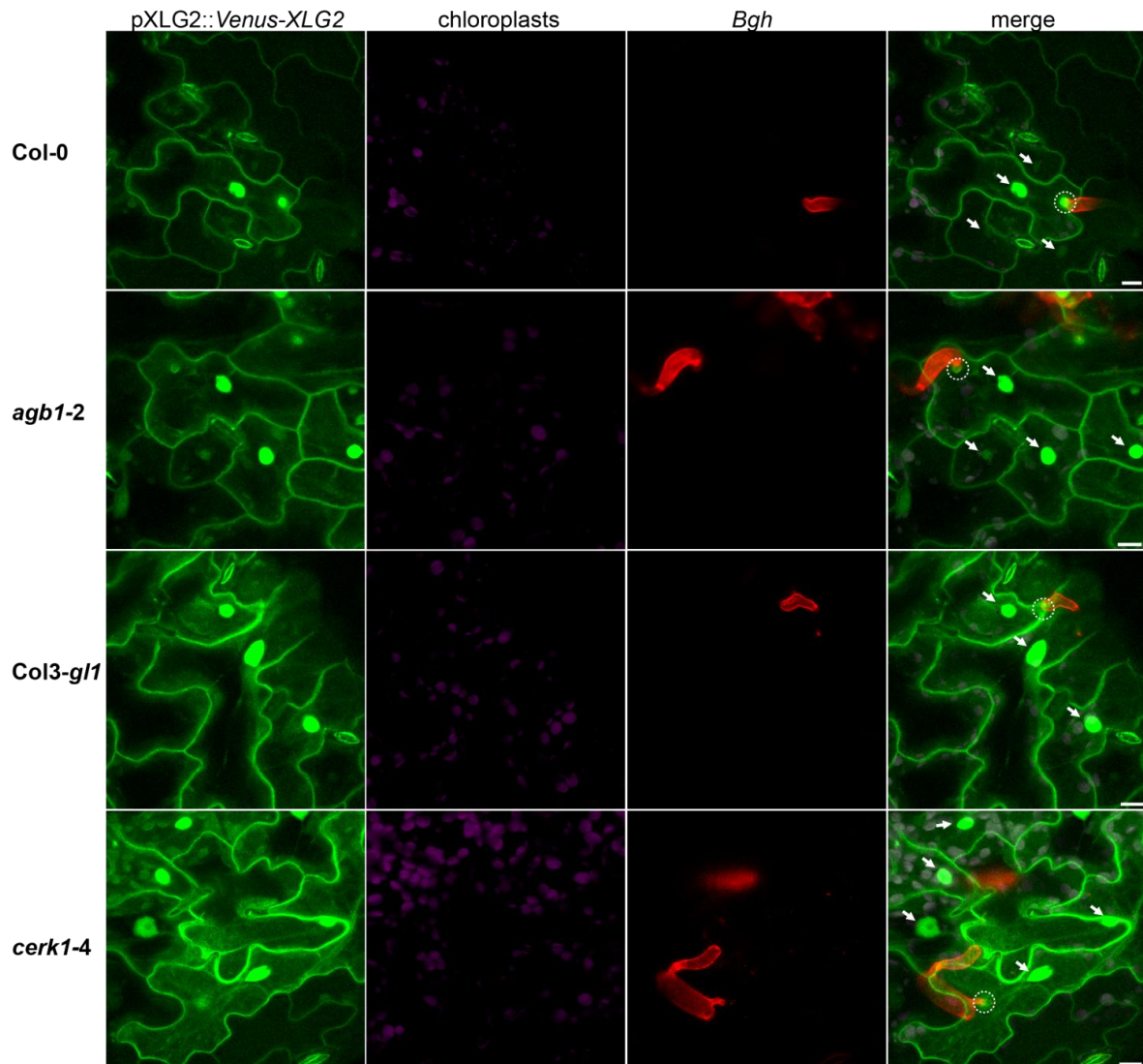


Figure 42. Venus-XLG2 accumulates in nuclei of *Bgh*-attacked and surrounding cells. Transgenic plants expressing Venus-XLG2 from the XLG2 promoter in Col-0, *agb1-2*, Col-3 *g11* or *cerk1-4* were inoculated with *Bgh*. Analysis by confocal laser scanning microscopy was performed two days after infection. Leaf discs were incubated in FB28 for 30 seconds to stain fungal structures. Images represent maximum projections of 10 single focal plane images taken 1 μm apart. White arrows denote nuclei. Size bar indicates 10 μm.

4. Discussion

Ectodomain shedding is a common regulatory mechanism of many membrane-anchored proteins in animals (Hayashida *et al.*, 2010). In plants it has been described only recently for the *Arabidopsis* receptor-like kinase CERK1 (Petutschnig *et al.*, 2014). A CERK1 mutant (*cerk1-4*) was isolated which shows altered abundance of the shed ectodomain and enhanced cell death upon pathogen inoculation (Petutschnig *et al.*, 2014). The first part of this study focused on the generation of a non-shedding CERK1 mutant to decipher the function of CERK1 ectodomain shedding and its role in development of the *cerk1-4* phenotype.

Extra-large G-proteins (XLGs) are unusual GTPases which can only be found in the plant kingdom (Urano *et al.*, 2013). They play roles in root development, hormone signaling, pathogen resistance and cell death (Ding *et al.*, 2008; Maruta *et al.*, 2015; Pandey *et al.*, 2008; Zhu *et al.*, 2009). A genetic screen to identify components of *cerk1-4* cell death execution identified XLG2 as a key regulator (Marnie Stolze, unpublished). The second part of this work focused on identification of a novel XLG2 allele fully suppressing the *cerk1-4* phenotype and the investigation of XLG2 subcellular localization.

4.1 Analysis of CERK1 ectodomain shedding

4.1.1 Prolines within the extracellular stalk of CERK1 modulate the abundance of the CERK1 ectodomain fragment

In *Arabidopsis thaliana* Columbia accessions, CERK1 is proteolytically processed to release its ectodomain. *cerk1* mutants lacking the soluble ectodomain are characterized by deregulated cell death upon pathogen attack (Petutschnig *et al.*, 2014). Natural variation between *Arabidopsis* accessions with regard to immune receptor complement is well documented (Gomez-Gomez *et al.*, 1999; Noel *et al.*, 1999; Rose *et al.*, 2004; Zhang *et al.*, 2013).

To investigate if there is also natural variation for CERK1 ectodomain shedding, different *Arabidopsis* accessions were analyzed with respect to CERK1 ectodomain fragment abundance. All 24 tested accessions showed a signal in immunoblots for the soluble CERK1 ectodomain, but in Mh-1, Rsch-4, Shakdara, Wt-5 and Sorbo, ectodomain levels were reduced compared to Col-0 (Figure 6A). The fact that none of the tested *Arabidopsis*

accessions completely lacked the CERK1 ectodomain points to the importance of CERK1 ectodomain shedding.

The reduced CERK1 ectodomain fragment abundance in these five accessions could be due to decreased stability like in the *cerk1-4* mutant or it could be the result of decreased shedding. Sequence analysis revealed amino acid changes in the extracellular stalk region of these accessions in comparison to Col-0 (Figure 6B). Especially the proline to alanine substitution in position 221 was regarded as potentially interesting. Prolines are known to disrupt secondary structures (Vanhoof *et al.*, 1995) which can cause structural disorder and may increase protease accessibility (Paetzel *et al.*, 1998). Also, proline-containing motifs play a role in ectodomain shedding of metazoan receptor kinases (Cheng *et al.*, 2003; Thorp *et al.*, 2011; Turk *et al.*, 2001; Yuan *et al.*, 2003). Thus, it seemed possible that the lack of proline 221 caused reduced CERK1 shedding in the five ecotypes with lower ectodomain fragment abundance.

Indeed, P²²¹ was found to be part of several potential EGFR-like cleavage motifs (P/G-X₅₋₇-P/G) within the extracellular stalk (Figure 8A). This motif is required for ectodomain shedding of EGFR family RTKs in animals (Cheng *et al.*, 2003; Yuan *et al.*, 2003). EGFRs can be shed by ADAMs (Rio *et al.*, 2000) which are not present in plants (Seals & Courtneidge, 2003). However, the related class of MMP proteases do occur in plants (Maidment *et al.*, 1999) and have been reported to recognize similar motifs to ADAMs (Caescu *et al.*, 2009; Turk *et al.*, 2001).

The amino acid directly N-terminal of P²²¹ is also a proline (P²²⁰). It is therefore conceivable that the two adjacent prolines at positions 220 and 221 might play redundant roles in CERK1 ectodomain shedding. This would also be an explanation for the fact that the CERK1 ectodomain fragment abundance is reduced in the ecotypes lacking P²²¹, but the fragment is not completely gone. In an attempt to generate a non-shedding CERK1 mutant, both prolines were mutated to alanine (*cerk1 cvg1*). Alanine is a helix-forming amino acid (Rohl *et al.*, 1999) promoting a secondary structure that possibly interferes with protease accessibility. When this construct was expressed in *Arabidopsis* plants, the *cerk1 cvg1* protein indeed showed lower levels of soluble ectodomain fragment, which is consistent with the idea of prolines being modulators of CERK1 ectodomain shedding. However, the cleaved CERK1 ectodomain was still detectable in *cerk1 cvg1*, which argues against P²²⁰ and P²²¹ redundantly mediating ectodomain shedding, unless there is another redundant amino acid. In *cerk1 cvg1* there is one remaining proline within the extracellular stalk in position 215. It cannot be ruled out completely that P²¹⁵ might contribute to ectodomain shedding and be sufficient for the residual ectodomain fragment observed. However, based on mass spectrometry analyses, the size of the ectodomain fragment and a series of domain swap

constructs the cleavage site is probably close to the or within the transmembrane domain (see section 4.1.5 below), which starts at amino acid 233 and is relatively far from P²¹⁵. Also, a CERK1-FLS2 domain swap construct (FLS2TMex3), in which P²¹⁵, P²²⁰ and P²²¹ are missing, still showed shed ectodomain. In this construct the extracellular stalk and transmembrane domain of CERK1 were replaced with the stalk and transmembrane domain of FLS2. The stalk of FLS2 also contains two proline residues. It is theoretically possible, that these two prolines (or one of them) mediate cleavage (potentially in addition to other sites – see section 4.1.5 below), which would suggest that prolines can promote proteolysis in a wide variety of sequence contexts. The fact that prolines have been reported to be modulators of ectodomain shedding in different types of transmembrane proteins supports this idea. For example, the mutation of a proline within the extracellular stalk of human p75 TNF receptor was shown to prevent protein kinase C-mediated ectodomain shedding (Herman & Chernajovsky, 1998).

Several *cerk1 cvg1* expressing lines showed lower overall CERK1 signal in immunoblots than the Col-0 control. It is normal for transgenic lines to show some variation in transgene expression, thus the lower CERK1 abundance could be attributed to this fact. However, immunoblot experiments with *cerk1-4 cvg1* expressing plants (also see below) revealed the full length protein to be unstable. This raises the possibility that the *cvg1* mutation alone might have a destabilizing effect on the CERK1 ectodomain and that lower ectodomain abundance is not caused by reduced shedding. This is reminiscent of the *cerk1-4* mutation. When present alone, it destabilizes the shed ectodomain (Petutschnig *et al.*, 2014). When combined with another mutation, *cerk1-5*, which likely also destabilizes the ectodomain, the full length *cerk1-4* protein appears to become unstable as well. Similar to *cerk1-4* plants, *cerk1-5* plants also develop the enhanced cell death phenotype. (Petutschnig *et al.*, 2014). The *cerk1-4* and *cerk1-5* mutation lie in close vicinity within the second LysM domain and might lead to the formation of a degradation product triggering the cell death phenotype, which is not formed in *cerk1 cvg1*. When a *cerk1-4 cerk1-5* double mutant *cerk1* variant is expressed in *cerk1-2*, no full length protein can be detected in immunoblots and transgenic plants do not develop a *cerk1-4* phenotype (Petutschnig and Horlacher, unpublished).

4.1.2 Reduced abundance of the CERK1 ectodomain cannot suppress the *cerk1-4* phenotype

One topic of this work was the influence of CERK1 ectodomain shedding on development of the *cerk1-4* phenotype. Since a non-shedding CERK1 variant could not be generated and

cerk1 cvg1 showed reduced ectodomain fragment abundance, the *cerk1 cvg1* mutation was chosen to be combined with the *cerk1-4* mutation. Plants expressing *cerk1-4 cvg1* strongly resembled *cerk1-4* mutants, indicating that the *cvg1* mutation can neither suppress the *cerk1-4* enhanced cell death phenotype upon pathogen challenge nor the senescence phenotype (Figure 10A, Figura 11A).

Surprisingly, very little *cerk1-4 cvg1* protein was detected in immunoblots, even though the plants developed a very clear *cerk1-4*-like phenotype. The cleaved *cerk1-4* ectodomain is likely to be unstable (Petutschnig *et al.*, 2014). One theory to explain the *cerk1-4* cell death phenotype is that a degradation product of the shed ectodomain acts as a DAMP and triggers cell death via an unknown receptor. This could also be the case in *cerk1-4 cvg1* plants. Very little full length protein might be left, but sufficient amounts of degradation product(s) might still be formed to trigger the *cerk1-4* phenotype.

4.1.3 CERK1 ectodomain shedding cannot be suppressed by mutating potential protease cleavage motifs

The prolines acting as possible modulators of CERK1 ectodomain shedding were part of potential EGFR cleavage motifs. Additional putative EGFR cleavage motifs within the CERK1 extracellular stalk containing glycines could be found (Figure 8A). Furthermore, sequences with similarities to cleavage motifs of rhomboid proteases were identified within the CERK1 transmembrane domain. Most rhomboid proteases were shown to depend on the presence of helix-relaxing amino acids in the outermost third of their substrate transmembrane domain (N-terminal part of type I transmembrane proteins) (Urban, 2006; Urban & Freeman, 2003). Also, the presence of small amino acids in this region promotes rhomboid cleavage (Urban & Freeman, 2003). For example, replacing a glycine with phenylalanine in the outer part of the transmembrane domain could successfully suppress cleavage by *Drosophila* Rhomboid-1 (Urban & Freeman, 2003). *cerk1 cvg2* and *cerk1 cvg3* were designed to harbor amino acid substitutions of helix-relaxing glycines within the N-terminal part of the transmembrane domain and at the same time target putative EGFR cleavage motifs that overlapped with the CERK1 extracellular stalk and transmembrane domain (Figure 8B). Both CERK1 variants exhibited slightly enhanced ectodomain abundance when expressed in *Arabidopsis*. Thus *cerk1 cvg2* and *cvg3* mutations certainly did not suppress ectodomain shedding. EGFRs are shed by MMPs and ADAMs (Carey *et al.*, 2005; Rio *et al.*, 2000), the latter of which do not occur in plants (Seals & Courtneidge, 2003). Other, yet unknown proteases may compensate

for the lack of ADAMs in plants. These proteases might rely on amino acid sequences completely different from ADAMs.

Apart from EGFR cleavage motifs, *cerk1 cvg3* harbored mutations aiming at inhibiting cleavage by rhomboid proteases. For this purpose, the helix-relaxing amino acid glycine was replaced by phenylalanine. The preference of rhomboid protease cleavage towards such helix-relaxing amino acids seems to be rather strict (Urban, 2006; Urban & Freeman, 2003). This is further supported by *ATRBL2*, an *Arabidopsis* rhomboid homologue, which was shown to exhibit a cleavage motif preference similar to its *Drosophila* counterpart Rho-1 (Kanaoka *et al.*, 2005). Taking this into consideration along with the fact that extracellular and cytoplasmic domains of substrate do not influence rhomboid activity (Urban & Freeman, 2003) makes it unlikely for CERK1 to be a rhomboid substrate.

Plant ectodomain shedding might resemble animal ectodomain shedding in the sense that proteins can be subject to proteolytic cleavage by not only one, but a variety of proteases (Hayashida *et al.*, 2010). It might be therefore possible that even though in the generated CERK1 mutants actual cleavage motifs were mutated, cleavage motifs for other proteases still existed or were even created. Furthermore, shedding of the CERK1 ectodomain might not occur at a distinct cleavage site, but at a fixed distance from the transmembrane domain, which was also suggested for APP (Sisodia, 1992).

In immunoblots after chitin pull-down, CERK1 often shows multiple bands at around 40 kDa whose exact identity and function is unknown (Figure 8C). These multiple bands could potentially be precursors of the cleaved CERK1 ectodomain. In contrast to the CERK1 ectodomain fragment, these bands are membrane-associated and their size suggests that in addition to the ecto- and transmembrane domain they also harbor parts of the intracellular domain. Interestingly, the intracellular juxtamembrane domain of CERK1 harbors potential EGFR cleavage motifs, similar to the extracellular domain (Figure 9A). Such motifs were also found in the intracellular juxtamembrane domains of several rice RLKs (Ding *et al.*, 2009) and phosphorylation of sites flanked by the cleavage motifs was reported to inhibit cleavage of the rice RLK XA21 (Xu *et al.*, 2006). By deleting potential corresponding motifs in CERK1, *cerk1 clx* aimed at repressing the generation of the 40 kDa fragment group. However, *cerk1 clx* was neither successful in inhibiting the generation of 40 kDa signals nor did it inhibit generation of the soluble CERK1 ectodomain derivative (Figure 9C). In *cerk1 clx* immunoblots it seemed like the highest of the multiple bands around 40 kDa was shifted upwards. This could indicate that the cleavage site for generation of this particular 40 kDa fragment was shifted to the C-terminus. However, at present it is not known if the multiple bands around 40 kDa arise from cleavage at multiple, adjacent sites. Alternatively CERK1 might be cleaved in only one position and the different apparent molecular weights might be

caused by protein modifications such as phosphorylation or differential patterns of glycosylation.

4.1.4 Reduction of extracellular stalk length cannot suppress CERK1 ectodomain shedding

Results of mutational analysis of possible CERK1 cleavage motifs revealed that other factors than the sole amino acid sequence might be critical for CERK1 ectodomain shedding. Ectodomain shedding of the transmembrane proteins L-selectin (Migaki *et al.*, 1995), the interleukin 6-receptor (Baran *et al.*, 2013) and the p75 neurotrophin receptor (Weskamp *et al.*, 2004) were reported to depend on the length of their extracellular stalk. Based on these studies CERK1 extracellular stalk deletion constructs were generated (Figure 12A). Shortening the CERK1 extracellular stalk by five amino acids could not repress ectodomain shedding. While for L-selectin deletion of five amino acids was sufficient for inhibition of ectodomain shedding (Migaki *et al.*, 1995), an extracellular stalk deletion of 15 amino acids was required with the p75 TNF receptor (Weskamp *et al.*, 2004). The 15 amino acid deletion left only two amino acids of the extracellular stalk and could successfully repress p75 TNF proteolytic cleavage. It was speculated that long deletions place the ectodomain in close vicinity to the plasma membrane thereby abolishing protease accessibility. Consequently, a CERK1 variant with a deletion of 16 amino acids within the CERK1 extracellular stalk was generated (*cerk1 del2*). However, when the respective construct was stably expressed in *Arabidopsis*, none of the transformants contained any *cerk1 del2* protein. Long stalk deletions might interfere with proper membrane insertion of CERK1 resulting in protein degradation. Sterical hindrance between ectodomain and plasma membrane or transmembrane domain might also be a reason for *cerk1 del2* degradation. Nevertheless, a series of successive deletions of 6 to 15 amino acids might result in a CERK1 variant where the ectodomain is close enough to the plasma membrane to inhibit shedding but does not interfere with protein stability. It would be interesting to address this issue in future experiments.

4.1.5 The CERK1 extracellular stalk and transmembrane domain are not critical for ectodomain shedding

In order to narrow down which parts of CERK1 are required for ectodomain shedding, a series CERK1-FLS2 chimeras were generated (Figure 13A). In *cerk1 fls2tm*, the

transmembrane domain (TM) of CERK1 was replaced with the TM of FLS2. In *cerk1 fls2tmex3*, both the TM and extracellular stalk were replaced with the FLS2 counterparts. *cerk1 fls2tmex1* and *cerk1 fls2tmex2* variants contained the FLS2 transmembrane domain and a composite extracellular stalk with elements from CERK1 as well as FLS2. None of these domain swaps could suppress ectodomain shedding of CERK1 in *Nicotiana benthamiana*. The CERK1-FLS2 chimera *cerk1 fls2tm* and *cerk1 fls2tmex1* were also stably transformed into *Arabidopsis thaliana* where the corresponding transgenic proteins still showed ectodomain shedding.

The fact that the cleaved CERK1 ectodomain is soluble (Petutschnig *et al.*, 2014) implicates that cleavage occurs within the extracellular stalk or transmembrane domain. The *cerk1 fls2tmex* variant contained the complete FLS2 transmembrane domain and extracellular stalk and still underwent ectodomain shedding. Thus, the cleavage must have occurred within the FLS2 sequences and CERK1 ectodomain shedding obviously does neither depend on the CERK1 transmembrane domain nor on the CERK1 extracellular stalk. Consequently, the FLS2 sequences which were introduced into CERK1 must meet the structural and/or sequence criteria for ectodomain shedding. This suggests that FLS2 might also be subject to ectodomain shedding. Peptides corresponding to the extracellular domains of several LRR-RLKs could be found in the supernatants of cell cultures (see section 4.1.6) further supporting the possibility of FLS2 being subject to ectodomain shedding.

The chimeras *cerk1 fls2tmex1* and *cerk1 fls2tmex3* have longer extracellular stalks than CERK1 and accordingly showed a bigger signal for the full length receptor than wild type CERK1 (Figure 13B). Interestingly, the *cerk1 fls2tmex1* and *cerk1 fls2tmex3* ectodomain fragments differed markedly in size. The shed *cerk1 fls2tmex1* ectodomain was discernibly bigger than in the wild type, which was expected. However, it appeared as a double band. In contrast, the size of *cerk1 fls2tmex3* ectodomain fragment was comparable to the shed ectodomain of wild type CERK1. This implies an N-terminal shift of the cleavage site in *cerk1 fls2tmex3*. The fact that the *cerk1 fls2tmex1* ectodomain fragment appeared as a double band suggests that this new cleavage site might also be present in *cerk1 fls2tmex3*, likely in addition to a more C-terminal site. Additionally, mutation or deletion of a shared KS motif found in all CERK1 FLS2 chimeric constructs did not abolish ectodomain shedding (Figure 15B). All in all, the data indicate that ectodomain shedding is not dependent on a specific sequence or motif within the TM or extracellular stalk.

The three LysM domains of CERK1 might be of importance for ectodomain shedding. Ectodomain shedding of the angiotensin converting enzyme (ACE) was reported to depend on an N-terminal (distal) part of its ectodomain (Sadhukhan *et al.*, 1998). ACE and CD4 are transmembrane proteins, of which ACE is subject to ectodomain shedding and CD4 is not.

Chimeras of the distal ACE ectodomain with the extracellular stalk and transmembrane domain of CD4 were shed within the CD4 sequence. Combining the distal ectodomain of CD4 with the juxtamembrane and transmembrane domain of ACE did not lead to ectodomain shedding (Sadhukhan *et al.*, 1998). The extracellular domain of CERK1 or one of its three LysM domains might be critical for interaction with a protease which is involved in proteolytic cleavage of the CERK1 ectodomain, whereas the amino acid sequence of the extracellular stalk and transmembrane domain appear to be of minor importance.

4.1.6 The extracellular domain of many RLKs is proteolytically processed

The analysis of *Arabidopsis* cell culture supernatants and apoplastic wash fluids from leaves by mass spectrometry revealed the presence of peptides corresponding to the extracellular domains of numerous receptor-like kinases (Figure 16). The exon structure of many of those RLKs excludes the possibility of the extracellular domain being generated by alternative splicing. This suggests that many RLKs in addition to CERK1 may undergo ectodomain shedding. LRR-RLKs were the biggest group of RLKs found in the cell culture supernatants and apoplastic wash fluids. Based on the fact that LRR-RLKs are the largest family of RLKs in *Arabidopsis* (Shiu & Bleecker, 2001), this could be expected. Even though FLS2 is not among the identified LRR-RLKs, its ectodomain domain might also be released. This might explain why the CERK1-FLS2 chimeras were still subject to ectodomain shedding. Interestingly, some types of RLKs appeared to be enriched in the cell culture supernatant and apoplastic wash fluid samples. *Arabidopsis* contains four LRR-RLKs of the TMK family (Dai *et al.*, 2013), of which three were detected in this study. The remaining one (TMK2) is only expressed in reproductive organs (Dai *et al.*, 2013) and thus was probably not present in the samples investigated. TMKs contain two extracellular LRR-domains that are linked by a hinge domain (Liu *et al.*, 2013b). The peptides identified mapped to the entire ectodomains of the TMKs, indicating that they are subject to ectodomain shedding and not cleavage between extracellular subdomains (Figure 17A). The exon structure precludes alternative splicing as the source of soluble TMK forms, thus it is highly likely that the entire TMK family undergoes ectodomain shedding. Interestingly, TMK1 was found as a putative interactor of CERK1 in a yeast two hybrid screen (Lipka, unpublished). CERK1 and LYK5 were also detected in this study, confirming previous results (Petutschnig *et al.*, 2014). It is tempting to speculate that TMKs and LysM-RLKs interact and might undergo ectodomain shedding together. Also, many RLKs were found that contain malectin-like domains in their extracellular domains. The Malectin-LRR-RLK SYMRK is required for symbiosis in *Lotus japonicus*.

SYMRK releases its malectin-like domain and this process depends on the presence of a GDPC motif (Antolín-Llovera *et al.*, 2014). In the supernatant of cell cultures three Malectin-LRR-RLKs could be found. Like SYMRK, they also harbor a GDPC motif within their extracellular domain (Figure 17B). Only peptides N-terminal to this GDPC motif were found indicating that the malectin-like domain is released in a process similar to SYMRK. However, as cleavage via the GDPC motif does not occur in close vicinity to the transmembrane domain, this process is not referred to as ectodomain shedding (Antolín-Llovera *et al.*, 2014). Malectin cleavage of SYMRK enhances its interaction with the LysM-RLK NFR5 (Antolín-Llovera *et al.*, 2014). Some *Arabidopsis* Malectin-LRR-RLKs might also interact with LysM-RLKs such as CERK1 and the proteolytic processing might modulate the interaction. Comparable to cell culture supernatants, numerous peptides corresponding to the extracellular domains of RLKs including Malectin-LRR-RLKs were found in apoplastic wash fluids (Figure 20). In contrast to cell culture supernatants, single peptides C-terminal to the characteristic Malectin-LRR-RLK GDPC motif were found. Moreover, also few peptides corresponding to intracellular domains could be identified. These peptides probably derive from wounded plant tissue which is a consequence of the preparation method.

Table 12. RLKs identified in cell wall proteome studies. RLKs marked with an asterisk were also found in cell culture supernatants and/or apoplastic wash fluids.

Material	Identified RLKs	Reference
Cell suspension cultures	(LRR – RLK) - AT3G08680 (LRR – RLK) - AT3G02880* (LRR – RLK) - AT2G01210 (LRR – RLK) - AT2G01820 – TMK3* (LRR – RLK) - AT3G51740 (LRR – RLK) - AT5G16590 – LRR1* (LRR – RLK) - AT2G16250	Bayer <i>et al.</i> (2006)
Etiolated hypocotyls	(LRR – RLK) - AT3G02880* (LRR – RLK) - AT5G16590 – LRR1*	Zhang <i>et al.</i> (2011)
Etiolated hypocotyls	(LRR – RLK) - AT2G29000	Feiz <i>et al.</i> (2006)
Roots	(LRR – RLK) - AT3G02880* (LRR – RLK) - AT3G17840 – RLK902* (LRR – RLK) - AT3G28450 (LRR – RLK) - AT5G37450 (Malectin – LRR – RLK) - AT2G14510 (Malectin – LRR – RLK) - AT1G51850* (Malectin – LRR – RLK) - AT1G51890 (Malectin – LRR – RLK) - AT2G28990 (Malectin – LRR – RLK) - AT5G59680*	Nguyen-Kim <i>et al.</i> (2016)

RLKs could also be identified in studies analyzing the cell wall proteome. These RLKs belong to the group of LRR-RLKs and Malectin-LRR-RLKs, some of which could also be found in the present study (Table 12). However, the degree of contamination of the cell wall preparations and to which part of the RLKs the identified peptides match is not known. Nevertheless, these results add further evidence to the hypothesis that proteolytic processing of extracellular domains is a more widespread phenomenon in *Arabidopsis* than previously known.

4.1.7 Possible function of CERK1 ectodomain shedding

The function of ectodomain shedding in many animal RTKs is to reduce the amount of functional receptors on the cellular surface upon ligand binding (Chen & Hung, 2015). Proteolytic cleavage of the extracellular domain is often followed by intramembrane proteolysis to release the intracellular domain which can be transported to the nucleus. For example, the intracellular domain of erbB4/Her-4 translocates into the nucleus after being released from the plasma membrane by γ -secretase cleavage (Jones, 2008). In the nucleus it acts as a transcriptional co-activator and is involved in regulation of growth and differentiation of breast epithelium cells. Since CERK1 ectodomain shedding is chitin-independent, it is likely not involved in chitin signaling into the cell (Petutschnig *et al.*, 2014). Moreover, confocal microscopy of plants expressing CERK1-GFP fusions could not detect a signal within the nucleus (Erwig *et al.*, unpublished; Petutschnig *et al.*, 2014). Therefore, the function of CERK1 ectodomain shedding is probably different from erbB4/Her-4 ectodomain shedding. CERK1 is thought to form a chitin induced complex with the LysM-RLK LYK5 (Cao *et al.*, 2014). Proteolytic cleavage of the CERK1 ectodomain might be a prerequisite for separation of the receptor complex components. In this scenario CERK1 would remain at the plasma membrane, while LYK5 is removed from the plasma membrane via endocytosis (Erwig *et al.*, unpublished).

CERK1 ectodomain shedding was shown to be upregulated upon pathogen attack (Petutschnig *et al.*, 2014). Thus it seems conceivable that the released ectodomain binds chitin fragments within the extracellular space to prevent excessive receptor activation. The CERK1 ectodomain might also function as extracellular decoy. Pathogens secrete a variety of effectors in the plant apoplast (Jashni *et al.*, 2015). These effectors include proteases which might then target the CERK1 ectodomain instead of the full length plasma membrane bound receptor. Development of the *cerk1-4* phenotype was hypothesized to be triggered by degradation product(s) of the *cerk1-4* ectodomain (Petutschnig *et al.*, 2014) which could

activate DAMP signaling. In analogy to this, degradation of the wild type decoy CERK1 ectodomain by pathogenic effector proteases might also lead to the generation of degradation products which initiate DAMP signaling.

4.1.8 Conclusion

The findings of the present study could not reveal the sequence determinants or structurally relevant elements for CERK1 ectodomain shedding. Different approaches to generate non-shedding CERK1 mutants failed. This prevented investigation of the function of CERK1 ectodomain shedding and its involvement in generation of the *cerk1-4* phenotype. A non-shedding CERK1 would be required to investigate these topics.

The underlying mechanism and responsible proteases of CERK1 ectodomain shedding remain unclear. Mutation of potential protease cleavage motifs, deletion and domain swap mutants point to a rather relaxed sequence specificity of the responsible protease or participation of several proteases in this process. CERK1 FLS2 chimeras further raise the possibility of the three LysM domains to be the critical for ectodomain shedding and the amino acid sequence to be of secondary importance. The amount of ectodomain could be modulated by modifications within the CERK1 extracellular stalk. Prolines within the extracellular stalk were found to be possibly important for structural integrity of the ectodomain. Reducing the abundance of CERK1 ectodomain by mutating these prolines could not suppress the *cerk1-4* phenotype.

Mass spectrometry analysis of cell culture supernatants revealed the presence of peptides corresponding to the extracellular domains of numerous RLKs suggesting that not only CERK1 but several RLKs are subject to ectodomain shedding.

4.1.9 Outlook

This study could not reveal the mechanism and function of CERK1 ectodomain shedding. To decipher the function of CERK1 ectodomain shedding, a non-shedding CERK1 variant will be required. In this work, deletions of five amino acids within the extracellular stalk did not suppress CERK1 ectodomain shedding, while deletions of 16 amino acids led to structural instability of the protein. Intermediate deletion mutants might be successful in inhibiting ectodomain shedding. To test if the CERK1 LysM domains are critical for CERK1 ectodomain shedding, the CERK1 ectodomain could be replaced by the ectodomain of another RLK (e.g.

FLS2) and tested for ectodomain shedding. However, this would require an antibody for the respective ectodomain.

An alternative approach would be identification of the shedding protease. In animals, receptor kinases are shed by MMPs and ADAMs (Chen & Hung, 2015), the latter of which are not present in plants (Seals & Courtneidge, 2003). Preliminary studies with multiple *Arabidopsis* MMP mutants suggest that CERK1 ectodomain shedding is not MMP-dependent (Stolze, unpublished). Rhomboids could act as sheddases on CERK1. However, mutation of a putative rhomboid motif argues against this. Also rhomboids are a large family of proteases in *Arabidopsis*, making a reverse genetics approach not feasible. In animals, many proteins are cleaved by γ -secretase after ectodomain shedding. A recent study revealed the presence of a putative γ -secretase complex in *Arabidopsis* (Smolarkiewicz *et al.*, 2014). All components of the complex were shown to be expressed in leaves. T-DNA knockout mutants of components of the γ -secretase complex could be investigated. The fate of the C-terminal CERK1 fragment in these mutants would be of particular interest and could be investigated using C-terminally tagged CERK1 constructs. Moreover, expression of *cerk1-4* would reveal if the development of the *cerk1-4* phenotype is dependent on γ -secretase processing.

In plants, research on proteolytic processing of plasma membrane localized receptors is only in its infancies and much work will be required in the future to elucidate the underlying mechanisms and, importantly, the functional implications.

4.2 Analysis of *nole1-2* and XLG2 subcellular localization

4.2.1 XLG2 is a key regulator of *cerk1-4* cell death execution

A *cerk1-4* suppressing mutant was identified in the present study. The causal mutation was mapped to the N-terminal part of XLG2, where a glutamic acid (E) was replaced by a lysine (K) in a highly conserved region (Figure 26). Based on immunoblot analysis of *xlg2 E293K* expressing plants suppression of the *cerk1-4* phenotype is probably not caused by reduced protein stability. However, the function of XLG2 may be disturbed by replacement of negatively charged glutamic acid with positively charged lysine. Recently, *xlg2* and *agb1* single, as well as *agg1 agg2* double mutants were reported to suppress the cell death phenotype of a BIR1 mutant (*bir1-1*) (Liu *et al.*, 2013a; Maruta *et al.*, 2015). These results suggest that XLG2 together with G γ β -dimers can act in receptor-like kinase mediated cell death regulation. *xlg2 E293K* might be disturbed in perceiving or transducing signals within these pathways. However, findings from our laboratory (Elena Petutschnig, unpublished)

showed that *agb1* single and *agg1 agg2* double mutants cannot fully suppress the *cerk1-4* phenotype. This indicates that XLG2 acts independently from G $\beta\gamma$ -dimers in *cerk1-4* mediated cell death and that CERK1 and BIR1 mediate different cell death pathways. Furthermore, these results exclude the possibility that *cerk1-4* suppression in *nole1-2* mutants is caused by disturbed interaction with AGB1.

The N-terminal domain of XLG2 harbors a region of regularly spaced cysteines (Figure 26B). (Ding *et al.*, 2008), whose function is unclear. These cysteines resemble zinc-finger domains which are implicated in protein-DNA interactions (Leon & Roth, 2000) suggesting that XLG2 might act as transcriptional regulator. As the *nole1-2* mutation is in close vicinity to the cysteine rich domain, it might disturb XLG2 DNA binding. This is further supported by the fact that XLG2 is localized to the nucleus upon stimulus (Chapter 3.2.5.2).

Although a function as direct transcriptional regulator has to be confirmed, XLG2 was already shown to exhibit functions within the nucleus, where it was shown to promote the activation of the DNA binding protein RELATED TO VERNALIZATION 1 (RTV1) (Heo *et al.*, 2012). Apart from DNA binding, regularly spaced cysteines can also be involved in formation of disulphide bridges. One of the key regulators of SA signaling, NON-EXPRESSION OF PR1 (NPR1), was shown to form intermolecular disulphide bridges which result in oligomer formation (Mou *et al.*, 2003). Salicylic acid (SA) induced cellular redox changes lead to reduction of intermolecular disulphide bridges and NPR1 monomer formation. NPR1 monomers then accumulate in the nucleus and activate expression of PR1.

4.2.2 XLG2 localization is stimulus dependent

Previous studies on XLG2 localization were performed using the strong 35S or UBIQUITIN10 promoter (Chakravorty *et al.*, 2015; Ding *et al.*, 2008; Maruta *et al.*, 2015). In the present study, XLG2 localization was re-assessed using fluorescently labeled XLG2 under control of the endogenous XLG2 promoter. In a first approach, the C-terminus of XLG2 was chosen for fusion of GFP. Expression of XLG2 constructs in the *nole1-1 cerk1-4* or *nole1-2 cerk1-4* background provides the possibility to assess functionality of XLG2 constructs. Only functional constructs can restore the *cerk1-4* phenotype in these mutant backgrounds. Expression of XLG2-GFP in *nole1-1 cerk1-4* could not restore the *cerk1-4* phenotype and revealed this construct not to be functional (Figure 29). Previous studies encountered problems with protein accumulation even when expressing XLG2-GFP under control of the 35S promoter (Zhu *et al.*, 2009). However, as a signal in immunoblot and confocal microscopy could be detected (Figure 28) compromised protein stability may not be the

reason for missing functionality in the present study. On the contrary, a scenario is more likely in which other factors are responsible for functional insufficiency. In this context, it is important to note that one amino acid substitution within the GTPase domain of XLG2 was sufficient to abolish *in vitro* GTP binding capacity and to block interaction with downstream targets (*xlg2* T476N, falsely denoted as T475N) (Heo *et al.*, 2012). Thus, fusion of GFP to the C-terminus might cause GTP binding problems similar to the *xlg2* T476N mutant and therefore might not be functional. As the C-terminus of XLG2 was found not to be suitable for fluorescent tag fusions, an N-terminal XLG2 fusion with the fluorescent protein Venus was generated. Venus-XLG2 restored the *cerk1-4* phenotype in *nole1-1 cerk1-4* and was therefore considered functional. Studies using this construct in *Arabidopsis thaliana* showed localization to the cell periphery in Col-0, Col-3 *gl1* and *cerk1-4*. Considering previous studies, which reported nuclear localization for XLG2, this was surprising (Maruta *et al.*, 2015). After infiltration of H₂O however, nucleus localization became visible after three hours in all genotypes (Figure 34, Figure 38, Figure 39). The same held true for chitin and *flg22* infiltration, as well as wounding in Col-0 plants (Figure 35, Figure 36, Figure 37). As XLGs were found to be involved in responses to osmotic stress, hormones and pathogens (Ding *et al.*, 2008; Maruta *et al.*, 2015; Zhu *et al.*, 2009) it seems conceivable that XLG2 changes its localization pattern, when stress and/or defense responses are activated. Overexpression of XLG2 might be the cause for the results of previous studies, which reported XLG2 to be localized to the plasma membrane and nucleus even in untreated cells (Maruta *et al.*, 2015). As overexpression of XLG2 leads to the accumulation of abnormal defense related transcripts (Zhu *et al.*, 2009), it might also induce cellular defense responses which lead to XLG2 translocation into the nucleus.

In contrast to the canonical α -subunit GPA1, XLG2 does not possess a motif or domain for plasma membrane targeting (Adjobo-Hermans *et al.*, 2006; Urano *et al.*, 2013). It probably relies on interaction with other proteins, such as the G β γ -dimer, for plasma membrane tethering. The amount of interaction partners in XLG2 overexpressing lines might not be sufficient to sequester all XLG2 molecules to the plasma membrane. Unbound XLG2 proteins are then localized to the nucleus. In the opposite case, overexpression of G β γ -dimers in *Nicotiana benthamiana* sequestered XLG3 to the plasma membrane, which can be normally found in nuclei and the plasma membrane (Chakravorty *et al.*, 2015).

In *agb1* mutant plants, XLG2 was localized to the cell periphery and the nucleus even in unchallenged plants (Figure 40). Nuclear localization of XLG2 might be caused by a lack of interaction partners at the plasma membrane. However, the question remains how XLG2 is tethered to the membrane in *agb1* mutants. XLG2 was shown to interact with AGB1, but interaction with AGG1 and AGG2 remains controversial (Chakravorty *et al.*, 2015; Maruta *et*

et al., 2015; Zhu *et al.*, 2009). XLG2 might indeed be capable to directly interact with G γ -subunits or other proteins involved in G-protein signaling like AtRGS1. However, it is not known whether XLG2 is constitutively GTP bound like the canonical α -subunit GPA1 (Johnston *et al.*, 2007). It might therefore rely on activation by a yet unidentified GPCR which might be, at least partially, responsible for plasma membrane localization of XLG2.

To confirm plasma membrane localization of XLG2, microsomal fractions of untreated *Venus-XLG2* expressing lines in the Col-0, *agb1-2*, Col-3 *gl1* and *cerk1-4* background were prepared (Figure 41). Immunoblot analysis using a CERK1 antibody confirmed integrity of the prepared fractions, as full length CERK1 was only detectable in total and microsomal fractions, while the CERK1 ectodomain was present in total and soluble fractions. Anti-GFP immunoblot revealed the presence of Venus-XLG2 in total and soluble fractions, but not in microsomal fractions for all genotypes. This was surprising, as plasma membrane localization of XLG2 could be confirmed by heterologous expression in *Nicotiana benthamiana* (Figure 31) and was reported in previous studies (Maruta *et al.*, 2015). However, as XLG2 is no integral transmembrane protein and probably only localized to the plasma membrane via protein-protein interaction, microsomal fractionation might be too harsh to retain XLG2 in microsomal fractions. Microsomal fractionation involves ultracentrifugation steps that might cause dissociation of XLG2 from its interaction partner. This is probably the reason, why Venus-XLG2 can only be found in total and soluble, but not in microsomal fractions.

Co-localization studies using Venus-XLG2 and plasma membrane, cytosolic and nuclear marker, respectively, in *Nicotiana benthamiana* were performed in this study. In contrast to XLG2 localization in *Arabidopsis*, XLG2 localization studies in *N. benthamiana* confirmed previous studies (Figure 30, Figure 31, Figure 32) (Chakravorty *et al.*, 2015; Maruta *et al.*, 2015). However, under the already mentioned circumstances that XLG2 does not have any motif or domain for plasma membrane localization, it has to interact with other proteins like G $\beta\gamma$ dimers. Components from *Arabidopsis thaliana* which are responsible for XLG2 membrane tethering are absent from *N. benthamiana* indicating that XLG2 interacts with *N. benthamiana* proteins for membrane localization. However, *Agrobacterium* infiltration into leaves of *N. benthamiana* might, comparable to H₂O, chitin or flg22 infiltration in *Arabidopsis*, induce defense responses. Induction of defense responses does then, similar to *Arabidopsis*, lead to translocation of XLG2 to the nucleus.

4.2.3 XLG2 localization in *Bgh*-infected *cerk1-4* plants does not differ from wild type plants

The mechanism how XLG2 is involved in execution of cell death in *cerk1-4* plants upon *Bgh* infection is unknown. In wild type plants, cell death upon *Bgh* infection is restricted to single cells, whereas in *cerk1-4*, a deregulated cell death response leads to cell death of surrounding tissue (Petutschnig *et al.*, 2014). It was therefore of great interest to investigate the role of XLG2 in this deregulated cell death response. Two days after inoculation, Venus-XLG2 was localized to the nucleus in cells which were under fungal attack (Figure 42). Furthermore, cells surrounding those attack sites also accumulated XLG2 in the nucleus. This could be observed for all tested genotypes with no obvious differences. The expected scenario of deregulated cell death in *cerk1-4* included massive nuclear accumulation of XLG2 in attacked cells which then spreads throughout the tissue. However, nuclear XLG2 accumulation in *cerk1-4* was not stronger than in wild type plants. Therefore, the *cerk1-4* phenotype is probably not caused by upregulation and accumulation of XLG2 within the nucleus. Previous studies overexpressing either untagged or tagged XLG2 did not report cell death phenotypes, suggesting that overexpression of XLG2 alone is not sufficient to confer cell death phenotype (Heo *et al.*, 2012; Maruta *et al.*, 2015). As already mentioned, XLG2 was shown to function as an indirect transcriptional regulator (Heo *et al.*, 2012) and might also function as direct transcriptional regulator. In *cerk1-4* plants, *Bgh* attacked cells might translocate XLG2 into the nucleus, where it constitutively activates target genes. Since the *cerk1-4* phenotype is characterized by high levels of SA (Petutschnig *et al.*, 2014), XLG2 might be involved in activation of genes involved in SA synthesis or signaling. This notion is further supported by the fact that upon bacterial infection, induction of the SA-responsive gene PR1 in *xlg2* mutants is significantly reduced (Zhu *et al.*, 2009).

4.2.4 Conclusion

A novel mutant fully suppressing the *cerk1-4* phenotype was identified. The underlying mutation was mapped to the N-terminal part of the extra-large G-protein XLG2 where a glutamic acid was replaced by lysine. This glutamic acid is highly conserved from mosses to flowering plants. The investigation of the subcellular localization of XLG2 was contradictory to previous studies. XLG2 localization in untreated plants could be observed at the cell periphery, while upon stimulus, XLG2 was localized to the nucleus. In knockout plants of the *Arabidopsis* G-protein β -subunit (AGB1), XLG2 was localized to the nucleus already in

unstimulated cells. Further investigation of *Bgh* inoculated plants revealed no difference between *cerk1-4* and wild type plants.

4.2.5 Outlook

The present study identified XLG2 to be a key regulator of cell death downstream of CERK1. A mutation within the N-terminal part of XLG2 could fully suppress the cell death phenotype of *cerk1-4*. In order to get further insights into the mechanism of *cerk1-4* suppression by *nole1-2*, the function of the N-terminal part of XLG2 has to be elucidated. To test if cysteine rich region of XLG2 is able to bind DNA, electrophoretic mobility shift assays (EMSA) could be performed. If no non-specific DNA binding can be observed, XLG2 target genes could be identified by chromatin immunoprecipitation with subsequent sequencing (ChIP-Seq). Mutational analysis of the regularly spaced cysteines would then provide information whether this region is critical for DNA binding. Expression of these mutants in *nole1-1 erk1-4* or *nole1-2 erk1-4* would reveal if XLG2 DNA binding is critical for development of the *cerk1-4* phenotype. The question whether the XLG2 cysteine-rich region forms disulphide bridges and exhibits differences to *xlg2* E293K could be answered with methods to display the redox status of the examined protein (Rudyk & Eaton, 2014). Reduced thiol groups are blocked and remaining oxidized thiol groups are reduced and labeled. Labels of relatively large size induce band shifts in immunoblots and can be used to investigate differences in redox levels. It would further be interesting to know if nuclear localization of XLG2 is a prerequisite for development of the *cerk1-4* phenotype. Therefore, the noncanonical NLS of XLG2 (KKRAKIACAVF) (Chakravorty *et al.*, 2015) could be mutated to exclude nuclear localization. In this context, the addition of a second NLS could shift XLG2 localization completely to the nucleus and might answer the question if localization to both, cytoplasmic and plasma membrane is critical for *cerk1-4* phenotype development. It would be further interesting to perform pathogen assays with *nole1-2* plants, to see if they exhibit enhanced susceptibility to bacterial and necrotrophic fungal pathogens comparable to *xlg2* mutants.

In order to microscopically validate the localization of XLG2 in *Arabidopsis thaliana*, it will be essential to generate transgenic lines co-expressing Venus-XLG2 together with marker constructs for plasma membrane, nuclear and cytosolic localization.

In contrast to microsomal preparation, nuclear fractionation should be suitable to confirm nuclear localization of XLG2. Comparison of infiltrated versus unfiltered tissue could confirm that XLG2 nuclear localization is stimulus dependent.

The expression of Venus-XLG2 in single Gy-subunit mutants and in G $\beta\gamma$ higher order

mutants could reveal which G-protein components are involved in XLG2 localization.

To correlate XLG2 localization with cellular SA levels in treated and untreated cells, transgenic Venus-XLG2 lines should be crossed with SA reporter lines of the Colorful system developed in our laboratory (Hassan Ghareeb, unpublished). They consist of a fluorescence protein which is expressed under control of hormone responsive promoters. These are combined with a plasma membrane marker and a normalizer and allow quantification of hormonal levels.

Taken together, the mechanism of cell death execution mediated by XLG2 is unknown. The *nole1-1 cerk1-4* and *nole1-2 cerk1-4* mutants offer the unique possibility, to decipher the functions of XLG2 on a molecular level and will provide further insights into XLG2 mediated cell death execution.

5. References

- Adam Z. (2013) Emerging roles for diverse intramembrane proteases in plant biology. *Biochimica et biophysica acta*, **1828**, 2933–2936.
- Adjobo-Hermans M.J.W., Goedhart J., Gadella T.W.J. (2006) Plant G protein heterotrimers require dual lipidation motifs of Galpha and Ggamma and do not dissociate upon activation. *Journal of cell science*, **119**, 5087–5097.
- Antolín-Llovera M., Ried M.K., Binder A., Parniske M. (2012) Receptor kinase signaling pathways in plant-microbe interactions. *Annual review of phytopathology*, **50**, 451–473.
- Antolín-Llovera M., Ried M.K., Parniske M. (2014) Cleavage of the SYMBIOSIS RECEPTOR-LIKE KINASE ectodomain promotes complex formation with Nod factor receptor 5. *Current biology CB*, **24**, 422–427.
- Ao Y., Li Z., Feng D., Xiong F., Liu J., Li J.-F., Wang M., Wang J., Liu B., Wang H.-B. (2014) OsCERK1 and OsRLCK176 play important roles in peptidoglycan and chitin signaling in rice innate immunity. *The Plant journal for cell and molecular biology*, **80**, 1072–1084.
- Arribas J., Borroto A. (2002) Protein Ectodomain Shedding. *Chem. Rev.*, **102**, 4627–4638.
- Aster J.C., Pear W.S., Blacklow S.C. (2008) Notch signaling in leukemia. *Annual review of pathology*, **3**, 587–613.
- Axtell M.J., Staskawicz B.J. (2003) Initiation of RPS2-Specified Disease Resistance in Arabidopsis Is Coupled to the AvrRpt2-Directed Elimination of RIN4. *Cell*, **112**, 369–377.
- Baran P., Nitz R., Grötzinger J., Scheller J., Garbers C. (2013) Minimal interleukin 6 (IL-6) receptor stalk composition for IL-6 receptor shedding and IL-6 classic signaling. *The Journal of biological chemistry*, **288**, 14756–14768.
- Bayer E.M., Bottrill A.R., Walshaw J., Vigouroux M., Naldrett M.J., Thomas C.L., Maule A.J. (2006) Arabidopsis cell wall proteome defined using multidimensional protein identification technology. *Proteomics*, **6**, 301–311.
- Birnboim H.C., Doly J. (1979) A rapid alkaline extraction procedure for screening recombinant plasmid DNA. *Nucleic acids research*, **7**, 1513–1523.
- Blobel C.P. (2005) ADAMs: key components in EGFR signalling and development. *Nature reviews. Molecular cell biology*, **6**, 32–43.
- Boller T., Felix G. (2009) A renaissance of elicitors: perception of microbe-associated molecular patterns and danger signals by pattern-recognition receptors. *Annual review of plant biology*, **60**, 379–406.
- Bozkulak E.C., Weinmaster G. (2009) Selective use of ADAM10 and ADAM17 in activation of Notch1 signaling. *Molecular and cellular biology*, **29**, 5679–5695.

- Brachmann C.B., Davies A., Cost G.J., Caputo E., Li J., Hieter P., Boeke J.D. (1998) Designer deletion strains derived from *Saccharomyces cerevisiae* S288C: a useful set of strains and plasmids for PCR-mediated gene disruption and other applications. *Yeast (Chichester, England)*, **14**, 115–132.
- Bradford M.M. (1976) A rapid and sensitive method for the quantitation of microgram quantities of protein utilizing the principle of protein-dye binding. *Analytical Biochemistry*, **72**, 248–254.
- Buist I., Bredeweg S.W., van Mechelen W., Lemmink, Koen A P M, Pepping G.-J., Diercks R.L. (2008) No effect of a graded training program on the number of running-related injuries in novice runners: a randomized controlled trial. *The American journal of sports medicine*, **36**, 33–39.
- Cacas J.-L., Furt F., Le Guédard M., Schmitter J.-M., Buré C., Gerbeau-Pissot P., Moreau P., Bessoule J.-J., Simon-Plas F., Mongrand S. (2012) Lipids of plant membrane rafts. *Progress in lipid research*, **51**, 272–299.
- Caescu C.I., Jeschke G.R., Turk B.E. (2009) Active-site determinants of substrate recognition by the metalloproteinases TACE and ADAM10. *The Biochemical journal*, **424**, 79–88.
- Cao Y., Liang Y., Tanaka K., Nguyen C.T., Jedrzejczak R.P., Joachimiak A., Stacey G. (2014) The kinase LYK5 is a major chitin receptor in *Arabidopsis* and forms a chitin-induced complex with related kinase CERK1. *eLife*, **3**.
- Carey K.D., Dugger D.L., Schwall R.H., Sliwkowski M.X. (2005) ErbB2/Her2 ectodomain shedding is regulated by a membrane-associated metalloprotease. *Cancer Res*, **65**, 871.
- Carpenter G., Liao H.-J. (2009) Trafficking of receptor tyrosine kinases to the nucleus. *Experimental cell research*, **315**, 1556–1566.
- Chakravorty D., Gookin T.E., Milner M., Yu Y., Assmann S.M. (2015) Extra-Large G proteins (XLGs) expand the repertoire of subunits in *Arabidopsis* heterotrimeric G protein signaling. *Plant Physiol.*, pp.00251.2015.
- Chakravorty D., Trusov Y., Zhang W., Acharya B.R., Sheahan M.B., McCurdy D.W., Assmann S.M., Botella J.R. (2011) An atypical heterotrimeric G-protein γ -subunit is involved in guard cell K^+ -channel regulation and morphological development in *Arabidopsis thaliana*. *The Plant journal for cell and molecular biology*, **67**, 840–851.
- Chen J.-G., Gao Y., Jones A.M. (2006) Differential Roles of *Arabidopsis* Heterotrimeric G-Protein Subunits in Modulating Cell Division in Roots. *Plant Physiol.*, **141**, 887–897.
- Chen J.-G., Willard F.S., Huang J., Liang J., Chasse S.A., Jones A.M., Siderovski D.P. (2003) A seven-transmembrane RGS protein that modulates plant cell proliferation. *Science (New York, N.Y.)*, **301**, 1728–1731.

- Chen M.-K., Hung M.-C. (2015) Proteolytic cleavage, trafficking, and functions of nuclear receptor tyrosine kinases. *The FEBS journal*, **282**, 3693–3721.
- Cheng Q.-C., Tikhomirov O., Zhou W., Carpenter G. (2003) Ectodomain cleavage of ErbB-4: characterization of the cleavage site and m80 fragment. *The Journal of biological chemistry*, **278**, 38421–38427.
- Cheng Y.T., Germain H., Wiermer M., Bi D., Xu F., Garcia A.V., Wirthmueller L., Despres C., Parker J.E., Zhang Y., Li X. (2009) Nuclear Pore Complex Component MOS7/Nup88 Is Required for Innate Immunity and Nuclear Accumulation of Defense Regulators in Arabidopsis. *THE PLANT CELL ONLINE*, **21**, 2503–2516.
- Chillakuri C.R., Sheppard D., Lea S.M., Handford P.A. (2012) Notch receptor-ligand binding and activation: insights from molecular studies. *Seminars in cell & developmental biology*, **23**, 421–428.
- Chinchilla D., Bauer Z., Regenass M., Boller T., Felix G. (2006) The Arabidopsis receptor kinase FLS2 binds flg22 and determines the specificity of flagellin perception. *The Plant cell*, **18**, 465–476.
- Chinchilla D., Zipfel C., Robatzek S., Kemmerling B., Nürnberger T., Jones J.D.G., Felix G., Boller T. (2007) A flagellin-induced complex of the receptor FLS2 and BAK1 initiates plant defence. *Nature*, **448**, 497–500.
- Chow F.L., Fernandez-Patron C. (2007) Many membrane proteins undergo ectodomain shedding by proteolytic cleavage. Does one sheddase do the job on all of these proteins? *IUBMB life*, **59**, 44–47.
- Christianson T.W., Sikorski R.S., Dante M., Shero J.H., Hieter P. (1992) Multifunctional yeast high-copy-number shuttle vectors. *Gene*, **110**, 119–122.
- Clough S.J., Bent A.F. (1998) Floral dip: a simplified method for Agrobacterium-mediated transformation of Arabidopsis thaliana. *The Plant journal for cell and molecular biology*, **16**, 735–743.
- Colot H.V., Park G., Turner G.E., Ringelberg C., Crew C.M., Litvinkova L., Weiss R.L., Borkovich K.A., Dunlap J.C. (2006) A high-throughput gene knockout procedure for Neurospora reveals functions for multiple transcription factors. *Proceedings of the National Academy of Sciences of the United States of America*, **103**, 10352–10357.
- Dai N., Wang W., Patterson S.E., Bleecker A.B. (2013) The TMK subfamily of receptor-like kinases in Arabidopsis display an essential role in growth and a reduced sensitivity to auxin. *PLoS one*, **8**, e60990.
- Dangl J.L., Horvath D.M., Staskawicz B.J. (2013) Pivoting the plant immune system from dissection to deployment. *Science (New York, N.Y.)*, **341**, 746–751.

- David J.M., Rajasekaran A.K. (2012) Dishonorable discharge: the oncogenic roles of cleaved E-cadherin fragments. *Cancer research*, **72**, 2917–2923.
- Dawkins E., Small D.H. (2014) Insights into the physiological function of the β -amyloid precursor protein: beyond Alzheimer's disease. *Journal of neurochemistry*, **129**, 756–769.
- Dewdney J., Reuber T.L., Wildermuth M.C., Devoto A., Cui J., Stutius L.M., Drummond E.P., Ausubel F.M. (2000) Three unique mutants of Arabidopsis identify eds loci required for limiting growth of a biotrophic fungal pathogen. *Plant J*, **24**, 205–218.
- Ding L., Pandey S., Assmann S.M. (2008) Arabidopsis extra-large G proteins (XLGs) regulate root morphogenesis. *The Plant journal for cell and molecular biology*, **53**, 248–263.
- Ding X., Richter T., Chen M., Fujii H., Seo Y.S., Xie M., Zheng X., Kanrar S., Stevenson R.A., Dardick C., Li Y., Jiang H., Zhang Y., Yu F., Bartley L.E., Chern M., Bart R., Chen X., Zhu L., Farmerie W.G., Gribskov M., Zhu J.-K., Fromm M.E., Ronald P.C., Song W.-Y. (2009) A Rice Kinase-Protein Interaction Map. *Plant Physiol.*, **149**, 1478–1492.
- Dodds P.N., Rathjen J.P. (2010) Plant immunity: towards an integrated view of plant-pathogen interactions. *Nature reviews. Genetics*, **11**, 539–548.
- Eckardt N.A. (2008) Chitin signaling in plants: insights into the perception of fungal pathogens and rhizobacterial symbionts. *The Plant cell*, **20**, 241–243.
- Elenius K., Corfas G., Paul S., Choi C.J., Rio C., Plowman G.D., Klagsbrun M. (1997) A Novel Juxtamembrane Domain Isoform of HER4/ErbB4: ISOFORM-SPECIFIC TISSUE DISTRIBUTION AND DIFFERENTIAL PROCESSING IN RESPONSE TO PHORBOL ESTER. *Journal of Biological Chemistry*, **272**, 26761–26768.
- Erwig J., Ghareeb H., Kopischke M., Hacke R., Matei A., Petutschnig E.-K., Lipka V. (unpublished) Chitin-induced and CERK1 phosphorylation-dependent endocytosis of Arabidopsis LYK5.
- Falk A., Feys B.J., Frost L.N., Jones J.D.G., Daniels M.J., Parker J.E. (1999) EDS1, an essential component of R gene-mediated disease resistance in Arabidopsis has homology to eukaryotic lipases. *Proceedings of the National Academy of Sciences of the United States of America*, **96**, 3292–3297.
- Faulkner C., Petutschnig E., Benitez-Alfonso Y., Beck M., Robatzek S., Lipka V., Maule A.J. (2013) LYM2-dependent chitin perception limits molecular flux via plasmodesmata. *Proceedings of the National Academy of Sciences of the United States of America*, **110**, 9166–9170.
- Faull R.J., Stanley J.M., Fraser S., Power D.A., Leavesley D.I. (2001) HB-EGF is produced in the peritoneal cavity and enhances mesothelial cell adhesion and migration. *Kidney international*, **59**, 614–624.

- Feiz L., Irshad M., Pont-Lezica R.F., Canut H., Jamet E. (2006) Evaluation of cell wall preparations for proteomics: a new procedure for purifying cell walls from Arabidopsis hypocotyls. *Plant methods*, **2**, 10.
- Feng X.-H., Derynck R. (2005) Specificity and versatility in tgf-beta signaling through Smads. *Annual review of cell and developmental biology*, **21**, 659–693.
- Freeman M. (2009) Rhomboids: 7 years of a new protease family. *Seminars in cell & developmental biology*, **20**, 231–239.
- Gajria D., Chandarlapaty S. (2011) HER2-amplified breast cancer: mechanisms of trastuzumab resistance and novel targeted therapies. *Expert review of anticancer therapy*, **11**, 263–275.
- Ganten D., Birchmeier W., Epplen J.T., Genser K., Gossen M., Kersten B., Lehrach H., Nolte C., Oschkinat H., Ruckpaul K., Ruiz P. (Eds) (2006) *Encyclopedic Reference of Genomics and Proteomics in Molecular Medicine*. Springer-Verlag, Berlin, Heidelberg.
- Gao M., Wang X., Wang D., Xu F., Ding X., Zhang Z., Bi D., Cheng Y.T., Chen S., Li X., Zhang Y. (2009) Regulation of cell death and innate immunity by two receptor-like kinases in Arabidopsis. *Cell host & microbe*, **6**, 34–44.
- Garvey K.J., Saedi M.S., Ito J. (1986) Nucleotide sequence of Bacillus phage phi 29 genes 14 and 15: homology of gene 15 with other phage lysozymes. *Nucleic acids research*, **14**, 10001–10008.
- Gimenez-Ibanez S., Ntoukakis V., Rathjen J.P. (2009) The LysM receptor kinase CERK1 mediates bacterial perception in Arabidopsis. *Plant signaling & behavior*, **4**, 539–541.
- Glazebrook J., Rogers E.E., Ausubel F.M. (1996) Isolation of Arabidopsis Mutants With Enhanced Disease Susceptibility by Direct Screening. *Genetics*, **143**, 973–982.
- Golldack D., Popova O.V., Dietz K.-J. (2002) Mutation of the matrix metalloproteinase At2-MMP inhibits growth and causes late flowering and early senescence in Arabidopsis. *The Journal of biological chemistry*, **277**, 5541–5547.
- Gomez-Gomez L., Felix G., Boller T. (1999) A single locus determines sensitivity to bacterial flagellin in Arabidopsis thaliana. *The Plant journal for cell and molecular biology*, **18**, 277–284.
- Gómez-Gómez L., Boller T. (2000) FLS2. *Molecular Cell*, **5**, 1003–1011.
- Guruharsha K.G., Kankel M.W., Artavanis-Tsakonas S. (2012) The Notch signalling system: recent insights into the complexity of a conserved pathway. *Nature reviews. Genetics*, **13**, 654–666.
- Gust A.A. (2015) Peptidoglycan Perception in Plants. *PLoS pathogens*, **11**, e1005275.

- Gust A.A., Willmann R., Desaki Y., Grabherr H.M., Nürnberger T. (2012) Plant LysM proteins: modules mediating symbiosis and immunity. *Trends in plant science*, **17**, 495–502.
- Haass C., Hung A.Y., Schlossmacher M.G., Teplow D.B., Selkoe D.J. (1993) beta-Amyloid peptide and a 3-kDa fragment are derived by distinct cellular mechanisms. *The Journal of biological chemistry*, **268**, 3021–3024.
- Haass C., Kaether C., Thinakaran G., Sisodia S. (2012) Trafficking and proteolytic processing of APP. *Cold Spring Harbor perspectives in medicine*, **2**, a006270.
- Hann D.R., Rathjen J.P. (2007) Early events in the pathogenicity of *Pseudomonas syringae* on *Nicotiana benthamiana*. *The Plant journal for cell and molecular biology*, **49**, 607–618.
- Hartwig B., James G.V., Konrad K., Schneeberger K., Turck F. (2012) Fast isogenic mapping-by-sequencing of ethyl methanesulfonate-induced mutant bulks. *Plant physiology*, **160**, 591–600.
- Hayafune M., Berisio R., Marchetti R., Silipo A., Kayama M., Desaki Y., Arima S., Squeglia F., Ruggiero A., Tokuyasu K., Molinaro A., Kaku H., Shibuya N. (2014) Chitin-induced activation of immune signaling by the rice receptor CEBiP relies on a unique sandwich-type dimerization. *Proceedings of the National Academy of Sciences of the United States of America*, **111**, E404-13.
- Hayashida K., Bartlett A.H., Chen Y., Park P.W. (2010) Molecular and cellular mechanisms of ectodomain shedding. *Anatomical record (Hoboken, N.J. 2007)*, **293**, 925–937.
- He K., Gou X., Yuan T., Lin H., Asami T., Yoshida S., Russell S.D., Li J. (2007) BAK1 and BKK1 regulate brassinosteroid-dependent growth and brassinosteroid-independent cell-death pathways. *Current biology CB*, **17**, 1109–1115.
- Heese A., Hann D.R., Gimenez-Ibanez S., Jones A.M.E., He K., Li J., Schroeder J.I., Peck S.C., Rathjen J.P. (2007) The receptor-like kinase SERK3/BAK1 is a central regulator of innate immunity in plants. *Proceedings of the National Academy of Sciences of the United States of America*, **104**, 12217–12222.
- Hellens R.P., Edwards E.A., Leyland N.R., Bean S., Mullineaux P.M. (2000) pGreen: a versatile and flexible binary Ti vector for *Agrobacterium*-mediated plant transformation. *Plant Mol Biol*, **42**, 819–832.
- Heo J.B., Sung S., Assmann S.M. (2012) Ca²⁺-dependent GTPase, extra-large G protein 2 (XLG2), promotes activation of DNA-binding protein related to vernalization 1 (RTV1), leading to activation of floral integrator genes and early flowering in *Arabidopsis*. *The Journal of biological chemistry*, **287**, 8242–8253.
- Herman C., Chernajovsky Y. (1998) Mutation of Proline 211 Reduces Shedding of the Human p75 TNF Receptor. *J Immunol*, **160**, 2478–2487.

- Higashiyama S., Nanba D., Nakayama H., Inoue H., Fukuda S. (2011) Ectodomain shedding and remnant peptide signalling of EGFRs and their ligands. *Journal of biochemistry*, **150**, 15–22.
- Hok S., Danchin E.G.J., Allasia V., Panabières F., Attard A., Keller H. (2011) An Arabidopsis (malectin-like) leucine-rich repeat receptor-like kinase contributes to downy mildew disease. *Plant, cell & environment*, **34**, 1944–1957.
- Hollmén M., Liu P., Kurppa K., Wildiers H., Reinvall I., Vandorpe T., Smeets A., Deraedt K., Vahlberg T., Joensuu H., Leahy D.J., Schöffski P., Elenius K. (2012) Proteolytic Processing of ErbB4 in Breast Cancer. *PloS one*, **7**.
- Hollmén M., Määttä J.A., Bald L., Sliwkowski M.X., Elenius K. (2009) Suppression of breast cancer cell growth by a monoclonal antibody targeting cleavable ErbB4 isoforms. *Oncogene*, **28**, 1309–1319.
- Hubbard S.R., Miller W.T. (2007) Receptor tyrosine kinases: mechanisms of activation and signaling. *Current opinion in cell biology*, **19**, 117–123.
- Hueck C.J. (1998) Type III protein secretion systems in bacterial pathogens of animals and plants. *Microbiology and molecular biology reviews MMBR*, **62**, 379–433.
- Humphry M., Bednarek P., Kemmerling B., Koh S., Stein M., Göbel U., Stüber K., Pislewska-Bednarek M., Loraine A., Schulze-Lefert P., Somerville S., Panstruga R. (2010) A regulon conserved in monocot and dicot plants defines a functional module in antifungal plant immunity. *Proceedings of the National Academy of Sciences of the United States of America*, **107**, 21896–21901.
- Iizasa E., Mitsutomi M., Nagano Y. (2010) Direct binding of a plant LysM receptor-like kinase, LysM RLK1/CERK1, to chitin in vitro. *The Journal of biological chemistry*, **285**, 2996–3004.
- Jashni M.K., Mehrabi R., Collemare J., Mesarich C.H., de Wit, Pierre J G M (2015) The battle in the apoplast: further insights into the roles of proteases and their inhibitors in plant-pathogen interactions. *Frontiers in plant science*, **6**, 584.
- Jirage D., Tootle T.L., Reuber T.L., Frost L.N., Feys B.J., Parker J.E., Ausubel F.M., Glazebrook J. (1999) Arabidopsis thaliana PAD4 encodes a lipase-like gene that is important for salicylic acid signaling. *Proceedings of the National Academy of Sciences*, **96**, 13583–13588.
- Johnston C.A., Taylor J.P., Gao Y., Kimple A.J., Grigston J.C., Chen J.-G., Siderovski D.P., Jones A.M., Willard F.S. (2007) GTPase acceleration as the rate-limiting step in Arabidopsis G protein-coupled sugar signaling. *Proceedings of the National Academy of Sciences of the United States of America*, **104**, 17317–17322.

- Jones A.M., Assmann S.M. (2004) Plants: the latest model system for G-protein research. *EMBO reports*, **5**, 572–578.
- Jones F.E. (2008) HER4 Intracellular Domain (4ICD) Activity in the Developing Mammary Gland and Breast Cancer. *Journal of mammary gland biology and neoplasia*, **13**, 247–258.
- Jones J.D.G., Dangl J.L. (2006) The plant immune system. *Nature*, **444**, 323–329.
- Joo J.H., Wang S., Chen J.G., Jones A.M., Fedoroff N.V. (2005) Different Signaling and Cell Death Roles of Heterotrimeric G Protein α and β Subunits in the Arabidopsis Oxidative Stress Response to Ozone. *Plant Cell*, **17**, 957–970.
- Josso N., Di Clemente N. (1997) Serine/threonine kinase receptors and ligands. *Current Opinion in Genetics & Development*, **7**, 371–377.
- Kadota Y., Sklenar J., Derbyshire P., Stransfeld L., Asai S., Ntoukakis V., Jones J.D., Shirasu K., Menke F., Jones A., Zipfel C. (2014) Direct regulation of the NADPH oxidase RBOHD by the PRR-associated kinase BIK1 during plant immunity. *Molecular Cell*, **54**, 43–55.
- Kaku H., Nishizawa Y., Ishii-Minami N., Akimoto-Tomiyama C., Dohmae N., Takio K., Minami E., Shibuya N. (2006) Plant cells recognize chitin fragments for defense signaling through a plasma membrane receptor. *Proceedings of the National Academy of Sciences of the United States of America*, **103**, 11086–11091.
- Kaku H., Shibuya N. (2011) [Chitin receptor for plant innate immunity]. *Seikagaku. The Journal of Japanese Biochemical Society*, **83**, 31–36.
- Kanaoka M.M., Urban S., Freeman M., Okada K. (2005) An Arabidopsis Rhomboid homolog is an intramembrane protease in plants. *FEBS Letters*, **579**, 5723–5728.
- Kearse M., Moir R., Wilson A., Stones-Havas S., Cheung M., Sturrock S., Buxton S., Cooper A., Markowitz S., Duran C., Thierer T., Ashton B., Meintjes P., Drummond A. (2012) Geneious Basic: an integrated and extendable desktop software platform for the organization and analysis of sequence data. *Bioinformatics (Oxford, England)*, **28**, 1647–1649.
- Kemmerling B., Schwedt A., Rodriguez P., Mazzotta S., Frank M., Qamar S.A., Mengiste T., Betsuyaku S., Parker J.E., Müssig C., Thomma, Bart P H J, Albrecht C., Vries S.C. de, Hirt H., Nürnberger T. (2007) The BRI1-associated kinase 1, BAK1, has a brassinolide-independent role in plant cell-death control. *Current biology CB*, **17**, 1116–1122.
- Khokha R., Murthy A., Weiss A. (2013) Metalloproteinases and their natural inhibitors in inflammation and immunity. *Nature reviews. Immunology*, **13**, 649–665.
- Kloppfleisch K., Phan N., Augustin K., Bayne R.S., Booker K.S., Botella J.R., Carpita N.C., Carr T., Chen J.-G., Cooke T.R., Frick-Cheng A., Friedman E.J., Fulk B., Hahn M.G.,

- Jiang K., Jorda L., Kruppe L., Liu C., Lorek J., McCann M.C., Molina A., Moriyama E.N., Mukhtar M.S., Mudgil Y., Pattathil S., Schwarz J., Seta S., Tan M., Temp U., Trusov Y., Urano D., Welter B., Yang J., Panstruga R., Uhrig J.F., Jones A.M. (2011) Arabidopsis G-protein interactome reveals connections to cell wall carbohydrates and morphogenesis. *Molecular systems biology*, **7**, 532.
- Kmiec-Wisniewska B., Krumpke K., Urantowka A., Sakamoto W., Pratje E., Janska H. (2008) Plant mitochondrial rhomboid, AtRBL12, has different substrate specificity from its yeast counterpart. *Plant molecular biology*, **68**, 159–171.
- Koncz C., Schell J. (1986) The promoter of TL-DNA gene 5 controls the tissue-specific expression of chimaeric genes carried by a novel type of Agrobacterium binary vector. *Molec Gen Genet*, **204**, 383–396.
- König S., Feussner K., Schwarz M., Kaefer A., Iven T., Landesfeind M., Ternes P., Karlovsky P., Lipka V., Feussner I. (2012) Arabidopsis mutants of sphingolipid fatty acid α -hydroxylases accumulate ceramides and salicylates. *The New phytologist*, **196**, 1086–1097.
- Koonin E.V., Makarova K.S., Rogozin I.B., Davidovic L., Letellier M.-C., Pellegrini L. (2003) Koonin et al 2003. *Genome Biol*, **4**, R19.
- Kopan R., Ilagan M.X.G. (2004) Gamma-secretase: proteasome of the membrane? *Nature reviews. Molecular cell biology*, **5**, 499–504.
- Kopan R., Ilagan M.X.G. (2009) The canonical Notch signaling pathway: unfolding the activation mechanism. *Cell*, **137**, 216–233.
- Kouzai Y., Mochizuki S., Nakajima K., Desaki Y., Hayafune M., Miyazaki H., Yokotani N., Ozawa K., Minami E., Kaku H., Shibuya N., Nishizawa Y. (2014a) Targeted gene disruption of OsCERK1 reveals its indispensable role in chitin perception and involvement in the peptidoglycan response and immunity in rice. *Molecular plant-microbe interactions MPMI*, **27**, 975–982.
- Kouzai Y., Nakajima K., Hayafune M., Ozawa K., Kaku H., Shibuya N., Minami E., Nishizawa Y. (2014b) CEBiP is the major chitin oligomer-binding protein in rice and plays a main role in the perception of chitin oligomers: Plant Molecular Biology. *Plant Mol Biol*, **84**, 519–528.
- Kullander K., Klein R. (2002) Mechanisms and functions of Eph and ephrin signalling. *Nature reviews. Molecular cell biology*, **3**, 475–486.
- Kunze G., Zipfel C., Robatzek S., Niehaus K., Boller T., Felix G. (2004) The N terminus of bacterial elongation factor Tu elicits innate immunity in Arabidopsis plants. *The Plant cell*, **16**, 3496–3507.

- Lal M., Caplan M. (2011) Regulated intramembrane proteolysis: signaling pathways and biological functions. *Physiology (Bethesda, Md.)*, **26**, 34–44.
- Lee S., Rojas C.M., Ishiga Y., Pandey S., Mysore K.S. (2013a) Arabidopsis heterotrimeric G-proteins play a critical role in host and nonhost resistance against *Pseudomonas syringae* pathogens. *PloS one*, **8**, e82445.
- Lee S.-W., Han S.-W., Sririyanum M., Park C.-J., Seo Y.-S., Ronald P.C. (2009) A type I-secreted, sulfated peptide triggers XA21-mediated innate immunity. *Science (New York, N.Y.)*, **326**, 850–853.
- Lee S.-W., Han S.-W., Sririyanum M., Park C.-J., Seo Y.-S., Ronald P.C. (2013b) Retraction. A type I-secreted, sulfated peptide triggers XA21-mediated innate immunity. *Science (New York, N.Y.)*, **342**, 191.
- Lee Y.-R., Assmann S. (1999) Arabidopsis thaliana 'extra-large GTP-binding protein' (AtXLG1): a new class of G-protein: Plant Molecular Biology. *Plant Mol Biol*, **40**, 55–64.
- Lefebvre B., Furt F., Hartmann M.-A., Michaelson L.V., Carde J.-P., Sargueil-Boiron F., Rossignol M., Napier J.A., Cullimore J., Bessoule J.-J., Mongrand S. (2007) Characterization of lipid rafts from *Medicago truncatula* root plasma membranes: a proteomic study reveals the presence of a raft-associated redox system. *Plant physiology*, **144**, 402–418.
- Leon O., Roth M. (2000) Zinc fingers: DNA binding and protein-protein interactions. *Biol. Res.*, **33**.
- Li D., Zhang H., Song Q., Wang L., Liu S., Hong Y., Huang L., Song F. (2015) Tomato SI3-MMP, a member of the Matrix metalloproteinase family, is required for disease resistance against *Botrytis cinerea* and *Pseudomonas syringae* pv. tomato DC3000. *BMC plant biology*, **15**, 143.
- Li J., Wen J., Lease K.A., Doke J.T., Tax F.E., Walker J.C. (2002) BAK1, an Arabidopsis LRR Receptor-like Protein Kinase, Interacts with BRI1 and Modulates Brassinosteroid Signaling. *Cell*, **110**, 213–222.
- Lichtenthaler S.F., Haass C., Steiner H. (2011) Regulated intramembrane proteolysis-- lessons from amyloid precursor protein processing. *Journal of neurochemistry*, **117**, 779–796.
- Liebrand T.W.H., van den Burg, Harrold A, Joosten, Matthieu H A J (2014) Two for all: receptor-associated kinases SOBIR1 and BAK1. *Trends in plant science*, **19**, 123–132.
- Lin K.-T., Sloniowski S., Ethell D.W., Ethell I.M. (2008) Ephrin-B2-induced cleavage of EphB2 receptor is mediated by matrix metalloproteinases to trigger cell repulsion. *The Journal of biological chemistry*, **283**, 28969–28979.

- Lipka V., Dittgen J., Bednarek P., Bhat R., Wiermer M., Stein M., Landtag J., Brandt W., Rosahl S., Scheel D., Llorente F., Molina A., Parker J., Somerville S., Schulze-Lefert P. (2005) Pre- and postinvasion defenses both contribute to nonhost resistance in *Arabidopsis*. *Science (New York, N. Y.)*, **310**, 1180–1183.
- Litterst C., Georgakopoulos A., Shioi J., Ghersi E., Wisniewski T., Wang R., Ludwig A., Robakis N.K. (2007) Ligand binding and calcium influx induce distinct ectodomain/gamma-secretase-processing pathways of EphB2 receptor. *The Journal of biological chemistry*, **282**, 16155–16163.
- Liu B., Li J.-F., Ao Y., Qu J., Li Z., Su J., Zhang Y., Liu J., Feng D., Qi K., He Y., Wang J., Wang H.-B. (2012a) Lysin motif-containing proteins LYP4 and LYP6 play dual roles in peptidoglycan and chitin perception in rice innate immunity. *The Plant cell*, **24**, 3406–3419.
- Liu C., Xu P., Lamouille S., Xu J., Derynck R. (2009) TACE-mediated ectodomain shedding of the type I TGF- β receptor downregulates TGF- β signaling. *Molecular Cell*, **35**, 26–36.
- Liu J., Ding P., Sun T., Nitta Y., Dong O., Huang X., Yang W., Li X., Botella J.R., Zhang Y. (2013a) Heterotrimeric G proteins serve as a converging point in plant defense signaling activated by multiple receptor-like kinases. *Plant physiology*, **161**, 2146–2158.
- Liu J., Elmore J.M., Lin Z.-J.D., Coaker G. (2011) A receptor-like cytoplasmic kinase phosphorylates the host target RIN4, leading to the activation of a plant innate immune receptor. *Cell host & microbe*, **9**, 137–146.
- Liu P., Hu Z., Zhou B., Liu S., Chai J. (2013b) Crystal structure of an LRR protein with two solenoids. *Cell research*, **23**, 303–305.
- Liu P.C., Liu X., Li Y., Covington M., Wynn R., Huber R., Hillman M., Yang G., Ellis D., Marando C., Katiyar K., Bradley J., Abremski K., Stow M., Rupa M., Zhuo J., Li Y.-L., Lin Q., Burns D., Xu M., Zhang C., Qian D.-Q., He C., Sharief V., Weng L., Agrios C., Shi E., Metcalf B., Newton R., Friedman S., Yao W., Scherle P.A., Hollis G., Burn T.C. (2006) Identification of ADAM10 as a major source of HER2 ectodomain sheddase activity in HER2 overexpressing breast cancer cells. *Cancer Biology & Therapy*, **5**, 657–664.
- Liu T., Liu Z., Song C., Hu Y., Han Z., She J., Fan F., Wang J., Jin C., Chang J., Zhou J.-M., Chai J. (2012b) Chitin-induced dimerization activates a plant immune receptor. *Science (New York, N. Y.)*, **336**, 1160–1164.
- Llorente F., Alonso-Blanco C., Sanchez-Rodriguez C., Jorda L., Molina A. (2005) ERECTA receptor-like kinase and heterotrimeric G protein from *Arabidopsis* are required for resistance to the necrotrophic fungus *Plectosphaerella cucumerina*. *The Plant journal for cell and molecular biology*, **43**, 165–180.

- Lo Presti L., Lanver D., Schweizer G., Tanaka S., Liang L., Tollot M., Zuccaro A., Reissmann S., Kahmann R. (2015) Fungal effectors and plant susceptibility. *Annual review of plant biology*, **66**, 513–545.
- Lovering A.L., Safadi S.S., Strynadka N.C.J. (2012) Structural perspective of peptidoglycan biosynthesis and assembly. *Annual review of biochemistry*, **81**, 451–478.
- Lu D., Wu S., Gao X., Zhang Y., Shan L., He P. (2010) A receptor-like cytoplasmic kinase, BIK1, associates with a flagellin receptor complex to initiate plant innate immunity. *Proceedings of the National Academy of Sciences of the United States of America*, **107**, 496–501.
- Macho A.P., Zipfel C. (2014) Plant PRRs and the activation of innate immune signaling. *Molecular Cell*, **54**, 263–272.
- Maidment J.M., Moore D., Murphy G.P., Murphy G., Clark I.M. (1999) Matrix Metalloproteinase Homologues from *Arabidopsis thaliana*: EXPRESSION AND ACTIVITY. *Journal of Biological Chemistry*, **274**, 34706–34710.
- Manners J.M., Penninckx I.A., Vermaere K., Kazan K., Brown R.L., Morgan A., Maclean D.J., Curtis M.D., Cammue B.P., Broekaert W.F. (1998) The promoter of the plant defensin gene PDF1.2 from *Arabidopsis* is systemically activated by fungal pathogens and responds to methyl jasmonate but not to salicylic acid. *Plant molecular biology*, **38**, 1071–1080.
- Maruta N., Trusov Y., Brenya E., Parekh U., Botella J.R. (2015) Membrane-localized extra-large G proteins and Gbg of the heterotrimeric G proteins form functional complexes engaged in plant immunity in *Arabidopsis*. *Plant physiology*, **167**, 1004–1016.
- Migaki G.I., Kahn J., Kishimoto T.K. (1995) Mutational analysis of the membrane-proximal cleavage site of L-selectin: relaxed sequence specificity surrounding the cleavage site. *The Journal of experimental medicine*, **182**, 549–557.
- Miya A., Albert P., Shinya T., Desaki Y., Ichimura K., Shirasu K., Narusaka Y., Kawakami N., Kaku H., Shibuya N. (2007) CERK1, a LysM receptor kinase, is essential for chitin elicitor signaling in *Arabidopsis*. *Proceedings of the National Academy of Sciences of the United States of America*, **104**, 19613–19618.
- Morel J., Claverol S., Mongrand S., Furt F., Fromentin J., Bessoule J.-J., Blein J.-P., Simon-Plas F. (2006) Proteomics of plant detergent-resistant membranes. *Molecular & cellular proteomics MCP*, **5**, 1396–1411.
- Mou Z., Fan W., Dong X. (2003) Inducers of plant systemic acquired resistance regulate NPR1 function through redox changes. *Cell*, **113**, 935–944.

- Mullis K., Faloona F., Scharf S., Saiki R., Horn G., Erlich H. (1986) Specific enzymatic amplification of DNA in vitro: the polymerase chain reaction. *Cold Spring Harbor symposia on quantitative biology*, **51 Pt 1**, 263–273.
- Murphy M.P., LeVine H. (2010) Alzheimer's disease and the amyloid-beta peptide. *Journal of Alzheimer's disease JAD*, **19**, 311–323.
- Muzzarelli R.A.A. (1977) *Chitin*. Pergamon Pr, Oxford: 309 pp.
- Nakamura S., Mano S., Tanaka Y., Ohnishi M., Nakamori C., Araki M., Niwa T., Nishimura M., Kaminaka H., Nakagawa T., Sato Y., Ishiguro S. (2010) Gateway binary vectors with the bialaphos resistance gene, bar, as a selection marker for plant transformation. *Bioscience, biotechnology, and biochemistry*, **74**, 1315–1319.
- Nawrath C., Métraux J.-P. (1999) Salicylic Acid Induction–Deficient Mutants of Arabidopsis Express PR-2 and PR-5 and Accumulate High Levels of Camalexin after Pathogen Inoculation. *Plant Cell*, **11**, 1393–1404.
- Newman M.-A., Sundelin T., Nielsen J.T., Erbs G. (2013) MAMP (microbe-associated molecular pattern) triggered immunity in plants. *Frontiers in plant science*, **4**, 139.
- Nguyen-Kim H., San Clemente H., Balliau T., Zivy M., Dunand C., Albenne C., Jamet E. (2016) Arabidopsis thaliana root cell wall proteomics: Increasing the proteome coverage using a combinatorial peptide ligand library and description of unexpected Hyp in peroxidase amino acid sequences. *Proteomics*, **16**, 491–503.
- Ni C.Y., Murphy M.P., Golde T.E., Carpenter G. (2001) gamma -Secretase cleavage and nuclear localization of ErbB-4 receptor tyrosine kinase. *Science (New York, N. Y.)*, **294**, 2179–2181.
- Nitta Y., Ding P., Zhang Y. (2015) Heterotrimeric G proteins in plant defense against pathogens and ABA signaling. *Environmental and Experimental Botany*, **114**, 153–158.
- Noe V., Fingleton B., Jacobs K., Crawford H.C., Vermeulen S., Steelant W., Bruyneel E., Matrisian L.M., Mareel M. (2001) Release of an invasion promoter E-cadherin fragment by matrilysin and stromelysin-1. *Journal of cell science*, **114**, 111–118.
- Noel L., Moores T.L., van Der Biezen, E A, Parniske M., Daniels M.J., Parker J.E., Jones J.D. (1999) Pronounced intraspecific haplotype divergence at the RPP5 complex disease resistance locus of Arabidopsis. *The Plant cell*, **11**, 2099–2112.
- Nürnberg T., Lipka V. (2005) Non-host resistance in plants: new insights into an old phenomenon. *Molecular plant pathology*, **6**, 335–345.
- Paetzel M., Dalbey R.E., Strynadka N.C. (1998) Crystal structure of a bacterial signal peptidase in complex with a beta-lactam inhibitor. *Nature*, **396**, 186–190.

- Pandey S., Monshausen G.B., Ding L., Assmann S.M. (2008) Regulation of root-wave response by extra large and conventional G proteins in *Arabidopsis thaliana*. *The Plant journal for cell and molecular biology*, **55**, 311–322.
- Park C.-J., Bart R., Chern M., Canlas P.E., Bai W., Ronald P.C. (2010) Overexpression of the endoplasmic reticulum chaperone BiP3 regulates XA21-mediated innate immunity in rice. *PloS one*, **5**, e9262.
- Park C.-J., Ronald P.C. (2012) Cleavage and nuclear localization of the rice XA21 immune receptor. *Nature Communications*, **3**, 920.
- Paulick M.G., Bertozzi C.R. (2008) The glycosylphosphatidylinositol anchor: a complex membrane-anchoring structure for proteins. *Biochemistry*, **47**, 6991–7000.
- Petutschnig E.K., Jones, Alexandra M E, Serazetdinova L., Lipka U., Lipka V. (2010) The lysin motif receptor-like kinase (LysM-RLK) CERK1 is a major chitin-binding protein in *Arabidopsis thaliana* and subject to chitin-induced phosphorylation. *The Journal of biological chemistry*, **285**, 28902–28911.
- Petutschnig E.K., Stolze M., Lipka U., Kopischke M., Horlacher J., Valerius O., Rozhon W., Gust A.A., Kemmerling B., Poppenberger B., Braus G.H., Nürnberger T., Lipka V. (2014) A novel *Arabidopsis* CHITIN ELICITOR RECEPTOR KINASE 1 (CERK1) mutant with enhanced pathogen-induced cell death and altered receptor processing. *The New phytologist*, **204**, 955–967.
- Piepkorn M., Pittelkow M.R., Cook P.W. (1998) Autocrine regulation of keratinocytes: the emerging role of heparin-binding, epidermal growth factor-related growth factors. *The Journal of investigative dermatology*, **111**, 715–721.
- Postina R., Schroeder A., Dewachter I., Bohl J., Schmitt U., Kojro E., Prinzen C., Endres K., Hiemke C., Blessing M., Flamez P., Dequenne A., Godaux E., van Leuven F., Fahrenholz F. (2004) A disintegrin-metalloproteinase prevents amyloid plaque formation and hippocampal defects in an Alzheimer disease mouse model. *J. Clin. Invest.*, **113**, 1456–1464.
- Pruitt R.N., Schwessinger B., Joe A., Thomas N., Liu F., Albert M., Robinson M.R., Chan L.J.G., Luu D.D., Chen H., Bahar O., Daudi A., Vleeschauwer D. de, Caddell D., Zhang W., Zhao X., Li X., Heazlewood J.L., Ruan D., Majumder D., Chern M., Kalbacher H., Midha S., Patil P.B., Sonti R.V., Petzold C.J., Liu C.C., Brodbelt J.S., Felix G., Ronald P.C. (2015) The rice immune receptor XA21 recognizes a tyrosine-sulfated protein from a Gram-negative bacterium. *Science Advances*, **1**, e1500245-e1500245.
- Raffler N.A., Rivera-Nieves J., Ley K. (2005) L-selectin in inflammation, infection and immunity. *Drug Discovery Today: Therapeutic Strategies*, **2**, 213–220.

- Rappsilber J., Mann M., Ishihama Y. (2007) Protocol for micro-purification, enrichment, pre-fractionation and storage of peptides for proteomics using StageTips. *Nat Protoc*, **2**, 1896–1906.
- Rio C. (2000) Tumor Necrosis Factor-alpha -converting Enzyme Is Required for Cleavage of erbB4/HER4. *Journal of Biological Chemistry*, **275**, 10379–10387.
- Rio C., Buxbaum J.D., Peschon J.J., Corfas G. (2000) Tumor necrosis factor-alpha-converting enzyme is required for cleavage of erbB4/HER4. *The Journal of biological chemistry*, **275**, 10379–10387.
- Robatzek S., Bittel P., Chinchilla D., Kochner P., Felix G., Shiu S.-H., Boller T. (2007) Molecular identification and characterization of the tomato flagellin receptor LeFLS2, an orthologue of Arabidopsis FLS2 exhibiting characteristically different perception specificities. *Plant molecular biology*, **64**, 539–547.
- Rohl C.A., Fiori W., Baldwin R.L. (1999) Alanine is helix-stabilizing in both template-nucleated and standard peptide helices. *Proceedings of the National Academy of Sciences of the United States of America*, **96**, 3682–3687.
- Rose L.E., Bittner-Eddy P.D., Langley C.H., Holub E.B., Michelmore R.W., Beynon J.L. (2004) The maintenance of extreme amino acid diversity at the disease resistance gene, RPP13, in Arabidopsis thaliana. *Genetics*, **166**, 1517–1527.
- Ross E.M., Wilkie T.M. (2000) GTPase-activating proteins for heterotrimeric G proteins: regulators of G protein signaling (RGS) and RGS-like proteins. *Annual review of biochemistry*, **69**, 795–827.
- Rotz R.C. von, Kohli B.M., Bosset J., Meier M., Suzuki T., Nitsch R.M., Konietzko U. (2004) The APP intracellular domain forms nuclear multiprotein complexes and regulates the transcription of its own precursor. *Journal of cell science*, **117**, 4435–4448.
- Roux M., Schwessinger B., Albrecht C., Chinchilla D., Jones A., Holton N., Malinovsky F.G., Tör M., Vries S.d., Zipfel C. (2011) The Arabidopsis Leucine-Rich Repeat Receptor-Like Kinases BAK1/SERK3 and BKK1/SERK4 Are Required for Innate Immunity to Hemibiotrophic and Biotrophic Pathogens. *Plant Cell*, **23**, 2440–2455.
- Rudyk O., Eaton P. (2014) Biochemical methods for monitoring protein thiol redox states in biological systems. *Redox biology*, **2**, 803–813.
- Rutledge B.J., Zhang K., Bier E., Jan Y.N., Perrimon N. (1992) The Drosophila spitz gene encodes a putative EGF-like growth factor involved in dorsal-ventral axis formation and neurogenesis. *Genes & development*, **6**, 1503–1517.
- Rzeniewicz K., Neue A., Rey Gallardo A., Davies J., Holt M.R., Patel A., Charras G.T., Stramer B., Molenaar C., Tedder T.F., Parsons M., Ivetic A. (2015) L-selectin shedding is activated specifically within transmigrating pseudopods of monocytes to regulate cell

- polarity in vitro. *Proceedings of the National Academy of Sciences of the United States of America*, **112**, E1461-70.
- Sadhukhan R., Sen G.C., Ramchandran R., Sen I. (1998) The distal ectodomain of angiotensin-converting enzyme regulates its cleavage-secretion from the cell surface. *Proceedings of the National Academy of Sciences of the United States of America*, **95**, 138–143.
- Saftig P., Reiss K. (2011) The "A Disintegrin And Metalloproteases" ADAM10 and ADAM17: novel drug targets with therapeutic potential? *European journal of cell biology*, **90**, 527–535.
- Schlessinger J. (2000) Cell Signaling by Receptor Tyrosine Kinases. *Cell*, **103**, 211–225.
- Schulze B., Mentzel T., Jehle A.K., Mueller K., Beeler S., Boller T., Felix G., Chinchilla D. (2010) Rapid heteromerization and phosphorylation of ligand-activated plant transmembrane receptors and their associated kinase BAK1. *The Journal of biological chemistry*, **285**, 9444–9451.
- Schwessinger B., Roux M., Kadota Y., Ntoukakis V., Sklenar J., Jones A., Zipfel C. (2011) Phosphorylation-dependent differential regulation of plant growth, cell death, and innate immunity by the regulatory receptor-like kinase BAK1. *PLoS genetics*, **7**, e1002046.
- Seals D.F., Courtneidge S.A. (2003) The ADAMs family of metalloproteases: multidomain proteins with multiple functions. *Genes & development*, **17**, 7–30.
- Selkoe D.J. (2001) Alzheimer's disease: genes, proteins, and therapy. *Physiological Reviews*, **81**, 741–766.
- Seubert P., Oltersdorf T., Lee M.G., Barbour R., Blomquist C., Davis D.L., Bryant K., Fritz L.C., Galasko D., Thal L.J. (1993) Secretion of beta-amyloid precursor protein cleaved at the amino terminus of the beta-amyloid peptide. *Nature*, **361**, 260–263.
- Shimizu T., Nakano T., Takamizawa D., Desaki Y., Ishii-Minami N., Nishizawa Y., Minami E., Okada K., Yamane H., Kaku H., Shibuya N. (2010) Two LysM receptor molecules, CEBiP and OsCERK1, cooperatively regulate chitin elicitor signaling in rice. *The Plant journal for cell and molecular biology*, **64**, 204–214.
- Shinya T., Motoyama N., Ikeda A., Wada M., Kamiya K., Hayafune M., Kaku H., Shibuya N. (2012) Functional characterization of CEBiP and CERK1 homologs in arabidopsis and rice reveals the presence of different chitin receptor systems in plants. *Plant & cell physiology*, **53**, 1696–1706.
- Shinya T., Nakagawa T., Kaku H., Shibuya N. (2015) Chitin-mediated plant-fungal interactions: catching, hiding and handshaking. *Current opinion in plant biology*, **26**, 64–71.

- Shinya T., Yamaguchi K., Desaki Y., Yamada K., Narisawa T., Kobayashi Y., Maeda K., Suzuki M., Tanimoto T., Takeda J., Nakashima M., Funama R., Narusaka M., Narusaka Y., Kaku H., Kawasaki T., Shibuya N. (2014) Selective regulation of the chitin-induced defense response by the Arabidopsis receptor-like cytoplasmic kinase PBL27. *The Plant journal for cell and molecular biology*, **79**, 56–66.
- Shiu S.H., Bleecker A.B. (2001) Receptor-like kinases from Arabidopsis form a monophyletic gene family related to animal receptor kinases. *Proceedings of the National Academy of Sciences of the United States of America*, **98**, 10763–10768.
- Siegel P.M., Massagué J. (2003) Cytostatic and apoptotic actions of TGF-beta in homeostasis and cancer. *Nature reviews. Cancer*, **3**, 807–821.
- Singh A.B., Harris R.C. (2005) Autocrine, paracrine and juxtacrine signaling by EGFR ligands. *Cellular signalling*, **17**, 1183–1193.
- Singh A.B., Tsukada T., Zent R., Harris R.C. (2004) Membrane-associated HB-EGF modulates HGF-induced cellular responses in MDCK cells. *Journal of cell science*, **117**, 1365–1379.
- Sisodia S.S. (1992) Beta-amyloid precursor protein cleavage by a membrane-bound protease. *Proceedings of the National Academy of Sciences of the United States of America*, **89**, 6075–6079.
- Smalley D.M., Ley K. (2005) L-selectin: Mechanisms and physiological significance of ectodomain cleavage. *J Cellular Mol Med*, **9**, 255–266.
- Smolarkiewicz M., Skrzypczak T., Michalak M., Leśniewicz K., Walker J.R., Ingram G., Wojtaszek P. (2014) Gamma-secretase subunits associate in intracellular membrane compartments in Arabidopsis thaliana. *Journal of experimental botany*, **65**, 3015–3027.
- Song W.-Y., Wang G.-L., Chen L.-L., Kim H.-S., Pi L.-Y., Holsten T., Gardner J., Wang B., Zhai W.-X., Zhu L.-H., Fauquet C., Ronald P. (1995) A Receptor Kinase-Like Protein Encoded by the Rice Disease Resistance Gene, Xa21. *Science*, **270**, 1804–1806.
- Spoel S.H., Dong X. (2012) How do plants achieve immunity? Defence without specialized immune cells. *Nature reviews. Immunology*, **12**, 89–100.
- Stahl E.A., Dwyer G., Mauricio R., Kreitman M., Bergelson J. (1999) Dynamics of disease resistance polymorphism at the Rpm1 locus of Arabidopsis. *Nature*, **400**, 667–671.
- Stracke S., Kistner C., Yoshida S., Mulder L., Sato S., Kaneko T., Tabata S., Sandal N., Stougaard J., Szczyglowski K., Parniske M. (2002) A plant receptor-like kinase required for both bacterial and fungal symbiosis. *Nature*, **417**, 959–962.
- Takai R., Isogai A., Takayama S., Che F.-S. (2008) Analysis of flagellin perception mediated by flg22 receptor OsFLS2 in rice. *Molecular plant-microbe interactions MPMI*, **21**, 1635–1642.

- Tanz S.K., Castleden I., Hooper C.M., Vacher M., Small I., Millar H.A. (2013) SUBA3: a database for integrating experimentation and prediction to define the SUBcellular location of proteins in Arabidopsis. *Nucleic acids research*, **41**, D1185-91.
- Tax F., Kemmerling B. (Eds) (2012) *Receptor-like Kinases in Plants: From Development to Defense*, 2012nd edn. Signaling and Communication in Plants, 13. Springer, Berlin.
- Temple B.R.S., Jones A.M. (2007) The plant heterotrimeric G-protein complex. *Annual review of plant biology*, **58**, 249–266.
- Ternes P., Feussner K., Werner S., Lerche J., Iven T., Heilmann I., Riezman H., Feussner I. (2011) Disruption of the ceramide synthase LOH1 causes spontaneous cell death in Arabidopsis thaliana. *The New phytologist*, **192**, 841–854.
- Thompson E.P., Smith S.G.L., Glover B.J. An Arabidopsis rhomboid protease has roles in the chloroplast and in flower development. *J. Exp. Bot.*, ers012.
- Thompson E.P., Smith S.G.L., Glover B.J. (2012) An Arabidopsis rhomboid protease has roles in the chloroplast and in flower development. *Journal of experimental botany*, **63**, 3559–3570.
- Thorp E., Vaisar T., Subramanian M., Mautner L., Blobel C., Tabas I. (2011) Shedding of the Mer Tyrosine Kinase Receptor Is Mediated by ADAM17 Protein through a Pathway Involving Reactive Oxygen Species, Protein Kinase C δ , and p38 Mitogen-activated Protein Kinase (MAPK)*. *The Journal of biological chemistry*, **286**, 33335–33344.
- Thung L., Trusov Y., Chakravorty D., Botella J.R. (2012) G γ 1+G γ 2+G γ 3=G β : the search for heterotrimeric G-protein γ subunits in Arabidopsis is over. *Journal of plant physiology*, **169**, 542–545.
- Torres M.A., Morales J., Sánchez-Rodríguez C., Molina A., Dangl J.L. (2013) Functional interplay between Arabidopsis NADPH oxidases and heterotrimeric G protein. *Molecular plant-microbe interactions MPMI*, **26**, 686–694.
- Trdá L., Boutrot F., Claverie J., Brulé D., Dorey S., Poinssot B. (2015) Perception of pathogenic or beneficial bacteria and their evasion of host immunity: pattern recognition receptors in the frontline. *Frontiers in plant science*, **6**, 219.
- Trusov Y., Rookes J.E., Chakravorty D., Armour D., Schenk P.M., Botella J.R. (2006) Heterotrimeric G Proteins Facilitate Arabidopsis Resistance to Necrotrophic Pathogens and Are Involved in Jasmonate Signaling¹. *Plant physiology*, **140**, 210–220.
- Trusov Y., Rookes J.E., Tilbrook K., Chakravorty D., Mason M.G., Anderson D., Chen J.-G., Jones A.M., Botella J.R. (2007) Heterotrimeric G Protein γ Subunits Provide Functional Selectivity in G $\beta\gamma$ Dimer Signaling in ArabidopsisOA. *The Plant cell*, **19**, 1235–1250.
- Turk B.E., Huang L.L., Piro E.T., Cantley L.C. (2001) Determination of protease cleavage site motifs using mixture-based oriented peptide libraries. *Nature biotechnology*, **19**, 661–667.

- Ullah H., Chen J.-G., Temple B., Boyes D.C., Alonso J.M., Davis K.R., Ecker J.R., Jones A.M. (2003) The β -Subunit of the Arabidopsis G Protein Negatively Regulates Auxin-Induced Cell Division and Affects Multiple Developmental Processes. *Plant Cell*, **15**, 393–409.
- Urano D., Chen J.-G., Botella J.R., Jones A.M. (2013) Heterotrimeric G protein signalling in the plant kingdom. *Open biology*, **3**, 120186.
- Urano D., Jones A.M. (2014) Heterotrimeric G protein-coupled signaling in plants. *Annual review of plant biology*, **65**, 365–384.
- Urano D., Jones J.C., Wang H., Matthews M., Bradford W., Bennetzen J.L., Jones A.M. (2012a) G protein activation without a GEF in the plant kingdom. *PLoS genetics*, **8**, e1002756.
- Urano D., Phan N., Jones J.C., Yang J., Huang J., Grigston J., Taylor J.P., Jones A.M. (2012b) Endocytosis of the seven-transmembrane RGS1 protein activates G-protein-coupled signalling in Arabidopsis. *Nature cell biology*, **14**, 1079–1088.
- Urban S. (2006) Rhomboid proteins: conserved membrane proteases with divergent biological functions. *Genes & development*, **20**, 3054–3068.
- Urban S., Freeman M. (2003) Substrate Specificity of Rhomboid Intramembrane Proteases Is Governed by Helix-Breaking Residues in the Substrate Transmembrane Domain. *Molecular Cell*, **11**, 1425–1434.
- Urban S., Lee J.R., Freeman M. (2001) Drosophila Rhomboid-1 Defines a Family of Putative Intramembrane Serine Proteases. *Cell*, **107**, 173–182.
- van der Hoorn R.A., Kamoun S. (2008) From Guard to Decoy: a new model for perception of plant pathogen effectors. *The Plant cell*, **20**, 2009–2017.
- van Roy F., Berx G. (2008) The cell-cell adhesion molecule E-cadherin. *Cellular and molecular life sciences CMLS*, **65**, 3756–3788.
- Vanhoof G., Goossens F., Meester I.D., Hendriks D., Scharpé S. (1995) Proline motifs in peptides and their biological processing. *FASEB J*, **9**, 736–744.
- Wakatsuki S., Kurisaki T., Sehara-Fujisawa A. (2004) Lipid rafts identified as locations of ectodomain shedding mediated by Meltrin beta/ADAM19. *Journal of neurochemistry*, **89**, 119–123.
- Walcheck B., Alexander S.R., St Hill C.A., Matala E. (2003) ADAM-17-independent shedding of L-selectin. *Journal of Leukocyte Biology*, **74**, 389–394.
- Wan J., Tanaka K., Zhang X.-C., Son G.H., Brechenmacher L., Nguyen, Tran Hong Nha, Stacey G. (2012) LYK4, a lysin motif receptor-like kinase, is important for chitin signaling and plant innate immunity in Arabidopsis. *Plant physiology*, **160**, 396–406.

- Wan J., Zhang X.-C., Stacey G. (2008) Chitin signaling and plant disease resistance. *Plant signaling & behavior*, **3**, 831–833.
- Wang Z.Y., Seto H., Fujioka S., Yoshida S., Chory J. (2001) BRI1 is a critical component of a plasma-membrane receptor for plant steroids. *Nature*, **410**, 380–383.
- Weigel D., Mott R. (2009) The 1001 genomes project for Arabidopsis thaliana. *Genome biology*, **10**, 107.
- Weiss A., Attisano L. (2013) The TGFbeta superfamily signaling pathway. *Wiley interdisciplinary reviews. Developmental biology*, **2**, 47–63.
- Weskamp G., Schlondorff J., Lum L., Becherer J.D., Kim T.-W., Saftig P., Hartmann D., Murphy G., Blobel C.P. (2004) Evidence for a critical role of the tumor necrosis factor alpha convertase (TACE) in ectodomain shedding of the p75 neurotrophin receptor (p75NTR). *The Journal of biological chemistry*, **279**, 4241–4249.
- Wessel D., Flügge U.I. (1984) A method for the quantitative recovery of protein in dilute solution in the presence of detergents and lipids. *Analytical Biochemistry*, **138**, 141–143.
- Wildermuth M.C., Dewdney J., Wu G., Ausubel F.M. (2001) Isochorismate synthase is required to synthesize salicylic acid for plant defence. *Nature*, **414**, 562–565.
- Willmann R., Lajunen H.M., Erbs G., Newman M.-A., Kolb D., Tsuda K., Katagiri F., Fliegmann J., Bono J.-J., Cullimore J.V., Jehle A.K., Götz F., Kulik A., Molinaro A., Lipka V., Gust A.A., Nürnberger T. (2011) Arabidopsis lysin-motif proteins LYM1 LYM3 CERK1 mediate bacterial peptidoglycan sensing and immunity to bacterial infection. *Proceedings of the National Academy of Sciences of the United States of America*, **108**, 19824–19829.
- Winter D., Vinegar B., Nahal H., Ammar R., Wilson G.V., Provart N.J. (2007) An “Electronic Fluorescent Pictograph” Browser for Exploring and Analyzing Large-Scale Biological Data Sets. *PLOS ONE*, **2**, e718.
- Wolfenstetter S., Chakravorty D., Kula R., Urano D., Trusov Y., Sheahan M.B., McCurdy D.W., Assmann S.M., Jones A.M., Botella J.R. (2015) Evidence for an unusual transmembrane configuration of AGG3, a class C Gy subunit of Arabidopsis. *The Plant journal for cell and molecular biology*, **81**, 388–398.
- Xu W.-H., Wang Y.-S., Liu G.-Z., Chen X., Tinjuangjun P., Pi L.-Y., Song W.-Y. (2006) The autophosphorylated Ser686, Thr688, and Ser689 residues in the intracellular juxtamembrane domain of XA21 are implicated in stability control of rice receptor-like kinase. *The Plant journal for cell and molecular biology*, **45**, 740–751.
- Yamazaki S., Iwamoto R., Saeki K., Asakura M., Takashima S., Yamazaki A., Kimura R., Mizushima H., Moribe H., Higashiyama S., Endoh M., Kaneda Y., Takagi S., Itami S., Takeda N., Yamada G., Mekada E. (2003) Mice with defects in HB-EGF ectodomain

- shedding show severe developmental abnormalities. *The Journal of cell biology*, **163**, 469–475.
- Yuan C.-X., Lasut A.L., Wynn R., Neff N.T., Hollis G.F., Ramaker M.L., Rupar M.J., Liu P., Meade R. (2003) Purification of Her-2 extracellular domain and identification of its cleavage site. *Protein expression and purification*, **29**, 217–222.
- Zhang J., Li W., Xiang T., Liu Z., Laluk K., Ding X., Zou Y., Gao M., Zhang X., Chen S., Mengiste T., Zhang Y., Zhou J.-M. (2010) Receptor-like cytoplasmic kinases integrate signaling from multiple plant immune receptors and are targeted by a *Pseudomonas syringae* effector. *Cell host & microbe*, **7**, 290–301.
- Zhang W., Fraiture M., Kolb D., Loffelhardt B., Desaki Y., Boutrot F.F.G., Tor M., Zipfel C., Gust A.A., Brunner F. (2013) Arabidopsis receptor-like protein30 and receptor-like kinase suppressor of BIR1-1/EVERSHED mediate innate immunity to necrotrophic fungi. *The Plant cell*, **25**, 4227–4241.
- Zhang Y., Giboulot A., Zivy M., Valot B., Jamet E., Albenne C. (2011) Combining various strategies to increase the coverage of the plant cell wall glycoproteome. *Phytochemistry*, **72**, 1109–1123.
- Zhou N., Tootle T.L., Tsui F., Klessig D.F., Glazebrook J. (1998) PAD4 Functions Upstream from Salicylic Acid to Control Defense Responses in Arabidopsis. *Plant Cell*, **10**, 1021–1030.
- Zhou W., Carpenter G. (2000) Heregulin-dependent trafficking and cleavage of ErbB-4. *The Journal of biological chemistry*, **275**, 34737–34743.
- Zhu H., Li G.-J., Ding L., Cui X., Berg H., Assmann S.M., Xia Y. (2009) Arabidopsis extra large G-protein 2 (XLG2) interacts with the Gbeta subunit of heterotrimeric G protein and functions in disease resistance. *Molecular plant*, **2**, 513–525.
- Ziegler Y. (2015) *The Role Of The Putative Receptor-Like Cytoplasmic Kinase CLR1 In Chitin Signalling*. PhD Thesis, Göttingen.
- Zimina E.P., Bruckner-Tuderman L., Franzke C.-W. (2005) Shedding of collagen XVII ectodomain depends on plasma membrane microenvironment. *The Journal of biological chemistry*, **280**, 34019–34024.
- Zipfel C. (2014) Plant pattern-recognition receptors. *Trends in immunology*, **35**, 345–351.
- Zipfel C., Kunze G., Chinchilla D., Caniard A., Jones J.D.G., Boller T., Felix G. (2006) Perception of the bacterial PAMP EF-Tu by the receptor EFR restricts Agrobacterium-mediated transformation. *Cell*, **125**, 749–760.
- Zipfel C., Robatzek S., Navarro L., Oakeley E.J., Jones J.D.G., Felix G., Boller T. (2004) Bacterial disease resistance in Arabidopsis through flagellin perception. *Nature*, **428**, 764–767.

6. Supplemental material

Table S1. Predicted localization of proteins from cell culture supernatants. SUBA3 localization prediction of proteins found in cell culture supernatants of *Arabidopsis*.

Predicted localization	Sample 01		Sample 02		Sample 03		Sample 04	
	Proteins (%)							
Extracellular	167 (46.4)	4061 (74.1)	201 (34.2)	3678 (50.0)	151 (27.7)	4448 (52.8)	128 (34.6)	2715 (56.9)
Cytosol	65 (18.1)	467 (8.5)	140 (23.8)	1432 (19.5)	168 (30.8)	1979 (23.5)	107 (28.9)	1044 (21.9)
PM	52 (14.4)	457 (8.3)	79 (13.4)	772 (10.5)	59 (10.8)	563 (6.7)	35 (9.5)	356 (7.5)
Plastid	30 (8.3)	159 (2.9)	60 (10.2)	497 (6.8)	81 (14.9)	726 (8.6)	46 (12.4)	299 (6.2)
Mitochondrion	19 (5.3)	114 (2.1)	42 (7.1)	334 (4.5)	45 (8.3)	432 (5.1)	25 (6.8)	190 (3.9)
Vacuole	20 (5.6)	202 (3.7)	29 (4.9)	472 (6.4)	15 (2.8)	134 (1.6)	10 (2.7)	70 (1.5)
Peroxisome	3 (0.8)	8 (0.15)	11 (1.9)	48 (0.7)	9 (1.7)	71 (0.7)	6 (1.6)	22 (0.5)
ER	3 (0.8)	9 (0.2)	10 (1.8)	64 (0.9)	9 (1.7)	47 (0.5)	7 (1.9)	53 (1.1)
Nucleus	1 (0.3)	3 (0.05)	16 (2.7)	58 (0.7)	7 (1.3)	39 (0.5)	6 (1.6)	22 (0.5)
Total	360 (100)	5480 (100)	588 (100)	7355 (100)	544 (100)	8439 (100)	370 (100)	4771 (100)

Table S2. Receptor-like kinases and receptor-like proteins found in cell culture supernatant (Sample01).

Unused	Total	%Cov	%Cov(50)	%Cov(95)	Accession	Name	Peptides (95 %)	
							extra-cellular	Intra-cellular
2.02	2.02	4.3	2.72	2.72	AT1G06840	Leucine-rich repeat protein kinase family protein	5	0
4.01	6.01	17.31	17.31	17.31	AT1G21880	lysm domain GPI-anchored protein 1 precursor	6	0
3.42	3.55	4.82	4.82	2.23	AT1G30570	hercules receptor kinase 2, HERK2	5	0
4	4	4.58	4.58	4.58	AT1G53730	STRUBBELIG-receptor family 6, SRF6	2	0
12.51	12.5	46.34	46.1	34.99	AT1G77630	Peptidoglycan-binding LysM domain-containing protein	11	0
4.66	4.78	4.02	3.244	3.24	AT1G51800	Leucine-rich repeat protein kinase family protein	3	0
38.32	38.3	35.84	34.99	34.04	AT2G01820	Leucine-rich repeat protein kinase family protein	71	1
9.96	10.0	16	16	16	AT2G17120	lysm domain GPI-anchored protein 2 precursor	5	0
2.54	2.6	6.07	4.86	4.86	AT2G26730	Leucine-rich repeat protein kinase family protein	2	1
4.79	4.87	7.12	5.03	5.03	AT2G39360	Protein kinase superfamily protein	3	0
5.69	5.79	3.65	3.65	2.43	AT3G02130	receptor-like protein kinase 2	3	0
5.57	5.64	5.9	5.9	5.9	AT3G02880	Leucine-rich repeat protein kinase family protein	3	0
5.06	5.29	7.11	6.03	4.79	AT3G17840	receptor-like kinase 902	3	0
10.22	10.2	8.84	7.87	6.57	AT3G23750	Leucine-rich repeat protein kinase family protein	5	0
20.15	20.2	32.91	32.91	27.39	AT3G46280	protein kinase-related	16	0
6.46	6.5	7.71	6.37	6.37	AT3G51550	Malectin/receptor-like protein kinase family protein	4	0
2.29	2.32	5.54	5.54	5.54	AT4G03390	STRUBBELIG-receptor family 3, SRF3	2	0
3.52	3.66	4.01	2.67	2.01	AT4G08850	Leucine-rich repeat protein kinase family protein	4	0
7.87	7.96	13.69	13.69	12.3	AT4G18760	receptor like protein 51	5	0
4.99	5.18	6.48	3.83	3.83	AT4G21410	cysteine-rich RLK (RECEPTOR-like protein kinase) 29	5	0
6.09	6.2	5.69	4.52	4.01	AT4G39400	Leucine-rich receptor-like protein kinase family protein	8	0
3.43	3.55	4.34	2.99	2.06	AT5G01890	Leucine-rich repeat protein kinase family protein	3	1

Table S3. Receptor-like kinases and receptor-like proteins found in cell culture supernatant (Sample02).

Unused	Total	%Cov	%Cov(50)	%Cov(95)	Accession	Name	Peptides (95 %)	
							extra-cellular	Intra-cellular
10.42	11.4	10.06	8.91	8.18	AT1G06840	Leucine-rich repeat protein kinase family protein	8	0
4	4	3.21	3.21	2.26	AT1G11330	S-locus lectin protein kinase family protein	2	0
6.89	6.95	6.4	6.4	6.4	AT1G15530	Concanavalin A-like lectin protein kinase family protein	4	0
2.44	4.65	13.22	13.22	11.54	AT1G21880	lysm domain GPI-anchored protein 1 precursor	4	0
10.92	10.9	8.6	8.6	8.6	AT1G30570	hercules receptor kinase 2	7	0
6.04	6.05	5.07	4.95	4.95	AT1G34300	lectin protein kinase family protein	3	0
5.7	5.8	3.47	3.47	3.47	AT1G51800	Leucine-rich repeat protein kinase family protein	3	0
13.03	13.1	11.91	11.79	11.79	AT1G51850	Leucine-rich repeat protein kinase family protein	11	0
7.12	7.36	15.42	15.42	15.42	AT1G53730	STRUBBELIG-receptor family 6	5	0
14.54	14.5	8.71	8.03	7.94	AT1G56140	Leucine-rich repeat transmembrane protein kinase	8	0
6.38	10.8	7.7	7.03	7.03	AT1G56145	Leucine-rich repeat transmembrane protein kinase	7	0
11.13	11.8	13.38	12.63	9.13	AT1G66150	transmembrane kinase 1	6	0
7.88	8.05	19.39	19.39	17.73	AT1G77630	Peptidoglycan-binding LysM domain-containing protein	6	0
51.94	51.9	34.68	34.04	33.93	AT2G01820	Leucine-rich repeat protein kinase family protein	113	0
15.2	15.2	22	22	22	AT2G17120	lysm domain GPI-anchored protein 2 precursor	10	0
6	6	11.85	11.85	11.85	AT2G26730	Leucine-rich repeat protein kinase family protein	5	0
2	2	1.96	1.96	1.96	AT2G33580	Protein kinase superfamily protein	2	0
12.24	12.2	10.71	7.92	7.92	AT2G37050	Leucine-rich repeat protein kinase family protein	8	0
17.4	17.4	14.36	14.36	13.01	AT2G39360	Protein kinase superfamily protein	9	0
8.24	8.42	8.34	7.56	4.43	AT3G02130	receptor-like protein kinase 2	5	0
9.98	10.1	9.89	9.89	9.89	AT3G02880	Leucine-rich repeat protein kinase family protein	13	0
11.43	11.5	8.59	8.59	6.1	AT3G13380	BR11-like 3	9	0

Table S3 (continued).

Unused	Total	%Cov	%Cov(50)	%Cov(95)	Accession	Name	Peptides (95 %)	
							extra-cellular	Intra-cellular
13.09	13.12	13.53	13.53	13.53	AT3G14350	STRUBBELIG-receptor family 7	9	0
11.07	11.23	9.74	9.74	9.74	AT3G17840	receptor-like kinase 902	7	0
6	6	10.7	10.7	8.27	AT3G21630	chitin elicitor receptor kinase 1	3	0
23.56	23.58	20.69	20.69	20.69	AT3G23750	Leucine-rich repeat protein kinase family protein	19	0
9.14	9.2	8.72	8.6	8.6	AT3G51550	Malectin/receptor-like protein kinase family protein	5	0
19.82	19.88	13.3	13.3	13.3	AT4G08850	Leucine-rich repeat receptor-like protein kinase family	12	0
8	8.23	13.69	13.46	13.46	AT4G18760	receptor like protein 51	5	0
9.41	9.51	9.72	9.57	7.66	AT4G21410	cysteine-rich RLK (RECEPTOR-like protein kinase) 29	6	0
3.2	3.39	4.73	4.73	4.15	AT4G23250	kinases;protein kinases	3	0
9.07	9.2	5.43	4.6	4.01	AT4G39400	Leucine-rich receptor-like protein kinase family protein	5	0
4.33	6.46	8.96	8.96	7.84	AT5G16590	Leucine-rich repeat protein kinase family protein	6	0
13.37	13.45	11.75	11.02	10.28	AT5G49760	Leucine-rich repeat protein kinase family protein	7	0
2.97	3.13	3.86	3.86	2.69	AT5G54380	protein kinase family protein	3	0
4.1	4.12	3.92	3.92	3.92	AT5G61350	Protein kinase superfamily protein	3	0
8	8	6.09	6.09	6.09	AT5G65240	Leucine-rich repeat protein kinase family protein	4	0

Table S4. Receptor-like kinases and receptor-like proteins found in cell culture supernatant (Sample03).

Sample03									
Unused	Total	%Cov	%Cov(50)	%Cov(95)	Accession	Name	Peptides (95 %)		
							extra-cellular	intra-cellular	
6,11	6,43	26,44	26,44	21,88	AT1G21880	lysm domain GPI-anchored protein 1 precursor	6	0	0
6,24	6,26	4,71	4,71	4,71	AT1G30570	hercules receptor kinase 2	4	0	0
6,32	6,34	6,82	4,47	3,47	AT1G51800	Leucine-rich repeat protein kinase family protein	4	0	0
4,42	4,46	8,61	8,61	8,61	AT1G53730	STRUBBELIG-receptor family 6	3	0	0
3,2	3,3	3,68	3,68	2,9	AT1G56140	Leucine-rich repeat transmembrane protein kinase	3	0	0
2,04	3,12	4,14	3,4	2,44	AT1G66150	transmembrane kinase 1	4	0	0
9,45	9,55	48,46	48,23	45,39	AT1G77630	Peptidoglycan-binding LysM domain-containing protein	12	0	0
37,89	37,9	35,1	33,83	30,22	AT2G01820	Leucine-rich repeat protein kinase family protein	59	0	0
14	14,1	22	22	22	AT2G17120	lysm domain GPI-anchored protein 2 precursor	8	0	0
8,75	8,93	7,39	7,39	5,78	AT2G37050	Leucine-rich repeat protein kinase family protein	5	0	0
3,81	3,95	6,03	4,79	3,71	AT3G17840	receptor-like kinase 902	4	0	0
8,25	8,28	6,25	6,25	6,25	AT3G23750	Leucine-rich repeat protein kinase family protein	5	0	0
11,3	11,3	11,17	9,72	9,72	AT3G51550	Malectin/receptor-like protein kinase family protein	7	0	0
7,09	7,2	9,19	7,46	5,26	AT4G08850	Leucine-rich repeat receptor-like protein kinase family protein	3	5	5
4,58	4,86	5,94	5,94	2,17	AT4G39400	Leucine-rich receptor-like protein kinase family protein	5	3	3
3,52	3,6	5,06	3,23	3,23	AT5G03140	Concanavalin A-like lectin protein kinase family protein	2	1	1

Table S5. Receptor-like kinases and receptor-like proteins found in cell culture supernatant (Sample04).

Sample04									
Unused	Total	%Cov	%Cov(50)	%Cov(95)	Accession	Name	Peptides (95 %)		
							extra-cellular	Intra-cellular	
16.4	16.42	30.05	26.68	25	AT1G21880	lysm domain GPI-anchored protein 1 precursor	26	0	
6.61	6.88	7.07	7.07	7.07	AT1G49730	Protein kinase superfamily protein	4	0	
4.99	5.07	3.24	3.24	3.24	AT1G51800	Leucine-rich repeat protein kinase family protein	3	0	
10.55	14.73	36.88	36.88	35.22	AT1G77630	Peptidoglycan-binding LysM domain-containing protein	16	0	
39.51	39.53	30.43	30.22	30.22	AT2G01820	Leucine-rich repeat protein kinase family protein	57	0	
16.63	16.65	26.86	25.14	23.14	AT2G17120	lysm domain GPI-anchored protein 2 precursor	12	0	
2.57	4.83	4.68	4.68	4.68	AT3G19300	Protein kinase superfamily protein	3	0	
6.6	6.77	8.72	8.6	8.6	AT3G51550	Malectin/receptor-like protein kinase family protein	5	0	
8.71	8.79	5.93	5.26	5.26	AT4G08850	Leucine-rich repeat receptor-like protein kinase family	5	0	
4.15	4.41	3.34	2.76	2.17	AT4G39400	Leucine-rich receptor-like protein kinase family protein	3	0	

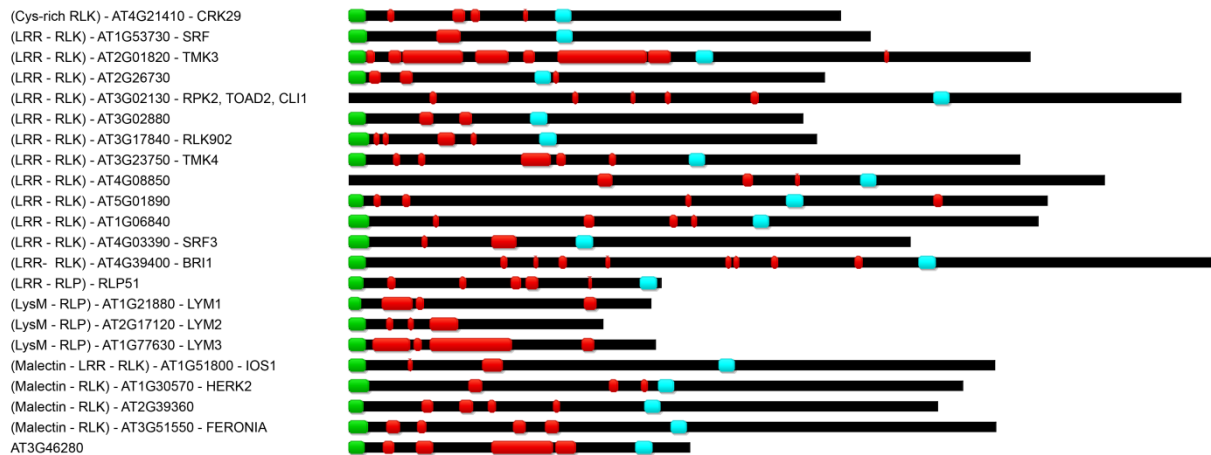


Figure S1. Receptor-like kinases and receptor-like proteins found in Col-0 cell culture supernatants of Sample01. Identified peptides were mapped to the amino acid sequence of the respective receptor-like kinase or receptor-like protein and peptide coverage is shown in red. Predicted signal peptides are given in green and transmembrane domain in light blue.

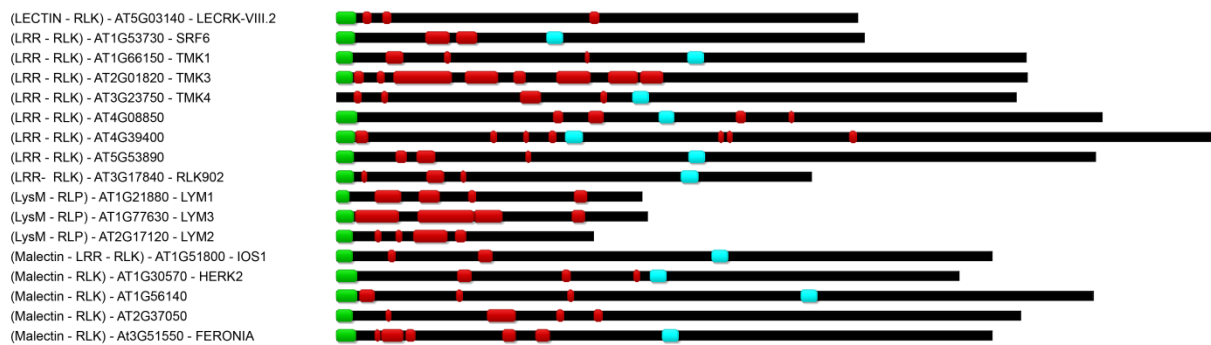


Figure S2. Receptor-like kinases and receptor-like proteins found in Col-0 cell culture supernatants of Sample03. Identified peptides were mapped to the amino acid sequence of the respective receptor-like kinase or receptor-like protein and peptide coverage is shown in red. Predicted signal peptides are given in green and transmembrane domain in light blue.

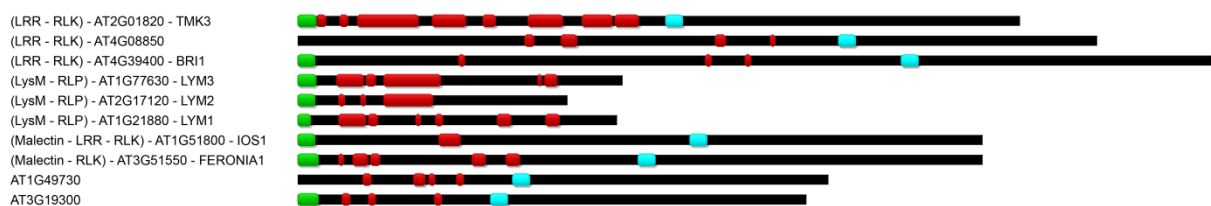


Figure S3. Receptor-like kinases and receptor-like proteins found in Col-0 cell culture supernatants of Sample04. Identified peptides were mapped to the amino acid sequence of the respective receptor-like kinase or receptor-like protein and peptide coverage is shown in red. Predicted signal peptides are given in green and transmembrane domain in light blue.

Supplemental file 1: 01. Sample01_localization.xlsx
Localization prediction of proteins identified in Sample01.

Supplemental file 2: 02. Sample02_localization.xlsx
Localization prediction of proteins identified in Sample02.

Supplemental file 3: 03. Sample03_localization.xlsx
Localization prediction of proteins identified in Sample03.

Supplemental file 4: 04. Sample04_localization.xlsx
Localization prediction of proteins identified in Sample04.

Supplemental file 5: 05. Sample01_TAIR10_repGeneModel.group
Raw data of Sample01.

Supplemental file 6: 06. Sample01_TAIR10_repGeneModel__FDR.xlsx
Raw data of Sample01.

Supplemental file 7: 07. Sample02_TAIR10_repGeneModel.group
Raw data of Sample02.

Supplemental file 8: 08. Sample02_TAIR10_repGeneModel__FDR.xlsx
Raw data of Sample02.

Supplemental file 9: 09. Sample03_TAIR10_repGeneModel.group
Raw data of Sample03.

Supplemental file 10: 10. Sample03_TAIR10_repGeneModel__FDR.xlsx
Raw data of Sample03.

Supplemental file 11: 11. Sample04_TAIR10_repGeneModel.group
Raw data of Sample04.

Supplemental file 12: 12. Sample04_TAIR10_repGeneModel__FDR.xlsx
Raw data of Sample04.

List of tables

Table 1. <i>Arabidopsis</i> accessions used in this study.	26
Table 2. Mutant <i>Arabidopsis</i> lines used in this study.....	27
Table 3. Transgenic <i>Arabidopsis</i> lines used in this study.....	28
Table 4. Vectors used in this study.....	30
Table 5. Primer used in this study.	32
Table 6. Buffers used in this study.	38
Table 7. Antibodies used in this study.	42
Table 8. Settings for fluorophore detection.....	57
Table 9. Predicted localization of proteins from cell culture supernatants.	78
Table 10. Predicted localization of proteins from apoplastic wash fluids.	82
Table 11. Summary of characteristics of noce mutants including results from sequencing of candidate suppressor genes..	88
Table 12. RLKs identified in cell wall proteome studies.....	118

List of figures

Figure 1. The plant immune system.	2
Figure 2. Chitin perception in plants.	7
Figure 3. Cycle of heterotrimeric G-protein activation in animals and in <i>Arabidopsis</i>	10
Figure 4. Ectodomain shedding and RIP of integral membrane proteins.	17
Figure 5. Proteolytic processing of amyloid precursor protein.	19
Figure 6. CERK1 ectodomain shedding is reduced in some <i>Arabidopsis</i> accessions.	60
Figure 7. Wt-5 ectodomain shedding is also reduced in <i>cerk1-2</i>	61
Figure 8. CERK1 cleavage motif mutants could not fully suppress CERK1 ectodomain shedding.	63
Figure 9. Deletion of potential intracellular cleavage motifs could not suppress CERK1 ectodomain shedding.	66
Figure 10. The <i>cvg1</i> mutation cannot suppress the <i>Bgh</i> -induced <i>cerk1-4</i> phenotype.	68
Figure 11. The <i>cvg1</i> mutation cannot suppress the <i>cerk1-4</i> senescence phenotype.	70
Figure 12. Deletion within the extracellular stalk did not suppress CERK1 ectodomain shedding.	72
Figure 13. Replacement of the CERK1 extracellular stalk and transmembrane domain could not suppress CERK1 ectodomain shedding.	74
Figure 14. CERK1 and FLS2 extracellular stalk share a lysine-serine motif.	76
Figure 15. The KS motif within the FLS2 and CERK1 extracellular stalk is most likely not a cleavage motif.	77
Figure 16. Receptor-like kinases found in Col-0 cell culture supernatants.	79
Figure 17. Detailed analysis of TMK1-3 and Malectin-LRR-RLKs.	80
Figure 18. Receptor like proteins found in Col-0 cell culture supernatant.	81
Figure 19. Only soluble ectodomain can be found in cell culture supernatants.	82
Figure 20. Receptor-like kinases found in apoplastic wash fluids of Col-3 <i>gl1</i> leaves.	83
Figure 21. Receptor-like proteins found in Col-3 <i>gl1</i> apoplastic wash fluids.	84

Figure 22. Sphingolipid mutants show enhanced CERK1 ectodomain shedding. .85	
Figure 23. Different <i>noce</i> mutants fully suppress the <i>cerk1-4</i> phenotype.86	
Figure 24. Supression of the <i>cerk1-4</i> phenotype is genetically linked to the <i>xlg2</i> E293K (<i>noce4/6</i>) mutation.89	
Figure 25. Expression of a genomic wild type XLG2 fragment can restore the <i>cerk1-4</i> phenotype in <i>nole6-1</i> plants.90	
Figure 26. The glutamatic acid mutated in <i>nole1-2</i> , E293, is located within a highly conserved region of the N-terminal part of XLG2.92	
Figure 27. XLG2-GFP and <i>xlg2</i> E293K-GFP are located to the nucleus and the cell periphery in <i>N. benthamiana</i>93	
Figure 28. XLG2-GFP localization is stimulus dependent.95	
Figure 29. XLG2-GFP is not functional.96	
Figure 30. N-terminal XLG2 fusions are localized to the cell periphery and the nucleus.97	
Figure 31. Venus-XLG2 co-localizes with LYK5-mKate at the plasma membrane.98	
Figure 32. Venus-XLG2 is also found in cytoplasmic strands.98	
Figure 33. N-terminal XLG2 fusions are functional.99	
Figure 34. XLG2 is localized to the cell periphery in unchallenged plants and appears in nuclei after H ₂ O infiltration in Col-0 plants.101	
Figure 35. XLG2 is localized to the cell periphery in unchallenged plants and appears in nuclei after chitin infiltration in Col-0 plants.102	
Figure 36. XLG2 is localized to the cell periphery in unchallenged plants and appears in nuclei after flg22 infiltration in Col-0 plants.103	
Figure 37. XLG2 is localized to the cell periphery in unchallenged plants and appears in nuclei after wounding in Col-0 plants.104	
Figure 38. XLG2 is localized to the cell periphery in unchallenged plants and appears in nuclei after H ₂ O infiltration in Col-3 <i>gl1</i> plants.105	
Figure 39. XLG2 is localized to the cell periphery in unchallenged plants and appears in nuclei after H ₂ O infiltration in <i>cerk1-4</i> plants.106	
Figure 40. XLG2 is localized to the cell periphery and nucleus in unchallenged and challenged <i>agb1-2</i> plants.107	

Figure 41. Venus-XLG2 can be found in soluble protein fractions, but not in microsomes.	108
Figure 42. Venus-XLG2 accumulates in nuclei of <i>Bgh</i> -attacked and surrounding cells.	109

List of supplemental tables

Table S1. Predicted localization of proteins from cell culture supernatants	149
Table S2. Receptor-like kinases and receptor-like proteins found in cell culture supernatant (Sample01)	150
Table S3. Receptor-like kinases and receptor-like proteins found in cell culture supernatant (Sample02)	151
Table S4. Receptor-like kinases and receptor-like proteins found in cell culture supernatant (Sample03)	153
Table S5. Receptor-like kinases and receptor-like proteins found in cell culture supernatant (Sample04)	154

List of supplemental figures

Figure S1. Receptor-like kinases and receptor-like proteins found in Col-0 cell culture supernatants of Sample01	155
Figure S2. Receptor-like kinases and receptor-like proteins found in Col-0 cell culture supernatants of Sample03	155
Figure S3. Receptor-like kinases and receptor-like proteins found in Col-0 cell culture supernatants of Sample04	155

Danksagung

Nach fast 4 Jahren gibt es doch einige Leute, bei denen ich mich für die Unterstützung bei der Fertigstellung dieser Arbeit bedanken möchte.

Bei Prof. Dr. Volker Lipka möchte ich für die Überlassung des Themas und die Möglichkeit diese Arbeit in seinem Labor anzufertigen, bedanken. Jede Phase dieser Arbeit wurde von ihm intensiv und professionell begleitet. Die Freiheiten vor allem beim Thema des Ectodomain shedding habe ich sehr genossen. Neben der professionellen Unterstützung waren es auch die Gespräche über Themen abseits vom Laborleben, die für eine positive Grundstimmung innerhalb der Arbeitsgruppe gesorgt haben:

Großer Dank gebührt Dr. Elena Petutschnig möchte ich für die Betreuung während der Anfertigung dieser Arbeit bedanken. Ihre Hilfe im täglichen Laboralltag, ständige Diskussionsbereitschaft, auch bei teilweise abstrusen Ideen und die damit verbundene konstruktive Kritik haben maßgeblich zum Gelingen dieser Arbeit beigetragen. Danke vor allem auch für die zuletzt zahlreichen Stunden am Schreibtisch um diese Arbeit auf Herz und Nieren zu überprüfen.

Danke an PD. Dr. Thomas Teichmann für die Übernahme des Korreferats, sowie Hilfe bei kleinen und großen Problemen des Laboralltags.

Prof. Dr. Ivo Feußner, Dr. Martin Fulda, Prof. Dr. Gatz und Prof. Dr. Andrea Polle bedanke ich mich für die Bereitschaft zusammen mit meinem Betreuungsausschuss meine Prüfungskommission zu bilden.

Vielen Dank an Dr. Andrzej Majcherczyk für die massenspektrometrischen Analysen und die Hilfe bei der Interpretation und Auswertung der daraus resultierenden Daten.

Bei Kathi, Ludmilla und Sabine möchte ich mich für die Hilfe im Labor bedanken. DNA und vor allem RNA waren manchmal einfach nicht meine Freunde. Danke auch für die Herstellung von Puffern, das Aufräumen von Laborbänken und nicht zu vergessen die Übernahme des Spüldienstes, wenn der mal wieder vergessen wurde.

Den Gärtnern Feli, Susanne und Herrn Wedemeyer danke ich für das Stopfen von Töpfen

und Siebearbeiten, die das Laborleben um einiges vereinfacht haben. Feli danke ich darüber hinaus für die zahlreichen Äpfel vom heimischen Apfelbaum.

Danke an alle aktuellen und ehemaligen Mitglieder der Arbeitsgruppe, für Grillaktionen, Geburtstagskuchen und vieles mehr. Großen Dank an Hassen, der einem jeder Zeit mit Rat und Tat bei Mikroskopieproblemen zur Seite stand. Marcel, danke für die Verwaltung der Kaffeekasse und das regelmäßige Auffüllen des Kaffeevorrats. Auch bei Anja möchte ich mich für die Überwindung so einiger bürokratischer Hürden bedanken.

Danke auch an alle aktuellen und ehemaligen „Mitreiter“ Marnie, Charlotte, Yvonne, Karin, Jan, Merlin, Johanna, Dimitri und Sabine. Ohne Martin und Zubi wäre der Freitag niemals eine so gute Einleitung des Wochenendes gewesen. Danke.

Bei Sebastian möchte ich mich für die Übernahme des Korreferats eines Sky-Abos bedanken. Das waren 2 gute Jahre, leider gingen sie viel zu schnell vorbei. Bei Matthias möchte ich mich darüber hinaus für das von ihm geschriebene Programm zur Auswertung der Massenspektrometrie Daten bedanken. Ohne dies wäre die Fertigstellung dieser Arbeit im Jahr 2016 nicht möglich gewesen.

Bei den Jungs in und um Osnabrück möchte ich mich für die Urlaube, zahlreichen Feiern und die Verfügbarkeit von Sofas zum Übernachten bedanken.

Ein großer Dank geht natürlich auch an meine Familie. Ohne die großartige Unterstützung der letzten Jahre wäre diese Arbeit niemals zustande gekommen.

Curriculum vitae

Personal information

Name: Christopher Meusel
Adress: Planckstr. 10, 37073 Göttingen
Date of birth: 05.12.1985
Place of birth: Ankum

Education

05/2012 – present **Georg-August-University of Göttingen**
Schwann-Schleiden Centre, Plant Cell Biology
PhD
Title of PhD thesis: *Analysis of CERK1 ectodomain shedding and the role of extra-large g-protein 2 (XLG2) in cerk1-4 cell death execution*

10/2009 – 03/2012 **Philipps-University of Marburg**
Course of study: Molecular and Cellular Biology
Degree: Master of Science (grade: 1.5)

10/2006 – 09/2009 **Leibniz-University of Hanover**
Course of study: Biology
Degree: Bachelor of Science (grade: 2.3)

08/1996 – 07/2005 **Integrierte Gesamtschule Fürstenau**
Qualification for university entrance: A levels/
Abitur (grade: 1.7)

Research experience

09/2010 – 01/2011 **Department of Biochemistry and Molecular Biology**
Universidad de Valencia (UV), Spain
Internship in the group of Dr. Ismael Mingarro

Additional skills

Languages: German (native language)
 Englisch (fluent)

IT skills: MS-Office: Word, Excel, PowerPoint
 Photoshop, Illustrator
 Geneious, Clone manager

Conferences

- 07/2014 XVI International Congress on Molecular Plant
Microbe Interactions, Rhodos (Greece)
Poster: *Ectodomain shedding – A general post-
translational modification of plant PRRs?*
- 03/2013 Gemeinsame Jahrestagung der DPG-Arbeitskreise
Mykologie und Wirt-Parasit-Beziehungen, Göttingen
(Germany)
Talk: *Analysis of CERK1 ectodomain shedding*